METALLODITHIOLATE LIGANDS AS BUILDING BLOCKS FOR MOLECULAR CONSTRUCTIONS

A Dissertation

by

STEPHEN PAUL JEFFERY

Submitted to the Office of Graduate Studies of
Texas A&M University
in partial fulfillment of the requirements for the degree of

DOCTOR OF PHILOSOPHY

May 2006

Major Subject: Chemistry

METALLODITHIOLATE LIGANDS AS BUILDING BLOCKS FOR MOLECULAR CONSTRUCTIONS

A Dissertation

by

STEPHEN PAUL JEFFERY

Submitted to the Office of Graduate Studies of
Texas A&M University
in partial fulfillment of the requirements for the degree of

DOCTOR OF PHILOSOPHY

Approved by:

Chair of Committee,	Marcetta Y. Darensbourg
Committee Members,	Kim R. Dunbar
	François P. Gabbaï
	Edward D. Harris
Head of Department,	Emile A. Schweikert

May 2006

Major Subject: Chemistry

ABSTRACT

Metallodithiolate Ligands as Building Blocks for Molecular Constructions. (May 2006)

Stephen Paul Jeffery, B.S., Texas A&M University

Chair of Advisory Committee: Dr. Marcetta Y. Darensbourg

NiN_2S_2 moieties have been used as a unique class of ligand in organometallic chemistry behaving as innocent mono- and bidentate ligands to metals bound via their thiolate sulfur donor atoms. We have established the donor ability of these ligands with respect to conventional ligands, e.g., diphosphines and diimines, by synthesizing a series of $(NiN_2S_2)W(CO)_4$ complexes and using infrared spectroscopy to obtain the ν(CO) stretching frequencies as a report of the electron density on the metal. In comparison to the analogous tungsten complexes utilizing traditional ligands, the NiN_2S_2 ligands were found to be far better donors than the diphosphines as evidenced by significantly lower ν(CO) values, and much closer to diimine ligands.

Sulfur's ability to form aggregates is well documented. The metallodithiolate ligands **Ni-1** and **Ni-1'** have been used resulting in numerous molecular constructions, specifically C_3 and C_4 paddlewheels of the composition M_2Ni_x. Whereas many paddlewheels in the literature employing NiN_2S_2 ligands were formed largely unintended, a synthetic approach was designed utilizing multiply-bonded dimetal units of various bond orders. These explorations have extended the range of metal-metal distances accommodated by NiN_2S_2 units in our library from 2.14 Å to 4.35 Å.

The complexes discussed in this dissertation are polymetallic clusters with high positive charges associated with them. Electrochemical studies reveal that the redox activity of the NiN_2S_2 unit can be deconvoluted from the dimetal unit and that sulfur metallation causes the reduction potential of the NiN_2S_2 ligand (approximately -2.0 V) to become more positive. With each subsequent reduction, the overall positive charge is lessened which causes the corresponding reduction potentials to be more negative. Solvent dependent studies suggest a partial dissociation of the NiN_2S_2 ligand reminiscent of the mechanism calculated for Acetyl CoA Synthase. Mixed-ligand species proved unstable in any solvent.

As rhodium is an intrinsically catalytic metal, investigations were performed to observe if stable complexes could be prepared to serve as models to study industrially relevant processes. The metalloligands **Ni-1** and **Ni-1'** were found to stabilize multiple oxidation states of rhodium resulting in structural forms such as a heterobimetallic (Rh^{I}), a C_4 paddlewheel (Rh^{II}), and tetrametallic analog to Rubpy (Rh^{III}).

DEDICATION

This work is dedicated to the head of my life Jesus Christ. Through Him all things are possible (Phil. 4:13). To my parents, Curtis and Leona Jeffery, thank you for all the love, encouragement, and advice you have given me throughout my twenty-eight years. You never limited me in my thinking or in the setting or obtaining of goals. Most importantly, thank you for your brutal honesty and for the many sacrifices you have made over the years.

To my cousin, Reginald Carmen, you will be truly missed. I was glad to know I made you proud—and that you never had to use those "hammers". Chapter VII, I dedicate to my friend, Mervin J. Bazile, Jr. Thank you for the ideas and discussions on the dirhodium chemistry. You had an eye for detail and a passion for the science. I hope to see y'all again in glory.

ACKNOWLEDGMENTS

In my stay here, I have been blessed to have met many people and developed numerous long-lasting bonds and camaraderie. To the many friends and contacts I've made, I thank you for just being there. I will do my best to keep in touch. In this section, I have attempted to acknowledge everyone; however, in the event I omitted you, charge it to my mind, not to my heart.

First, I wish to thank my advisor Marcetta Y. Darensbourg for guiding me through the rigors of obtaining a Ph.D. degree. You have mentored me on how to be a successful educator and researcher. Your passion and ease in teaching is something I strive for. Your drive for perfection in chemical research is nonpareil. Although a great deal of knowledge has been obtained through laboratory and class work, over the years we've known each other that which I have learned outside these arenas from you was of far greater value. You have taught by example and have shown me how to critically evaluate my work and how to express my findings through various media. The camaraderie between the MYD and DJD groups conveyed a sense of belonging and togetherness. Don's giggle and sarcastic wit brought many a smile to my face. P. S., Marcetta, I apologize for not sharing my French fries with you in London.

I owe much gratitude to my advisory committee members, Drs. Kim R. Dunbar François P. Gabbaï, and Edward D. Harris for their advice and willingness to answer questions. A special thanks goes to Dr. Donald J. Darensbourg who has been an valuable asset in the infrared studies. To Drs. Abraham Clearfield, Simon W. North, and

Eric E. Simanek, thank you for your encouraging words or simple a smile in the hall. They always seemed to come when I needed it most.

No amount of words can be used to express my sincere thanks and appreciation to Dr. Joseph H. Reibenspies. Your expertise in the field of x-ray crystallography to the world is immense, yet your friendship and **patience** with a tyro like me has been invaluable. I must also thank Drs. Damon G. Billodeaux and Cesar G. Ortiz for their assistance and guidance on many a crystal structure during their tenure as graduate students. You have passed your knowledge on to me and I have done the same.

I appreciate all the help I received from former students and postdocs while at A&M. Each of you has taught or mentored me in some form which has shaped my development and helped me mature as a scientist: Drs. Daesung Chong, James P. Donahue, Melissa L. Golden, Penglin Huang, Jonghyuk Lee, Tongbu Lu, Ahmed Mohammed, and Chad C. Wilkinson. Thank you all for letting me pluck your nerves time and time again.

Thank you to past MYD group members whom I did not work with directly, Chao-Yi Chiang (Joey) and Rosario Mejia-Rodriguez, I valued your input and suggestions. Thanks to current members of the MYD and DJD groups, Elky Almaraz, Jeremy Andreatta, Megan Arnold, Scott Brothers, Angelica Cantillo, Cody Carson, Wonsook Choi, Shawn Fitch, Eric Frantz, Kayla Green, Roxanne Jenkins, Tianbiao Liu (Leo), Adriana Moncada, Carlos Montalvo, Cass Richers, Michael Singleton, Sarah Stranahan, Jesse Tye, Hsaio-Wan Wang (Ivy). Your friendships have meant a lot to me. I can only hope you have learned as much from me as I have from you. Special thanks

to Kayla for always having an ear to listen, letting me take you under my wing and teach you things, for reading several drafts of this dissertation, and also for having my back. Thank you for being such a good friend and colleague. To Jesse, laughter is golden and you kept me in stitches. You've also shown me how to look at my work from a different perspective. Mind the gap! An extra special thanks goes to Sue Winters for formatting this dissertation and showing me various ways to manipulate software for my presentations. My advice to current and future students, if I may be so bold, is that you get out of this degree what you put into it. Find a project that you believe in and put your heart and soul in it. Learn everything you can about its functions. It can be rough out there, so persevere. It'll be greater, later.

To "Shorty," Kirsten, thank you for being by my side and enduring my many mood swings and putting up with my idiosyncrasies. For what you lack in stature, you more than make up in heart. You're a trooper and have been an unwavering beacon of encouragement and one of my biggest fans and supporters. It's been a long, hard road. I made it to the end of the tunnel and didn't get hit by a train!

Last, but certainly not least, I would like to thank the men and women who make our jobs as researchers a little easier. A heart-felt thanks goes to employees of the physical plant, maintenance, custodial, glass and machine shops. You may go unseen, but your labors do not. Thank you.

TABLE OF CONTENTS

CHAPTER Page

Page

LIST OF TABLES

TABLE Page

LIST OF FIGURES

FIGURE Page

FIGURE Page

FIGURE Page

FIGURE Page

FIGURE Page

FIGURE Page

LIST OF SCHEMES

SCHEME Page

CHAPTER I

INTRODUCTION

That *cis*-dithiolato metal compounds might serve as important building blocks for the synthesis of heterobimetallic complexes has long been recognized. Two decades ago D. W. Stephan and co-workers directed efforts towards the preparation of early-late heterobimetallic (EHLB) complexes, presumably for their potential as catalysts, utilizing $(\eta^5\text{-}C_5H_5)_2Ti(SCH_2CH_2PPh_2)_2$ as a metallodithiolate ligand. The complex shown in Figure I-1 depicts this compound as a tetradentate chelating ligand to a copper(I) source.[1] While other structures were prepared and characterized, there were no reports of catalytic activity.

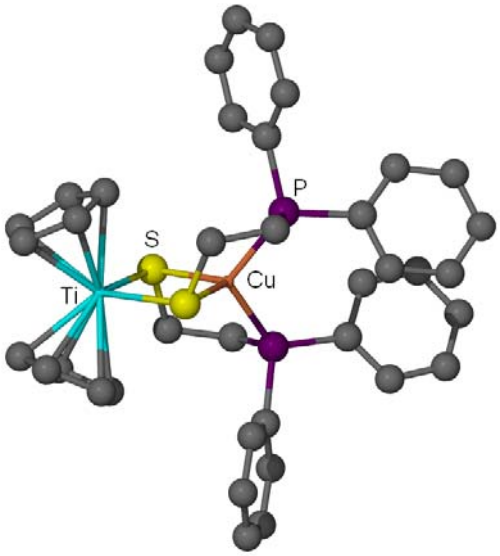

Figure I-1. Archetypical example of Stephan's metallodithiolate ligation.

This dissertation follows the style and format of *Journal of the American Chemical Society.*

NiN_2S_2 as ligand to transition metals

The remarkable ability of nickel *cis*-thiolates to act as bidentate ligands to metals has been known for quite some time. Since the seminal work by Jicha and Busch in the 1960's,[2] the library of NiN_2S_2 metallodithiolate ligands has increased tremendously. These ligands, aided by sulfur's affinity to aggregate, have served as the building block or subunit for myriad molecular constructions found in the literature. The number of complexes formed by NiN_2S_2 units serving as ligands has traversed the transition metals as shown in Scheme I-1.

Scheme I-1. Scope of transition metals ligated by NiN_2S_2 metallodithiolate ligands shown in bold with contributions from the M. Y. Darensbourg laboratories shown in *italics*.

Sc	Ti	V	Cr	Mn	***Fe***	***Co***	***Ni***	***Cu***	***Zn***
Y	Zr	Nb	***Mo***	Tc	***Ru***	***Rh***	***Pd***	***Ag***	**Cd**
La	Hf	Ta	***W***	Re	Os	Ir	**Pt**	**Au**	**Hg**

A recent report by Holm and co-workers summarized the extensive structural vocabulary of NiN_2S_2 and added 27 new structures to the ever growing library of polymetallic complexes.[3] This serves as testimony to the aggregative ability of metallodithiolates and more importantly sulfur ($Ni(\mu\text{-}SR)_2M'$). A presentation of possible structures based on NiN_2S_2 metallodithiolates is given in Figure I-2. While many of the aforementioned complexes resulted from thermodynamically controlled processes, it has become evident over the years that the aggregative products may be controlled by stoichiometry, ligand modification, and nature of the exogenous metal.

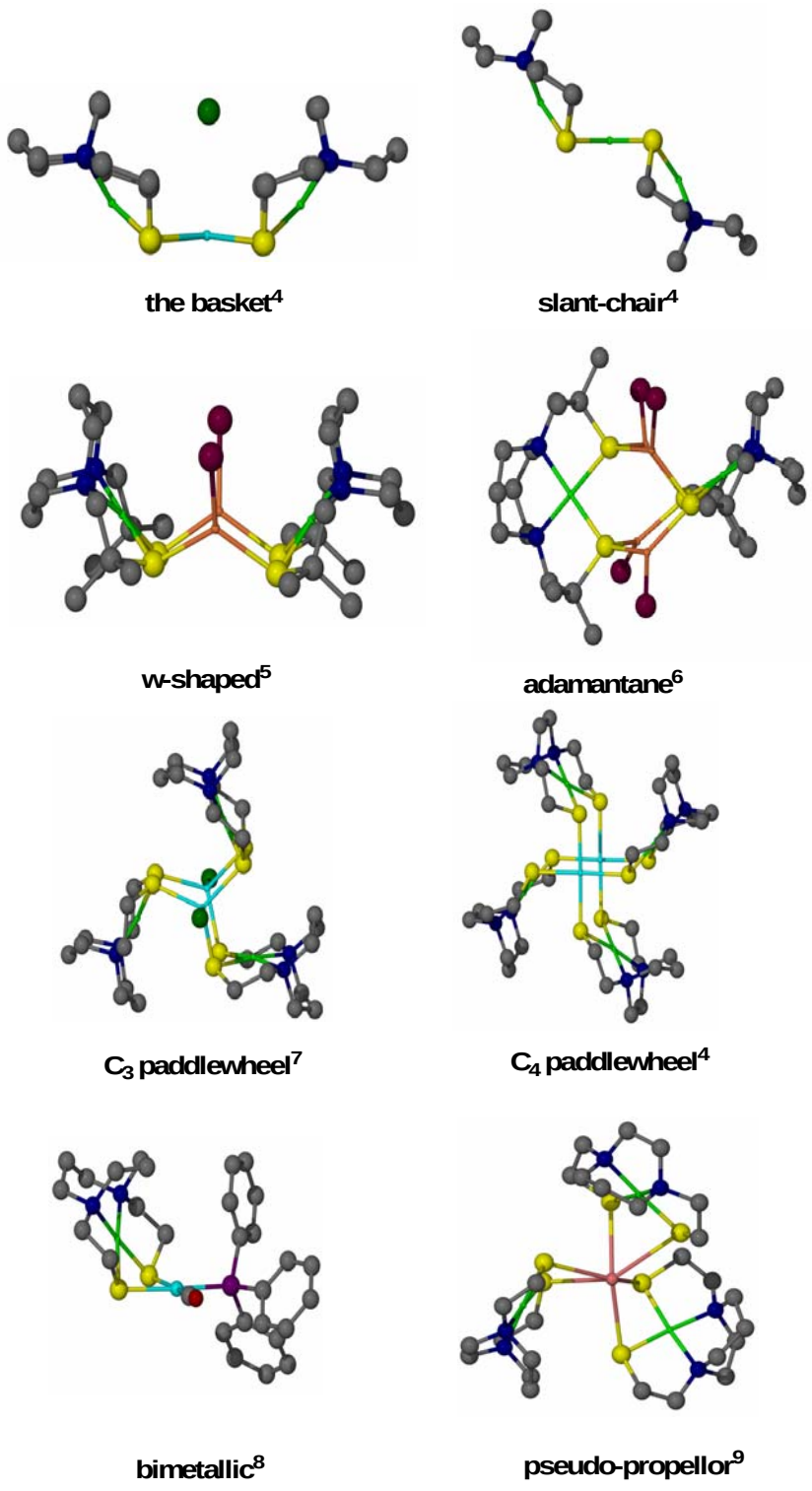

Figure I-2. Structures of polymetallics in our $M'_y(NiN_2S_2)_x$ collection derived from x-ray crystallographic analyses.

Nature's NiN_2S_2 ligand

The trapping of exogenous metals by *cis*-dithiolato complexes of nickel including $(P\text{-}S)_2Ni$ or $(N\text{-}S)_2Ni$ is also well established. In fact, through detailed structural studies of the metalloprotein Acetyl CoA Synthase, ACS, it is now known that the active site is a binuclear complex containing a dicysteinate nickel as a $Ni(\mu\text{-}SR)_2$ donor to a second, catalytically functional, nickel atom shown in Figure I-3.[10] This discovery was completely consistent with complexes based on NiN_2S_2 as metallodithiolate ligands, including those from the M. Y. Darensbourg group involving bis(mercaptoethyl)-*N,N'*-1,5-diazacyclooctane)nickel, Ni(bme-daco), **Ni-1**[11] and (bis(mercaptoethyl)-*N,N'*-1,5-diazacycloheptane)nickel, Ni(bme-dach), **Ni-1'**[12] shown in Figure I-4 as used in Figure I-2.

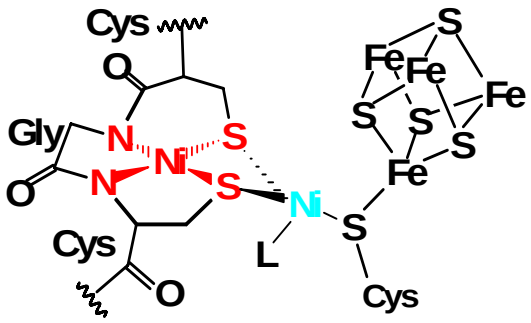

Figure I-3. Depiction of the ACS enzyme with the Cys-Gly-Cys NiN_2S_2 moiety in red and the catalytically active metal in light blue.

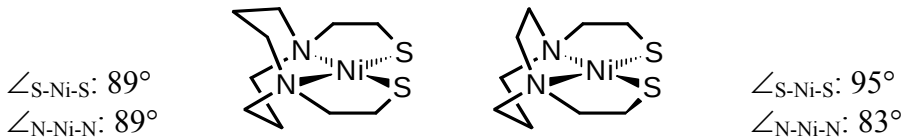

Ni-1 **Ni-1'**

Figure I-4. Metallodithiolate ligands utilized in this study with relevant bond angles listed.

It also suggests the possibility that such NiN_2S_2 complexes should be capable of supporting organometallic reactivity at a ligated metal. In order to be effectively exploited, the properties of a ligand must be well understood. The NiN_2S_2 units utilized in the Darensbourg labs were originally postulated as mimics to diphosphine ligands based on similar binding abilities to metal carbonyl complexes. A structural comparison of nickel chelated by *dppm* and by **Ni-1** revealed comparable metric data.[13,14] This dissertation concerns itself with reactivity at the thiolate sulfur lone pairs which results in an assortment of polymetallic molecular constructions comprised of NiN_2S_2 units, including metal-metal bonded clusters.

Metal-metal bonding

The chemistry of metal-metal bonded complexes is a remarkable field based on the chemistry of compounds with multiple metal centers bound to each other and surrounded by ligands. It was not until the early 1960's that a new outlet for transition metal chemistry had begun to take shape galvanized by investigations of the rhenium atoms in the cluster $[Re_3Cl_{12}]^{3-}$ which subsequently led to the discovery of the quadruply-bonded $[Re_2Cl_8]^{2-}$ anion. Previously, chemists relied on a Wernerian view of the role of metal atoms in chemistry where a single metal ion is surrounded by ligands bound by dative bonds.[15]

In the discussion of metal-metal bonding, it is easiest to describe the quadruple bond. Since all multiple bonds contain elements of the former, it is thus a good starting point for discussion. Metal-metal bonding is best explained by using a molecular orbital

approach. The quadruple bond, which exists for transition metals, can therefore be explained using *d*-orbitals. In molecular orbital theory, bonding is defined as the overlap of orbitals of the same symmetry. The quadruple bond is composed by the overlap of the d_{z^2}, d_{xz} and d_{yz}, and d_{xy} orbitals which make up one σ, two π, and one δ interactions as shown in Figure I-5. The $d_{x^2-y^2}$ orbital is not included in the bonding scheme because it is the same symmetry as the ligands. The bond order can be derived by subtracting the number of electrons in bonding orbitals from the number of electrons in antibonding. Dimolybdenum tetraacetate ($Mo_2(OAc)_4$), for example, consists of two Mo^{2+} cations containing eight valence electrons. Thus the orbital from bonding overlaps are filled and using the molecular orbital diagram in Figure I-6, $Mo_2(OAc)_4$ can be shown to have a bond order of four. The Rh^{II}-Rh^{II} containing compound $Rh_2(OAc)_4$ consists of two Rh^{2+} cations, containing 14 valence electrons, gives a bond order of one and likewise two Pd^{2+} cations with 16 valence electrons gives a bond order of zero.

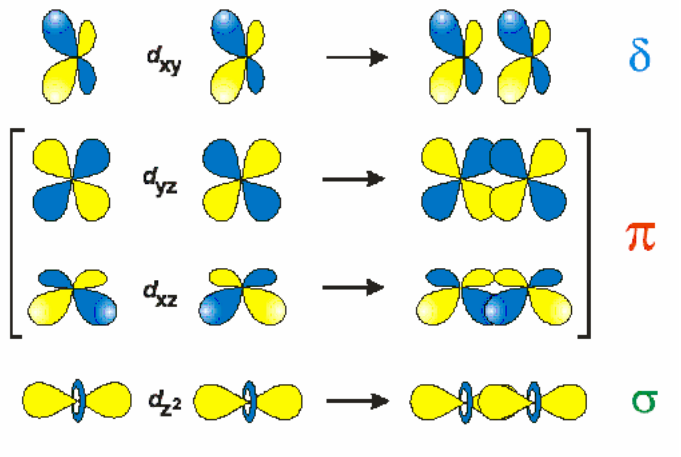

Figure I-5. Overlap of *d* orbitals utilized in the multiple bonding of metal atoms.[16]

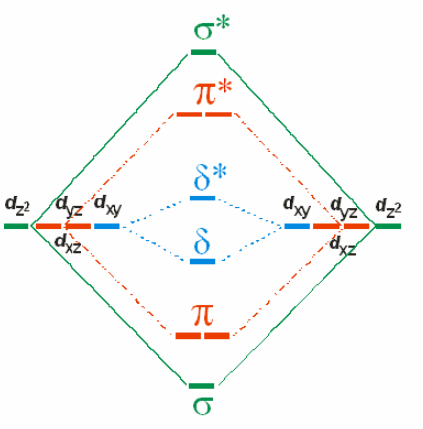

Figure I-6. Molecular orbital diagram explaining multiple bonding between transition metal atoms.[16]

For the purpose of this dissertation, the metal-metal bonded complexes described herein are best described as paddlewheel complexes. A paddlewheel complex can be loosely defined as a compound with a major rotation axis, commonly a four-fold, containing multiple metal atoms and four bidentate bridging which ligands containing at least three atoms. Figure I-7 lists the three common categories of bridging ligands in metal-metal bonded chemistry. Interestingly however, there are very few examples of metalloligands used to bridge multiply-bonded dimetal centers.[17] Two examples are shown in Figure I-8.[18] Metalloligands have been demonstrated to serve as linkers between metal-metal bonded complexes in the synthesis of supramolecular arrays.[19]

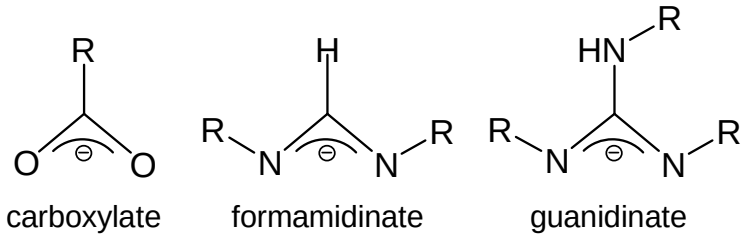

Figure I-7. A sample of the most common bridging ligands in metal-metal bonded chemistry where R is any organic group.

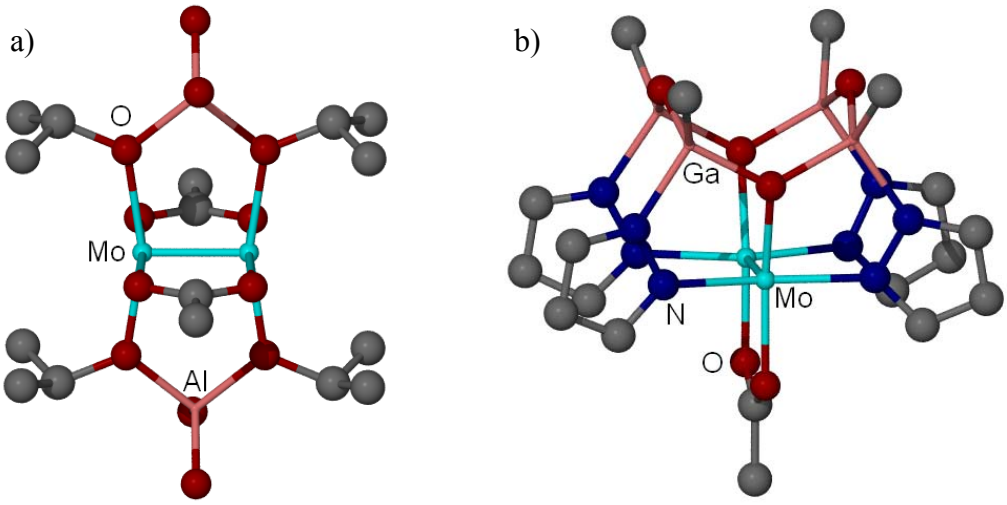

Figure I-8. Ball and stick drawings of a) *trans*-bis(μ-acetato)-(bis(μ-tetraisopropoxy)aluminate) dimolybdenum and b) (μ-acetato)[1,3,5,7-tetramethyl-1,3,5,7-tetrakis(pyrazol-1-yl) cyclotetragalloxanato]dimolybdenum anion.

A common theme with the ligands associated with paddlewheel complexes is a relatively flat five-membered dimetallocycle comprised of the dimetal unit, with ligating bridging atoms similar to those depicted in Figure I-9. Last but not least, it is worthwhile to mention that a paddlewheel complex may possess zero, one, or two axial ligands coordinated to the dimetal unit.

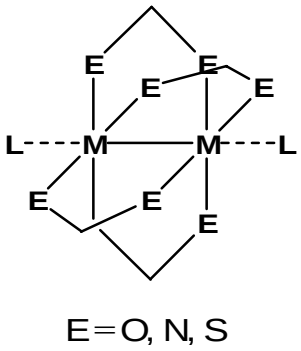

Figure I-9. General scheme for C_4 paddlewheel complexes with bidentate bridging ligands.

This dissertation consists of four major sections. The first part describes the explorations carried out to determine the donor ability of nickel metallodithiolate ligands via infrared spectroscopy by examination of a series of heterobimetallic tungsten tetracarbonyl complexes. Cotton-Kraihanzel force constants have been calculated and the complexes were ranked amongst the more traditional ligands such as diphosphines and diimines. All the compounds of this series were structurally characterized and my contributions will be discussed first followed by analysis of the entire series. This work will be followed by ligand substitution studies with monodentate phosphines.

In the second part of this dissertation, the NiN_2S_2 metallodithiolate ligands have been used as bidentate bridging ligands for a designed series of multiply-bonded dimetal complexes. Unlike diphosphine ligands whose steric bulk is located on the donor atoms, the steric bulk of the metallodithiolate is located abaft making them relatively flat ligands like bipyridine or the carboxylate ligands used in metal-metal bonded chemistry for example. The literature contains several dimolybdenum compounds with transoid bridging diphosphine ligands and halogen or pseudohalogen ligands residing in the equatorial plane like the one shown in Figure I-10.[20] Full substitution is not achieved and only two phosphines bind to the dimetal center presumably due to steric limitations. In contrast, the sterically unencumbered ligands of Figure I-7 and the square planar NiN_2S_2 ligands show full coordination. It is my goal to use NiN_2S_2 units as bidentate bridging ligands to multiply-bonded M_2^{n+} units resulting in M_2Ni_4 complexes and to determine the full scope of metal-metal distances possible in NiN_2S_2 paddlewheel type complexes.

If NiN_2S_2 units indeed prove viable as ligands for metal-metal bonded complexes, it is important to know if the electrochemistry of the metallodithiolate can be deconvoluted from that of the M_2^{n+} unit. To determine this, various mixed-ligand clusters formulated as $Mo_2Ni_2L_2$ and Mo_2Ni_3L were prepared and analyzed. As a comparison to these new studies, various polymetallics and paddlewheel complexes from our collection of complexes have been characterized electrochemically as well.

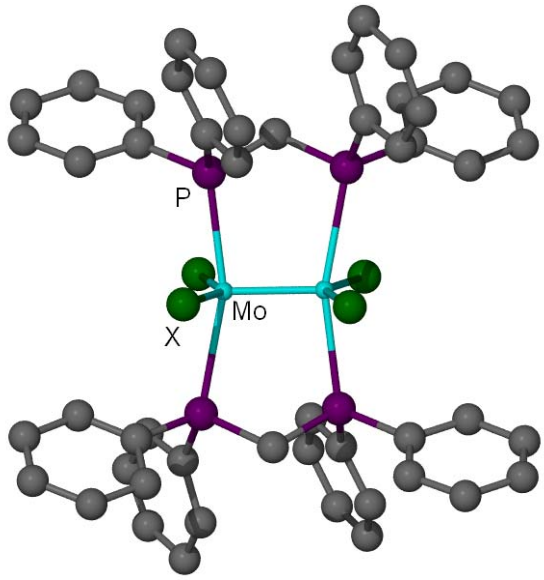

Figure I-10. Ball and stick representation of complexes of the type $Mo_2(dppm)_2X_4$, where X = Cl, Br, I, SCN.

Lastly, the pursuit of the dirhodium hexametallic metal-metal bonded complex led to the discovery of a tetrametallic structural mimic of $Ru(bpy)_3^{2+}$ formulated as $[Rh^{III}(NiN_2S_2)_3]^{3+}$. Isolation of this complex may aid in further study the analogy of NiN_2S_2 to diimines. Metallodithiolate ligands will be shown to stabilize Rh in other oxidation states which resulted in another paddlewheel for our collection,

$[Rh^{II}_2(NiN_2S_2)_4]^{4+}$, and heterobimetallics, $[Rh^{I}(NiN_2S_2)(CO)_2]^{+}$, for potential use in industrially relevant processes.

CHAPTER II

EXPERIMENTAL/SYNTHESIS OF COMPOUNDS AND REACTIVITY STUDIES CHAPTERS III-VII

General procedures and physical methods

Syntheses and manipulations were performed using standard Schlenk-line and syringe/rubber septa techniques under N_2 or in an argon atmosphere glovebox unless specifically stated. Filtrations of solutions used airless-ware glass frits typically with 1-2 cm pads of Celite. Solvents were reagent grade, purified according to published procedures, and freshly distilled under nitrogen prior to use.[21]

UV-Vis spectra were recorded in MeCN and DMF on a Hewlett Packard HP8452A diode array spectrometer using quartz cells (1.00 cm path length). Elemental analyses were performed by Canadian Microanalytical Services, Ltd., Delta, British Columbia, Canada. Infrared spectra were recorded on a Matteson Galaxy Series 6021 FTIR spectrometer or a Bruker Tensor 27 spectrometer in CaF_2 solution cells of 0.1 mm path length. Photolysis experiments were performed using a 450 W UV mercury arc vapor immersion lamp purchased from the Ace Glass Co. Electron spray ionization mass spectrometry measurements were obtained at the Laboratory for Biological Mass Spectrometry, Texas A&M University, College Station, Texas, using MDS Series Quasar Pulsar with a spray voltage of 5 eV.

Cyclic voltammograms were obtained under an argon atmosphere at room temperature using a BAS100W potentiostat equipped with three electrodes: a 3.0 mm glassy carbon working electrode, a platinum wire auxiliary electrode, and 0.01 M

$Ag/AgNO_3$ reference electrode in MeCN. The reversibility of the reductions waves was poorer when a platinum working electrode is used as compared to glassy carbon due to plating of the electrode resulting from sulfur's affinity for heavy metals. For studies performed in DMF, THF, and CH_2Cl_2, a Ag/Ag^+ reference electrode was used and prepared by anodizing a silver wire in 1.0 M HCl. Measurements were taken in MeCN, THF, and DMF of 1 mM analyte in 0.1 M n-Bu_4NBF_4 supporting electrolyte at ambient temperature. All potentials were reported to the normal hydrogen electrode (NHE) using $Cp^*_2Fe/Cp_2^*Fe^+$ referenced to -130 mV in MeCN according to the literature (under the same conditions ferrocene was found at 640 mV) as the internal standard.[22] The Fc/Fc^+ couple in THF and DMF was found at 0.56 and 0.45 V respectively. All cyclic voltammograms were reported at a scan rate of 200 mV/s; all square wave voltammograms have an amplitude of 25 mV, frequency of 15 Hz, and E_{step} of 4 mV.

X-ray structure analysis

The x-ray data were obtained from the Crystal and Molecular Structure Laboratory Center for Chemical Characterization and Analysis at Texas A&M University. The crystals were mounted on a nylon loop with a small amount of oil and attached to a goniometer head. X-ray data were obtained on a SMART 1000 diffractometer unless specifically stated. Low temperature (110K) x-ray diffraction data were collected on a BRUKER SMART CCD-based diffractometer (Mo-Kα radiation, $\lambda = 0.71073$ Å).

The space groups were determined based on systematic absences and intensity statistics using the SMART program[23] for data collection and cell refinement. Raw data frame integration was performed with SAINT+. The structures were solved by direct methods. Hydrogen atoms were added at idealized positions and refined with fixed isotropic displacement parameters equal to 1.2 times the isotropic displacement parameters of the atoms to which they were attached. Anisotropic displacement parameters were determined for all non-hydrogen atoms. Programs used for data collection and cell refinement, Bruker XSCANS; data reduction, SHELXTL; absorption correction,[24] SADABS; structure solution, SHELXS-97 (Sheldrick);[25] structure refinement, SHELXL-97 (Sheldrick),[26] and molecular graphics and preparation of material for publication, SHELXTL-PLUS, version 5.1 or later (Bruker).

Integrated intensity information for each reflection was obtained by reduction of the data frames with the program SAINT V6.63.[27] The integration method employed a three dimensional profiling algorithm and all data were corrected for Lorentz and polarization factors, as well as for crystal decay effects. Finally the data was merged and scaled to produce a suitable data set. The absorption correction program SADABS was employed to correct the data for absorption effects. X-Seed was employed for the final data presentation and structure plots.[28]

Experimental details for Chapter III

Materials. CH_2Cl_2, Et_2O, benzene, hexane, MeOH, and CH_2Cl_2 were purified according to published procedures under an N_2 atmosphere.[21] PMe_3 and PPh_3 were purchased from

Aldrich Chemical Co and 99.9% anhydrous dimethylformamide (DMF) was purchased from Acros Chemical Co.

Syntheses. The **Ni-1**,[11] **Ni-1'**,[12] Ni(bme-Me_2PDA),[29] and *cis*-$(pip)_2W(CO)_4$ [30] complexes were synthesized according to previously published procedures. PPh_3 was recrystallized from hot MeOH prior to use. The (**Ni-1**)$W(CO)_4$ and (**Ni-1'**)$W(CO)_4$ complexes were prepared by graduate student Marilyn Rampersad in a manner similar to the $(NiN_2S_2)W(CO)_4$ complexes shown below. Definitions: **Ni-1** = (1,5-bis(2-mercaptoethyl)-1,5-diazacyclooctane)nickel; **Ni-1'** = (1,5-bis(2-mercaptoethyl)-1,5-diazacycloheptane)nickel; Ni(bme-Me_2PDA) = (*N,N'*-dimethyl-*N,N'*-1,5-bis(2-mercaptoethyl)-1,5-dimethyl propylamine)nickel

((*N,N'*-dimethyl-*N,N'*-bis-2-mercaptoethyl-1,3-propanediamine)nickel)tungsten tetracarbonyl, (Ni(bme-Me_2PDA)$W(CO)_4$. Under an N_2 atmosphere to a Schlenk flask containing 15 mL of MeOH, Ni(bme-Me_2PDA) (0.3 g, 1.1 mmol) and *cis*-$(pip)_2W(CO)$ (0.50 g, 1.1 mmol) were added. The nickel complex immediately dissolved with stirring yielding a brown solution. The yellow tungsten complex remained undissolved. Upon heating to approximately 60°C for 10 min, the tungsten complex dissolved yielding a dark brown solution. The product was precipitated out of solution with 80 mL of Et_2O and washed with Et_2O and benzene to remove excess piperidine (2 x 20 mL). The brown black solid was dried *in vacuo* yielding 0.50 g (80%). Dark brown crystals were obtained by dissolving the residue in a minimum of CH_2Cl_2 and layering with hexanes. Anal.

Calc'd (found): C: 27.2 (26.9%), H: 3.51 (3.51), N: 4.87 (4.60). Vis/UV in DMF solution: λ_{max} (ε) = 310 (7695), 414 (1325), 454 (1077), 494 nm (597). ^{13}C NMR (DMF): 213.4, 210.1, 204.2 ppm. ν(CO), DMF: 1993, 1876, 1843, 1826 cm^{-1}.

((1,5-bis(2-mercaptoethyl)-1,5-diazacyclooctane)nickel) tungsten tetracarbonyl, (Ni-1)WCO_4. Under an N_2 atmosphere to a Schlenk flask containing 15 mL CH_2Cl_2, **Ni-1** (0.20 g, 0.687 mmol) and *cis*-$(pip)_2W(CO)_2$ (0.146 g, 0.313 mmol) were dissolved with stirring in 15 mL CH_2Cl_2. The solution was refluxed for approximately 15 min yielding a brown solution. The product was precipitated out of solution with 80 mL of hexanes and washed with Et_2O and benzene to remove excess piperidine (2 x 20 mL). The brown, air-stable solid was dried *in vacuo*. ν(CO), DMF: 1995, 1871, 1853, 1819 cm^{-1}. Diffractometer quality crystals were grown from a concentrated DMF solution layered with Et_2O. Needle-shaped crystals formed after 7 days.

(1,5-bis(2-mercaptoethyl)-1,5-diazacycloheptane)nickel) tungsten tetracarbonyl, (Ni-1')WCO_4. In an identical manner, the **Ni-1'** derivative was isolated. ν(CO), DMF: 1996, 1873, 1852, 1817 cm^{-1}. Diffractometer quality crystals were grown from a concentrated DMF solution layered with Et_2O. Needle-shaped crystals formed after seven days.

Ligand substitution studies with PR_3, R = Me, Ph. In a typical reaction, (**Ni-1'**)$W(CO)_4$ (0.200 g, 0.349 mmol) was dissolved in 20 mL of DMF and reacted with 10

equivalents of the appropriate phosphine (PMe_3: 50 μL, PPh_3: 0.117 g) at room temperature. An infrared spectrum was obtained after one hour. PMe_3 reaction, ν(CO): 2000, 1886, 1864, 1820. After three hours, the reaction with PPh_3 did not reach completion. Increasing the amount of PPh_3 used in the reaction by equivalents of 10 caused a noticeable change in the infrared spectrum yielding multiple bands (ν(CO): 2036, 2002, 1976, 1945, 1916, 1892, 1868, 1825 cm^{-1}).

Experimental details for Chapter IV

Materials. CH_2Cl_2, THF, MeCN, Et_2O, hexane, MeOH, and CH_2Cl_2 were purified according to published procedures under an N_2 atmosphere.[21] PPh_3 was purchased from Aldrich Chemical Co. Anhydrous dimethylformamide (DMF) 99.9% was purchased from Acros Chemical Co.

Syntheses. The **Ni-1**,[11] (**Ni-1**)$W(CO)_5$,[31] and Ni(mese-daco)[14] complexes were synthesized according to previously published procedures. PPh_3 was recrystallized from hot MeOH prior to use. Definition: Ni(mese-daco) = [(mercaptoethyl)(sulfinatoethyl) diazacyclooctane)]nickel

X-ray structure analysis. The **Ni-1**$(W(CO)_5)_2$ complex was analyzed on a BRUKER D8 GADDS general-purpose three-circle X-ray diffractometer was employed for sample screening and data collection. The goniometer was controlled using the GADDS software suite (Microsoft Win 2000 operating system). The mounted tube was then

placed on the diffractometer and in a cold nitrogen stream (Oxford) maintained at 110K. The sample was optically centered with the aid of a video camera such that no translations were observed as the sample was rotated through all positions. The detector was set at 12 cm from the sample (MWPC Hi-Star Detector, 1024 x 1024 pixel). The X-ray radiation employed was generated from a Cu sealed X-ray tube (K_α = 1.54184Å with a potential of 40 kV and a current of 40 mA) and filtered with a graphite monochromator in the parallel mode (175 mm collimator with 0.5 mm pinholes). The goniometer was controlled using the GADDS software.

Ligand substitution studies with PPh_3. In a typical reaction, (**Ni-1**)$W(CO)_5$ (0.166 g, 0.270 mmol) was dissolved in 30 mL of DMF and reacted with PPh_3 at 60˚C. The amount of PPh_3 was increased until it was ascertained that 75 equivalents (5.317 g, 20.25 mmol) were required to cause noticeable changes in the IR spectrum after 18 hours (ν(CO): 2065, 2043, 2017, 1992, 1967, 1942, 1919, 1909, 1890, 1869, 1843, 1828, 1811 cm^{-1}). The reaction repeated in refluxing CH_2Cl_2 yielded a similar IR spectrum (ν(CO): 2088, 2064, 2027, 2017, 1992, 1967, 1942, 1919, 1909, 1890, 1869, 1843, 1828, 1811 cm^{-1}). Diffractometer quality crystals were grown from the reaction solution by layering with diethyl ether. The product can be synthesized directly as shown below.

Preparation of Ni-1$(W(CO)_5)_2$. To a Schlenk flask containing 20 mL of THF, $W(CO)_6$ (0.241 g, 0.68 mmol) was added. This clear solution was transferred to a photolysis cell and photolyzed using a mercury lamp for approximately 1 h after which an IR was

obtained of the resultant yellow solution (ν(CO), THF: 2075, 1975, 1930, 1892 cm^{-1}). This yellow solution was transferred via cannula to a Schlenk flask containing a purple solution of **Ni-1** (0.100 g, 0.343 mmol) in 10 mL of CH_2Cl_2. Upon mixing the solution turned dark red brown. This solution was vigorously stirred for 1 day at ambient temperature. The solution was concentrated to half the volume and excess hexanes added to precipitate a dark red brown solution. The supernatant solution was decanted and the leftover solid washed with hexanes (3 x 15 mL). To obtain diffractometer quality crystals, the solid material was dissolved in CH_2Cl_2 and layered with hexanes. Large, dark reddish-brown crystals formed in approximately one week. 57.3% yield (0.184 g). IR (νCO, cm^{-1}) DMF: 2065, 1974, 1931, 1912, 1881 cm^{-1}; THF: 2065, 1976, 1926, 1913, 1890 cm^{-1}; CH_2Cl_2: 2067, 1979, 1925, 1914, 1884 cm^{-1}. Calc'd (found): C, 25.1 (25.6); H, 1.97 (2.15) ; N, 2.94 (2.98).

Preparation of (Ni(mese-daco))$_2$CuBr. Ni(mese-daco) (0.032 g, 0.099 mmol) was added to a Schlenk flask and dissolved in 20 mL MeCN giving a brown solution. In a separate flask CuBr (0.0050 g, 0.035 mmol) was added and dissolved in 20 mL MeCN giving a colorless solution. The Ni(mese-daco) solution was transferred via cannula to the flask over a period of 15 min. The resulting orange solution was stirred for 3 h at room temperature. The solution was concentrated and the product precipitated out of solution using 10 mL hexanes and 50 mL of Et_2O yielding a red-orange solid. The solid was filtered and washed with Et_2O. Diffractometer quality crystals were grown by dissolving the solid in 15 mL of MeOH and layering that solution with Et_2O. After five

days, red crystals formed. Yield 0.0476 g. Calc'd (found): C: 30.4 (30.6); H: 5.11 (5.24); N: 7.10 (6.91).

Experimental details for Chapter V

Materials. MeCN, Et_2O, and MeOH were purified according to published procedures under an N_2 atmosphere.[21] Palladium(II)bromide was purchased from Strem Chemical Co.

Syntheses. The **Ni-1**,[11] **Ni-1'**,[12] and $[Mo_2(MeCN)_{10}][BF_4]_4$ [32] complexes were prepared according to published procedures.

Preparation of $[Mo_2(Ni\text{-}1)_4][BF_4]_4 \cdot 6MeCN$. To a Schlenk flask containing 15 mL of MeCN, $[Mo_2(MeCN)_{10}][BF_4]_4$ (0.10 g, 1.0 mmol) and **Ni-1** (0.12 g, 3.9 mmol) were added. The solution immediately turned dark red brown with stirring. The solution was stirred for 2.5 h at ambient temperature. The solution was then transferred to a test tube and layered with Et_2O. Reddish-brown crystals formed in approximately one week, giving 45.1% yield (0.080 g). UV-Vis: λ_{max}: MeCN, nm (ε) = 226 (11248), 272 (10691), 316 (4067), 440 (852), 530 (497). Calc'd (found): C, 28.2 (28.4); H, 4.73 (4.74) ; N, 6.58 (6.87). ESI-MS (MeCN, m/z) {(**Ni-1**)$_2$Ni^{2+}} 320 (100), {$N_2S_2H)^+$} 233 (64.6), {[Mo_2(**Ni-1**)$_4$]$^{4+}$} 339 (7.68), {[(**Ni-1**)$_2$Ni]$^{2+}$} 727 (4.65), {[Mo_2(**Ni-1**)$_4$](BF_4)$_2^{2+}$} 765 (4.81).

$[Mo_2(Ni\text{-}1')_4][BF_4]_4 \cdot 4MeCN$. In an identical manner, the **Ni-1'** derivative was isolated in 73.3% yield (0.142 g) UV-Vis: λ_{max}: MeCN, nm (ε) = 226 (10252), 270 (7485), 306 (4322), 408 (1156), 536 (523). Calc'd (found): C, 25.8 (25.4); H, 4.32 (4.77); N, 6.87 (6.16). ESI-MS (MeCN, m/z) {[**Ni-1'**]$^+$} 276 (100), {[Mo_2(**Ni-1'**)$_2$(MeCN)$_{3.5}$](BF_4)$_2^{2+}$} 531 (50.8), {[(**Ni-1'**)$_2$Ni]$^{2+}$} 306 (40.5), {[Mo_2(**Ni-1'**)$_4$]$^{4+}$} 325 (23.8), {[Mo_2(**Ni-1'**)$_2$(MeCN)$_3$](BF_4)$_2^{2+}$} 520 (11.8), {[Mo_2(**Ni-1'**)$_4$](BF_4)$_2^{2+}$} 737 (8.67).

$[Pd_2(Ni\text{-}1')_4][Br]_4 \cdot 6MeOH$. A Schlenk flask containing **Ni-1'** (0.139 g, 0.513 mmol) was placed under vacuum and loaded into the drybox to which $PdBr_2$ (0.133 g, 0.500 mmol) was added. The flask was degassed and 30 mL of MeOH added. This suspension was stirred overnight at room temperature. The next day the solution had turned from brown to dark red-brown with a precipitate of the same color. The solution was concentrated anaerobically, filtered, and the supernatant transferred to a test tube for crystallization. This MeOH solution was layered with Et_2O. After two days, dark red orange crystals formed. Crystalline yield 0.087 (10.6%).

Experimental details for Chapter VI

Materials. 99.9% Anhydrous MeCN, DMF, CH_2Cl_2, and THF were purchased from Acros Chemical Co. $AgNO_3$ was purchased from the Spectrum Chemical Mfg. Co and used as received.

Syntheses. The complexes **Ni-1**,[11] **Ni-1'**,[12] $[Mo_2(OAc)_2(MeCN)_6][BF_4]_2$,[32] $[Mo_2(OAc)(MeCN)_7][BF_4]_3$,[33] $(CuBr)_2$(**Ni-1**)$_3$,[34] and $[Pd_2$(**Ni-1'**$)_4][NO_3]_4$[4] were synthesized according to previously published procedures. The $[Ag_2$(**Ni-1'**$)_3][NO_3]_2$ complex was prepared from a modified procedure of $[Ag_2$(**Ni-1'**$)_3][ClO_4]_2$.[9]

Preparation of $[Mo_2(OAc)_2$(Ni-1$)_2][BF_4]_2$. $[Mo_2(OAc)_2(MeCN)_6][BF_4]_2$ (0.47 g, 0.51 mmol) and **Ni-1** (0.30 g, 2.06 mmol) were added to a Schlenk flask containing 15 mL of MeCN. The solution immediately turned from violet red to dark red brown and was stirred for a further 2.5 h at ambient temperature. Excess Et_2O was added to the solution to precipitate the product. Calc'd (found): C, 27.0 (26.7); H, 4.34 (4.36); N, 5.24 (5.60). ESI-MS (MeCN, m/z) $\{[Mo_2(OAc)_2$(**Ni-1**$)_2]^{2+}\}$ 446 (100%), $\{$(**Ni-1**$)_2Ni^{2+}\}$ 320 (18.0%), $\{[Mo_2(OAc)_2$(**Ni-1**$)_3$(MeCN)$]^{2+}\}$ 659 (15.1%). Attempts to grow crystals from a concentrated MeCN solution layered with diethyl ether resulted in the previously published Mo_2Ni_4 species.

$[Mo_2(OAc)_2$(Ni-1'$)_2][BF_4]_2$. In an identical manner, the **Ni-1'** derivative was isolated. Calc'd (found): C, 25.4 (25.5); H, 4.07 (4.39); N, 5.39 (5.20). ESI-MS (MeCN, m/z) $\{[Mo_2(OAc)($**Ni-1'**$)_3]^{3+}\}$ 361 (100%), $\{Mo_2(OAc)_2($**Ni-1'**$)_2]^{2+}\}$ 432 (84.0%), $\{$(**Ni-1'**$)_2Ni^{2+}\}$ 306 (60.0%). Attempts to grow crystals from a concentrated MeCN solution layered with diethyl ether resulted in the previously published Mo_2Ni_4 species.

$[Mo_2(OAc)(Ni\text{-}1)_3][BF_4]_3$. $[Mo_2(OAc)(MeCN)_7][BF_4]_3$ (0.47 g, 1.22 mmol) and **Ni-1** (0.30 g, 3.09 mmol) were added to a Schlenk flask containing 15 mL of MeCN. The solution immediately turned from dark violet to dark red brown. The solution was stirred for 2.5 h at ambient temperature. Excess Et_2O was added to the solution to precipitate the product. Calc'd (found): C, 29.5 (29.6); H, 4.74 (4.94); N, 7.64 (7.04). ESI-MS (MeCN, m/z) $\{[Mo_2(OAc)_2(\mathbf{Ni\text{-}1})_2]^{2+}$ 446 (100%), $\{[Mo_2(OAc)(\mathbf{Ni\text{-}1})_3]^{3+}\}$ 374 (34.0%), $\{[Mo_2(OAc)_2(\mathbf{Ni\text{-}1})_3(MeCN)]^{2+}\}$ 591 (30.0%), $\{(\mathbf{Ni\text{-}1})_2Ni\}^{2+}$ 320 (17.0%), $[Mo_2(OAc)_2(\mathbf{Ni\text{-}1})_3]^{2+}$ 571 (6.00%). Attempts to grow crystals from a concentrated MeCN solution layered with diethyl ether resulted in the previously published Mo_2Ni_4 species.

$[Mo_2(OAc)(Ni\text{-}1')_3][BF_4]_3$. In an identical manner, the **Ni-1'** derivative was isolated. Calc'd (found): C, 25.9 (26.5); H, 4.28 (4.16); N, 6.26 (6.90). ESI-MS (MeCN, m/z) $\{[Mo_2(OAc)_2(\mathbf{Ni\text{-}1'})_2]^{2+}$ 431 (100%), $\{[Mo_2(OAc)_2(\mathbf{Ni\text{-}1})_3]^{2+}$ 361 (80.0%). Attempts to grow crystals from a concentrated MeCN solution layered with diethyl ether resulted in the previously published Mo_2Ni_4 species.

$[Ag_2(Ni\text{-}1')_3][NO_3]_2$. $AgNO_3$ (0.123 g, 0.72 mmol) and **Ni-1'** (0.30 g, 3.25 mmol) were added to a Schlenk flask containing 15 mL of MeOH. The solution immediately turned dark red brown. The solution was stirred for overnight at ambient temperature. The solvent was removed *in vacuo* leaving behind a dark red solid which was recrystallized from a concentrated MeOH solution layered with Et_2O. Red crystals formed overnight.

Calc'd (found): C, 27.8 (27.6); H, 4.67 (4.44); N, 9.61 (9.07). ESI-MS (MeCN, m/z) {$[Ag_2(Ni\text{-}1')_3]^{2+}$} 523 (100%).

Experimental details for Chapter VII

Materials. MeCN, Et_2O were purified according to standard procedures and were freshly distilled under N_2 prior to use.[21] $[Rh(CO)_2Cl]_2$, $Rh(CO)Cl(PPh_3)_2$, and $TlPF_6$ were purchased from Strem Chemical Co. Et_3OBF_4, $NaBF_4$ and NBu_4BF_4 were purchased from Aldrich Chemical Co. The NBu_4BF_4 electrolyte and $NaBF_4$ were oven dried prior to use.

Syntheses. Manipulations were performed under an atmosphere of N_2 using standard Schlenk techniques. The starting materials **Ni-1**,[11] **Ni-1'**,[12] **Ni-1***,[36] and $[NEt_4]_2[Ni(ema)]$,[37] and $Rh_2(O_2CCF_3)_4$,[38] were synthesized according to published procedures.

Preparation of [(Ni-1)Rh(CO)$_2$][PF$_6$]. A sample of the $[Rh(CO)_2Cl]_2$ (0.0281 g, 0.072 mmol), ν_{CO} (MeCN) 2097, 2026 cm^{-1}, starting material was dissolved in 5 mL MeCN resulting in a pale yellow solution. In a separate flask, **Ni-1** (0.042 g, 0.144 mmol) and $TlPF_6$ (0.0503 g, 0.144 mmol) were mixed and dissolved in 10 mL MeCN resulting in a purple solution. The $[Rh(CO)_2Cl]_2$ solution was transferred via cannula to the **Ni-1** solution which immediately turned orange-red with a yellow precipitate of TlCl. This solution was stirred for 2 h and then filtered through a Celite pad yielding a clear orange

solution with ν_{CO}, MeCN: 2077(s), 2017(s) cm^{-1}. The solvent was removed *in vacuo* leaving behind a red brown solid, 0.0882 g, 42.4 % yield. ESI-MS (MeCN): {[(**Ni-1**)$Rh(CO)_2]^+$} 420 (100%). Diffractometer quality crystals were grown in a test tube by layering a concentrated MeCN solution with diethyl ether. Red needles formed after 4 days. Calc'd (found): C, 24.2 (24.5); H, 3.39 (3.49); N, 4.72 (4.83).

[(Ni-1*)$Rh(CO)_2$][PF_6]. In the same manner, $[Rh(CO)_2Cl]_2$ (0.050 g, 0.129 mmol), **Ni-1*** (0.089 g, 0.256 mmol) and $TlPF_6$ (0.090 g, 0.257 mmol) were reacted. Crude product isolated 0.167 g. 58.1% yield. ν_{CO}, MeCN: 2075 (s), 2015 (s) cm^{-1}. ESI-MS (MeCN): {[(**Ni-1***)$Rh(CO)]^+$} 477 (100%), {[(**Ni-1***)$Rh(CO)_2]^+$} 505 (97.0%). Calc'd (found): C, 29.5 (29.5); H, 4.34 (4.42); N, 4.31 (4.27).

[NEt_4]$_2${[Ni(ema)$Rh(CO)_2$]$_2$}. The red solid $(Rh(CO)_2Cl)_2$ (30 mg, 0.077 mmol) and red solid $(Et_4N)_2$Ni(ema) (80 mg, 0.154 mmol) were dissolved in 25 mL of CH_3CN, stirred for 1 hour, and filtered through Celite. A red-brown solid was obtained after precipitation with ether, removal of supernatant fluid via cannula, and washing with ether. Crude product 0.434 g. 54% yield. ESI-MS (MeCN): {[Ni(ema)$Rh(CO)_2$]}$^-$ 420 (100%). ν(CO), MeCN: 2061s, 1996s cm^{-1}.

[(Ni-1)$Rh(CO)PPh_3$][Cl]·H_2O. A degassed sample of $Rh(CO)(Cl)(PPh_3)_2$ (0.24 g, 0.34 mmol) in 40 mL of CH_2Cl_2 produced a yellow slurry to which a purple solution of **Ni-1** (0.10 g, 0.34 mmol) dissolved in 10 mL of CH_2Cl_2 was added drop wise. The resulting

orange-red slurry was stirred overnight. The solvent was concentrated to about 10 mL, addition of 40 mL of pentane produced a precipitate which was filtered through a sintered frit. The orange solid was washed twice with 25 mL of ether to remove PPh_3, twice with 25 mL of toluene and dried under vacuum, 0.14 g. (55%) of [(**Ni-1**)Rh(CO)(PPh_3)][Cl]. X-ray quality crystals were obtained by layering a CH_2Cl_2 solution of the product with hexane. Calc'd (found): C, 48.4 (48.2); H, 4.90 (4.54); N, 3.89 (2.98). ν(CO), CH_2Cl_2: 1988 cm^{-1}. UV-Vis in CH_2Cl_2 solution: λ_{max} (ε) 232 (26002), 254 (17552), 282 (15466), 358 (3030), 486 (515) nm. ESI-MS (CH_3CN/CH_2Cl_2): {[(**Ni-1**)Rh(CO)(PPh_3)]$^+$} 683 (100 %).

[Rh_2(Ni-1')$_4$][O_2CCF_3]$_4$·3MeCN. $Rh_2(O_2CCF_3)_3$ (0.20 g, 0.304 mmol) and **Ni-1'** (0.337 g, 1.24 mmol) were weighed in separate flasks and stored under a N_2 atmosphere. To the flask containing the rhodium dimer was added 20 mL MeCN resulting in a dark bluish green solution. This solution was transferred by cannula to the flask containing **Ni-1'** solid, resulting in a dark red orange solution which was stirred overnight. The solution was filtered through Celite to remove any unreacted **Ni-1'**. The solvent was removed *in vacuo* leaving a dark red residue. Diffractometer quality crystals were obtained by diffusion of Et_2O into a concentrated solution of MeCN. 0.498 g, 72.6% yield. ESI-MS (MeCN): {[Rh(**Ni-1'**)3]$^{3+}$}, 311 (100%), {[Rh(**Ni-1'**)$_3$(O_2CCF_3)]$^{2+}$} 523 (41.9%), {[Rh_2(**Ni-1'**)$_4$]$^{4+}$} 476 (34.7%), {[Rh_2(**Ni-1'**)$_4$(O_2CCF_3)$_2$]$^{2+}$} 769 (6.45%). Calc'd (found): C, 30.9 (30.6); H, 4.20 (4.31); N, 7.29 (7.89).

[Rh(Ni-1')$_3$][BF$_4$]$_3$. Samples of RhI_3 (0.020 g, 0.041 mmol) and **Ni-1'** (0.034 g, 0.125 mmol) were placed in a Schlenk flask to which 20 mL of MeCN were added. The solution was refluxed overnight. A sample of this solution was analyzed via ESI-MS. ESI-MS (MeCN): {[Rh(**Ni-1'**)$_3$][I]$^{2+}$} 530 (100%), {[Rh(**Ni-1'**)$_3$][I]$_2^+$} 907 (88.6%). The next day, heating was ceased and $NaBF_4$ added (0.014 g, 0.127 mmol). The solution was stirred for 1 day and the resulting red solution filtered through Celite to remove NaI and any unreacted material. The solvent was removed *in vacuo*. 0.050 g, 78.0% yield. ESI-MS (MeCN) {[Rh(**Ni-1'**)$_3$]$^{3+}$} 311 (74.5%), {[Rh(**Ni-1'**)$_3$(MeCN)(BF$_4$)]$^{2+}$} 530 (8.19%), {[Rh(**Ni-1'**)$_3$(BF$_4$)]$^{2+}$} 510 (2.13%). Calc'd (found): C, 27.1 (27.4); H, 4.56 (4.51); N, 7.04 (6.99).

[Rh(Ni-1')$_3$][PF$_6$]$_3$. In the same manner, the PF_6^- derivative can be prepared from [Rh(**Ni-1'**)][I]$_3$ using $TlPF_6$ (0.227 g, 0.650 mmol) for ion exchange. 0.141 g, 47.6% yield. ESI-MS (MeCN) {[Rh(**Ni-1'**)$_3$]$^{3+}$} 311 (100%). Calc'd (found): C, 23.7 (24.4); H, 3.98 (4.39); N, 6.14 (6.33).

Attempts at resolution of optical isomers. [Rh(**Ni-1'**)$_3$][I]$_3$ (0.226 g, 0.190 mmol) was placed in a Schlenk flask with disodium-L-tartrate (0.087 g, 0.380 mmol). The two solids were dissolved in 25 mL and stirred vigorously; the white precipitate NaI formed immediately. After 1 h, the solution was filtered over Celite leaving a clear red-orange solution. This solution was concentrated to nearly half its original volume. The flask was stored in the refrigerator overnight. Presumably, the Λ-isomer was collected via

filter cannula and pumped to dryness and collected in air (0.025 g). The solvent of supernatant solution was removed *in vacuo* and the Δ-isomer collected in air (0.116 g). Anion exchange of the Δ and Λ isomers was accomplished with $NaSbF_6$ (0.016 g and 0.075 g) respectively. Crystal growth was attempted by layering a concentrated MeCN solution with ether.

Reactivity studies. This reaction was performed as a one-pot synthesis. [Rh(**Ni-1'**)$_3$][I]$_3$ (0.050 g, 0.042 mmol), [Rh(cod)Cl]$_2$ (0.009 g, 0.018 mmol), **Ni-1'** (0.011 g, 0.040 mmol), and $TlPF_6$ (0.055 g, 0.158 mmol) were mixed in 20 mL of MeCN and refluxed overnight. The red-orange solution was filtered through a Celite pad, and the solvent was removed *in vacuo*. The remaining solid was analyzed via ESI-MS. {[Rh(**Ni-1'**)$_3$(MeCN)]$^{3+}$} 325 (100%), {[Rh(**Ni-1'**)$_3$$^{3+}$} 311 (25.2%).

CHAPTER III

THE NiN_2S_2 MOIETIES AS LIGANDS: DONOR ABILITY, SPECTROSCOPY, MECHANISTIC AND LABILIZATION STUDIES*

Development of a series

Tolman's well known electronic factors for phosphine ligands are based on a $R_3PNi(CO)_3$ model that used the ν(CO) A_1 band of the vibrational spectra to order the PR_3 donor ability with varying R groups. The degree of Ni→CO dative bonding correlated with donor ability of the PR_3 ligands.[39] In collaboration with group member Marilyn Rampersad, a similar approach was used to contrast the donor abilities of the NiN_2S_2 ligands (Figure III-1) which were originally proposed to be mimics of diphosphines.[10c,40] Their donating abilities, as determined by IR spectroscopy of $W(CO)_4$ derivatives, were compared with traditional bidentate ligands.[31,41]

The assortment of NiN_2S_2 complexes shown in Figure III-1 were chosen as ligands because of availability and inherent structural or electronic properties.[11,12,29,36,37,42] For instance, the **Ni-1** and **Ni-1*** compounds possess S-Ni-S angles close to 90˚ and a rigid diazacyclooctane framework links the *cis*-dithiolates. The constraint of a 2-carbon atom N to N link in the **Ni-1'** and **Ni(bmmp-dmed)** compounds opens the S-Ni-S angles to ca. 95˚. The open chain bme-Me_2PDA ligand with a 3-carbon N to N link constricts the S-Ni-S angle to 85˚. The **Ni-1*** and **Ni(bmmp-dmed)**

* Reproduced in part with permission from Rampersad, M. V.; Jeffery, S. P.; Golden, M. L.; Lee, J.; Reibenspies, J. H.; Darensbourg, D. J.; Darensbourg, M. Y. *J. Am. Chem. Soc.* **2005**, *127*, 17323. Copyright 2005 American Chemical Society.

compounds have gem dimethyl groups on the carbon atoms alpha to sulfur; such a substituent pattern is expected to provide steric hindrance at the donor sulfur sites as well as increase the electron donating ability of the sulfurs. The highly constrained, dianionic $Ni(ema)^{2-}$ complex has the largest S-Ni-S angle of 97˚.

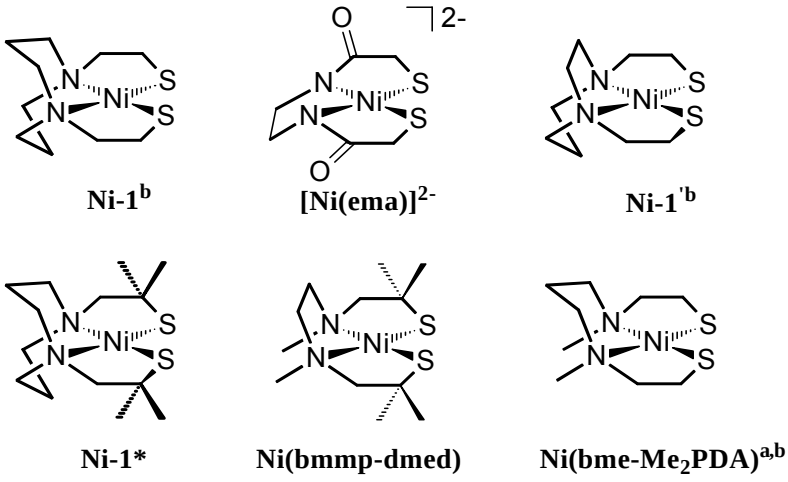

Ni-1*: (*N*,*N'*-bis(2-mercapto-2-methylpropane)(*N*,*N'*-diazacyclooctane))nickel
Ni(ema)$^{2-}$: (*N*,*N'*-ethylenebis(2-mercaptoacetamide))nickel
Ni(bme-Me$_2$PDA): (*N*,*N'*-dimethyl-*N*,*N'*-bis(2-mercaptoethyl-1,3-propanediamine)nickel
Ni-1: (*N*,*N'*-bis(2-mercaptoethyl)-*N*,*N'*-diazacyclooctane)nickel
Ni-1': (*N*,*N'*-bis(2-mercaptoethyl)-*N*,*N'*-diazacycloheptane)nickel
Ni(bmmp-dmed): (*N*,*N'*-bis(2-methyl-mercaptopropyl)-*N*,*N'*-dimethylethylenediamine)nickel

Figure III-1. Series of NiN_2S_2 complexes used in IR study for the determination of donating ability. a) compound prepared by the author; b) compounds structurally characterized by the author.

In this study, *cis*-$(pip)_2W(CO)_4$, pip = piperidine, served as the $W(CO)_4$ synthon.[30] Scheme III-1 outlines the synthesis used to generate the $(NiN_2S_2)W(CO)_4$ complexes. Piperidine, a labile ligand, is readily displaced upon introduction of another donor ligand such as a diphosphine or a metallodithiolate. The air-stable product precipitates from the CH_2Cl_2 solution on addition of hexanes. The resultant (L-

L)$W(CO)_4$ complexes were characterized by x-ray crystallography as octahedral $S_2W(CO)_4$ complexes of pseudo C_{2v} symmetry at tungsten.

Scheme III-1. Example of the synthetic procedure for the $(NiN_2S_2)W(CO)_4$ series.

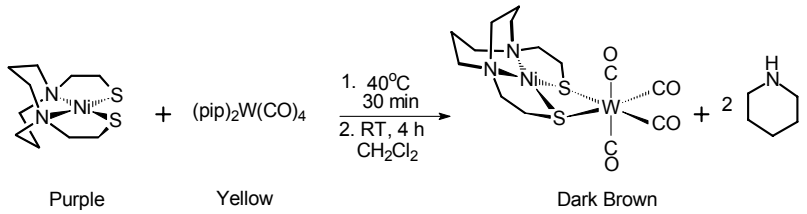

The $(NiN_2S_2)W(CO)_4$ series. Detailed structural data for three members

The solid state structures of the series of $(NiN_2S_2)W(CO)_4$ complexes is that of a heterobimetallic where the metallodithiolate unit behaves as a bidentate ligand to a $W(CO)_4$ moiety. Of the six compounds in the series, I prepared one, (Ni(bme-Me_2PDA))$W(CO)_4$ and structurally characterized three, (Ni(bme-Me_2PDA))-, (**Ni-1**), and (**Ni-1'**)$W(CO)_4$. These are shown as thermal ellipsoid plots in Figure III-2 and experimental crystallographic data is given in Table III-1. These compounds will first be described individually and then the entire series will be compared. These structures have been deposited into the Cambridge Crystallographic Database[43] and have been published in two separate accounts.[31,41] The molecular structures of the entire series are presented as ball and stick representations in the title of Table III-2 and selected metric data for both the free and bound ligand are shown.[11,12,29,36,37,42]

The ($Ni(bme\text{-}Me_2PDA)W(CO)_4$ complex crystallizes in the space group *P*nma and is shown as a thermal ellipsoid plot in Figure III-2a. Analysis of the Ni(bme-Me_2PDA) unit revealed the nickel to be in a square planar geometry as evident from a least-squares deviation from the N_2S_2 best plane of 0.0155 Å. There is no (0.0 Å) deviation of the N and S atoms from the best least squares plane. The thiolate arms are eclipsed across the N_2S_2 plane with the open chain backbone forming a metallocyclohexane ring in a chair conformation. The methyl groups on the nitrogens are in the *cis* position. The small $\angle_{S\text{-}Ni\text{-}S}$ angle of 83.83(11) provides a $\angle_{S\text{-}W\text{-}S}$ bite angle of 68.75(9). The dihedral angle, defined as the intersection of the NiN_2S_2 and S_2WC_2 planes, is 106.8˚. This dihedral angle enforces asymmetry on the $W(CO)_4$ unit, and positions one axial carbonyl at a Ni-C distance of 2.846 Å. The Ni-W distance is 3.033 Å. The axial W-C-O units deviate from linearity by approximately the same amount as seen in $(N\text{-}N)W(CO)_4$. The $W\text{-}C_{ax}$ bonds are also slightly longer than the $W\text{-}C_{eq}$ CO groups.

Table III-1. Experimental crystallographic data for $(NiN_2S_2)W(CO)_4$ complexes synthesized in this dissertation.

	(Ni(bme-Me$_2$PDA))W(CO)$_4$	**(Ni-1)W(CO)$_4$**	**(Ni-1')W(CO)$_4$**
Formula	$C_{13}H_{20}N_2NiO_4S_2W$	$C_{14}H_{18}N_2NiO_4S_2W$	$C_{13}H_{18}N_2NiO_4S_2W$
Formula Weight	574.99	584.98	572.97
Temperature (K)	110	110(2)	110(2)
Wavelength (Å)	0.71073	0.71073	0.71073
Z	4	4	4
D_{calcd} (Mg/cm^3)	2.184	2.128	2.247
m (mm^{-1})	7.906	7.573	8.162
Crystal System	Orthorhombic	Orthorhombic	Orthorhombic
Space Group	Pnma	Pnma	Pnma
Unit Cell			
a(Å)	19.713(6)	13.397(4)	12.721(5)
b(Å)	12.868(3)	12.386(4)	12.151(5)
c(Å)	6.894(3)	11.005(3)	11(2)
a	90	90	90
þ	90	90	90
g	90	90	90
Volume (Å^3)	1748.9(10)	1826.2(10)	1694(309)
Goodness-of-fit	1.296	1.144	1.164
R_1[a], wR_2[b](%) [I>2s(I)]	0.0389, 0.1006	0.0341, 0.0886	0.0717, 0.1761
R_1[a], wR_2[b](%) all data	0.0434, 0.1150	0.0341, 0.0895	0.0800, 0.1865

[a] $R_1 = \Sigma||F_o| - |F_c||/\Sigma F_o$.
[b] $wR_2 = [\Sigma[w(F_o^2 - F_c^2)^2/\Sigma w(F_o^2)^2]^{1/2}$.

The (**Ni-1**)W(CO)$_4$ complex crystallizes in the orthorhombic space group *P*nma and is shown as a thermal ellipsoid plot in Figure III-2b. The **Ni-1** unit finds the nickel to be in a square planar geometry as evident from a least-squares deviation from the N_2S_2 plane of 0.0286 Å. The best least squares plane finds no deviation of the N and S atoms. The thiolate arms are eclipsed across the square plane with the diazacycle backbone rings in a chair/boat conformation. The small $\angle_{S\text{-}Ni\text{-}S}$ angle of 87.76(8) provides a smaller bite $\angle_{S\text{-}W\text{-}S}$ of 72.08(6). The dihedral or hinge angle is 132.5º which yields a Ni-W distance of 3.35 Å. This is slightly smaller than the dihedral angle of (**Ni-1***)W(CO)$_4$ (136˚) due to absence of gem dimethyl groups on the carbon atoms

alpha to the donor sulfur atoms. The W-C bond lengths for the axial CO groups are also slightly longer than the equatorial CO groups and slightly bent away from NiN_2S_2 unit.

The (**Ni-1'**)$W(CO)_4$ complex crystallizes in same space group *P*nma and is shown as a thermal ellipsoid plot in Figure III-2c. Analysis of the **Ni-1'** unit showed the nickel atom to be in a square planar geometry as evidenced by a least-squares deviation from the N_2S_2 best plane of 0.1378 Å. There is no deviation of the N and S atoms from the best least squares plane. The thiolate arms are eclipsed with the six-membered nickel diazacyclohexane ring in a chair conformation. The large $\angle_{S\text{-}Ni\text{-}S}$ angle of 92.3(9)˚ provides a comparably large $\angle_{S\text{-}W\text{-}S}$ bite angle of 74.8(8)˚ due to a 2-carbon atom N to N linker with a dihedral angle of 127.5˚. Both the W-C(1)-O(1) and W-C(2)-O(2) angles deviate from linearity, with angles of 174.7(11)˚ and 174.9(10)˚, respectively. The S-C distances do not vary significantly; however, it is of note to mention the W-C bond lengths of the carbonyls *trans* to the metallodithiolato ligand are slightly shorter 1.96(15) Å for both W-C(3) and W-C(4).

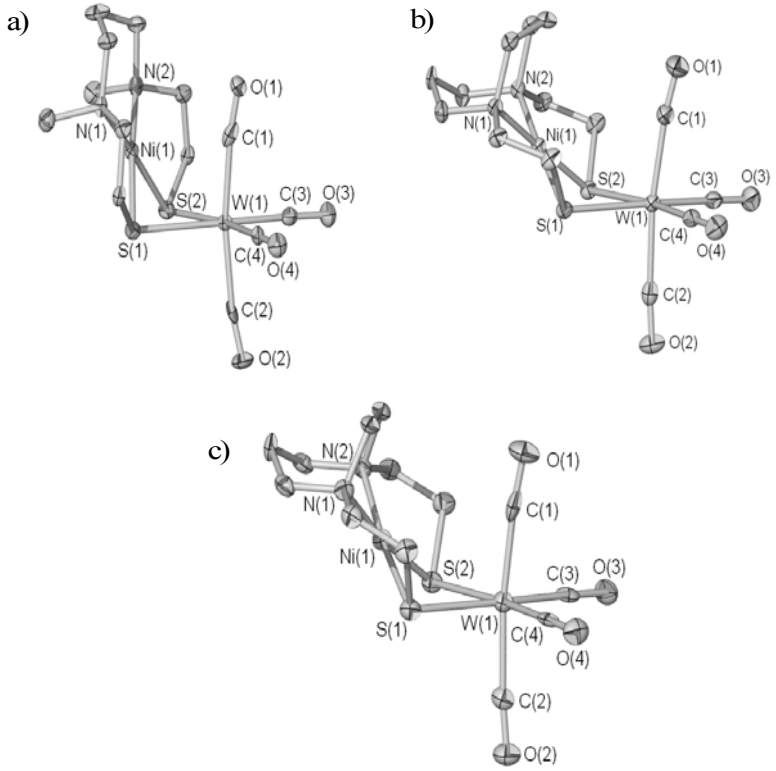

Figure III-2. Thermal ellipsoid plots (50% probability) of a) (Ni(bme-Me_2PDA))$W(CO)_4$ b) (**Ni-1**)$W(CO)_4$ c) (**Ni-1'**)$W(CO)_4$.

Overall comparison of structures

Table III-2 gives extensive metric data which compares the NiN_2S_2 free ligands with the $(NiN_2S_2)W(CO)_4$ complexes. There are minor metric differences between the free and bound nickel dithiolato ligands which are statistically insignificant. Nevertheless, the trends in this large series show an increase in the Ni-S distances and a concomitant decrease in the Ni-N distances when the NiN_2S_2 unit bound to $W(CO)_4$.

Table III-2. Selected bond distances and bond angles of complexes in the $(NiN_2S_2)W(CO)_4$ series and ball-and-stick representations with NiN_2S_2 ligands included for comparison. [a] Angle between best planes of NiN_2S_2 and $S_2W(CO)_2$.

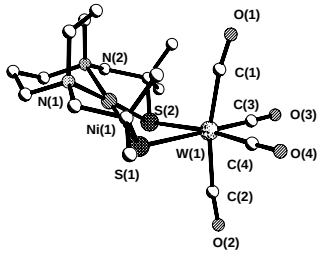

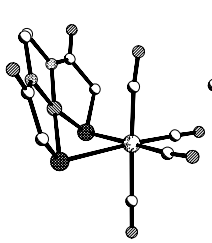
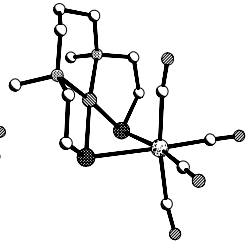
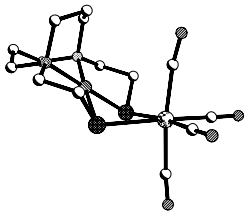
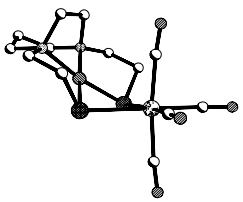
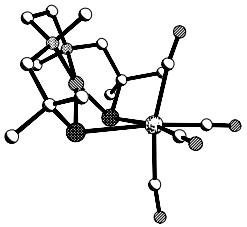

Bond distances	Ni-1* ref. 35	1	$[Et_4N]_2$[Ni(ema)] ref. 36	2	Ni(bme-Me_2PDA) ref. 28	3	Ni-1 ref. 11	4	Ni-1' ref. 12	5	Ni(bmmp-dmed) ref. 42	6
Ni-W		3.389		2.928		3.033		3.35		3.249		3.021
W-C1		2.001(14)		1.978(13)		2.023(13)		2.023(15)		2.03(4)		2.052(9)
W-C2		2.037(12)		2.042(12)		2.057(12)		2.047(11)		2.03(8)		2.040(9)
W-C3		1.951(10)		1.939(12)		1.952(8)		1.957(6)		1.96(15)		1.970(9)
W-C4		1.951(10)		1.937(12)		1.952(8)		1.957(6)		1.96(15)		1.944(9)
W-S1		2.589(3)		2.637(3)		2.591(2)		2.5792(14)		2.6(2)		2.649(2)
W-S2		2.589(3)		2.594(3)		2.591(2)		2.5792(14)		2.6(2)		2.592(2)
Ni-S1	2.152(1)	2.170(3)	2.179(1)	2.175(3)	2.176(1)	2.190(2)	2.159(3)	2.1893(15)	2.164(1)	2.17(16)	2.145(10)	2.152(2)
Ni-S2	2.152(1)	2.170(3)	2.179(1)	2.168(3)	2.174(1)	2.190(2)	2.159(3)	2.1893(15)	2.164(1)	2.17(16)	2.161(10)	2.157(2)
Ni-N1	1.995(3)	1.986(8)	1.857(3)	1.849(8)	1.999(3)	1.995(6)	1.979(7)	1.974(5)	1.940(4)	1.93(14)	1.930(3)	1.958(6)
Ni-N2	1.995(3)	1.986(8)	1.857(3)	1.842(8)	2.006(3)	1.995(6)	1.979(7)	1.974(5)	1.940(4)	1.93(14)	1.950(3)	1.930(7)
Bond Angles												
C(1)-W-C(2)		165.5(5)		176.5(5)		170.0(4)		172.4(3)		172.6(10)		165.5(3)
C(3)-W-C(4)		91.3(6)		90.8(5)		89.9(4)		90.7(3)		91(9)		91.3(4)
C(1)-W-C(3)		84.0(4)		89.6(5)		87.4(3)		86.6(3)		87(5)		81.2(3)
W-C(1)-O(1)		171.5(13)		173.4(11)		172.9(9)		171.7(7)		174.7(11)		173.8(8)
W-C(2)-O(2)		173.3(12)		179.3(11)		170.8(8)		175.5(8)		174.9(10)		178.8(8)
W-C(3)-O(3)		178.7(8)		177.4(10)		178.4(6)		177.1(6)		178.6(6)		171.4(8)
W-C(4)-O(4)		178.7(8)		175.1(11)		178.4(6)		177.1(6)		178.6(6)		178.3(8)
S(1)-W-S(2)		70.92(12)		75.06(9)		68.75(9)		72.08(6)		75(8)		71.16(6)
S(1)-Ni-S(2)	88.8(1)	87.62(15)	97.44(8)	94.42(11)	85.37(4)	83.83(11)	89.4(1)	87.76(8)	95.4(1)	92(9)	95.16(4)	91.49(9)
N(1)-Ni-N(2)	90.4(1)	92.2(5)	85.6(2)	86.04(4)	97.3(1)	98.3(4)	82.5(2)	91.5(3)	82.5(2)	83(7)	88.11(12)	89.8(3)
Dihedral[a]		135.9		107		106.8		132.5		127.5		114.4

The increase of the Ni-S bond distance is ascribed to donation of electron density from the sulfur atoms to the tungsten metal center.

A striking feature of these complexes is the hinge formed by the intersection of the NiN_2S_2 and $S_2W(CO)_2$ planes. The Ni-W distances fall within a nonbonding range of 2.92-3.39 Å. These values can be correlated to the span of the hinge angle of 107-136˚. The full steric capability of the $(NiN_2S_2)W(CO)_4$ series is seen in the overlay shown in Figure III-3. The hinge angle is a result of the residual lone pair on each sulfur donor. Differences within the $(NiN_2S_2)W(CO)_4$ series is dictated by the steric bulk of the pendant thiolate arms on the metalloligand. The $Ni(ema)^{2-}$ complex, for instance, has a relatively flat NiN_2S_2 plane with no steric influence from N to S linker arms; its hinge angle is 107˚. Another complex with a similar hinge angle of 107˚ is the (Ni(bme-Me_2PDA))$W(CO)_4$ complex. An overlay of the profile views the (Ni(ema))- and (Ni(bme-Me_2PDA)$W(CO)_4$ complexes is seen in Figure III-4.

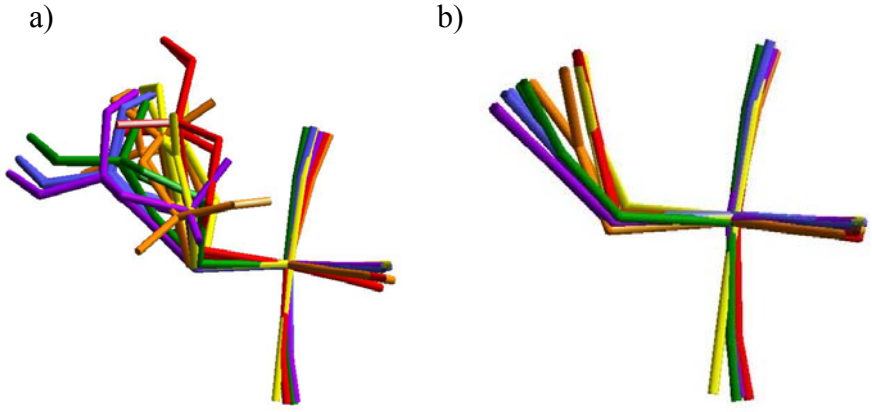

Figure III-3. Structural overlay of the $(NiN_2S_2)W(CO)_4$ complexes shown in the order of decreasing hinge angle with hydrogens omitted: purple (**Ni-1***)$W(CO)_4$, blue (**Ni-1**)$W(CO)_4$, green (**Ni-1'**)$W(CO)_4$, orange (Ni(bmmp-dmed))$W(CO)_4$, yellow $[NEt_4]_2[(Ni(ema))W(CO)_4]$, red (Ni(bme-$Me_2$PDA))$W(CO)_4$. a) with b) without hydrocarbons.

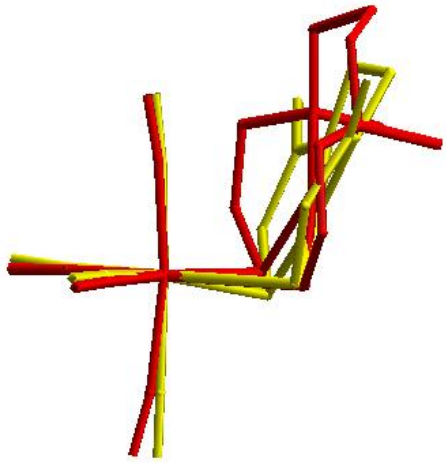

Figure III-4. Structural overlay of the profile views of $[(Ni(ema))W(CO)_4]^{2-}$ (**yellow**, 107˚) and (Ni(bme-Me_2PDA)$W(CO)_4$ (**red**, 106.8˚). The hinge angles are given in parentheses.

It was expected that the complexes possessing gem dimethyl groups would show greater hinge angles. Indeed, the (**Ni-1***)$W(CO)_4$ derivative, complex **1**, has the largest hinge angle of 136˚. Interestingly, the hinge angle of complex **6**, (Ni(bmmp-dmed))$W(CO)_4$, also with gem dimethyl groups, has a much smaller angle of 114˚.

Careful scrutiny of their molecular structures offers a suggestion as to why this is the case. Shown in Figure III-5 are the (**Ni-1***)$W(CO)_4$ and (Ni(bmmp-dmed))$W(CO)_4$ complexes. A major difference is found in the spatial positioning of their gem dimethyl groups. For the (**Ni-1***)$W(CO)_4$ complex, the methyl groups are positioned upright and directed toward the $W(CO)_4$ moiety as opposed to those in the Ni(bmmp-dmed) analog where the methyl groups are directed away from the $W(CO)_4$ moiety. A probable cause for this is a lack of flexibility afforded to the compound due to the 2-carbon linker in its open chain backbone. The torsion angles resulting from this rigidity extend into the N to S linkages and orient the substituent methyl groups such that they do not inhibit optimal W-S interaction. The result of this effect is evident in their W-S distances. Comparison of (**Ni-1***)- and (**Ni-1**)$W(CO)_4$ show the **Ni-1*** analog to have W-S distances that are 0.1 Å longer. Nevertheless, the W-S distances of the compounds possessing gem dimethyl groups, (Ni(bmmp-dmed))- and (**Ni-1***)$W(CO)_4$, are very similar. In fact, the W-S distances of the former are approximately 0.03 Å longer than that of the latter.

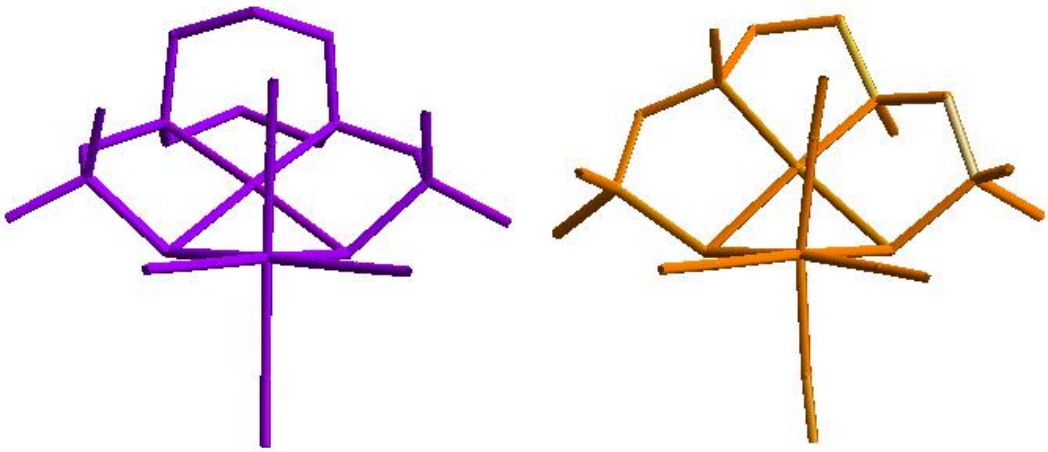

Figure III-5. Views of (**Ni-1***)$W(CO)_4$ (**purple,** 136˚) and (Ni(bmmp-dmed))$W(CO)_4$ (**orange**, 114.4˚) highlighting the difference in orientation of their gem dimethyl groups. The hinge angles are given in parentheses.

Another feature of these complexes worthy of note is the bending of axial CO ligands. A similar trend is observed with thioether metal carbonyl complexes.[44] Using simple steric arguments, a reasonable proposed explanation would be in claiming the carbonyl below the WS_2C_2 plane deviates from linearity due to repulsion from the extra lone pair on sulfur and the carbonyl above the plane from the repulsion of the NiN_2S_2 ligand. However, the same bending of axial CO ligands is observed in metal carbonyl complexes with ligands that possess only one lone pair, i.e. diphosphines and diimines.[45] Analysis of the crystal packing diagram for the (Ni(bme-Me_2PDA)$W(CO)_4$, (**Ni-1**)$W(CO)_4$, and (**Ni-1'**)$W(CO)_4$ complexes are shown in Figures III-6 to Figure III-8, reveals the bending of the CO ligands is caused by intermolecular steric repulsions of the CO ligands from neighboring molecules. The closest nonbonding contacts are in the range of 3.08-3.2 Å and relate to carbonyl oxygens oriented toward each other. Each

bimetallic cluster is related by a glide plane as approximate alternate inverted clusters across the unit cell. For the $[NEt_4]_2[(Ni(ema))W(CO)_4]$ salt, tetraethyl ammonium cations intersperse between sheets comprised of pairings of interdigitated anions a distance of 3.2-4.0 Å away.

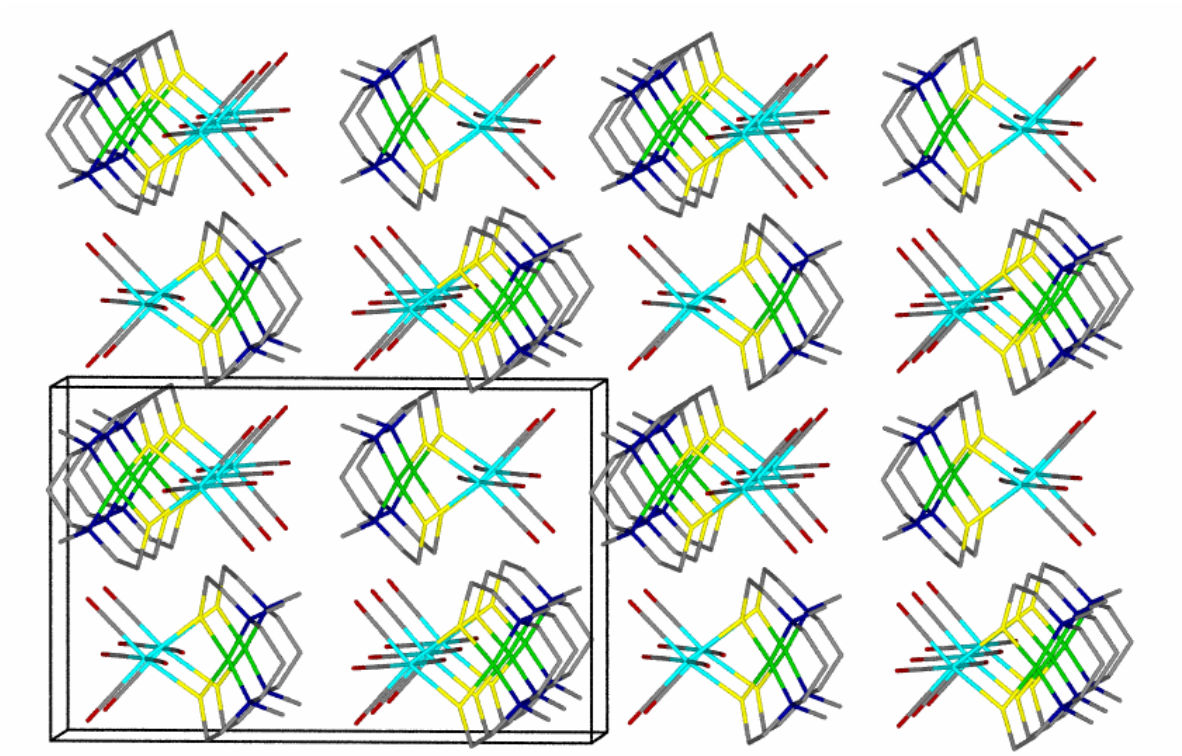

Figure III-6. Extended packing diagram of $(Ni(bme\text{-}Me_2PDA))W(CO)_4$ viewed down the c-axis.

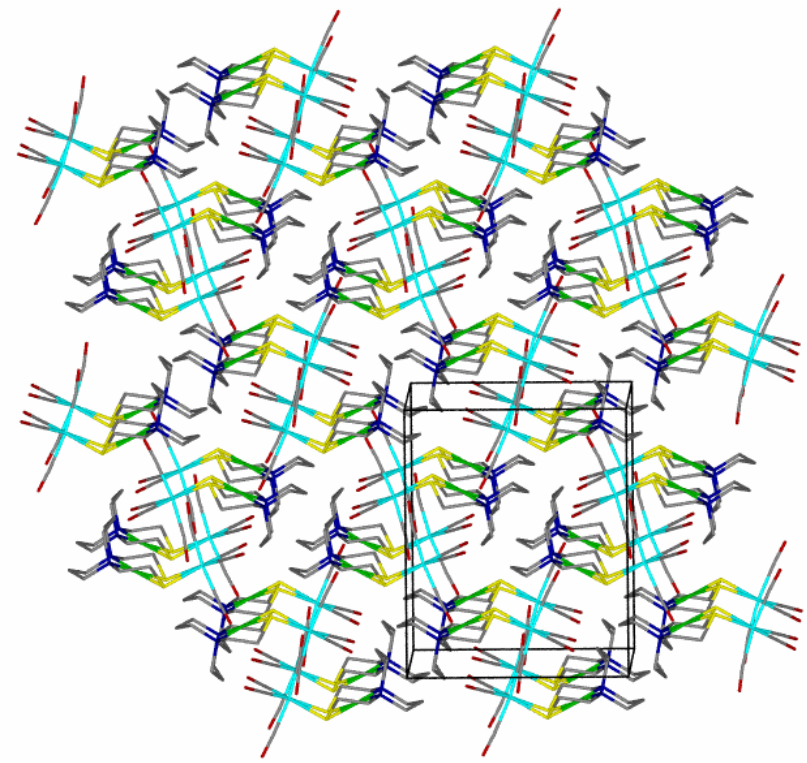

Figure III-7. Extended packing diagram of (**Ni-1**)$W(CO)_4$ viewed down the c-axis.

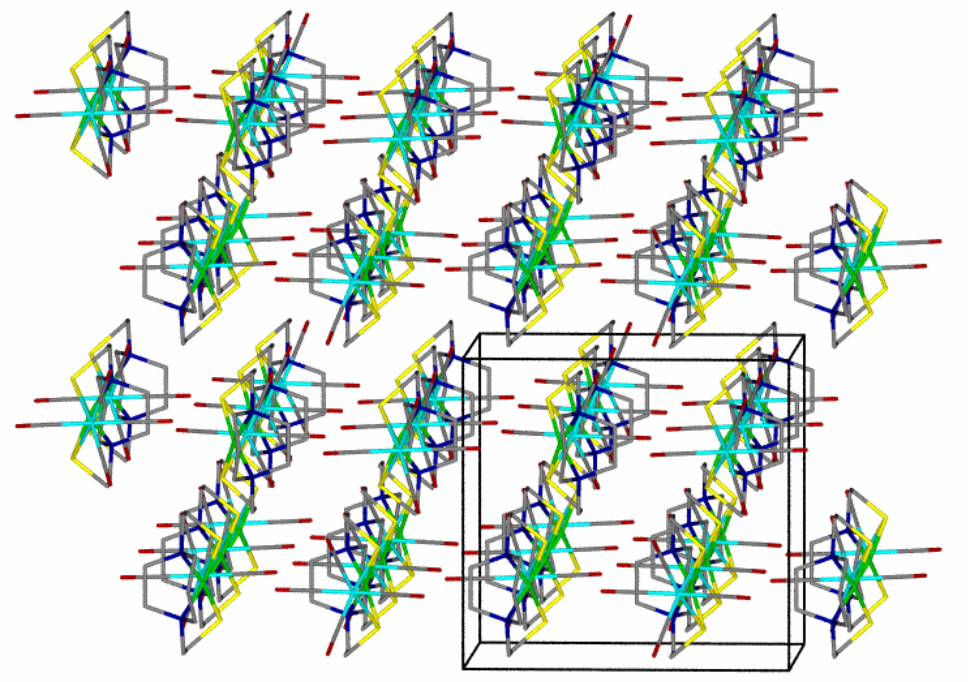

Figure III-8. Extended packing diagram of (**Ni-1'**)$W(CO)_4$ viewed down the a-axis.

A comparison of the $(NiN_2S_2)W(CO)_4$ complexes to their monodentate $(NiN_2S_2)W(CO)_5$ analogs

It was found that upon adding CO to a solution of (**Ni-1**)$W(CO)_4$ or (**Ni-1***)$W(CO)_4$, one of the W-S bonds breaks, thus creating an open site for CO to bind. Kinetic studies performed on (**Ni-1***)$W(CO)_4$ confirm the hemi-labile characteristic of the NiN_2S_2 ligand and establish the monodentate $(NiN_2S_2)W(CO)_5$ derivative to be more stable than the tetracarbonyl. Crystallographic analysis of the pentacarbonyl derivatives of **Ni-1** and **Ni-1*** show the remaining W-S bond decreases in length by 0.002 and 0.013 Å respectively. The results of this hemilabile comparison are shown in Figure III- 9.

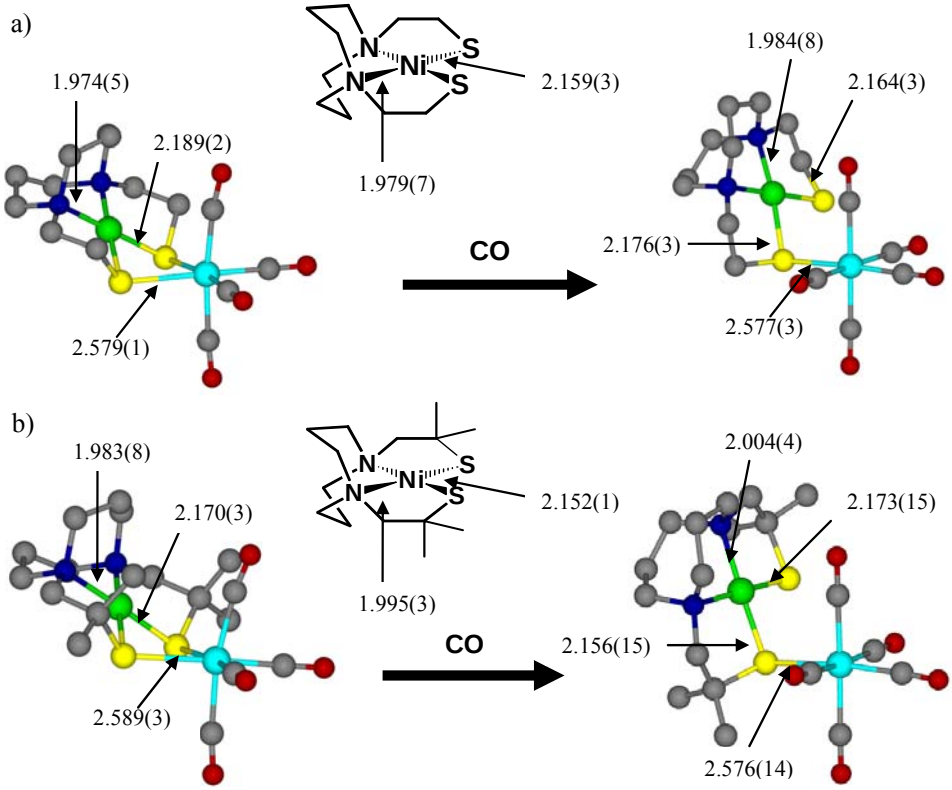

Figure III-9. Comparison of bond distances in the tungsten tetra- and pentacarbonyl derivatives of a) **Ni-1** b) **Ni-1***.

The unique "hinge" of the NiN_2S_2 ligand is well illustrated in the structural overlay of (**Ni-1***)- and (*o*-phenanthroline)$W(CO)_4$.[45e] Despite the differences in ligand orientation, the ν(CO) IR spectra are very similar for the 2 N donors of (*o*-phen)$W(CO)_4$ and the S_2 donor of (**Ni-1***)$W(CO)_4$, yielding a 4-band pattern with each assigned in C_{2v} symmetry as $2A_1 + B_1 + B_2$ shown in Figure III-10. Low solubility in non-interacting solvents necessitated using DMF as a solvent for the infrared spectroscopy studies. Force constants were calculated by graduate student Melissa Golden and Prof. D. J. Darensbourg for all complexes using the method of Cotton and Kraihanzel and are listed in Table III-3.[46]

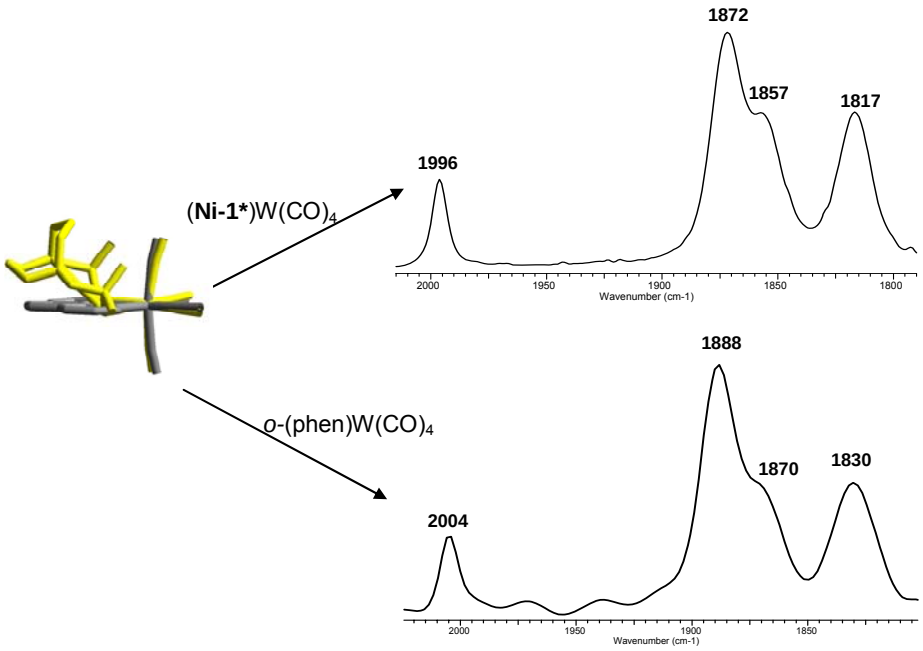

Figure III-10. Structural overlay of $W(CO)_4$ derivatives **Ni-1*** and *o*-phenanthroline matching the tungsten and (S/N atoms) with their respective ν(CO) infrared spectra in DMF.

Vibrational studies reflect donor abilities

The donor abilities of the metallodithiolate derivatives of $W(CO)_4$ were assigned according to their ν_{CO} stretching frequencies and their k_1 and k_2 force constants. The ν_{CO} values for the NiN_2S_2 ligand derivatives are lower than their diphosphine analogs. In fact, as presented in Table III-1, the NiN_2S_2 ligand of best donor ability, $Ni(ema)^{2-}$, donates more electron density to the $W(CO)_4$ unit than does piperidine, entry 10. The neutral NiN_2S_2 ligands are all of similar donor abilities according to $W(CO)_4$ as spectral probe. Their force constants match those of *cis*-$(pip)_2W(CO)_4$, entry 10.

This study is significant as it is the first comparison of NiN_2S_2 ligands which unequivocally defines their donor abilities with respect to traditional bidentate P- or N-donor ligands. The ranking of the metallothiolates with respect to increasing donor ability is shown in Scheme III-2. The diphosphines are the poorest donors, followed by the diimines which are equal to the neutral NiN_2S_2 compounds which are roughly the same in donor ability as evidenced by their CO-force constants. As noted above, the best donor by far is the dianion, $Ni(ema)^{2-}$. Surprisingly, the NiN_2S_2 complexes with gem dimethyl groups were not better donors than those lacking the substituents at the carbon α to sulfur. It should be noted that a less diffuse metal carbonyl probe, e.g., $Ni(CO)_3$ or $Rh(CO)_2$, could possibly distinguish between the donating abilities of the NiN_2S_2 ligands.

Scheme III-2. Ranking of donor ability for the NiN_2S_2 ligands related to each other and other neutral donors.

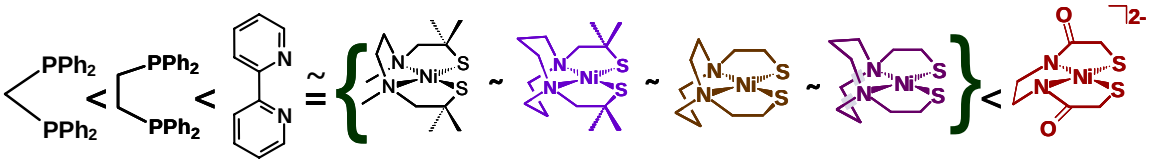

Stability of the $(NiN_2S_2)W(CO)_4$ complexes

All the $(NiN_2S_2)W(CO)_4$ complexes are stable in air as well as in solution as evidenced by the lack of changes in their infrared spectra when exposed to air. The $Ni(ema)^{2-}$ complex, however, rapidly decomposes on exposure to air. The neutral complexes are very soluble in DMF, and they show slight solubility in MeCN; they are largely insoluble in CH_2Cl_2. No precautions were taken to shield the complexes from ambient laboratory light.

The anionic NiN_2S_2 ligand may be partially displaced on sparging a MeCN solution of $[Et_4N]_2[(Ni(ema))W(CO)_4]$ with CO. This reaction was monitored via IR spectroscopy at room temperature, showing diminishing of ν(CO) bands with the concomitant growth of new bands at higher frequencies indicative of a mixture of products in solution, Figure III-11. The position and band envelope suggested formulation as $[(Ni(ema))W(CO)_4]^{2-}$ and $[(Ni(ema))W(CO)_5]^{2-}$. Similar behavior was observed during routine synthesis of the (**Ni-1**)$W(CO)_4$ complex in boiling CH_2Cl_2 in the absence of added CO. Attempts to grow crystals from this solution resulted in isolation of (**Ni-1**)$W(CO)_5$.

Table III-3. IR ν(CO) data establishing donating ability of metallodithiolate ligands compared to P- and N-donor ligands with calculated force constants.[a]

entry	$(NiN_2S_2)W(CO)_4$	A^1_1	B_1	A^1_2	B_2	k_1	k_2	k_i
1	(**Ni-1**)$W(CO)_4$	1995	1871	1853	1819	13.77	14.95	0.41
2	(Ni(bme-Me_2PDA))$W(CO)_4$	1993	1876	1843	1826	13.81	14.91	0.35
3	(**Ni-1'**)$W(CO)_4$	1996	1873	1852	1817	13.74	14.98	0.41
4	(**Ni-1***)$W(CO)_4$	1996	1871	1857	1816	13.74	14.99	0.43
5	(Ni(bmmp-dmed))$W(CO)_4$	1993	1878	1854	1821	13.77	15.00	0.38
6	$[Et_4N]_2$[(Ni(ema))$W(CO)_4$]	1986	1853	1837	1791	13.41	14.77	0.46
7	(dppm)$W(CO)_4$	2016	1906	1906	1870	14.50	15.43	0.38
8	(dppe)$W(CO)_4$	2015	1900	1900	1870	14.50	15.43	0.38
9	(dmpm)$W(CO)_4$	2007	1885	1885	1863	14.39	15.10	0.38
10	$(pip)_2W(CO)_4$	2000	1863	1852	1809	13.68	14.94	0.46
11	(phen)$W(CO)_4$	2004	1889	1871	1829	13.91	15.22	0.41
12	(bpy)$W(CO)_4$	2006	1886	1870	1830	13.94	15.19	0.41

[a] IR spectra obtained in DMF.

In both processes described above, a pentacarbonyl species was formed on creation of an open site by a chelate ring-opening process with concomitant trapping by an incoming CO ligand. In an attempt to trap this open site with another ligand, a 10 to 60-fold excess of phosphines, PMe_3 and PPh_3, was utilized to promote complete dissociation of the nickel dithiolate. Unfortunately the ν(CO) spectral monitor is unsatisfactory due to large overlap of the reactant and product bands, exacerbated by the use of DMF solvent. Nevertheless, the endpoints of the reactions were detectable such that qualitative conclusions could be made.

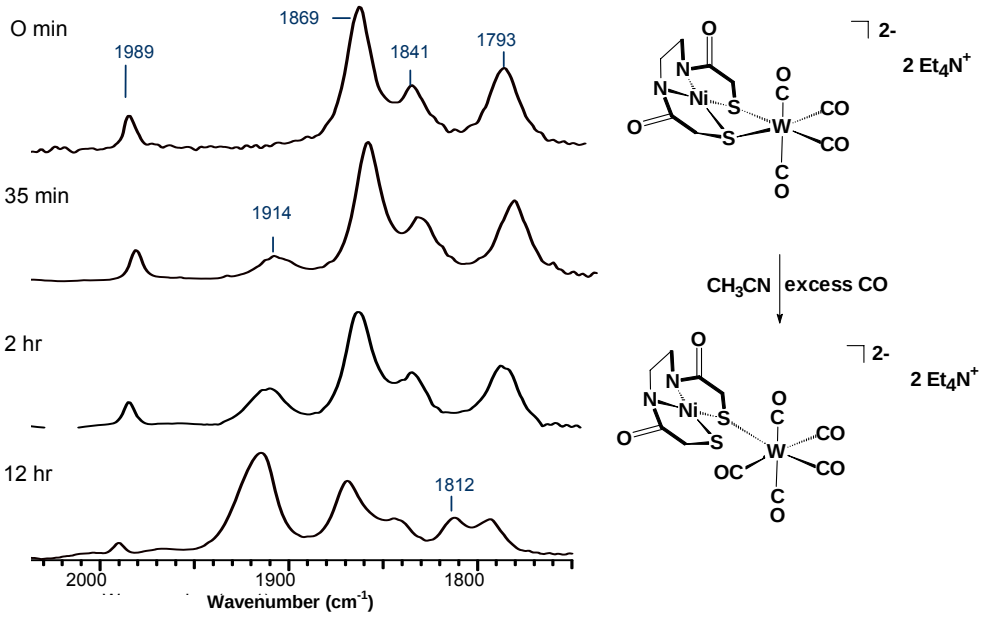

Figure III-11. Partial displacement of the $Ni(ema)^{2-}$ ligand in MeCN by CO using infrared spectroscopy as spectral monitor.

The ligand displacement experiments outlined in Scheme III-3 showed the reaction of (**Ni-1'**)$W(CO)_4$ and PMe_3 in 10-fold excess to reach completion in approximately one hour. In contrast, with PPh_3 as the incoming ligand in 10-fold excess the reaction did not reach completion after three hours. This qualitative study showed time-dependence for product formation, however it proved unsuccessful for detailed kinetic information due to severe overlap of bands in the infrared spectrum.

Scheme III-3. a) Observed reaction and b) suggested mechanism for NiN_2S_2 ligand displacement by PR_3.

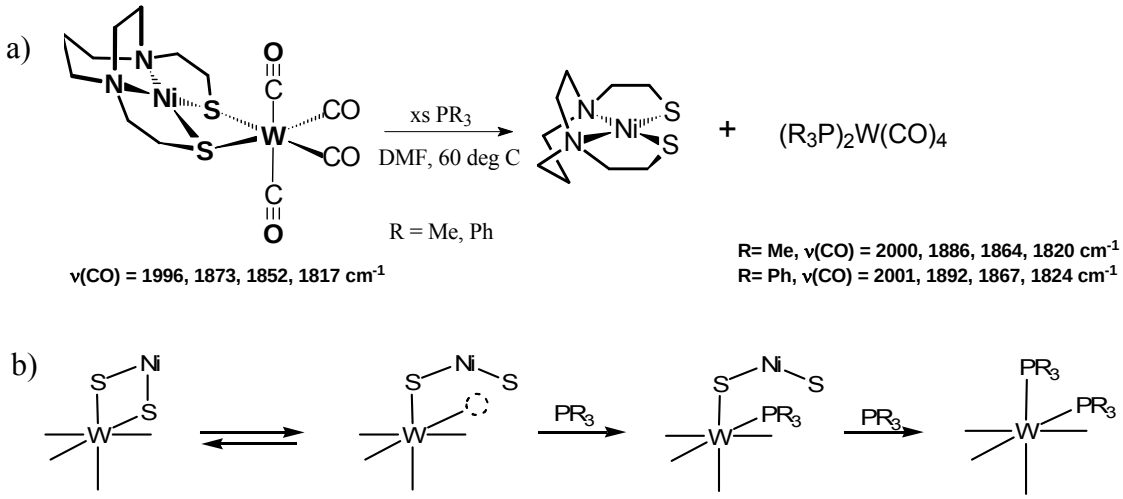

In a recent report by Don Darensbourg, Andrea Phelps, and co-workers the rates and rate parameters of NiN_2S_2 ring opening process was studied using (**Ni-1***)$W(CO)_4$ in DMF.[47] It was found that the pentacarbonyl and tetracarbonyl analogs exist in equilibrium under CO atmosphere as presented in Scheme III-4. From ^{13}CO labeling studies it was determined that the pentacarbonyl analog loses a carbonyl resulting in ring-closure with the ^{13}CO preferring a position *trans* to the thiolate sulfurs. Addition of CO to the tetracarbonyl derivative to form the pentacarbonyl derivative was followed

via *in situ* IR at a variety of temperatures and pressures. There was no evidence of W-S bond cleavage to form $W(CO)_6$. Analysis of the crystal structures of (**Ni-1***)$W(CO)_4$ and (**Ni-1***)$W(CO)_5$ revealed upon the breaking of the first W-S bond, the W-S bond of the remaining chelate arm contracts slightly suggesting that upon chelate opening the remaining W-S bond is strengthened. This result is confirmed by x-ray crystallographic results shown in Figure III-9.

Scheme III-4. Conclusion from ring opening study performed by Don Darensbourg and co-workers.[47]

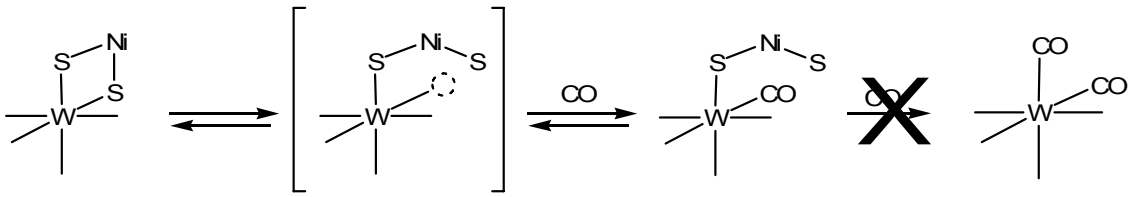

CHAPTER IV

CONTROL OF AGGREGATION: NiN_2S_2 AS A MONODENTATE LIGAND

The Ni-1$(W(CO)_5)_2$ complex

Inspired by "A Kinetic Study of the Ring-Opening Process in Tungsten Carbonyl Complexes Containing Hemilabile Metallodithiolate Ligands, a study by Don Darensbourg, Andrea Phelps, and co-workers,[47] the (**Ni-1**)$W(CO)_5$ complex was chosen for the basis of another ligand displacement study. The infrared spectrum of this compound in DMF is shown in Figure IV-1a. The goal was to displace the **Ni-1** bound as a monodentate ligand to the tungsten metal center with an excess of PPh_3 and monitor by IR spectroscopy to obtain the rates and activation parameters of the breakage of the W-S bond. After several preliminary runs, it was ascertained that a 75-fold excess of phosphine at 60°C was required to generate noticeable shifts in the infrared spectrum and after 18 hours shows a complex mixture of products formed in solution, Figure IV-1c. The reproducibility of this result is indicated by the spectrum in Figure IV-1b in which case the reaction again with large excesses of PPh_3 was attempted in CH_2Cl_2 at 30°C. The mixture could reasonably be deconvoluted into possibly seven compounds in solution: (**Ni-1**)$W(CO)_5$, (**Ni-1**)$W(CO)_4$, $(PPh_3)W(CO)_5$, *cis*-$(PPh_3)_2W(CO)_4$, *trans*-$(PPh_3)_2W(CO)_4$, $W(CO)_6$, and (**Ni-1**)$(PPh_3)W(CO)_4$.

The ^{31}P NMR spectrum of a microcrystalline sample of product that was isolated at the conclusion of the reaction was taken in CD_2Cl_2 solution at 22˚C. A sample of the PPh_3 used in the study shows a single resonance at -5.0 ppm which is consistent with

literature values of -5 to -6 ppm.[48] Literature values of PPh_3 bound to tungsten appear in the region of 20 to 30 ppm. The product sample showed no resonance attributable to PPh_3, either free or tungsten-bound.

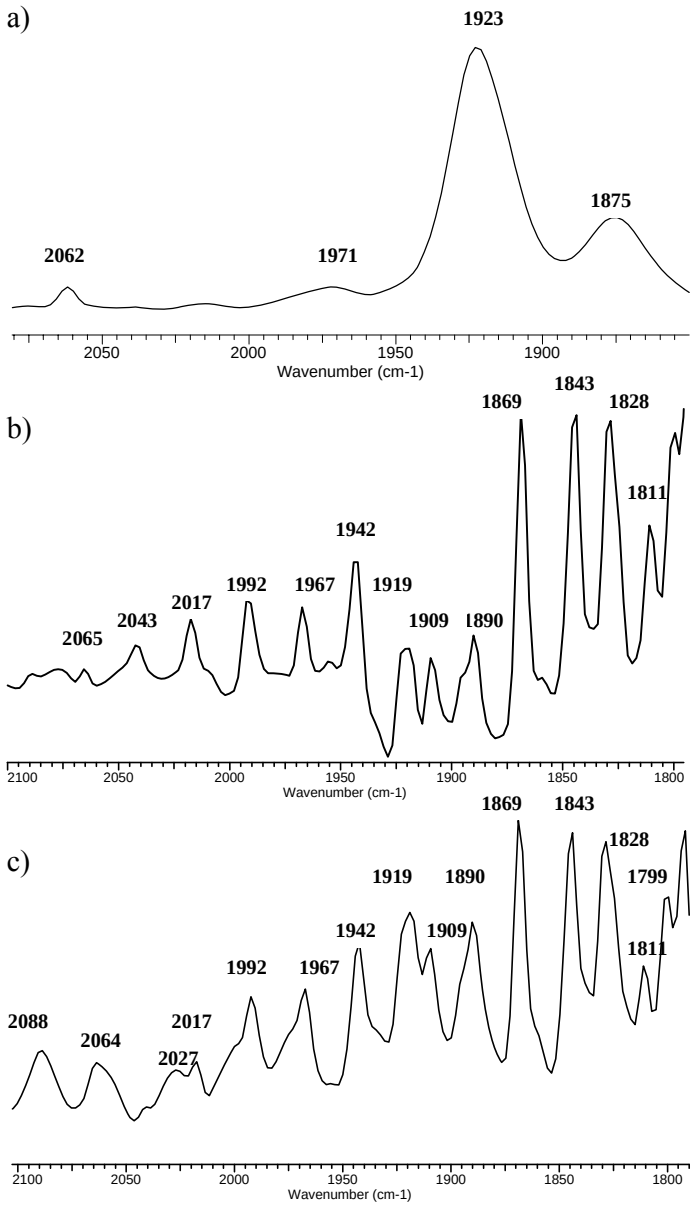

Figure IV-1. Infrared spectrum of a) (**Ni-1**)$W(CO)_5$ in DMF; b) mixture of products observed in the reaction of (**Ni-1**)$W(CO)_5$ with 10-fold excess of PPh_3 in CH_2Cl_2 at 30˚C; c) mixture of products observed in the reaction of (**Ni-1**)$W(CO)_5$ with 75-fold excess of PPh_3 in DMF at 60˚C.

Diffractometer quality crystals were obtained from the reaction mixture by ether diffusion into a concentrated solution of DMF. The single molecular structure obtained is for a complex of formula **Ni-1**$(W(CO)_5)_2$ and is shown in Figure IV-2. This compound can be synthesized directly, as outlined in Scheme IV-1, by photolysis of a THF solution of $W(CO)_6$ in a 2:1 ratio in the presence of **Ni-1**. Its ν(CO) spectrum revealed a five band pattern. A survey of the literature found many complexes with two or more tungsten pentacarbonyl groups bound to diphosphines or dithiolates. Complexes of this type show three to four ν(CO) IR bands typical of monometallic pentacarbonyl compounds.[49] There appears to be little coupling between the $W(CO)_5$ units.

Scheme IV-1. Synthetic route to **Ni-1**$(W(CO)_5)_2$.

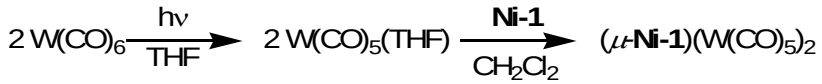

ν(CO): DMF = 2065, 1974, 1931, 1912, 1881 cm^{-1}
THF = 2065, 1976, 1926, 1913, 1890 cm^{-1}
CH_2Cl_2 = 2067, 1979, 1925, 1914, 1884 cm^{-1}

Structural description of Ni-1 as a monodentate ligand to two $W(CO)_5$ moieties

The **Ni-1**$(W(CO)_5)_2$ complex crystallizes in the triclinic space group *P*-1; a thermal ellipsoid plot and experimental crystallographic data can be found in Figure IV-2 and Table IV-1. Selected metric data for the **Ni-1**$(W(CO)_5)_2$ complex is shown in Table IV-2 and compared to that of the (**Ni-1**)$W(CO)_5$ and the free **Ni-1** complex. The molecular structure of **Ni-1**$(W(CO)_5)_2$ is that of a trimetallic species with each sulfur atom bound to a $W(CO)_5$ moiety oriented in transoid fashion with respect to the NiN_2S_2

plane with the tungsten atoms at a distance of 5.583 Å apart and a Ni-W distance of 4.021 Å. Two additional views of the compound are shown in Figure IV-3 as ball and stick representations. The Ni-S-W angles are 113.9(1)° and 117.5(1)°. The S-Ni-S angle of 89.25(9)° in the NiW_2 complex is essentially unchanged from that of free **Ni-1** 89.4(1)°; in the (**Ni-1**)$W(CO)_5$ complex, this angle is slightly compressed to 88.4(1)°. Analysis of the **Ni-1** unit revealed that the nickel remains in a square planar environment comprised of a N_2S_2 best plane with a least-squares deviation of 0.0024 Å. The average Ni-W distance is 4.021Å. The pendant thiolate arms are staggered giving a tetrahedral twist of intersecting NNiS planes of 13.7°, ca. 0.6° greater than that of the free ligand. The diazacycle rings are in the standard chair/boat conformation.

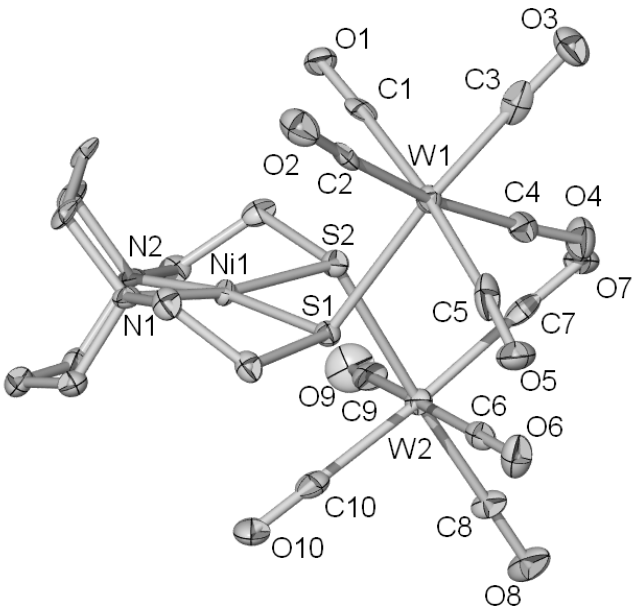

Figure IV-2. Thermal ellipsoid plot (50% probability) of **Ni-1**$(W(CO)_5)_2$ with select atoms labeled and hydrogen atoms omitted.

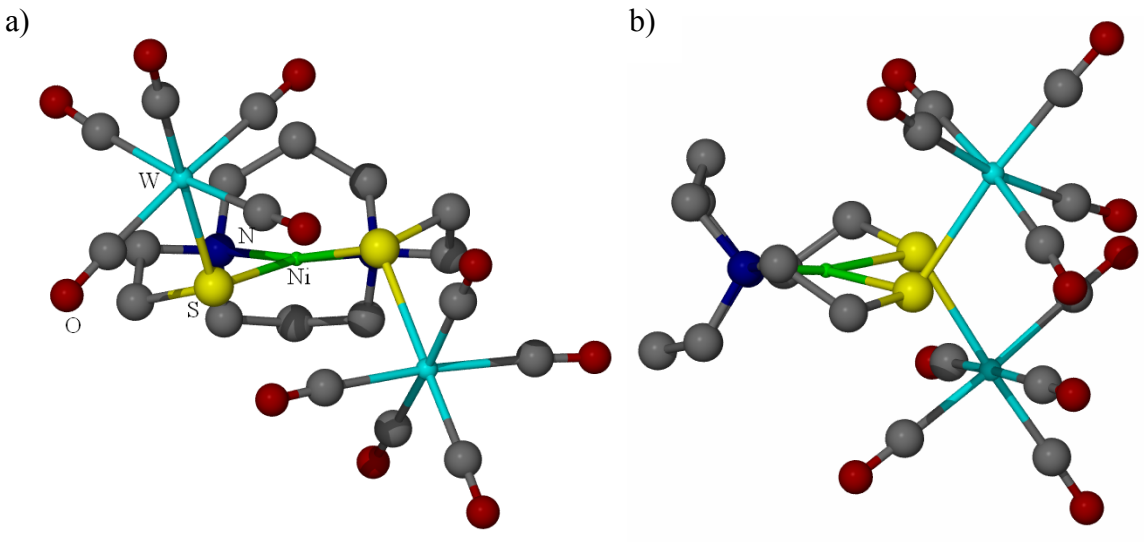

Figure IV-3. Ball and stick representation of **Ni-1**$(W(CO)_5)_2$ with hydrogen atoms omitted and select atoms labeled a) viewed down bisector of the $\angle_{S\text{-}Ni\text{-}S}$; b) viewed at 90˚ angle from a).

Table IV-1. Crystallographic experimental data for **Ni-1**$(W(CO)_5)_2$.

Formula	$C_{20}H_{20}N_2NiO_{10}S_2W_2$
Formula Weight	937.89
Temperature (K)	110(2)
Wavelength (Å)	1.54178
Z	1
D_{calcd} (Mg/cm^3)	2.366
μ (mm^{-1})	18.591
Crystal System	Triclinic
Space Group	*P*-1
Unit Cell	
a(Å)	10.4829(7)
b(Å)	10.5887(7)
c(Å)	13.7992(8)
α	106.304(5)
β	96.606(4)
γ	112.242(4)
Volume (Å^3)	1317.83(15)
Goodness-of-fit	1.079
$R_1{}^a$, $wR_2{}^b$(%) [I>2s(I)]	0.0376, 0.0849
$R_1{}^a$, $wR_2{}^b$(%) all data	0.0562, 0.0942

Table IV-2. Selected metric data for **Ni-1**$(W(CO)_5)_2$ with (**Ni-1**)$W(CO)_5$ and **Ni-1** shown for comparison.

	(**Ni-1**)$(W(CO)_5)_2$	(**Ni-1**)$W(CO)_5$	**Ni-1**
Bond distances			
Ni1-W1	3.969	3.894	
W1-C1	2.010(11)	2.031(11)	
W1-C2	2.081(12)	2.036(12)	
W1-C3	1.982(12)	2.019(11)	
W1-C4	2.053(12)	1.955(13)	
W1-C5	2.071(12)	2.067(12)	
W1-S1	2.572(3)	2.577(3)	
Ni1-W2	4.072		
W2-C6	2.038(12)		
W2-C7	2.035(12)		
W2-C8	1.968(13)		
W2-C9	2.037(12)		
W2-C10	2.055(11)		
W2-S2	2.571(2)		
Ni-S1 (···W)	2.186(3)	2.176(3)	2.159(3)
Ni-S2	2.170(2)	2.164(3)	2.159(3)
Ni-N1	1.984(7)	1.985(8)	1.979(7)
Ni-N2	1.984(8)	1.982(8)	1.979(7)

	(**Ni-1**)$(W(CO)_5)_2$	(**Ni-1**)$W(CO)_5$	**Ni-1**
Bond Angles			
W(1)-C(1)-O(1)	179.2(10)	178.3(9)	
W(1)-C(2)-O(2)	173.8(10)	177.5(12)	
W(1)-C(3)-O(3)	179.1(9)	175.7(11)	
W(1)-C(4)-O(4)	178.4(9)	176.5(11)	
W(1)-C(5)-O(5)	176.8(9)	172.6(10)	
S(1)-W(1)-S(2)			
W(1)-S(1)-Ni(1)	113.39(10)		
W(2)-C(6)-O(6)	174.8(9)		
W(2)-C(7)-O(7)	175.8(9)		
W(2)-C(8)-O(8)	177.2(10)		
W(2)-C(9)-O(9)	176.2(8)		
W(2)-C(10)-O(10)	177.2(8)		
W(2)-S(2)-Ni(1)	117.47(11)		
S(1)-Ni-S(2)	89.25(9)	88.45(11)	89.4(1)
N(1)-Ni-N(2)	90.9(3)	89.5(3)	82.5(2)
T_d twist	13.8	8.6	13.1

The W-C-O units are substantially linear. The closest intermolecular contacts are in the range of 3.01 to 3.30 Å which is slightly beyond the overlap of the van der Waals radii of 3.22 Å. The W-C distances do not vary by a significant amount; however, it is noteworthy to mention that the W-C bond lengths of the carbonyl *trans* to the donor sulfur atom are slightly shorter from the average *cis* W-C distances (1.982(12) Å, 1.968(13) Å) for W(1)-C(3) and W(2)-C(8) respectively. The W(1)-C(3) distance is slightly longer than W(2)-C(8) due to the deactivation of the sulfur donor atom upon being bound to the tungsten metal center. This effect is also reflected in the Ni-S distances (Ni(1)-S(1) 2.186(3) Å and Ni(1)-S(2) 2.170(2) Å). The W(1)-S(1) and W(2)-S(2) distances are the same at 2.572(3) Å and 2.571(2) Å, respectively.

A comparison of the bond distances and angles of the **Ni-1**$(W(CO)_5)_2$**,** (**Ni-1**)$W(CO)_5$, and **Ni-1** compounds reveals no appreciable change within the **Ni-1** unit. Mi nor lengthening of the Ni-S distances is ascribed to donation of electron density from the sulfur atoms to the tungsten metal center. The W-C bond distances of the $W(CO)_5$ moieties differ by no more than 0.04 Å.

A similar structure is found in our library of electrophile/NiN_2S_2 complex adducts which features SO_2 uptake of **Ni-1'**.[50] Ball and stick representations of the molecular structures of **Ni-1**$(W(CO)_5)_2$ and **Ni-1'**·$2SO_2$ adducts are shown in Figure IV-4. The latter is that of a square planar NiN_2S_2 unit with each sulfur bound to SO_2 groups oriented transoid to each other with the SO_2-sulfur atoms 6.035 Å apart. The S-SO_2 distances of 2.660(1) and 2.557(1) Å are comparable to the W-S distances found in the NiW_2 trimetallic 2.572(3) and 2.571(2) Å respectively. The Ni-S-W angles (113.4(1)

and 117.5(1)˚) are markedly larger than the corresponding Ni-S-SO_2 angles (105.2(3) and 102.4(3)˚) presumably due to the large steric bulk of the $W(CO)_5$ unit.

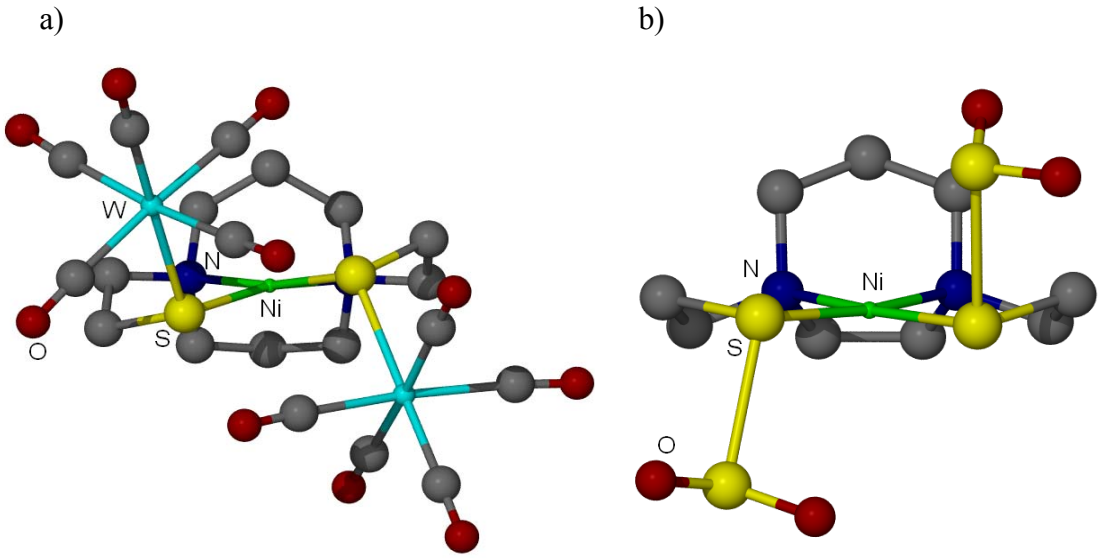

Figure IV-4. Ball and stick representations of a) **Ni-1**$(W(CO)_5)_2$ and b) **Ni-1'**$\cdot 2SO_2$ viewed from the bisector of the $\angle_{S\text{-}Ni\text{-}S}$.

In a study by Blinn and co-workers, reaction of the Nipe compound, 2,3-pentanedione-bis(*β*-mercaptoethylimino)nickel, with $W(CO)_6$ in refluxing toluene for six hours resulted in the proposed oligomeric complex $[NipeW(CO)_3]_2$ shown in Figure IV-5. This assignment is corroborated by the number IR of bands determined by group theory in the infrared spectrum and by elemental analysis.[51] Compounds such these are rare.[52] The aggregative ability of the NiN_2S_2 complex is aided by the low steric hindrance at the S-donor binding site. To corroborate this study, a similar investigation

of the reaction with $W(CO)_6$ was conducted with the open chain Ni(bme-Me_2PDA) complex.[28] Infrared spectroscopy revealed a forest of CO stretches similar to the one in Figure IV-1. An increase of the refluxing time by one hour revealed an IR spectrum identical to the one reported for the (Ni(bme-Me_2PDA))$W(CO)_4$ complex. This suggests the forest of IR bands is that of intermediates mediated perhaps by a similar tetrametallic with the Ni(bme-Me_2PDA) ligand.

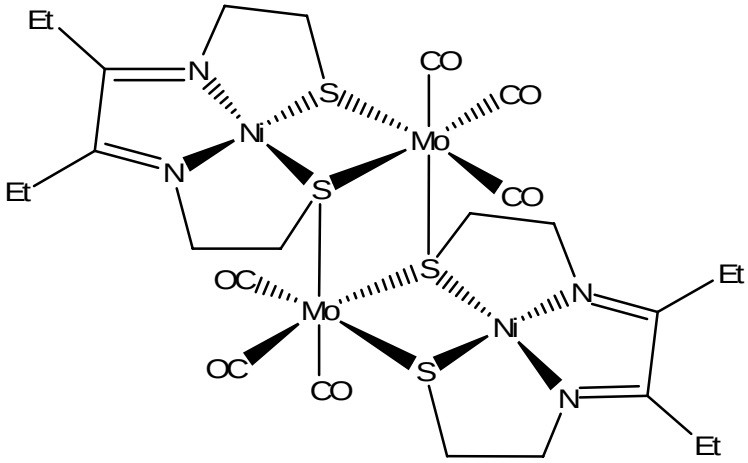

Figure IV-5. Proposed structure of the Ni_2W_2 tetrametallic reported by Blinn and co-workers.[51]

Inhibition of nickel dithiolate aggregation

In order to attenuate the donor ability of the nickel dithiolates, the sulfinato species Ni(mese-daco), (mercaptoethylsufinatoethyl-1,5-diazacyclooctane)nickel, was prepared.[14] The oxygenation of **Ni-1** to Ni(mese-daco) is known to reduce the nucleophilicity of the pendant nickel thiolate. Hence aggregation should be inhibited. An acetonitrile solution of Ni(mese-daco) was added to $W(CO)_5$(THF) in a 1:1 ratio with

expectation of the Ni(mese-daco)·$W(CO)_5$ adduct shown in Figure IV-6. Remarkably, no CO-containing product at all was observed in the infrared spectrum. As **Ni-1** is a mimic for diphosphines, and phosphine oxides are well-known CO labilizing agents,[53] the data could suggest Ni(mese-daco) has a similar CO-labilizing effect. Attempts to crystallize a product from this reaction were unsuccessful.

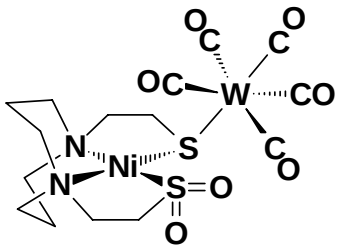

Figure IV-6. Proposed molecular structure of the Ni(mese-daco)·$W(CO)_5$ adduct.

In a further probe of the ability of Ni(mese-daco) to bind metal ions, the compound was reacted with copper(I)bromide in a 2:1 ratio. Consistent with the well-known affinity of nickel thiolates for copper, the crystals obtained from this reaction revealed a trimetallic compound where copper bromide is ligated by two Ni(mese-daco) units via its unoxidized sulfur atom. The molecular structure of $(Ni(mese\text{-}daco))_2CuBr$ is shown in Figure IV-7 as a thermal ellipsoid plot. Selected metric data and experimental crystallographic data are given in Tables IV-3 and 4.

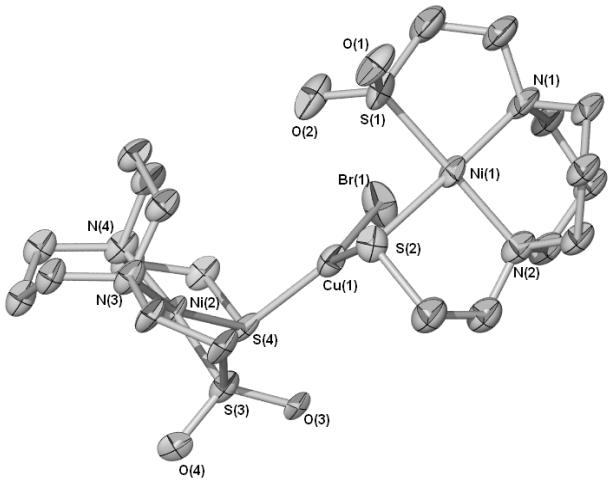

Figure IV-7. Thermal ellipsoid plot (50% probability) of $(Ni(mese\text{-}daco))_2CuBr$ with select atoms labeled and hydrogen atoms omitted.

Table IV-3. Selected metric data for $(Ni(mese\text{-}daco))_2CuBr$.

Bond Distances			
Ni1-S1	2.121	Ni2-S3	2.114
Ni1-S2	2.141	Ni2-S4	2.168
Ni1-N1	1.981	Ni2-N3	1.991
Ni1-N2	1.908	Ni2-N4	1.951
S1-O1	1.501	S3-O3	1.45
S1-O2	1.539	S3-O4	1.449
Cu1-S4	2.241	Ni1-Cu1	3.301
Cu1-S2	2.253	Ni2-Cu1	3.257
Cu1-Br1	2.42		
Bond Angles			
S1-Ni1-S2	90.88	O1-S1-O2	115.08
N1-Ni1-N2	93.05	O3-S3-O4	113.99
S3-Ni2-S4	88.7	S2-Cu1-S4	130.43
N3-Ni2-N4	93.31		

Table IV-4. Experimental crystallographic data for $(Ni(mese\text{-}daco))_2CuBr$.

Formula	$C_{20}H_{40}BrCuN_4Ni_2O_4S_4$
Formula Weight	394.84
Temperature (K)	110(2)
Wavelength (Å)	0.71073
Z	8
D_{calcd} (Mg/cm^3)	1.916
μ (mm^{-1})	3.932
Crystal System	orthorhombic
Space Group	$P2_12_12_1$
Unit Cell	
a(Å)	8.467(5)
b(Å)	11.600(7)
c(Å)	27.870(16)
α	90
β	90
γ	90
Volume ($Å^3$)	2737(3)
Goodness-of-fit	1.019
R_1[a], wR_2[b](%)	0.1353, 0.1682
R_1[a], wR_2[b](%) all data	0.077, 0.1451

[a] $R_1 = S||F_o| - |F_c||/SF_o$

[b] $wR_2 = [S[w(F_o^2 - F_c^2)^2/Sw(F_o^2)^2]^{1/2}$

This $(Ni(mese\text{-}daco))_2CuBr$ crystallizes in the orthorhombic space group $P2_12_12_1$. This trimetallic features two **Ni-1** units, each with one of its sulfur atoms doubly oxygenated into a sulfinate. A molecule of copper(I)bromide is bound by the remaining thiolate sulfur atoms as monodentate ligands. The copper(I) ion is in a trigonal planar S_2Br coordination environment with a copper-bromide distance of 2.421(3) Å. The donor sulfur atoms which complete the trigonal planar geometry are

positioned 2.247(5) Å from copper. The average deviation in the $CuBrS_2$ unit from the best least squares plane is 0.0009 Å. In fact the angle defined by the Ni(1)-S(2)-Cu(1)-Br(1) atoms displays a maximum torsion of 0.7 °. Similar behavior is observed in the (**Ni-1***)$_2$(CuBr)$_4$ cluster from our laboratories. This cluster contains four trigonal planar CuBr units. All of lone pairs on the donor sulfur atoms are bound to CuBr forming an adamantine-like $Ni_2S_4Cu_4$ core.

One of the NiN_2S_2 units is in a highly distorted square planar geometry caused by the bound thiolate sulfur deviating from the best $N_2S_{sulfinate}$ plane by 0.7620 Å. The S-Ni-S angle for each NiN_2S_2 unit is slightly contracted (90.75(18)° and 88.9(2)°) from its unbound form (91.8(1)°). In fact, for each Ni(mese-daco), the Ni-$S_{sulfinate}$ distances (Ni(1)-S(1): 2.102(5) Å and Ni(2)-S(3): 2.101(5) Å are shorter than in the unbound form (2.140(1) Å) whereas the Ni-$S_{thiolate}$ distances (Ni(1)-S(2): 2.141 Å and Ni(2)-S(4): 2.168 Å) are largely unchanged. Additional views of this compound are shown in Figure IV-8.

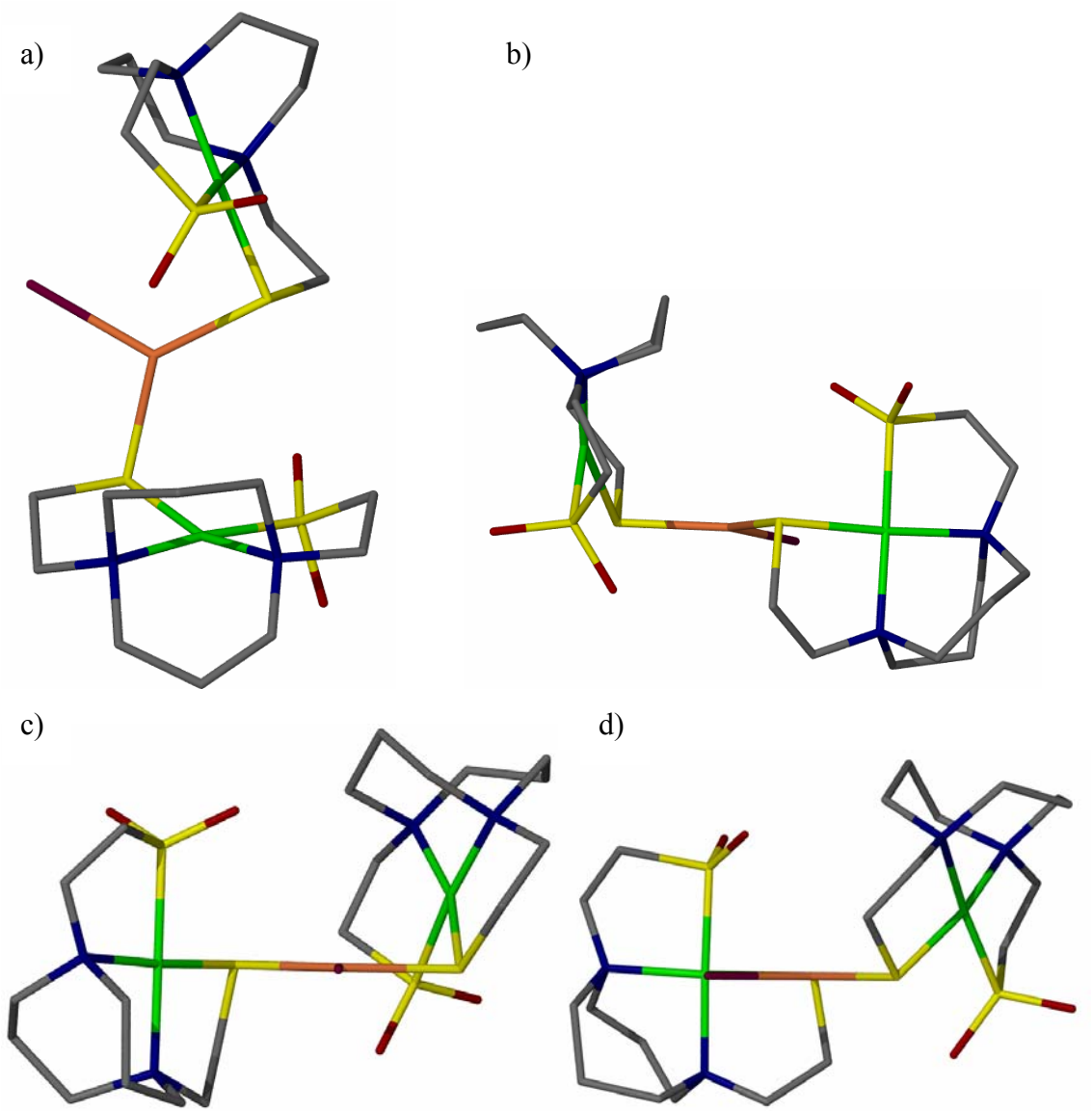

Figure IV-8. Wireframe models of $(Ni(mese\text{-}daco))_2CuBr$ with hydrogen atoms omitted a) viewed with S_2CuBr unit in the plane of the page b) viewed down eclipsed nitrogen atoms of Ni(mese-daco) unit c) viewed down CuBr vector d) view of eclipsed Ni-S-Cu-Br torsion angle.

CHAPTER V

NiN_2S_2 AS A BIDENTATE BRIDGING LIGAND: PADDLEWHEEL COMPLEXES WITH METAL-METAL BONDED UNITS*

The *cis*-dithiolates derived from structurally reinforced diazacycles as in Ni(bme-daco), **Ni-1** (1,5-bis(mercaptoethyl)-1,5-diazacyclooctane)nickel) and Ni(bme-dach), **Ni-1'** (1,4-bis(mercaptoethyl)-1,4-diazacycloheptane)nickel), have proven exceptional as metallodithiolate ligands which nucleate a broad scope of cluster complexes. Along with other NiN_2S_2 complexes, the donor abilities of **Ni-1** and N**i-1'** have been addressed via analysis of ν(CO) vibrational spectroscopy of NiN_2S_2 derivatives of $W(CO)_4$.[30,41] The thermally stable complexes have been subjected to x-ray diffraction studies for determination of solid state structures. In solution, facile chelate ring opening produces the (η^1-NiN_2S_2)$W(CO)_5$ in the presence of added CO. Such studies have established that the NiN_2S_2 metallodithiolate ligands bind to low valent metals with electron donor abilities comparable to amines, diphosphines and diimines.

Shown in Figure III-10 is a structural overlay of **Ni-1*** ((1,5-bis(2-mercapto-2-methylpropyl)-1,5-diazacyclooctane)nickel) and (*o*-phen)$W(CO)_4$. The relatively flat steric character of the nickel dithiolates, coupled with the hinge associated with the lone pairs of sulfur in bridging dithiolates, engenders a stereoorientational effect not seen in either the typically bulky diphosphines or the flat diimines. This unique steric character is responsible for the profusion of paddlewheel type clusters formed as Zn, Cu, Ag, and

* Reproduced in part with permission from Jeffery, S. P.; Lee, J.; Darensbourg, M. Y. *Chem. Commun.* **2005**, 1122. Copyright 2005 The Royal Society of Chemistry.

Pd derivatives.[4,7,9,35] Figure V-I lists formulations of such clusters in which M---M distances > 4 Å result from tetrahedral S_3X donor environments about Zn^{II} and Cu^{I}; planar S_4 or S_3 donor environments about Pd^{II} and Ag^{I} in the C_4 and C_3 paddlewheels, respectively, engender non-bonded M---M distances of around 3 Å. As the NiN_2S_2 ligands also serve as bidentate ligands to a single metal, a reasonable goal is the isolation of dinuclear multiply-bonded M_2^{n+} units. The latter are typically found as carboxylate and formamidinate derivatives which have been extensively chronicled in explorations of metal-metal bonds in the Cotton laboratories.[14] Thus, in order to determine whether the steric and donor characteristics of NiN_2S_2 ligands perform similarly to that of traditional bidentate bridging ligands of multiply-bonded dinuclear compounds, two complexes containing quadruply-bonded dimolybdenum (Mo_2^{4+}) units were prepared and characterized via x-ray crystallography, cyclic voltammetry, and electron spray ionization mass spectroscopy.[54]

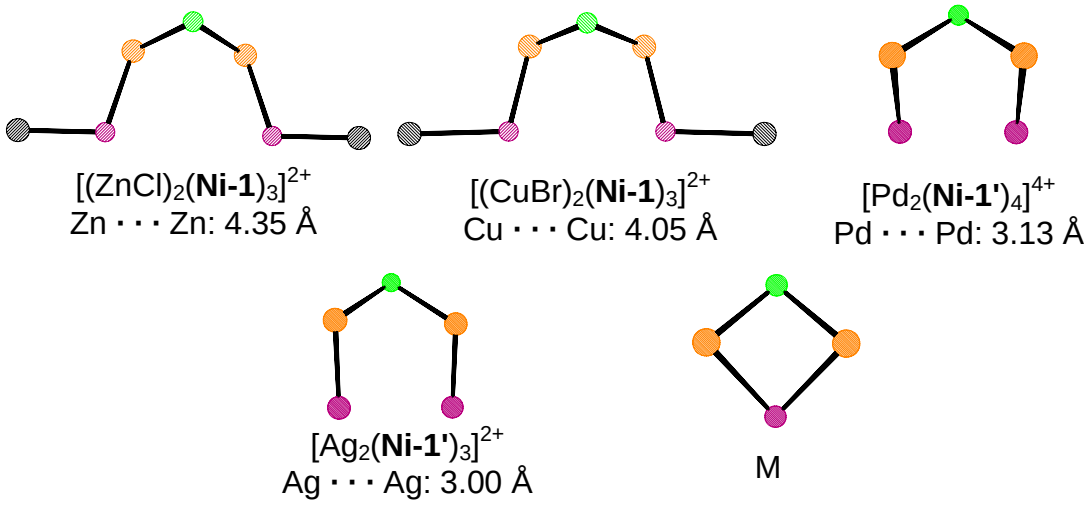

Figure V-1. Range of metal-metal distances afforded by NiN_2S_2 ligands; see text for description of structures.

Synthesis of the hexametallic clusters is readily accomplished by ligand displacement from $[Mo_2(MeCN)_{10}][BF_4]_4$ in MeCN at room temperature. The royal blue solution of $[Mo_2(MeCN)_{10}][BF_4]_4$ immediately turns dark brown-red upon reaction with NiN_2S_2. After stirring for 3 hours, the solvent is removed *in vacuo*, and the product is isolated in 60% yield. Diffractometer quality crystals were grown by layering a concentrated solution of MeCN with Et_2O.

Complexes $[Mo_2(\mathbf{Ni\text{-}1})_4][BF_4]_4$ and $[Mo_2(\mathbf{Ni\text{-}1'})_4][BF_4]_4$ crystallize as MeCN solvates, with six and four molecules of MeCN respectively, in the monoclinic space group $P2_1/n$. Shown in Figure V-2 are the thermal ellipsoid molecular structures of the Mo_2Ni_4 cations; Tables V-1 and 2 show selected metric and experimental crystal data respectively. There are two molecular cations in the unit cell with the four charge-balancing BF_4 anions residing within the lattice interstices. The central methylene carbons (C(4) and C(7)) on one of the diazacycles of compound $Mo_2(\mathbf{Ni\text{-}1})_4][BF_4]_4$ is disordered between two positions 70% of the time. One of the BF_4 anions of $[Mo_2(\mathbf{Ni\text{-}1'})_4][BF_4]_4$ is also disordered.

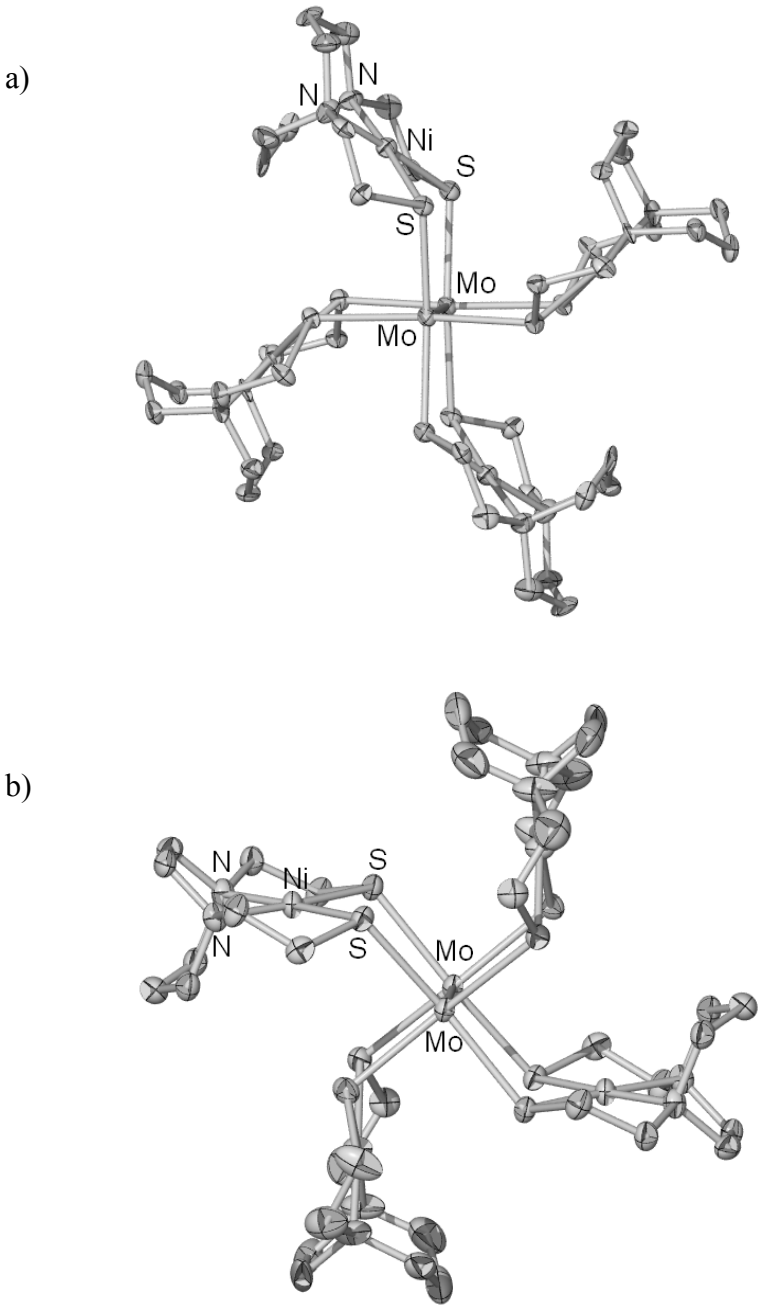

Figure V-2. Thermal ellipsoid plots (50% probability) of cations a) $[Mo_2(\mathbf{Ni\text{-}1})_4]^{4+}$ and b) $[Mo_2(\mathbf{Ni\text{-}1'})_4]^{4+}$.

Table V-1. Selected metric data for $[Mo_2(NiN_2S_2)_4]^{4+}$ complexes.

	$[Mo_2(\mathbf{Ni\text{-}1})_4][BF_4]_4\cdot 6MeCN$	$[Mo_2(\mathbf{Ni\text{-}1'})_4][BF_4]_4\cdot 4MeCN$	**Ni-1**	**Ni-1'**
M'-S_{avg}	2.526(3)	2.517(14)		
Ni-S_{avg}	2.160(3)	2.141(15)	2.159(3)	2.164(1)
Ni-N_{avg}	1.977(6)	1.921(9)	1.979(7)	1.940(4)
M'---Ni	3.921	3.73		
Ni---Ni	5.328	5.049		
M'---M'	2.143(18)	2.162(10)		
S-Ni-S	87.875(10)	92.62(6)	89.4(1)	95.4(1)
N-Ni-N	90.85(3)	83.305(10)	89.3(4)	82.5(2)
torsion	1.5	0.9		
dihedral	134.3	128.7		
axial interaction	2.827, BF_4^-	2.73, MeCN		

Table V-2. Experimental crystal data for $[Mo_2(NiN_2S_2)_4]^{4+}$ complexes.[a]

	$[Mo_2(\mathbf{Ni\text{-}1})_4][BF_4]_4\cdot 6MeCN$	$[Mo_2(\mathbf{Ni\text{-}1'})_4][BF_4]_4\cdot 4MeCN$
formula	$C_{52}H_{98}B_4F_{16}Mo_2N_{14}Ni_4S_8$	$C_{44}H_{84}B_4F_{16}Mo_2N_{12}Ni_4S_8$
formula weight	1949.88	1811.67
temperature (°C)	110(2)	110(2)
wavelength (Å)	0.71073	0.71073
Z	2	2
D_{calcd} (g/cm^3)	1.751	1.773
m (cm^{-1})	1.64	1.779
crystal system	monoclinic	monoclinic
space group	$P2_1/n$	$P2_1/n$
unit cell		
a (Å)	11.319 (5)	12.693 (4)
b (Å)	23.770 (10)	20.039 (5)
c (Å)	13.822 (6)	14.166 (4)
b (°)	96.057 (8)	109.659 (4)
volume (Å^3)	3698 (3)	3393.3 (16)
GOF	1.048	1.055
R_1[b], wR_2[c](%) [$I > 2s(I)$]	7.69, 16.45	6.18, 15.59
R_1[b], wR_2[c](%) all data	11.83, 18.46	5.84, 15.15

[a] Obtained using graphite-monochromatized Mo Ka radiation (l = 0.71073 Å) at 110K.
[b] $R_1 = S||F_o| - |F_c||/SF_o$.
[c] $wR_2 = [S[w(F_o^2 - F_c^2)^2/Sw(F_o^2)^2]^{1/2}$.

The Mo_2^{4+} coordination environment of the Mo_2Ni_4 clusters, shown in Figure V-3, are C_4 paddlewheels containing a Mo-Mo axis and eight sulfurs derived from four NiN_2S_2 bidentate bridging paddles. The **Ni-1** and **Ni-1'** moieties are in their common configurations with Ni-N and Ni-S distances essentially unchanged from their unbound forms.[11,12] A plane of symmetry perpendicular to the Mo-Mo C_4 rotation axis includes the four nickel ions and the central methylene carbons in the four diazacyclohexane rings of $[Mo_2(\mathbf{Ni\text{-}1})_4]^{4+}$; a similar plane of symmetry exists in the contracted diazacycle-ring derivative of $[Mo_2(\mathbf{Ni\text{-}1'})_4]^{4+}$. Thus, neglecting the diazacycle frameworks of complexes $[Mo_2(\mathbf{Ni\text{-}1})_4][BF_4]_4$ and $[Mo_2(\mathbf{Ni\text{-}1'})_4][BF_4]_4$, the molecular cations are of C_{4h} symmetry. It has been well established for quadruply-bonded compounds that the strength of the delta bond varies with the angle of torsional twist.[19c] The measure of torsion angles, shown in Figure V-3, is a quantitative way to measure the strength of the delta bond. The two MoS_4 planes are largely eclipsed, displaying a maximum torsion of 1.5°. A much greater torsion angle of up to 32° for example, has been observed in a $(NiN_2S_2)_4Ni_2$ structure.[55] The MoS_4 units of both complexes are essentially eclipsed, varying by no more than 1.5˚, indicating maximum overlap is achieved giving a strong quadruple bond.

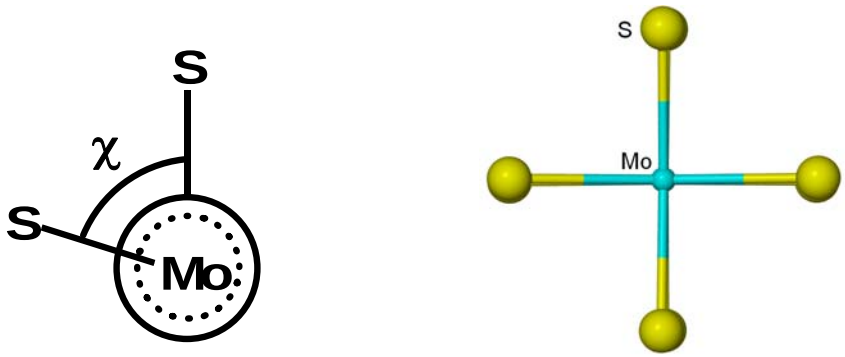

Figure V-3. a) Neumann projection defining torsion angle b) View of $[Mo_2(NiN_2S_2)_4]^{4+}$ cation down Mo-Mo axis showing eclipsed MoS_4 planes.

Ni-1 and **Ni-1'** coordinate to the dimolybdenum unit via their sulfur atoms with average Mo-S distances of 2.526(3) Å and 2.517(14) Å, respectively. These distances are ~0.1 Å longer than those in S-donor complexes, $Mo_2(S_2CR)_4$, and similar to those in $Mo_2(S_2PEt_2)_4$.[56] The Mo-Mo bond distances of 2.142(18) Å and 2.162(10) Å for $[Mo_2(\mathbf{Ni\text{-}1})_4][BF_4]_4$ and $[Mo_2(\mathbf{Ni\text{-}1'})_4][BF_4]_4$ respectively are not significantly different from each other or the $Mo_2(S_2CR)_4$ derivatives which represent quadruply-bonded Mo_2^{4+} units in neutral S-ligated C_4 structures.[57] The packing diagrams, given in Figures V-4 and 5, show no anion or solvent contacts within bonding distances.

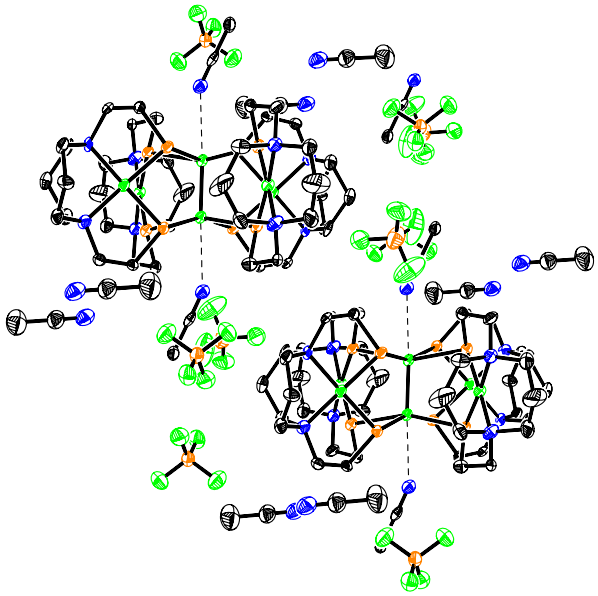

Figure V-4. Thermal ellipsoid plot of $[Mo_2(\mathbf{Ni\text{-}1})_4][BF_4]_4$ with focus on axially oriented MeCN molecules.

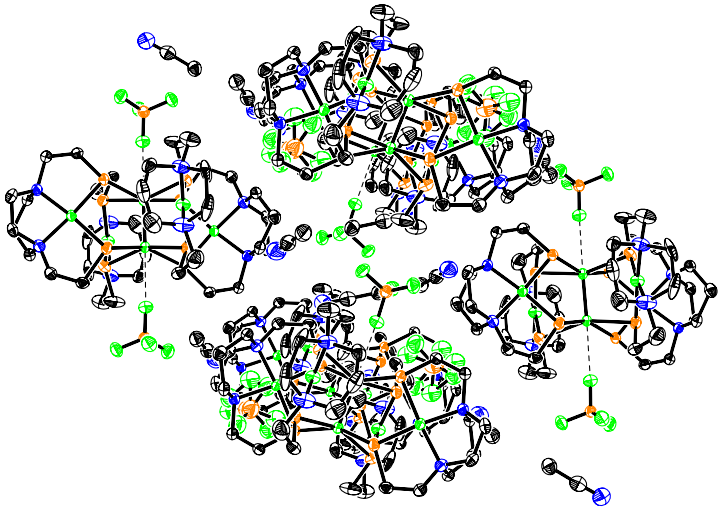

Figure V-5. Thermal ellipsoid plot of $[Mo_2(\mathbf{Ni\text{-}1'})_4][BF_4]_4$ with focus on BF_4 anions oriented axially.

The bidentate bridging ligands in $[Mo_2(\mathbf{Ni\text{-}1})_4][BF_4]_4$ and $[Mo_2(\mathbf{Ni\text{-}1'})_4][BF_4]_4$ display S-Ni-S angles that are compressed by ca. 2° from their free ligand values of 89.5 and 95.4° for **Ni-1** and **Ni-1'** respectively. The S···S distances within one ligand "paddle" are at 3.0 Å largely the same as those in the $Mo_2(S_2CR)_4$ analogs. Despite the apparent steric bulk of these ligands, the orientational possibilities of the square planar NiN_2S_2 ligand permit a structural meshing conducive to stable C_4 paddlewheel type complexes. Indeed the space filling models shown in Figure V-6 show clefts between the paddles, exposing sulfur and nickel atoms.

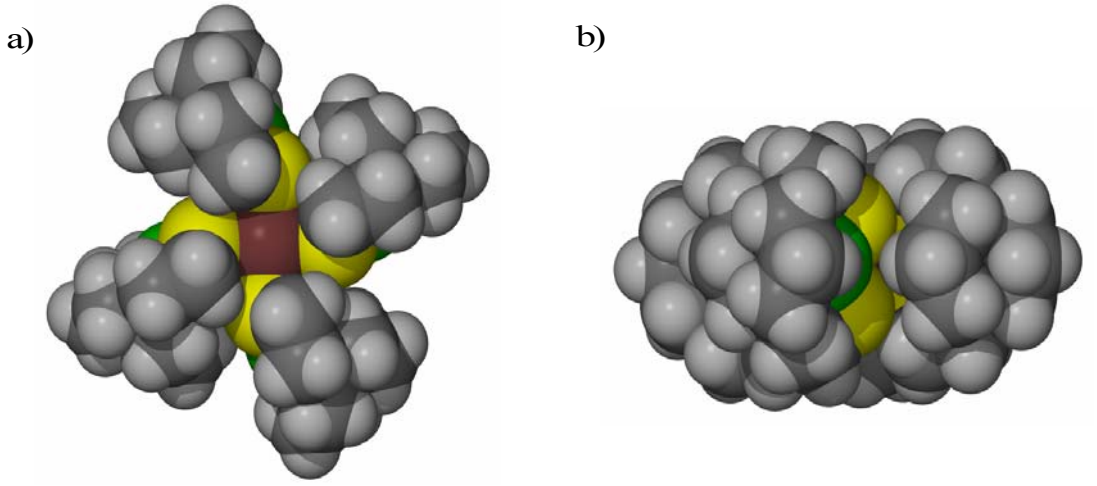

Figure V-6. Space filling models of the $[Mo_2(\mathbf{Ni\text{-}1})_4]^{4+}$ cation showing clefts which expose the nickel and sulfur atoms. a) viewed down Mo-Mo axis b) 90˚ rotation, viewed from above.

In collaboration with postdoctoral researcher Dr. Jonghyuk Lee, the redox behavior of the two dimolybdenum compounds in MeCN was examined at room temperature by cyclic voltammetry. Figure V-7 displays the CV and associated square wave (SWV) voltammogram of compound $[Mo_2(\mathbf{Ni\text{-}1'})_4][BF_4]_4$ in the cathodic potential

region. Consistent with earlier electrochemical studies of polynuclear compounds based on **Ni-1** and **Ni-1'**, the CV's of $[Mo_2(\mathbf{Ni\text{-}1})_4][BF_4]_4$ and $[Mo_2(\mathbf{Ni\text{-}1'})_4][BF_4]_4$ show multiple and overlapping redox events.[58] In the case of $[Mo_2(\mathbf{Ni\text{-}1'})_4][BF_4]_4$, the redox events commence at -0.70 V and, within the solvent window, finish with an apparently reversible wave at $E_{1/2}$ = -2.04 V. The SWV amplifies and separates the electrochemical events indicating six reductive processes, four of which are quite distinct with two others, at -0.70 V and -1.31 V, being weak and poorly defined.

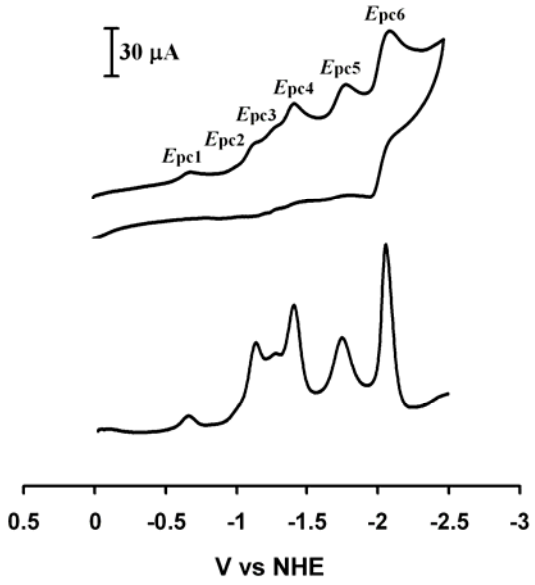

Figure V-7. Cyclic and square wave voltammograms of 1.0 mM solution of $[Mo_2(\mathbf{Ni\text{-}1'})_4][BF_4]_4$ in 0.1 M *n*-Bu_4NBF_4 with a glassy carbon electrode at a scan rate of 200 mV/s. Square-wave voltammogram shown in the bottom of the figure is initiated in the negative direction; square-wave voltammogram amplitude = 25 mV; frequency = 15 Hz; E_{step} = 4 mV. All potentials scaled to NHE via the Fc/Fc^+ reference.[21] E_{pc1} = -0.70 V, E_{pc2} = -1.18 V, E_{pc3} = -1.32 V, E_{pc4} = -1.43 V, E_{pc5} = -1.81 V, E_{pc6} = -2.11V.

The C_3 paddlewheel based on zinc, $[(\mathbf{Ni\text{-}1})_3(ZnCl)_2][BF_4]_2$, showed three cathodic events,[58] which were assigned to successive reductions of **Ni-1** units. Thus a likely scenario for the C_4 paddlewheel compound $[Mo_2(\mathbf{Ni\text{-}1'})_4][BF_4]_4$ is that the four

distinct reductions are based on the **Ni-1'** units while the minor waves are reasonably attributed to dimolybdenum unit. The latter possibility is supported by the redox behavior of the starting material $[Mo_2(MeCN)_{10}][BF_4]_4$ which shows, under similar electrochemical conditions, a reversible reduction at $E_{1/2}$ = -0.21 V and an irreversible reduction at E_{pc} = -0.96 V. As the NiN_2S_2 ligands are better electron donors than MeCN,[30,41,59] the more negative reductions of compounds $[Mo_2(\mathbf{Ni\text{-}1})_4][BF_4]_4$ and $[Mo_2(\mathbf{Ni\text{-}1'})_4][BF_4]_4$ are expected. The recently reported $Mo_2(hpp)_4$ (hpp = the anion of 1,3,4,6,7,8-hexahydro-2H-pyrimido[1,2-a]pyrimidine) also revealed two cathodic events of similar separation which were assigned to the dimolybdenum unit redox levels of $Mo_2^{6+/5+}$ and $Mo_2^{5+/4+}$.[60]

The electrochemical assignments have as a basic assumption that the hexanuclear cluster remains intact in MeCN solution. This assumption is challenged by the position of the most negative reduction wave which is very similar to that of the free NiN_2S_2 ligand. The attempted "spiking" of the electrochemical solution of compound $[Mo_2(\mathbf{Ni\text{-}1'})_4][BF_4]_4$ with **Ni-1'** resulted in minor differences in the CV largely due to the insolubility of **Ni-1'** in MeCN. For compound $[Mo_2(\mathbf{Ni\text{-}1})_4][BF_4]_4$, spiking with **Ni-1** produced some enhancement of the -2.1 V event and also a major anodic event wave at +0.17 V. As this oxidative event is characteristic of free NiN_2S_2 complexes and assigned to oxidation of thiolate to the thiyl radical,[61] we conclude that the absence of this oxidative wave in non-spiked $[Mo_2(\mathbf{Ni\text{-}1})_4][BF_4]_4$ solutions is indicative of the lack of dissociation of **Ni-1** in solutions of compound $[Mo_2(\mathbf{Ni\text{-}1})_4][BF_4]_4$. Additional studies

required for definitive assignments and further development of the electrochemistry are discussed in Chapter VI.

In a study of the "Construction of (N_2S_2)Ni-Pd Clusters,"[4] we uncovered various structural forms including a slant chair Ni_2Pd trimetallic, a basket, and a C_4 paddlewheel as the latter crystallized with nitrate ions as shown in Figure V-8. To elucidate the possibility of a counterion effect directing the formation of the $(\mathbf{Ni\text{-}1'})_2Pd^{2+}$ trimetallic containing chloride or the $(\mathbf{Ni\text{-}1'})_4Pd^{4+}$ hexametallic containing nitrate, **Ni-1'** was reacted with $PdBr_2$ in a 2:1 ratio in MeOH. This solution was concentrated and layered with Et_2O to obtain diffractometer quality crystals.[62]

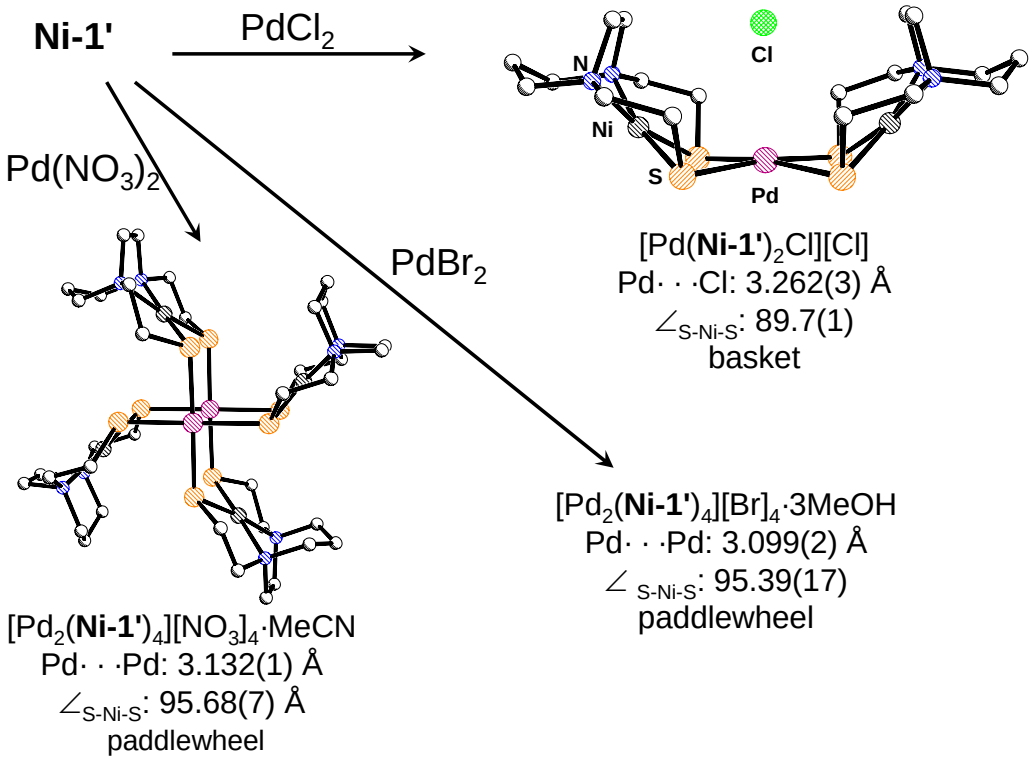

Figure V-8. Polymetallic clusters formed with **Ni-1'** when reacted with various palladium sources.

The complex $[Pd_2(\mathbf{Ni\text{-}1'})_4][Br]_4$ crystallizes in the triclinic space group *P*-1. The molecular structure of Pd_2Ni_4 cluster is shown in Figure V-9 as a thermal ellipsoid plot and selected metric parameters are listed in Table V-3. There are two molecular cations in the unit cell with four charge balancing bromide anions within the interstices. Each of the **Ni-1'** paddles are in their common configurations where the pendant thiolate arms are eclipsed. The six membered metallodiazacyclohexane rings are in a chair conformation. The Ni-N and Ni-S distances are essentially unchanged from their unbound forms. Like its Mo_2Ni_4 analog, a plane of symmetry exists perpendicular to the Pd-Pd rotation axis making the tetracation of nearly perfect C_{4h} symmetry.

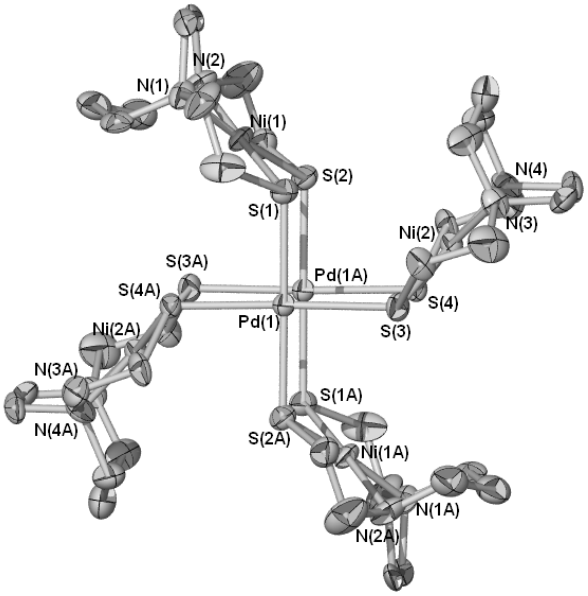

Figure V-9. Thermal ellipsoid plot (50% probability) of the $[Pd_2(\mathbf{Ni\text{-}1'})_4]^{4+}$ cation with hydrogen atoms omitted and select atoms labelled.

Table V-3. Selected metric parameters for $[Pd_2(\textbf{Ni-1'})_4][Br]_4$.

Pd(1)-Pd(1A)	3.099(2)	S(2)-Pd(1)-S(3)	88.79(14)
Pd(1)-S(2)	2.319(4)	S(2)-Pd(1)-S(1)	178.00(15)
Pd(1)-S(3)	2.329(4)	S(3)-Pd(1)-S(1)	90.82(14)
Pd(1)-S(1)	2.334(4)	S(2)-Pd(1)-S(4)	89.74(15)
Pd(1)-S(4)	2.345(4)	S(3A)-Pd(1)-S(4)	177.23(15)
		S(1A)-Pd(1)-S(4)	90.57(15)
Ni(1)-N(1)	1.916(12)		
Ni(1)-N(2)	1.948(14)	S(1)-Ni(1)-S(2)	95.60(15)
Ni(1)-S(1)	2.160(4)	S(3)-Ni(2)-S(4)	95.37(15)
Ni(1)-S(2)	2.167(4)		
Ni(2)-N(4)	1.921(12)		
Ni(2)-N(3)	1.930(12)		
Ni(2)-S(3)	2.141(4)		
Ni(2)-S(4)	2.144(4)		

The hexametallic cluster contains a Pd-Pd axis with four **Ni-1'** paddles comprised of NiN_2S_2 units which bind via sulfur donor atoms in a bidentate bridging manner to two palladium atoms spanning a distance of 3.099(2) Å. The two Pd^{II} ions are held in place by the four NiN_2S_2 "paddles"; there is no metal-metal bond. The Pd_2^{4+} coordination environment contains a Pd–Pd axis and eight sulfurs derived from four NiN_2S_2 bidentate bridging paddles. As in the structure with NO_3^-, the bromides are not bound to palladium. The Pd···Pd distances are largely the same as in the NO_3^- analog . The **Ni-1'** units coordinate to palladium with an average Pd-S distance of 2.333 Å. This distance is approximately 0.02 Å shorter than the Mo_2Ni_4 analog.

A survey of the literature reports six hexametallic clusters with a C_4 dipalladium unit ligated by nickel or palladium metallodithiolate ligands. The two shown in Figure V-10 are by Doug Stephan's and Takumi Konno's groups, respectively. Each complex is a C_4 paddlewheel made up of a dipalladium core ligated by four metallodithiolate ligands similar to the one reported in this work.[55,63] All metals are in a square planar environment with Pd---Pd distances ranging from of 3.02-3.19 Å. A variety of anionic

ligands were used to neutralize the charge. The Pd_2Ni_4 contribution from our laboratories is the median of metal-metal distances at 3.13 Å. All of the metalloligands are at a Pd-S distances of roughly 2.33 or 2.34 Å from the dipalladium core.

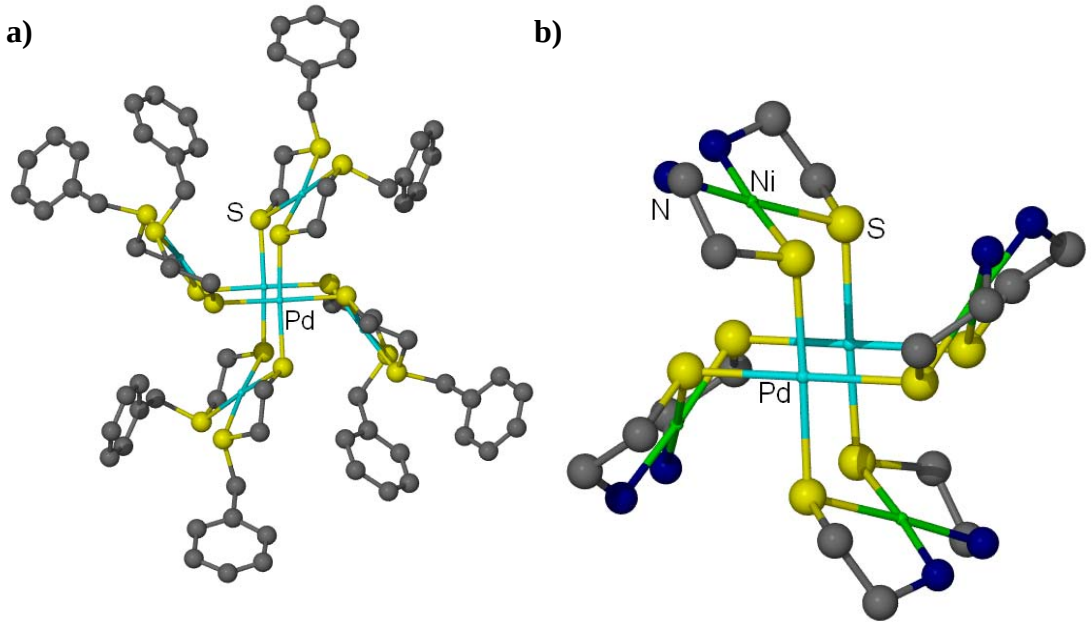

Figure V-10. Ball and stick representations of a) $[Pd_6(SCH_2CH_2SCH_2Ph)_8]^{4+}$ and b) $[Pd_2\{Ni(aet)_2\}_4]^{4+}$.

Experiments were performed to investigate whether the trimetallic, $[(\mathbf{Ni\text{-}1'})_2PdCl]^+$ could be converted to the paddlewheel structure. Reaction of $[(\mathbf{Ni\text{-}1'})_2PdCl]^+$ with $TlNO_3$ with ESI-MS as spectroscopic monitor revealed the isotopic envelope of $\{[Pd_2(\mathbf{Ni\text{-}1'})_4]^{4+}\}$ (m/z = 330) as the most abundant species, as well as the isotopic bundles of the hexametallic cluster in its mono-, di-, and tricationic states in much smaller abundances. Variable temperature NMR studies performed on $[(\mathbf{Ni\text{-}1'})_2PdCl]^+$ suggest there is no interconversion between $[(\mathbf{Ni\text{-}1'})_2PdCl]^+$ and the paddlewheel

structures as evidenced by no change in the ^{1}H NMR spectrum in the temperature range of 40 to -80ºC in CD_3OD at 400 MHz. This finding is confirmed by conductivity studies of $[(\mathbf{Ni\text{-}1'})_2PdCl]^+$ where a uni-uni electrolyte was reported indicating the chloride remained attached to the cluster in solution.[4] Thus it appears that the basket conformation is stabilized by the Pd-Cl interaction.

The efficacy of such non-classical ligands for metal-metal bonded units has been established for the hexametallic clusters with bond orders of four and zero. These compounds were produced by design, and they were characterized by x-ray diffraction analysis. The dirhodium analog, which has a bond order of one, will be discussed in Chapter VII.

CHAPTER VI

ELECTROCHEMISTRY

The trapping of exogenous metals by *cis*-thiolato complexes of nickel is the major feature of this dissertation. Changes in the nickel *cis*-thiolates upon derivatization at sulfur with reduction in the Ni-S π-electron density is quickly and easily probed using electrochemical methods. In collaboration with former postdoctoral researcher Dr. Jonghyuk Lee, the redox activities of several of the polymetallic clusters mentioned in this dissertation were characterized by cyclic and square wave voltammetry and are reported in this chapter.

Early studies of the metallated NiN_2S_2 aggregates addressed the issue of electrochemical reactions occurring at the NiN_2S_2 unit or at the exogenous, bound transition metal. As an approach to a background experiment, the $[(ZnCl)_2(\mathbf{Ni\text{-}1})_3]^{2+}$ C_3 paddlewheel type complex was prepared[7] and examined via electrochemical methods of cyclic and square wave voltammetry.[58] Figure VI-1 displays those results. The interpretation, also shown in Figure VI-1, is that successive uptake of 3 electrons occurs at three different nickel centers on intact clusters at potentials of -1.1, -1.3, and -1.5 V.

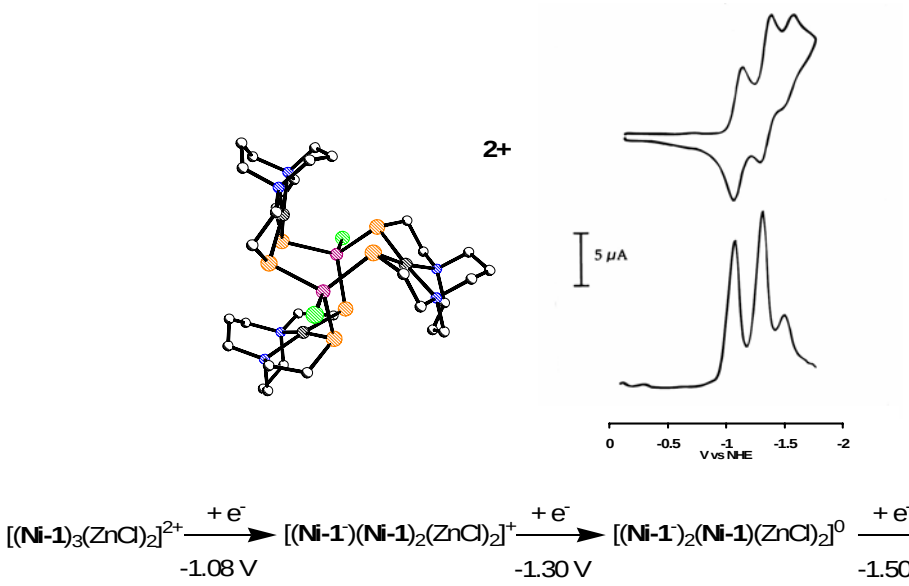

Figure VI-1. The $[(ZnCl)_2(\mathbf{Ni\text{-}1})_3]^{2+}$ reduction pathway.

This interpretation is generalized in Scheme VI-1 according to the upper track pathway for electron addition to intact clusters, without committing to a specific location of the added electrons. An alternate possibility follows the lower pathway where ligand loss with solvent molecule replacement could offer species with different reduction potentials. Scheme VI-2 addresses the specific sites of 1-electron reductions at the dimetal unit or at the bidentate bridging ligand. Clearly reduction of the $[(ZnCl)_2(\mathbf{Ni\text{-}1})_3]^{2+}$ compound is at the bidentate ligand rather than the dimetal site. Nevertheless, the particular pathway operative in Scheme VI-1 cannot be determined from studies that were published.[58]

Scheme VI-1. Redox activity and pathways for electron uptake by $M_2(L\text{-}L)_4$: Intact clusters or reduction with ligand loss.

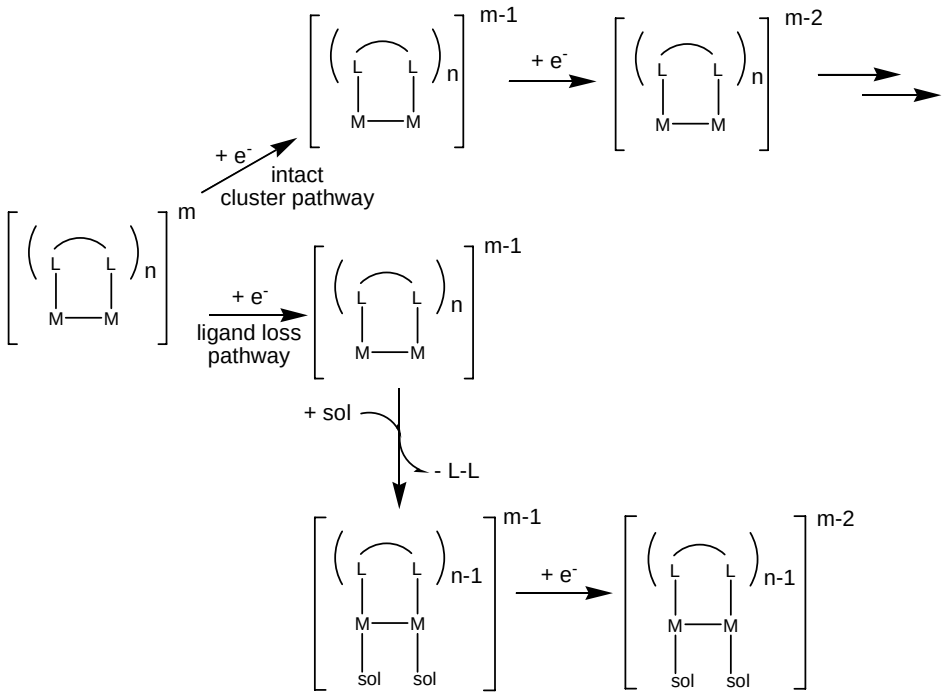

Scheme VI-2. Redox activity and pathways for electron uptake by $M_2(L\text{-}L)_4$: Alternate reduction sites, Dimetal unit vs. Nickel dithiolate ligand.

i) at M-M

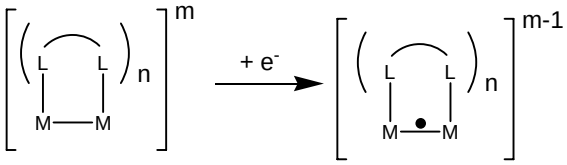

ii) at L-L

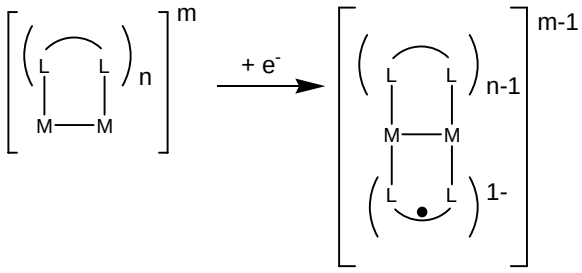

The cyclic and square wave voltammograms of the dimolybdenum complexes recorded at room temperature found multiple and overlapping redox events in the cathodic region. The CV and SWV of $[Mo_2(\mathbf{Ni\text{-}1'})_4]^{4+}$ are given in Chapter V as Figure V-7 and that of $[Mo_2(\mathbf{Ni\text{-}1})_4]^{4+}$ as Figures VI-2a and VI-2a'. While the redox events of the latter are severely overlapping, the SWV indicates similarity to the better-defined $[Mo_2(\mathbf{Ni\text{-}1'})_4]^{4+}$ congener. Within the MeCN solvent window, a total of six reductive events were observed for $[Mo_2(\mathbf{Ni\text{-}1})_4]^{4+}$ and $[Mo_2(\mathbf{Ni\text{-}1'})_4]^{4+}$, four of which were clearly defined and two that were of weaker intensity.

The cyclic voltammogram of the anodic region of $[Mo_2(\mathbf{Ni\text{-}1})_4][BF_4]_4$, shown in Figure VI-2a, shows four events labeled E_{pa1}- E_{pa4} in the range of 0.39 to 1.32 V. The event at E_{pa2} is reversible. The square wave corroborates these findings and shows the peak at E_{pa1} to be half the intensity of the other three peaks. The cyclic voltammogram cathodic region, shown in Figure VI-2b, is poorly defined yet reveals three reductions, of which the last is reversible. The square wave, which is vague, suggests the existence of six reductions of varying intensities labeled $E_{pc1} - E_{pc6}$ ranging from -0.71 to -2.11 V.

The cyclic voltammogram of the anodic region of $[Mo_2(\mathbf{Ni\text{-}1'})_4][BF_4]_4$, shown in Figure VI-2a', shows a reversible wave at E_{pa1} at 0.52 V, a quasireversible wave E_{pa2} at 1.01 V and an irreversible wave E_{pa3} at 1.38 V. These finding are in accordance with the SWV and finds three peaks of nearly equal intensity. The CV of the cathodic region finds multiple and overlapping redox events starting at –0.70 V and finishing at –2.11 V within the MeCN solvent window and are designated as $E_{pc1} - E_{pc6}$. The last wave (E_{pc6}) is at a slightly more negative potential than that of free **Ni-1'**. The square wave

voltammogram amplifies and separates these processes indicating six reductions, four of which that are quite distinct (E_{pc2} = -1.18 V, E_{pc4} = -1.43 V, E_{pc5} = -1.81 V, and E_{pc6} = -2.11) and two others (E_{pc1} = -0.70 V and E_{pc3} = -1.32 V) that are weak and poorly defined which are separated by 700 mV.

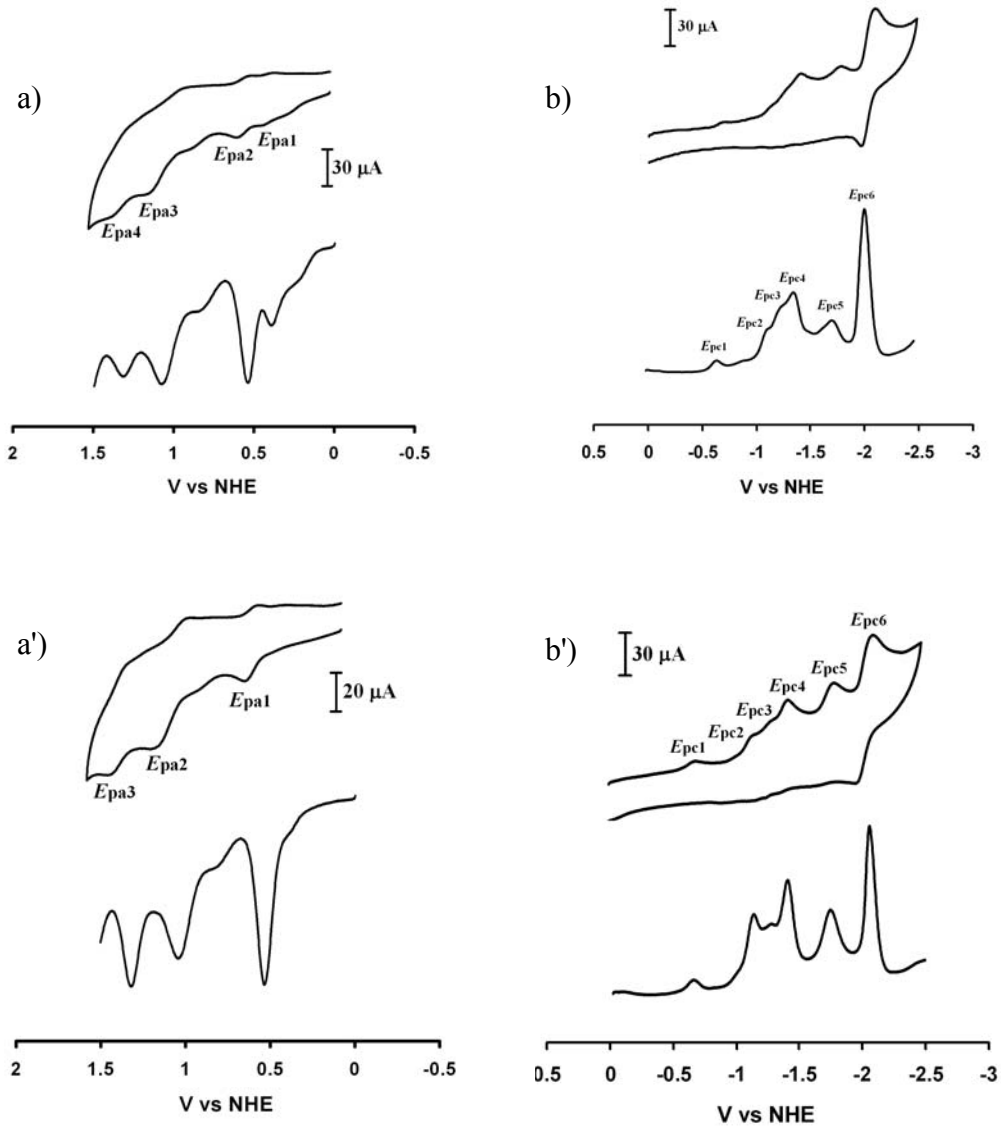

Figure VI-2. Cyclic and square wave voltammograms of the a) anodic and b) cathodic region of $[Mo_2(\mathbf{Ni\text{-}1})_4]^{4+}$ and the a') anodic and b') cathodic region of $[Mo_2(\mathbf{Ni\text{-}1'})_4]^{4+}$.

As mentioned above, the C_3 paddlewheel based on zinc, $[(ZnCl)_2(\mathbf{Ni\text{-}1})_3][BF_4]_2$, showed three cathodic events, assigned to successive reductions of **Ni-1** units attached to an intact Zn_2Ni_3 unit. This is reasonable as generation of an anionic NiN_2S_2 should favor binding to Zn^{2+}. Should this scenario apply to the C_4 dimolybdenum paddlewheel, the four distinct reductions would originate from the four **Ni-1** units; the two minor waves, separated by 700 mV, are reasonably attributed to the dimolybdenum unit. The latter possibility was supported by the redox behavior of the starting material $[Mo_2(MeCN)_{10}][BF_4]_4$ which shows under identical electrochemical conditions, two events in the cathodic region separated by ca. 700 mV. The $Mo_2(hpp)_4$ (hpp = the anion of 1,3,4,6,7,8-hexahydro-2H-pyrimido[1,2-a]pyrimidine), a neutral compound, also revealed two cathodic events at -0.44 and -1.27 V of similar separation.[60]

A bothersome issue for interpretation of the $[Mo_2(NiN_2S_2)_4]^{4+}$ CVs are the reduction events of major intensity at -2.1 V. As this position is similar to that of the free **Ni-1'** metallodithiolate ligand, see Figure VI-3, dissociation of NiN_2S_2 from the hexanuclear complex reasonably accounted for its presence. To examine this possibility further, several dimolybdenum complexes that contain fewer redox active nickel metallodithiolates were synthesized via the routes shown in Scheme VI-3.

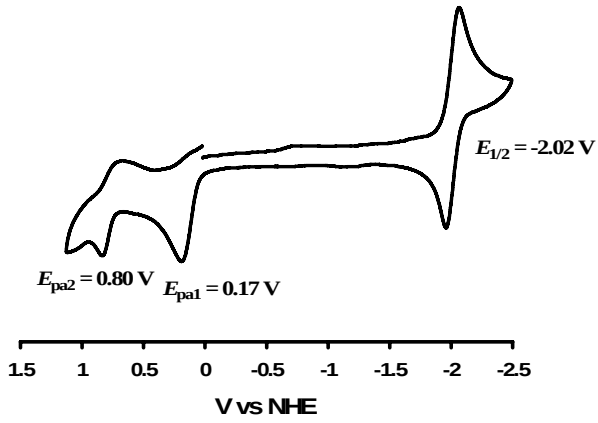

Figure VI-3. Cyclic voltammogram of a 1.0 mM MeCN solution of **Ni-1** in 0.1 M *n*-Bu_4NBF_4 at a scan rate of 200 mV/s.

Scheme VI-3. Synthetic route to the preparation of dimolybdenum complexes with fewer redox active ligands.

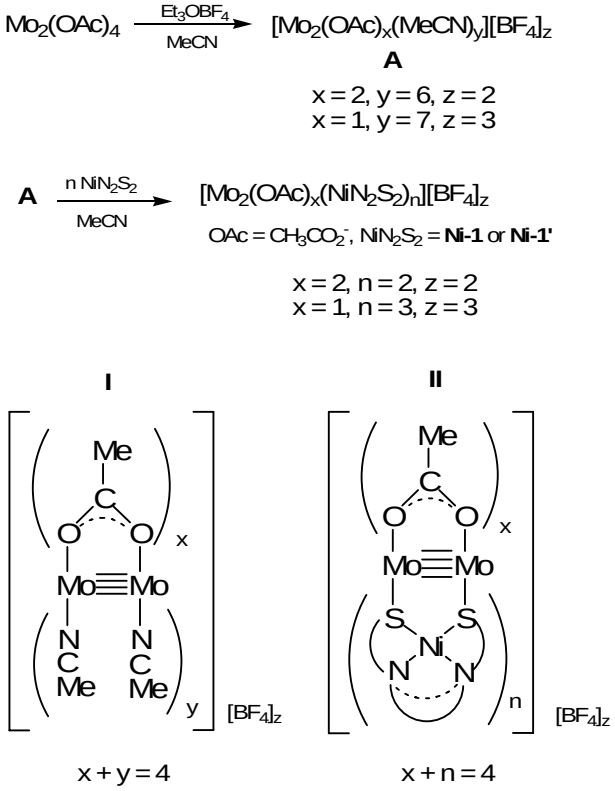

The mixed-ligand clusters are prepared by reacting $Mo_2(OAc)_4$, where OAc = acetate, with Et_3OBF_4 in a 1:2 or 1:3 ratio in a solution of MeCN to obtain the desired solvated dimolybdenum acetato synthon, where x = 2 and 1 for acetate and y = 6 and 7 for MeCN respectively, shown in **I** of Scheme VI-3. The acetate group is alkylated to produce ethyl acetate which removes it from the dimolybdenum unit forming open sites. These open sites are occupied by MeCN; the tetrafluoroborate ions neutralize the charge, z = 2 and 3. This material is then mixed with NiN_2S_2 (**Ni-1** or **Ni-1'**) in MeCN to produce the dimolybdenum acetato metallodithiolate mixed-ligand cluster labeled shown as **II** in the scheme as n = 2 or 3. The new polynuclear complexes are formulated to be $[Mo_2(OAc)_2(\mathbf{Ni\text{-}1})_2][BF_4]_2$, $[Mo_2(OAc)_2(\mathbf{Ni\text{-}1'})_2][BF_4]_2$, $[Mo_2(OAc)(\mathbf{Ni\text{-}1})_3][BF_4]_3$, and $[Mo_2(OAc)(\mathbf{Ni\text{-}1'})_3][BF_4]_3$.

As there are few reports in the area of such cluster electrochemistry, the results were gained along two lines. First, as just described, Mo_2^{4+} derivatives with fewer redox-active ligands were prepared. Secondly, other M_yNi_x complexes from our library formulated as $(CuBr)_2(\mathbf{Ni\text{-}1})_3$,[34] $[Pd_2(\mathbf{Ni\text{-}1'})_4][NO_3]_4$,[4] and $[Ag_2(\mathbf{Ni\text{-}1'})_3][NO_3]_2$ [9] were prepared and analyzed.

All cyclic voltammograms (CV) and square wave voltammograms (SWV) were recorded in MeCN containing 1.0 mM analyte and 0.1 M *n*-Bu_4NBF_4 supporting electrolyte at room temperature. Square wave voltammetry (SW) was used to enhance and corroborate complicated CVs. In the case of a reduction peak coupled with a return peak, the scan rate was varied in order to investigate reversibility of the wave. The cyclic voltammogram of free **Ni-1** is shown in Figure VI-3. The CV of **Ni-1** shows a

reversible wave at $E_{1/2}$ = -2.02 V assigned to the $Ni^{2+/1+}$ redox couple in the cathodic region. In the anodic region, there is an irreversible oxidation at E_{pa} = 0.17 V assigned to the oxidation of the thiolate to the thiyl radical,[61] a quasi-reversible wave assigned to the $Ni^{2+/3+}$ redox couple is at 0.80 V.[12,64]

The CV and SWV plots in the cathodic region for the starting material $[Mo_2(CH_3CN)_{10}][BF_4]_4$ used for the syntheses of $[Mo_2(\mathbf{Ni\text{-}1})_4][BF_4]_4$ and $[Mo_2(\mathbf{Ni\text{-}1'})_4][BF_4]_4$ was obtained for comparison to the hexametallic products and is shown in Figure VI-4. The CV of $[Mo_2(CH_3CN)_{10}][BF_4]_4$ scanned from 1.5 to -2.0 V shows only two events. Reversible and irreversible reductions are found at $E_{1/2}$ = -0.21 V and E_{pc} = -0.96 V respectively, which are separated by approximately 700 mV. The reduction peak at -0.25 V is coupled to a return peak E_{pa} at -0.18 V. The SWV verifies the presence of the reductions. Interestingly, however, the SWV also shows an additional peak at -0.69 V, a peak that is poorly defined in the CV. The reduction process occurring at -0.69 V is not consistently reproducible and has been not been assigned. The response is often very small, and we conclude it to be an impurity or decomposition product.

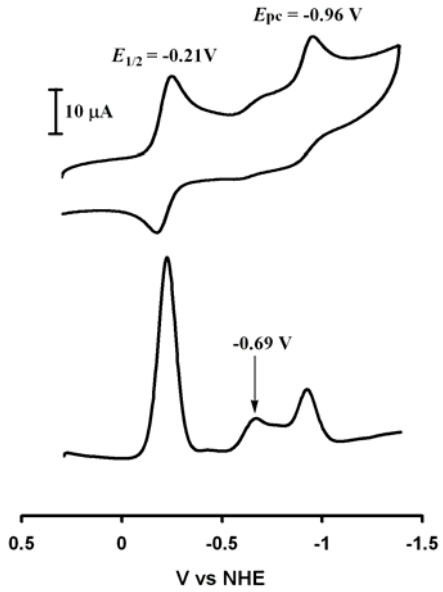

Figure VI-4. Cyclic and square wave voltammograms in the cathodic region of a 1.0 mM solution of $[Mo_2(MeCN)_{10}][BF_4]_4$ in 0.1 M *n*-Bu_4NBF_4 at a scan rate of 200 mV/s.

For purpose of comparison to the $[Mo_2(NiN_2S_2)_4][BF_4]_4$ complexes, the acetate substituted analogs were analyzed under identical conditions. Cyclic voltammetric analysis of the cathodic region of $[Mo_2(\mathbf{Ni\text{-}1'})_3(OAc)][BF_4]_3$ seen in Figure VI-5 shows two irreversible reductions at E_{pc2} = -1.32 V and E_{pc3} = -1.45 V and a reversible wave at E_{pc5} = -2.04 V. The SWV confirms these three reductions and shows E_{pc5} to be nearly twice the size of E_{pc2} and E_{pc3}. In addition to the three peaks of strong intensity, the SW finds two weak, ill-defined peaks at E_{pc1} = -0.69 V and E_{pc4} = -1.76 V. The SW also shows a pattern similar to that of $[Mo_2(\mathbf{Ni\text{-}1'})_4][BF_4]_4$. The peaks E_{pc1} and E_{pc2} of the Mo_2Ni_3 system have the same potential as E_{pc1} and E_{pc3} of the Mo_2Ni_4 system. Analysis of the anodic region shown in Figure VI-6 reveals a distinct reversible wave at E_{pa} = 0.56V.

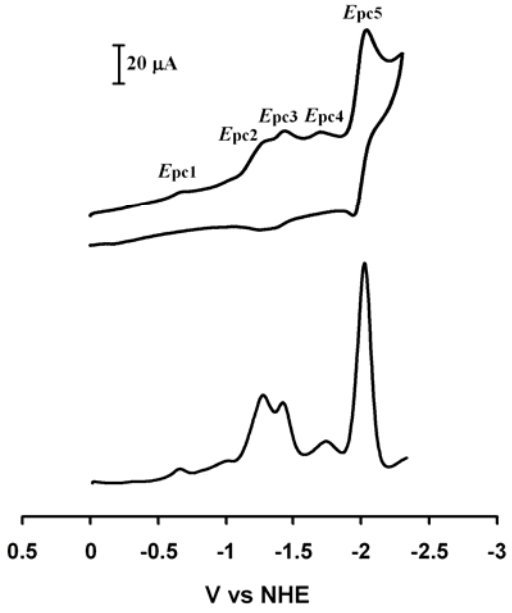

Figure VI-5. Cyclic and square wave voltammograms of the cathodic region of a 1.0 mM solution of $[Mo_2$ (**Ni-1'**$)_3$(OAc)][BF_4]$_3$ in 0.1 M *n*-Bu_4NBF_4 at a scan rate of 200 mV/s.

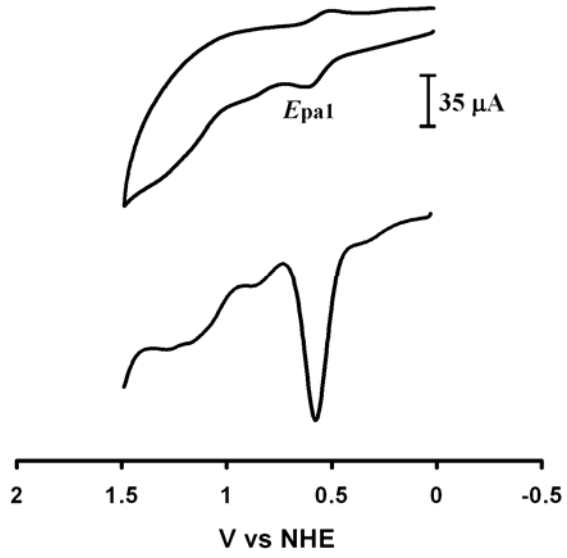

Figure VI-6. Cyclic and square wave voltammograms of the anodic region of a 1.0 mM solution of [Mo_2 (**Ni-1'**$)_3$(OAc)][BF_4]$_3$ in 0.1 M *n*-Bu_4NBF_4 at a scan rate of 200 mV/s.

Cyclic voltammetric analysis of $[Mo_2(\mathbf{Ni\text{-}1}')_2(OAc)_2][BF_4]_2$ resulted in irreproducible data and from this we conclude the compound to be unstable in solution. Despite the irreproducibility, a reversible wave was observed and found at the same potential as free ligand. The SWV consistently found four electrochemical events and showed a peak pattern similar to that of the Mo_2Ni_4 and Mo_2Ni_3 systems. The first two events (E_{pc1} = -0.69 V and E_{pc2} = -1.35 V) were poorly defined and exhibited a similar 700 mV separation.

In summary, the Mo_2Ni_4, Mo_2Ni_3L, and $Mo_2Ni_2L_2$ clusters all display multiple and overlapping waves in both the cathodic and anodic regions as shown by cyclic voltammetry. The most negative redox event of each complex is reversible and found at approximately -2.0 V, a potential which is more negative than the free NiN_2S_2 ligand. The anodic region shows one reversible event at approximately 0.50 V. Lastly, the SWVs all display multiple peaks of varying intensities. The weak and poorly defined peaks all exhibit a separation of 700 mV.

Electrochemical analysis of various paddlewheel clusters bridged by NiN_2S_2 ligands

It has been established that NiN_2S_2 adducts of Cu^I are extremely stable with log $\beta_{3,2}$ binding constants for the $(CuBr)_2(\mathbf{Ni\text{-}1})_3$ cluster of >30.[9] Thus it is reasonable to expect minor dissociation of $(CuBr)_2(\mathbf{Ni\text{-}1})_3$ in solution. The cyclic voltammogram of $(CuBr)_2(\mathbf{Ni\text{-}1})_3$, seen in Figure VI-7, shows two reversible waves in the cathodic region at E_{pc1} = -1.35 V and E_{pc2} = -2.01 V. The SWV corroborated these results and shows

two peaks of nearly equal intensity. Analysis of the anodic region, shown in Figure VI-8, reveals three irreversible oxidations at E_{pa1} = 0.25 V, E_{pa2} = 0.60 V, and E_{pa3} = 1.25 V.

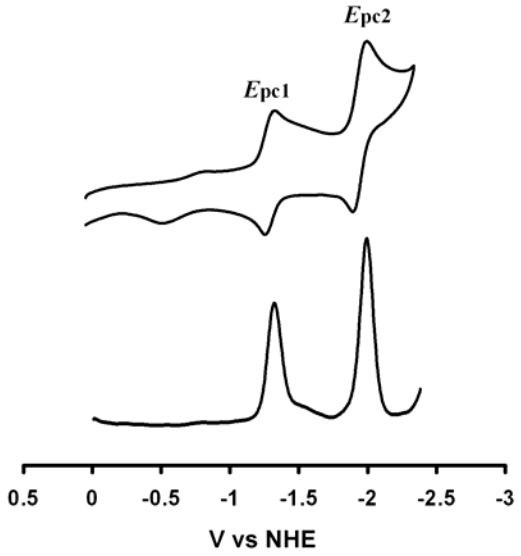

Figure VI-7. Cyclic and square wave voltammograms of the cathodic region of a 1.0 mM solution of $(CuBr)_2$(**Ni-1**)$_3$ in 0.1 M *n*-Bu_4NBF_4 at a scan rate of 200 mV/s.

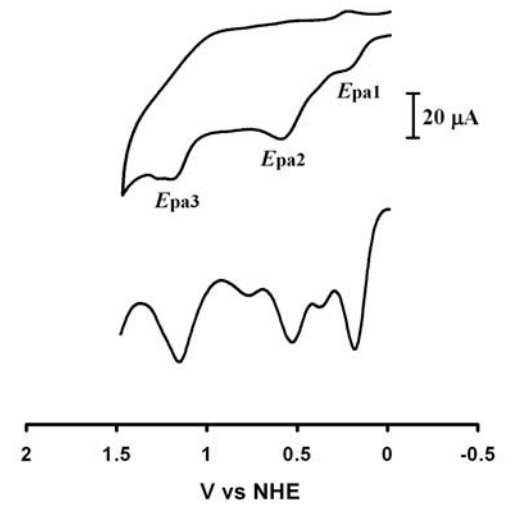

Figure VI-8. Cyclic and square wave voltammograms of the anodic region of a 1.0 mM solution of $(CuBr)_2$(**Ni-1**)$_3$ in 0.1 M *n*-Bu_4NBF_4 at a scan rate of 200 mV/s.

Much like the copper cluster, NiN_2S_2 adducts of Ag^I have been found to be extremely stable showing log $\beta_{3,2}$ binding constants for the $[Ag_2(\mathbf{Ni\text{-}1'})_3][NO_3]_2$ cluster of 26 [9] making it reasonable to expect little dissociation of the cluster in solution. The cyclic voltammogram of $[Ag_2(\mathbf{Ni\text{-}1'})_3][NO_3]_2$, displayed in Figure VI-9, shows an irreversible wave and a reversible wave designated as E_{pc1} = -1.40 V and E_{pc2} = -2.04 V. These findings agreed with the SWV; however, SWV shows E_{pc1} to be half the size of E_{pc2}. Analysis of the oxidative region, shown in Figure VI-10, reveals an irreversible wave at E_{pa} = 0.90 V.

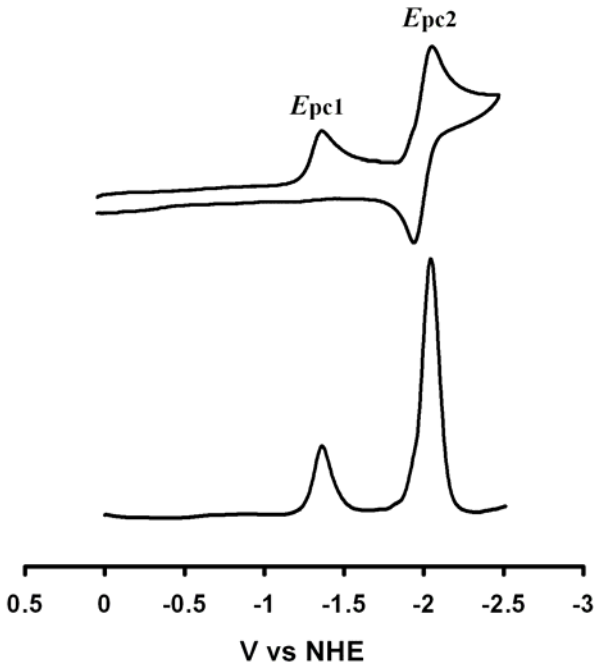

Figure VI-9. Cyclic and square wave voltammograms of the cathodic region of a 1.0 mM solution of $[Ag_2(\mathbf{Ni\text{-}1'})_3][NO_3]_2$ in 0.1 M *n*-Bu_4NBF_4 at a scan rate of 200 mV/s.

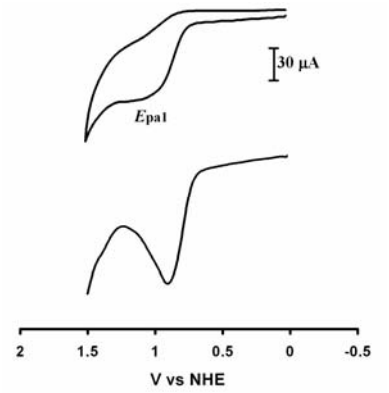

Figure VI-10. Cyclic and square wave voltammograms of the anodic region of a 1.0 mM solution of $[Ag_2(\textbf{Ni-1}')_3][NO_3]_2$ in 0.1 M *n*-Bu_4NBF_4 at a scan rate of 200 mV/s.

The cyclic voltammogram of $[Pd_2(\textbf{Ni-1}')_4][NO_3]_4$, shown in Figure VI-11, is obscure but shows two definite irreversible reductions designated as E_{pc2} = -1.09 V and E_{pc3} = -1.41 V. The reduction wave E_{pc2} has a shoulder labeled as E_{pc1} = -1.00 V. Lastly, there is a reversible reduction at E_{pc4} = -2.03 V. The SWV shows three distinct peaks, E_{pc1} and $E_{pc3,}$ of nearly equal intensity. The intensity of E_{pc4} is of much greater intensity than E_{pc1} and E_{pc3} combined. Analysis of the oxidative region, shown in Figure VI-12, reveals a quasi-reversible wave at E_{pa} = 0.77 V.

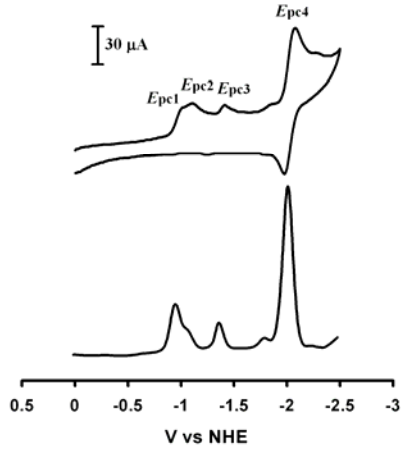

Figure VI-11. Cyclic and square wave voltammograms of the cathodic region of a 1.0 mM solution $[Pd_2(\textbf{Ni-1}')_4][NO_3]_4$ in 0.1 M *n*-Bu_4NBF_4 at a scan rate of 200 mV/s.

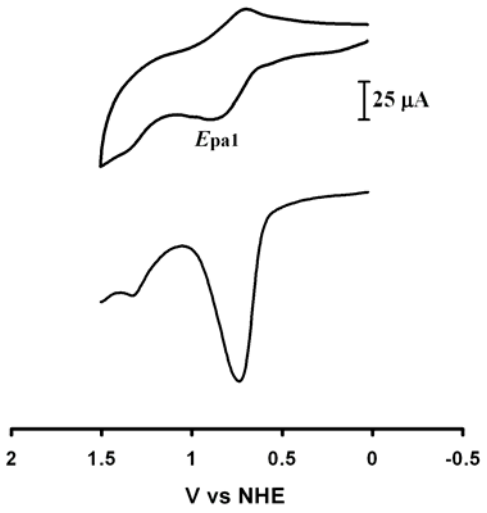

Figure VI-12. Cyclic and square wave voltammograms of the anodic region of a 1.0 mM solution $[Pd_2(\textbf{Ni-1}')_4][NO_3]_4$ in 0.1 M *n*-Bu_4NBF_4 at a scan rate of 200 mV/s.

Each of the paddlewheel complexes exhibits multiple redox events in the cathodic region. In the case of Cu_2 and Ag_2, only two reductions are observed within the MeCN solvent window while the Pd_2 complex is rather unclear. Each of the complexes shows at least one event in the anodic region. The exception to this is the Cu_2 complex which shows multiple events of varying intensity.

Ligand exchange and spiking studies

Since there were indications of NiN_2S_2 ligand dissociation in the electrochemistry of the $[Mo_2(NiN_2S_2)_4]^{4+}$ clusters, as evidenced by the prominent reduction feature that coincided with the potential of the free NiN_2S_2 ligand, experiments were designed to establish ligand loss in the $[Mo_2(NiN_2S_2)_4]^{4+}$ complexes. A MeCN solution of $[Mo_2(\textbf{Ni-1}')_4][BF_4]_4$ was mixed with one equivalent of **Ni-1** and stirred

overnight at room temperature. A solid sample was isolated by removing the solvent *in vacuo* and analyzed via ESI-MS. The results of this study are shown in Table VI-1. The signal of major abundance was a trinickel species, (**Ni-1**)$_2$Ni^{2+} (*m/z* = 320), which indicates the loss of ligand from the dimolybdenum unit as well as removal of nickel from the N_2S_2 core. The presence of several dimolybdenum mixed-ligand species ([Mo$_2$(**Ni-1'**)$_2$(**Ni-1**)$_2$](BF$_4$)$^{3+}$, [Mo$_2$(**Ni-1**)$_4$](BF$_4$)$_2^{2+}$, and [(**Ni-1**)$_2$Ni](BF$_4$)$^+$) suggests the possibility of ligand exchange. This finding is entirely reasonable. We know from Chapter III which described the study of the electron-donating ability of NiN_2S_2 ligands in the series of (NiN_2S_2)W(CO)$_4$ complexes that **Ni-1** and **Ni-1'** are quite similar.[30,41]

In fact, analysis of **Ni-1** by itself under identical conditions finds the parent compound in major abundance at *m/z* = 297 corresponding to the (**Ni-1** + Li)$^+$ molecular ion. In addition to the parent compound, the trinickel species, *m/z* = 320 (10.4%), was found as well as a degraded **Ni-1** species with only one pendant thiolate arm at *m/z* = 233 (7.29%). The possibility of ligand lability in solution is a likely cause for the difficulty in the assignment of redox events in the electrochemical studies.

Table VI-1. Results of the ligand exchange experiment using $[Mo_2(\textbf{Ni-1'})_4][BF_4]_4$ and **Ni-1** as analyzed via ESI-mass spectrometry.

species	mass	% abundance
$[(\textbf{Ni-1})_2Ni]^{2+}$	320	100
$[Mo_2(\textbf{Ni-1'})_4]^{4+}$	339	7.58
$[Mo_2(\textbf{Ni-1'})_2(\textbf{Ni-1})_2](BF_4)^{3+}$	472	3.03
$[Mo_2(\textbf{Ni-1})_4](BF_4)_2^{2+}$	765	3.03
$[(\textbf{Ni-1})_2Ni](BF_4)^{+}$	727	1.82
$[(\textbf{Ni-1'})_2Ni](BF_4)^{+}$	700	0.121

The possibility of ligand dissociation suggested by the final reversible wave at or beyond the potential of free ligand was investigated further by 'spiking' the electrochemical solutions of $[Mo_2(\textbf{Ni-1})_4][BF_4]_4$ and $[Mo_2(\textbf{Ni-1'})_4][BF_4]_4$ with free NiN_2S_2. The CVs of the reduction region for these complexes shows slight enhancements to the reversibility of the last redox event; however, the effects of the spiking experiments are much more prominent in the oxidative region. Figure VI-13 shows the SWV of $[Mo_2(\textbf{Ni-1})_4][BF_4]_4$ spiked with a 1 mM equivalent of **Ni-1**. When **Ni-1** is reduced at -2.03 V, it is believed Ni^{2+} is released from the N_2S_2 core and free dithiolate oxidized to thiyl radical on the return sweep at 0.17 V (Figure VI-13a). As shown in the ligand labilization studies, free Ni^{2+} is metalated by NiN_2S_2 to form a trinickel species. Due mostly to the insolubility of **Ni-1'** in MeCN solution, spiking the electrochemical solution with **Ni-1'** showed only slight differences observed in the CV and SWV. This is in vast contrast to the **Ni-1** analog where the shape of the final wave was enhanced and showed greater reversibility. In addition, the SWV shows the growth of an electrochemical event at 0.17 V (Figure VI-13c) indicative of disulfide that is not

seen in either $[Mo_2(\mathbf{Ni\text{-}1})_4][BF_4]_4$ (Figure VI-13b) or $[Mo_2(\mathbf{Ni\text{-}1'})_4][BF_4]_4$. The absence of a response at 0.17 V would indicate no formation of disulfide or diffusion of NiN_2S_2 into bulk solution before the anodic potential is reached.

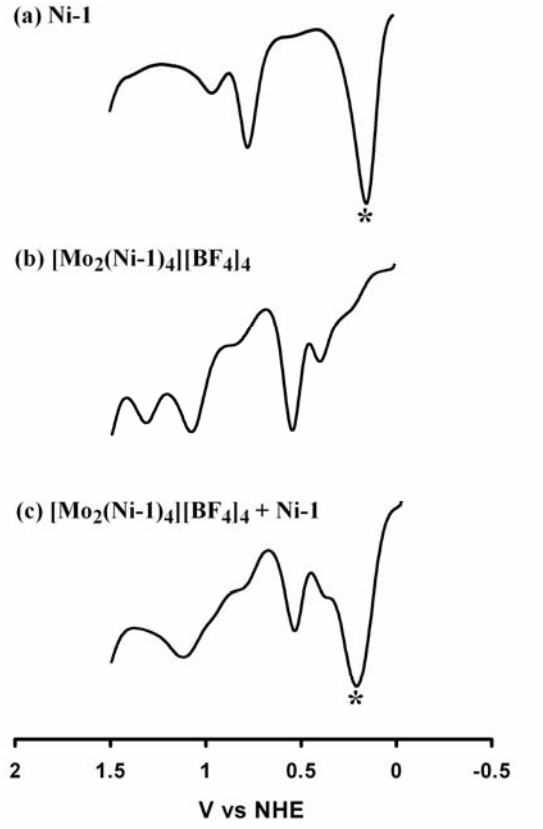

Figure VI-13. Square wave voltammograms of a) **Ni-1**, b) $[Mo_2(\mathbf{Ni\text{-}1})_4][BF_4]_4$, and c) spiked solution of $[Mo_2(\mathbf{Ni\text{-}1})_4][BF_4]_4$. The asterisk indicates the location of thiolate oxidation to thiyl radical.

Solvent effects

To investigate the possibility of ligand dissociation, partial or completely, the Mo_2Ni_x complexes were subjected to electrochemical studies performed in poor or noncoordinating solvents (ε = dielectric constant), i.e., CH_2Cl_2 (ε = 8.93), THF (ε = 7.58), and DMF (ε = 36.71) under identical conditions as the study in MeCN (ε = 38.8).

The complexes exhibited poor solubility in CH_2Cl_2 and THF; however, in DMF, solubility is akin to MeCN. In all cases, CH_2Cl_2 as solvent produced results which were uninterpretable attributed to a lack of solubility. For comparison, the metalldithiolate ligand **Ni-1** displays reversible waves at -2.01 and -1.91 V in DMF and THF solvents respectively as shown in Figure VI-14.

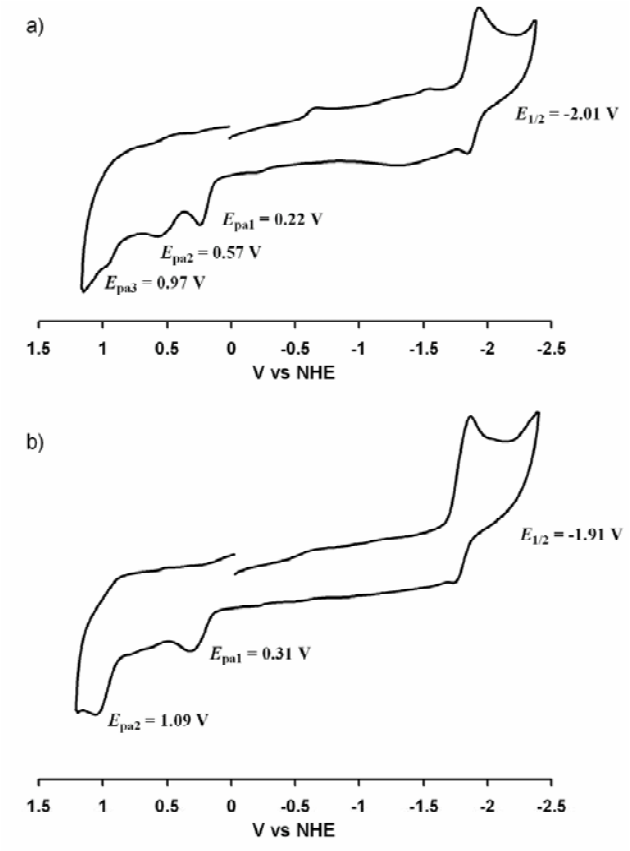

Figure VI-14. Cyclic voltammograms of a 1.0 mM solution of **Ni-1** at scan rates of 200 mV/s a) 0.1 M *n*-Bu_4NBF_4 in DMF and b) 0.2 M *n*-Bu_4NBF_4 in THF.

The CV analysis of $[Mo_2(\mathbf{Ni\text{-}1'})_4][BF_4]_4$ in THF exhibited four irreversible events assigned as E_{pc1} = -0.68, E_{pc2} = -1.14, E_{pc3} = -1.62, and E_{pc4} = -2.04 V as shown in Figure VI-15. This finding was corroborated with SWV which showed four peaks of

nearly equal intensity. When the complex was examined in DMF under identical conditions, shown in Figure VI-16, four irreversible events were observed designated as E_{pc1} = -0.36, E_{pc2} = -0.85, E_{pc3} = -0.98, and E_{pc4} = -1.29 V respectively. In addition, two reversible events were observed at $E^1_{1/2}$ = -1.70 and $E^2_{1/2}$ = -2.22.

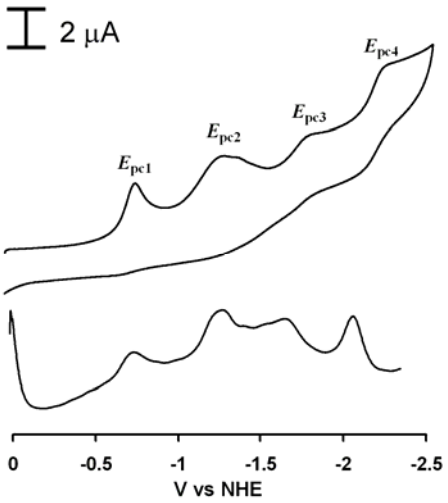

Figure VI-15. Cyclic and square wave voltammograms of the cathodic region of a 1.0 mM THF solution of $[Mo_2(\mathbf{Ni\text{-}1}')_4][BF_4]_4$ in 0.1 M *n*-Bu_4NBF_4 at a scan rate of 20 mV/s.

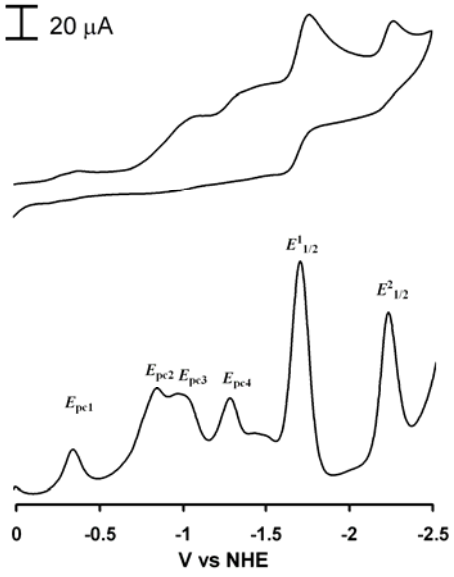

Figure VI-16. Cyclic and square wave voltammograms of the cathodic region of a 1.0 mM DMF solution of $[Mo_2(\textbf{Ni-1}')_4][BF_4]_4$ in 0.1 M *n*-Bu_4NBF_4 at a scan rate of 100 mV/s.

The CV of $[Mo_2(OAc)(\textbf{Ni-1}')_3][BF_4]_3$ recorded in THF, shown in Figure VI-17, reveals three irreversible events at E_{pc1} = -1.10, E_{pc2} = -1.28, and E_{pc3} = -2.01 V. SWV analysis corroborates these results and finds E_{pc1} and E_{pc2} to be half the size of E_{pc3}. When the Mo_2Ni_3 complex was examined in DMF (Figure VI-18), five irreversible reductions are observed designated as E_{pc1} = -0.91, E_{pc2} = -1.03, E_{pc3} = -1.65, E_{pc4} = -2.18, and E_{pc5} = -2.46 V. The SWV confirms these findings and finds E_{pc3} to be twice as intense as the remaining four peaks.

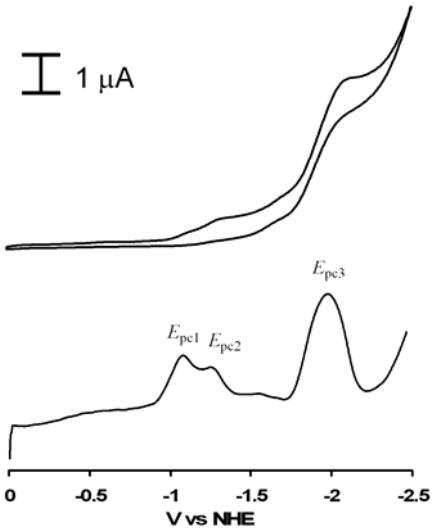

Figure VI-17. Cyclic and square wave voltammograms of the cathodic region of a 1.0 mM THF solution of $[Mo_2(OAc)(\textbf{Ni-1}')_3][BF_4]_3$ in 0.1 M *n*-Bu_4NBF_4 at a scan rate of 20 mV/s.

The CV of $[Mo_2(OAc)_2(\textbf{Ni-1}')_2][BF_4]_2$ in THF gave poor results; however, the SW suggests the existence of two or three reduction events. In DMF (Figure VI-19), three irreversible events at E_{pc1} = -0.88, E_{pc2} = -1.61, and E_{pc3} = -2.14 V, respectively are observed. The SWV confirms these findings and shows the wave labeled E_{pc2} is nearly three times the intensity of the other two peaks.

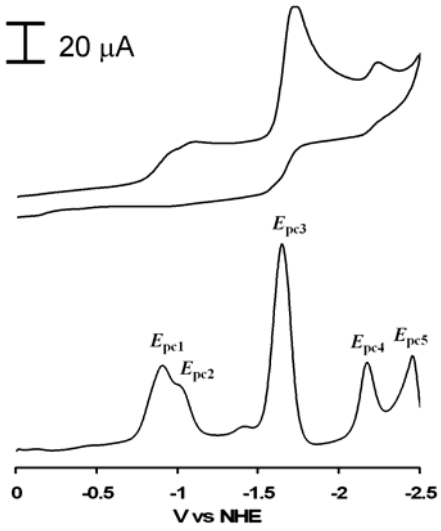

Figure VI-18. Cyclic and square wave voltammograms of the cathodic region of a 1.0 mM DMF solution of $[Mo_2(OAc)(\textbf{Ni-1}')_3][BF_4]_3$ in 0.1 M *n*-Bu_4NBF_4 at a scan rate of 100 mV/s.

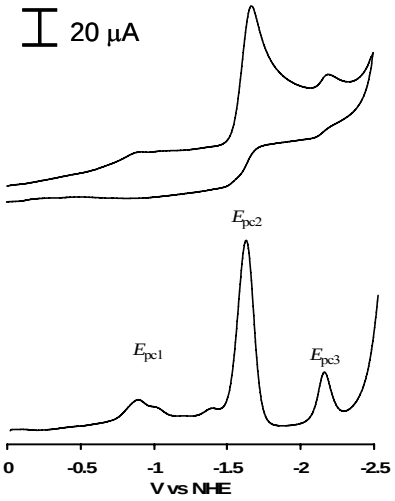

Figure VI-19. Cyclic and square wave voltammograms of the cathodic region of a 1.0 mM DMF solution of $[Mo_2(OAc)_2(\textbf{Ni-1}')_2][BF_4]_4$ in 0.1 M *n*-Bu_4NBF_4 at a scan rate of 100 mV/s.

The cyclic voltammograms of the Mo_2Ni_4 performed in MeCN (Figure VI-2b') and DMF (Figure VI-16) show striking similarity. Each CV reveals a total of six

multiple and overlapping redox events with the SWV showing a combination of strong and weak intensity peaks. However, when the CV and SWV are recorded in THF, only four equal intensity irreversible events are seen. This could suggest that the greater coordinating solvents, MeCN and DMF, promote partial dissociation of the metalloligands.

The CVs of Mo_2Ni_3 and Mo_2Ni_2 performed in DMF show striking similarity to those in MeCN. The CVs show more redox events than available redox active ligands bound to the dimetal unit. In fact, the CVs performed in THF, a poor coordinating solvent, have an equal number of redox events and redox active ligands. More importantly, all three complexes, Mo_2Ni_4, Mo_2Ni_3, and Mo_2Ni_2, exhibit one redox event, typically the median potential, ca. -1.6 V, which is much larger than the other events. This might suggest decomposition or a major structural rearrangement which liberates free ligand. This possibility is supported by multiple attempts to structurally characterize the mixed-ligand species in MeCN resulting in the Mo_2Ni_4 species. Figure VI-20 depicts the proposed and expected molecular structures of the Mo_2Ni_2 and Mo_2Ni_3 complex cations. For the Mo_2Ni_2 structure (Figures VI-20a and b), the steric influence of the NiN_2S_2 unit on the acetate ligand in *cis* and *trans* isomers appears to be about the same. By inspection, no one preferred isomer can be determined. On the other hand, the Mo_2Ni_3 structure (Figure VI-20c) may incur some steric hinderance by the NiN_2S_2 unit.

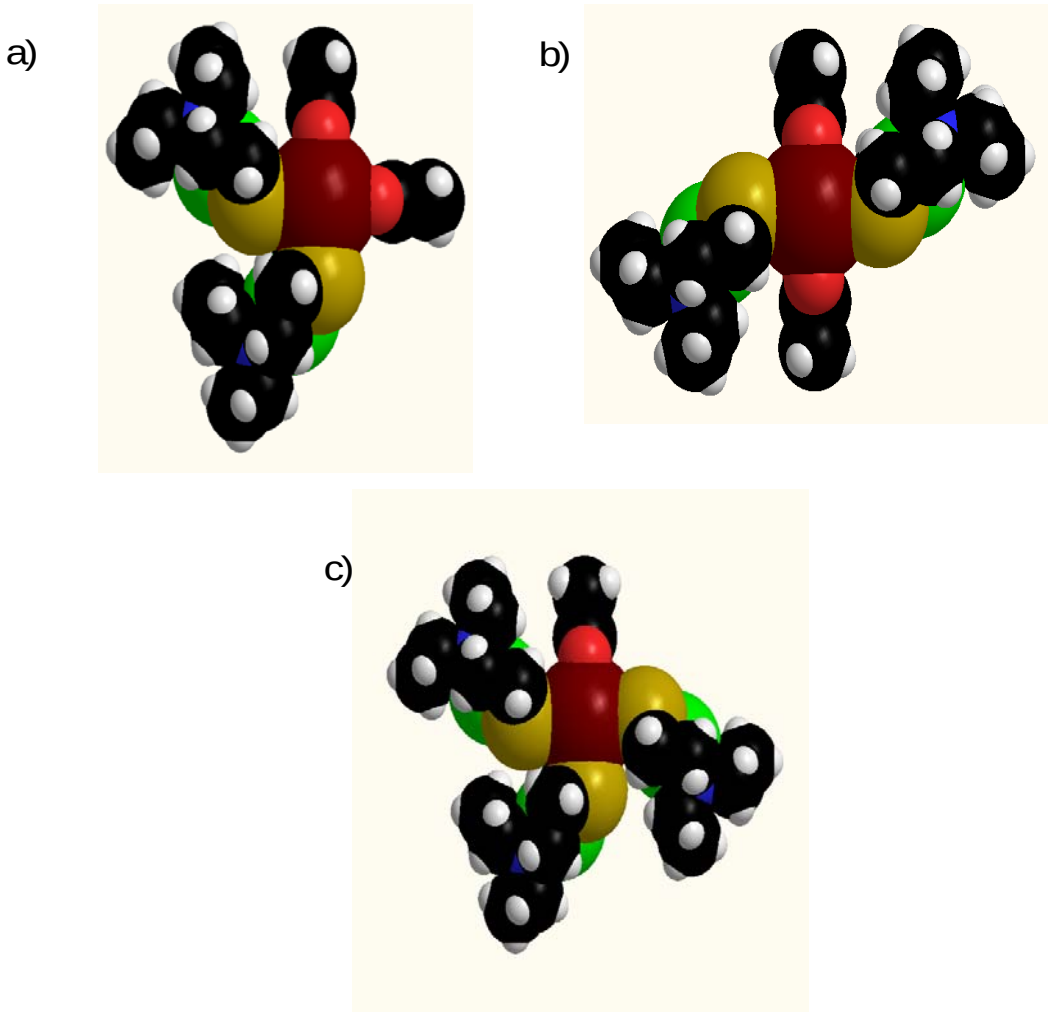

Figure VI-20. Proposed molecular structures of a) *cis*- b) *trans*-$[Mo_2(OAc)_2(\mathbf{Ni\text{-}1})_2]^{2+}$. Expected molecular structure of c) $[Mo_2(OAc)(\mathbf{Ni\text{-}1})_3]^{3+}$. All structures are shown as space filling models.

Other complexes as controls, $[Mo_2(ZnN_2S_2)_4]^{4+}$ and $Mo_2(ZnN_2S_2Cl)_4$

To verify the existence of dimolybdenum reduction in the Mo_2Ni_4 species, an approach similar to the one taken in the Zn_2Ni_3 complex was attempted. Synthesis of dimolybdenum complexes which utilize ZnN_2S_2 complexes[7,65] as ligands from our collection, aptly named **Zn-1** and **Zn-1'** after their nickel congeners, was attempted. As hypothesis, Zn^{2+} of the ZnN_2S_2 unit, is redox inactive and sulfur oxidation occurs at 0.17

V based on findings from the **Ni-1** and **Ni-1'**; therefore, any redox events that are observed would have to belong to the dimolybdenum unit.

Reaction **1**, shown in Scheme VI-4, was attempted by refluxing a chloride salt (Li or PPN) in a 2:1 ratio with $(ZnN_2S_2)_2$ in MeCN overnight with the intention of synthesizing an anionic metallodithiolate chloride that would be less likely to dissociate from the dimetal unit. The solvent was removed *in vacuo* and the white solid that remained was analyzed via ESI-MS. Analysis found no identifiable peaks indicative of the $[ZnN_2S_2Cl]^-$ species or the starting material. As a result, reaction **2** could not be performed.

Reaction **3** was performed by reacting $[Mo_2(MeCN)_8]^{4+}$ and $(ZnN_2S_2)_2$ in a 1:2 ratio in MeCN. The royal blue dimolybdenum solution was transferred to a flask containing the clear zinc compound which immediately formed a dark green solution. After stirring for three hours, the solvent was removed *in vacuo* and the remaining solid analyzed via ESI-MS. There were no clusters in the mass spectrum matching the isotopic envelope of Mo_2Zn_4 or any species that could be identified.

Scheme VI-4. Attempted (failed) syntheses performed to elucidate the existence of a dimolybdenum reduction for the Mo_2Ni_4 complex.

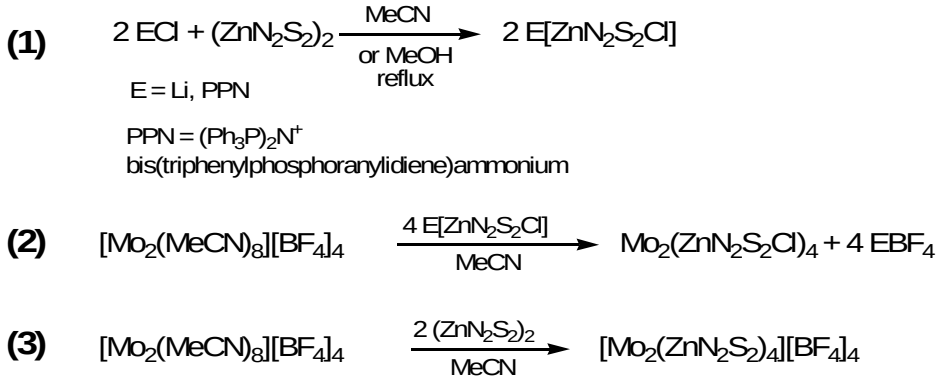

Mo_2Ni_4 clusters in perspective: overview of electrochemistry of C_3 and C_4 paddlewheels

The observation of multiple redox events in the cathodic region for the complexes analyzed in this study is similar to the $[(ZnCl)_2(\textbf{Ni-1})_3][BF_4]_2$ complex. For this complex, the successive redox events were assigned to reductions of Zn-bound NiN_2S_2 units. The most negative feature of the CV is 500 mV more positive than the **Ni-1** reduction potential. While it would be reasonable to suggest that the new paddlewheel complexes behave in a similar fashion, the consistent observation of reversible redox events at potentials near and in cases beyond that of the free ligand indicated NiN_2S_2 dissociation. A summary of the reductions and oxidations of the preceding electrochemical series are shown in Tables VI-2 and 3 respectively.

Table VI-2. Summary of electrochemical reductions for the complexes utilized in the paddlewheel series performed in MeCN (potentials shown in volts). Potentials in bold at or beyond the potential for free NiN_2S_2 ligand. Potentials in italics are proposed dimolybdenum reductions

	E_{pc1}	E_{pc2}	E_{pc3}	E_{pc4}	E_{pc5}	E_{pc6}
$[(ZnCl)_2(\textbf{Ni-1})_3][BF_4]_2$	-1.08	-1.30	-1.50			
$(CuBr)_2(\textbf{Ni-1})_3$	-1.35	**-2.01**				
$[Ag_2(\textbf{Ni-1'})_3][NO_3]_2$	-1.40	**-2.04**				
$[Pd_2(\textbf{Ni-1'})_4][NO_3]_4$	-1.00	-1.09	-1.41	**-2.03**		
$[Mo_2(\textbf{Ni-1})_4][BF_4]_4$	*-0.71*	-1.19	*-1.33*	-1.43	-1.80	**-2.11**
$[Mo_2(\textbf{Ni-1'})_4][BF_4]_4$	*-0.70*	-1.18	*-1.32*	-1.43	-1.81	**-2.11**
$[Mo_2(OAc)(\textbf{Ni-1})_3][BF_4]_3$	*-0.69*	-1.30	*-1.45*	-1.76	**-2.04**	

Table VI-3. Summary of electrochemical oxidations for the complexes utilized in the paddlewheel series performed in MeCN (potentials shown in volts).

	E_{pa1}	E_{pa2}	E_{pa3}	E_{pa4}
$(CuBr)_2$(**Ni-1**)$_3$	0.25	0.60	1.25	
$[Ag_2$(**Ni-1'**)$_3][NO_3]_2$	0.90			
$[Pd_2$(**Ni-1'**)$_4][NO_3]_4$	0.77			
$[Mo_2$(**Ni-1**)$_4][BF_4]_4$	0.39	0.55	1.08	1.32
$[Mo_2$(**Ni-1'**)$_4][BF_4]_4$	0.52	1.01	1.38	
$[Mo_2(OAc)$(**Ni-1**)$_3][BF_4]_3$	0.56			

Table VI-4. Summary of electrochemical reductions for the complexes utilized in the Mo_2Ni_x solvent dependence study (potentials shown in volts). Potentials in **bold** at or beyond the potential for free NiN_2S_2 ligand.

	solvent	E_{pc1}	E_{pc2}	E_{pc3}	E_{pc4}	E_{pc5}	E_{pc6}
$[Mo_2$(**Ni-1'**)$_4][BF_4]_4$	THF	-0.68	-1.14	-1.62	**-2.04**		
$[Mo_2$(**Ni-1'**)$_4][BF_4]_4$	DMF	-0.36	-0.85	-0.98	-1.29	-1.70	**-2.22**
$[Mo_2(OAc)$(**Ni-1'**)$_3][BF_4]_3$	THF	-1.10	-1.28	**-2.01**			
$[Mo_2(OAc)$(**Ni-1'**)$_3][BF_4]_3$	DMF	-0.91	-1.03	-1.65	**-2.18**	**-2.46**	
$[Mo_2(OAc)_2$(**Ni-1'**)$_2][BF_4]_2$	DMF	-0.88	-1.61	**-2.14**			
Ni-1'	THF	-1.98					
Ni-1'	DMF	-2.01					

The literature contains many precedents for dimolybdenum redox chemistry. The reversible waves around 0.50 V are attributed to the $Mo_2^{4+/5+}$ redox couple. For comparison, the one electron oxidation of $Mo_2(O_2C$-*t*-Bu$)_4$ occurred at 0.38 V in MeCNvs. SCE.[66] The quasi- and irreversible waves beyond 1.0 V are assigned to $Ni^{2+/3+}$ redox couple. Comparable values are reported by N-macrocylic systems under aqueous conditions.[67]

Work in our laboratories has shown that the palladium analog of **Ni-1**, designated as **Pd-1**, shows a $Pd^{2+/1+}$ redox couple at -2.10 V, while the reduction of S-methylated, dicationic $[Me_2\text{-}\mathbf{Pd\text{-}1}]^{2+}$ is at approximately -1.0 V under similar electrochemical conditions. As well, the trimetallic complexes $[(\mathbf{Zn\text{-}1})(OCH_3)]_2Pd^{2+}$ and $[(\mathbf{Ni\text{-}1})_2]Pd^{2+}$ show no reduction at the palladium metal center. To this end, it could be concluded the $Pd^{2+/1+}$ couple is not observed. The reversible anodic event at E_{pa} = 0.77 V can be reasonably attributed to the $Pd^{2+/3+}$ couple.[68]

The major redox events for the $(CuBr)_2(\mathbf{Ni\text{-}1})_3$ complex 0.25 and 0.60 V are within the range of $Cu^{1+/2+}$ redox couple. There are several examples with S- and N-macrocycle complexes are found throughout the literature such as the Cu^{I}(hexathia-18-crown-6) complex reported by Cooper and co-workers which exhibits an oxidation at 0.72 V vs. SCE.[69] The oxidative event for $(CuBr)_2(\mathbf{Ni\text{-}1})_3$ at 1.25 V vs. NHE is ascribed to the $Ni^{2+/3+}$ couple. Investigations done by the Rorabacher laboratories found the range of $Cu^{II/I}$ reductions for a series of thioether complexes to be from 0.43 to 0.65 V vs. SCE performed in 80% aqueous methanol.[70] An explanation for the appearance of the weakly defined peaks is suggested in a paper by Joseph Fox, Glenn Yap and coworkers.[71] In this work, poorly defined responses in the CV of a copper salophen peptidomimetic complex were eliminated by performing electrochemical experiments in non-coordinating solvents. For the $[Ag_2(\mathbf{Ni\text{-}1'})_3][NO_3]_2$ complex, the irreversible oxidation at 0.90 V is assigned to the $Ag^{1+/2+}$ redox couple. This claim is supported by reports conducted by Laguna[72] on the $[Ag(Fc2qpy)]^+$ complex and Kamigata[73] on the [Ag(15-

UT-5)] and [Ag(16-UT-6)] complexes whose work utilizes bis(ferrocenyl)polypyridyl and thiacrown ether silver ligands respectively.

The electrochemical behavior of the $Mo_2Ni_x(OAc)_{4-x}$ species (x = 2, 3, 4), in solution is perplexing and poses unresolved issues. The first is the appearance of peaks in the SWV of both strong and weak intensities where the weak intensity peaks are found at the same potentials for all three complexes. The second issue is the most negative reduction wave for each of the complexes is very similar to the free NiN_2S_2 in reversible shape and position. It was proposed initially that the four distinct waves were based on the **Ni-1'** units while the two minor waves, exhibiting a separation of approximately 700 mV, could be attributed to the dimolybdenum.[54] The latter is supported by the redox behavior of the starting material $[Mo_2(CH_3CN)_{10}][BF_4]_4$ and the $Mo_2(hpp)_4$ compound which show a similar separation. Additionally, there are other $[M_2(RCN)_{10}][BF_4]_4$ systems in the literature, where M = Tc, Rh, Re; R = Me, Et, that behave in the same manner.[74]

The Mo_2Ni_4 species contains four redox active NiN_2S_2 ligands and a redox active dimolybdenum unit. Due to the difficulty in assigning the CV and SW, there are multiple possibilities for the six reductions observed: 1) any of five reduction steps for shown in Scheme VI-2; 2) dissociation of NiN_2S_2 units facilitated by reduction; 3) uptake of six electrons by an intact Mo_2Ni_4 species; or 4) uptake of 4 electrons by the four NiN_2S_2 units and uptake of 2 electrons attributed to solvated species caused by partial dissociation of the NiN_2S_2 unit.

Scheme VI-5. Alternative scheme proposed to explain the multiple reductions of the $Mo_2Ni_4^{4+}$ species.

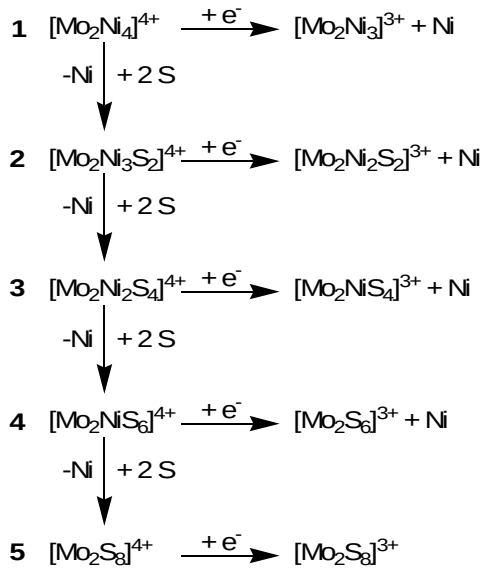

Results from the ligand exchange experiments suggest that labilization is possible as evidenced by several mixed-ligand species observed in the mass spectrum. It remains unanswered, however, if this substitution occurs in solution or the ion beam. **Ni-1'** could easily be displaced by **Ni-1** as they are very similar in donor ability as discussed in Chapter III which supports the possibility for complete NiN_2S_2 ligand dissociation from the dimolybdenum unit and the open coordination sites filled by two molecules of acetonitrile as seen in Scheme VI-5. This dissociative process could occur *before* or after electron transfer shown in steps **1-5** of Scheme VI-5. It difficult to determine what extent this process would occur in solution. Step **5** is highly unlikely and thus can be eliminated from the scheme because it is a known compound with redox properties that have been discussed earlier in this report (*cf.* $[Mo_2(MeCN)_{10}][BF_4]_4$, Figure VI-4). In addition, potentials belonging to this compound are observed in neither the CV nor SW; therefore, it can be concluded that $[Mo_2(MeCN)_{10}][BF_4]_4$ is not being

generated in solution. Even though no solvated species have ever been observed in the mass spectrum for the mixed-metal clusters mentioned above, this explanation cannot be entirely ruled out.

Dimolybdenum complexes containing xanthate ($^{-}S_2COR$), thioxanthate ($^{-}S_2CSR$), and dithiocarboxylate ($^{-}S_2CR$) ligands, $[Mo_2(S_2CR)_4]^0$ are known for their interesting electrochemistry.[14] The ligands, which are themselves redox active, form stable dimolybdenum complexes containing a Mo_2S_8 core exhibiting two one-electron reductions as shown by cyclic voltammetry. After the second reduction, ligand dissociation occurs and the ligand is oxidized on the return sweep. The resultant dication is unstable and undergoes chemical reactions to form a more stable species which itself is redox active.[75]

By analogy, the Mo_2Ni_4 system could behave similarly. The four redox active metallodithiolates are bound to the dimolybdenum unit via their sulfur donor atoms composing a Mo_2S_8 core. We have tentatively assigned the weak and poorly defined peaks separated by ~700 mV as reductions of the dimolybdenum unit as nearly identical behavior is found for both the Mo_2Ni_2 and Mo_2Ni_3 complexes. Reduction of the dimolybdenum unit occurring at nearly the same potential could in fact be evidence for ligand dissociation. A buildup of electron density on molybdenum would encourage ligand dissociation. Explanation two is unlikely as free NiN_2S_2 ligand can be reduced and the thiolate sulfurs of are subsequently oxidized to disulfide.

Metallation and a high positive charge (M_2^{4+}) shifts the $Ni^{II/I}$ reduction potential to more positive values as compared to the free ligand. By analogy, the opposite could

be justified in dimolybdenum unit. The labilization of **Ni-1'** from the dimolybdenum unit and concomitant replacement by a poorer donating ligand, MeCN, would cause the reduction potential of the dimolybdenum unit to be more positive.[59] This phenomena could explain the similarity in reduction potentials for the dimolybdenum unit in Mo_2Ni_4, Mo_2Ni_3, and Mo_2Ni_2. Moreover, molar conductivity measurements performed on the $[Pd_2(\mathbf{Ni\text{-}1'})_4][NO_3]_4$ complex indicated two to three ions in solution, indicative of the Pd_2Ni_4 tetracation and two long range nitrate interactions.[4] The tetrafluoroborate ions associated with the large Mo_2Ni_4 tetracation would have a similar effect on not only the molar conductivity but the reduction potentials as well.

CHAPTER VII

NiN_2S_2 COMPLEXES AS METALLODITHIOLATE LIGANDS TO Rh^I, Rh^{II}, AND Rh^{III}

As evidenced by the ν(CO) stretching frequencies in the IR spectra, NiN_2S_2 metallodithiolate ligands bound to the $W(CO)_4$ fragment have electron donor properties similar to diimines such as bipyridine. This comparison is intriguing since the bipyridine (bipy) ligand has been prominent in inorganic chemistry for over 30 years. For example, the $Ru(bipy)_3^{2+}$ (ruthenium tris(2,2'-bipyridine)) complex, or "Rubpy" as it is commonly referred, has a host of literature documenting its ability to absorb light and photocatalyze bimolecular electron transfer reactions.[76] Rubpy's photo-electroactive abilities have been used to modify the redox capabilities of metal electrodes and induce oxidative polymerization reactions.[77] To further explore the analogy of NiN_2S_2 ligands to bipy, we have synthesized new complexes which utilize NiN_2S_2 moieties as a tris(bidentate) ligand to d^6 metal center. While our attempts to synthesize the $RuNi_3$ analog were unsuccessful, we were able to isolate and characterize a $RhNi_3$ cluster.

The first $[Rh^{III}(NiN_2S_2)_3]^{3+}$ complex prepared in our laboratories was obtained via serendipity from attempts to synthesize a hexametallic cluster $[Rh^{II}_2(NiN_2S_2)_4][BF_4]_4$ analogous to $[Mo^{II}_2(NiN_2S_2)_4][BF_4]_4$,[54] which has been derived from $[Mo^{II}_2(MeCN)_8][BF_4]_4$.[31] A reasonable thought progression was to use the analogous starting material, $[Rh_2(MeCN)_8][BF_4]_4$.[78] However, upon exposure to light, this material undergoes a reversible photodisproportionation reaction which is said to result from

cleavage of the single Rh-Rh bond and generation of metastable species such as $Rh^{III}L_6$ and a mixed-valent $(Rh^{II}Rh^{II}Rh^{I})L_n$ species, where L = MeCN.[79] Upon crystallization of products obtained from this reaction, we derived the crystals of $[Rh(NiN_2S_2)_3][BF_4]_3$ in low yield (< 10%). A direct synthesis from RhI_3 produced the complex in better yields.

In this chapter, I describe polymetallics as Rhbpy analogs formulated as $[Rh^{III}(NiN_2S_2)_3]^+$; we have added to our paddlewheel series by the preparation of $[Rh_2(NiN_2S_2)_4]^{4+}$;[4,7,9,34,54] and I and my colleagues synthesized the $(NiN_2S_2)Rh^{I}(CO)_2$ compounds for potential use in catalytic processes such as the Monsanto Acetic Acid or hydroformylation processes. These complexes have been characterized using infrared spectroscopy, X-ray crystallography, electron spray ionization-mass spectrometry (ESI-MS), and electrochemical methods.

Syntheses of $[Rh(NiN_2S_2)]$ complexes

The Rh^{I} complexes.[8,80] The $[(NiN_2S_2)Rh(CO)_2][PF_6]$ complexes (NiN_2S_2 = **Ni-1** and **Ni-1***) were synthesized via $[Rh(CO)_2Cl]_2$ dimer cleavage followed by salt metathesis as shown in Equation 1. The ν(CO) spectra for the salts show two bands of equal intensity as expected for *cis*-CO groups at 90˚ angles to each other.

$$[Rh(CO)_2Cl]_2 + 2\ NiN_2S_2 \xrightarrow[MeCN,\ 22°]{2\ TlPF_6} [Rh(NiN_2S_2)(CO)_2][PF_6] + 2\ TlCl$$

NiN_2S_2 = **Ni-1** and **Ni-1***

u(CO), **Ni-1**: 2077, 2017 cm^{-1}
Ni-1*: 2077, 2015 cm^{-1}

The positions of the bands for the derivatives of **Ni-1** and **Ni-1*** are not significantly different. ESI-mass spectroscopy of the **Ni-1** derivative in MeCN shows the parent ion at 420 (100%); analysis of the [Rh(**Ni-1***)$(CO)_2$][PF_6] analog under identical conditions shows the parent ion at m/z = 477 (100%) and a monocarbonyl species at m/z = 505 (97.0%). No other clusters of higher nuclearity were observed in the mass spectrum for either compound. The [(NiN_2S_2)Rh$(CO)_2$][PF_6] complexes are air stable in solution. In fact a MeCN solution of [(**Ni-1***)Rh$(CO)_2$][PF_6] was exposed to air for four days without a change in the IR spectrum or color of solution.

Synthesis of these complexes was also attempted with (acac)Rh$(CO)_2$ as starting material, where acac = acetylacetonate. In this reaction, a one molar equivalent of acid (HBF_4) in MeCN was required for protonolysis of the acac ligand. Without acid, the reaction did not reach completion as indicated by the IR monitor even after 24 h. Upon addition of the acid, the reaction occurs within 30 min. Crystals were difficult to obtain, presumably due to difficulty in removing 2,4-pentanedione (Hacac) from the product. All attempts led to oils.

Synthesis of the $[NEt_4]_2${[Ni(ema)Rh$(CO)_2]_2$} was performed by fellow graduate student Kayla Green. Under an argon atmosphere, the red solids $[NEt_4]_2$[Ni(ema)] and [Rh$(CO)_2Cl]_2$ were loaded into a Schlenk flask and dissolved in about 20 mL of acetonitrile. After stirring for 2 hours and filtering over a bed of Celite, the resulting red-brown solution had two ν(CO) bands of equal intensity at 2061 and 1996 cm^{-1}. Red, air sensitive crystals suitable for x-ray diffraction analysis were obtained by layering an acetonitrile solution with ether. It is unclear if the tetrametallic complex that crystallized

is the same as what is studied in solution. The air instability of the crystals prevented further characterization by IR spectroscopy.

The [(**Ni-1**)Rh(CO)(PPh_3)][Cl] complex was synthesized by co-worker Marilyn Rampersad *via* displacement of a PPh_3 and a chloride ion from Rh(CO)(PPh_3)$_2$Cl.[37] The infrared spectrum in MeCN shows a single ν(CO) stretch in the terminal CO bound region at 1987 cm^{-1}, shifted to higher wavenumbers from the starting complex (ν(CO) 1978 cm^{-1}). The infrared results can be rationalized as follows: In Chapter III we have shown that NiN_2S_2 ligands have donor abilities far better than phosphine ligands. Nevertheless, the binding of NiN_2S_2 displaces the chloride ion and a triphenylphosphine ligand from the neutral square planar Rh(CO)(PPh_3)$_2$Cl, starting material, Scheme VII-1. The product is a cationic complex in which the Rh(I) is less π-backbonding to the CO ligand. ESI mass spectroscopy confirmed that 100% of the product was [(**Ni-1**)Rh(CO)(PPh_3)]$^+$, with a mass to charge ratio of 683. No other clusters of higher nuclearity were observed in the mass spectrum.

Scheme VII-1. Rationale for ν(CO) values in synthesis of [Rh(**Ni-1**)(CO)(PPh_3)][Cl].

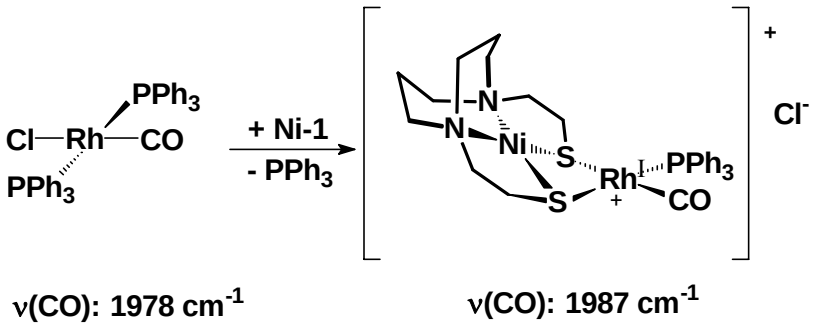

A stack plot of the IR spectra of the $[Rh(NiN_2S_2)(CO)_2]^n$ complexes from this dissertation and from our collection is shown in Figure VII-1. Each spectrum shows a two band pattern of relatively equal intensity. The bands of the starting material, $[Rh(CO)_2Cl]_2$, are the most positive of the series. Conversely, the $[NEt_4]_2\{[(Ni(ema))Rh(CO)_2]_2\}$ complex, is the most negative of the series which is to be expected as it is a dianion. The $[Rh(\mathbf{Ni\text{-}1})(CO)_2]^+$ and $[Rh(\mathbf{Ni\text{-}1^*})(CO)_2]^+$ complexes are virtually indistinguishable. Interestingly, the $[NEt_4]_2\{[(Ni(ema))Rh(CO)_2]_2\}$ complex exhibits ν(CO) values very similar to $[Rh(CO)_2I_2]^-$, the precatalyst in the Monsanto Acetic Acid Process (ν(CO), KBr: 2060, 1988).[81]

The Rh^{II}-Rh^{II} complex.[8] Synthesis of the $[Rh_2(\mathbf{Ni\text{-}1'})_4]^{4+}$ compound is readily accomplished via ligand displacement from $Rh_2(O_2CCF_3)_4$ in MeCN solution. The reaction can be performed in ambient laboratory light and under a N_2 atmosphere. The dark blue solution of $Rh_2(O_2CCF_3)_4$ quickly turned red-orange upon reaction with **Ni-1'**. After stirring overnight, the solvent was removed *in vacuo* and the product was isolated as a red-orange air stable solid in 73% yield. Mass spectrometry confirmed the existence of the hexametallic cluster in smaller quantities ($\{[Rh_2(\mathbf{Ni\text{-}1'})_4]^{4+}\}$ m/z = 476 (34.7%), $\{[Rh_2(\mathbf{Ni\text{-}1'})_4(O_2CCF_3)_2]^{2+}\}$ m/z = 769 (6.45%)) and showed as well the formation of tetrametallic clusters at much higher relative intensity ($\{[Rh(\mathbf{Ni\text{-}1'})_3]^{3+}\}$, m/z = 311 (100%), $\{[Rh(\mathbf{Ni\text{-}1'})_3(O_2CCF_3)]^{2+}\}$ m/z = 523 (41.9%)).

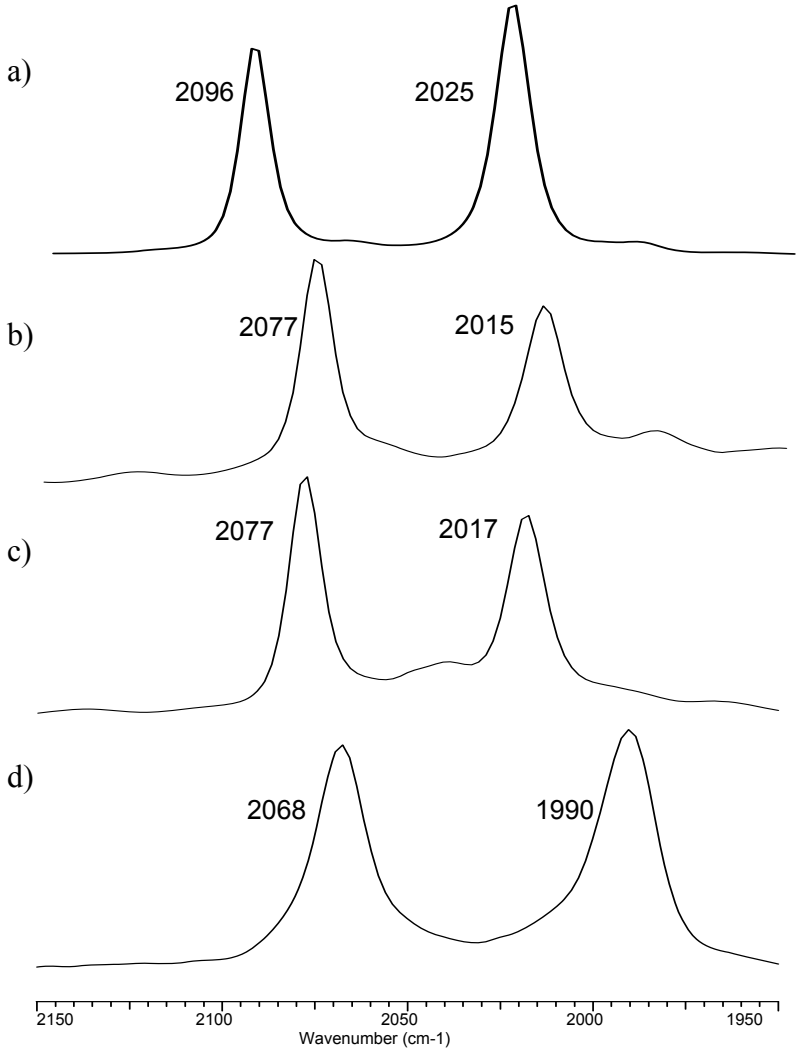

Figure VII-1. Stack-plot of the $[Rh(NiN_2S_2)(CO)_2]^+$ ν(CO) infrared spectra in MeCN. a) Starting material $[Rh(CO)_2Cl]_2$ b) [Rh(**Ni-1***)$(CO)_2$][PF_6] c) [Rh(**Ni-1**)$(CO)_2$][PF_6] d) $[NEt_4]_2\{[(Ni(ema))Rh(CO)_2]_2\}$.

An alternate synthesis of the $[Rh_2(\mathbf{Ni\text{-}1'})_4]^{4+}$ complex was attempted via ligand displacement from $[Rh_2(MeCN)_{10}][BF_4]_4$ in MeCN solution in a manner similar to the successful approach for the dimolybdenum analog, $[Mo_2(NiN_2S_2)_4][BF_4]_4$.[54] Unfortunately, the extensive photo- and subsequent air sensitivity of this complex in solution led to oxidation and a mono-rhodium product. Crystals obtained from the reaction of the dirhodium decakis(acetonitrile) complex with 4 equivalents of NiN_2S_2 revealed a tetrametallic complex formulated as $[Rh^{III}(NiN_2S_2)_3]^{3+}$ in low yield (~10%). A direct route to this coordination complex of Rh^{III} is described Scheme VII-2. Should this dimer cleavage of $[Rh^{II}_2(MeCN)_{10}][BF_4]_4$ be operative, one might propose the generation of two rhodium(II)pentakis(acetonitrile) monomers as has been suggested James, Dunbar and co-workers.[79] Upon exposure to excess NiN_2S_2, the monomer is prevented from reforming the dimer. During this time or during recrystallization, the unstable rhodium(II) monomer was oxidized giving a tetranuclear rhodium(III) complex. The reaction was repeated in the dark, however only small quantities, approximately eight percent intensity observed via ESI-MS, of the desired hexametallic cluster were obtained.

Scheme VII-2. Proposed mechanism for the photochemical cleavage of $[Rh_2(MeCN)_{10}][BF_4]_4$ resulting in the formation of the $[Rh(NiN_2S_2)_3]^{3+}$ cluster.

$$[Rh_2(MeCN)_{10}][BF_4]_4 \overset{h\nu}{\rightleftharpoons} 2[Rh(MeCN)_5][BF_4]_2$$

$$[Rh(MeCN)_5][BF_4]_2 \xrightarrow{NiN_2S_2} [Rh(NiN_2S_2)_3][BF_4]_2$$

$$[Rh(NiN_2S_2)_3][BF_4]_2 \xrightarrow{O_2} [Rh(NiN_2S_2)_3][BF_4]_3$$

The Rh^{III} complex. The tetranuclear $[Rh(NiN_2S_2)_3]^{3+}$ complex can be synthesized directly and in high yield from RhI_3 and NiN_2S_2 in refluxing MeCN followed by salt metathesis with $NaBF_4$ or $TlPF_6$ as shown in Scheme VII-3.

Scheme VII-3. Synthesis of the RhNi tetrametallic complex cation.

$$RhI_3 + 3\ \textbf{Ni-1'} \xrightarrow[\Delta,\ MeCN]{3\ NaBF_4} [Rh(\textbf{Ni-1'})_3][BF_4]_3 + 3\ NaI$$

While anion exchange leads to higher yield and purer products, the $[Rh(NiN_2S_2)_3][I]_3$ salt can be isolated. For this salt, mass spectrometry shows the existence of the $\{[Rh(NiN_2S_2)_3][I]^{2+}\}$ species, m/z = 529 at maximum intensity as well as several other unidentifiable peaks. Addition of $NaBF_4$ or $TlPF_6$ to precipitate iodide salts drives the reaction towards the products giving only the $\{[Rh(NiN_2S_2)_3]^{3+}\}$ species. Attempts to resolve the $RhNi_3$ complex into its optical isomers has been undertaken as indicated in Scheme VII-4. Crystals are still being sought.

Scheme VII-4. Synthetic route to the resolution of optical isomers.

$$RhI_3 + 3\ NiN_2S_2 \xrightarrow[\text{or MeCN reflux}]{\text{MeOH}} [Rh(NiN_2S_2)_3][I]_3$$

$$[Rh(NiN_2S_2)_3][I]_3 + \text{sodium L-tartrate dihydrate} \xrightarrow{MeCN} [Rh(NiN_2S_2)_3][I][\text{L-tartrate}] + 2NaI$$

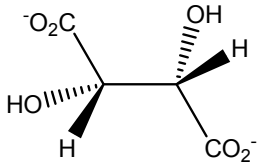

Attempts to prepare $RuNi_3$

Leigh and co-workers developed the $[Ru(MeCN)_6][I_4]$ complex as a synthon for octahedral coordination ruthenium complexes.[82] Parenthetically, the I_4^{2-} dianion developed during this reaction as an unusual counterion which yielded well-behaved solids. This was expected to be a suitable precursor for the $RuNi_3$ complex. Under N_2 in MeCN solution, three equivalents of **Ni-1'** were mixed with $[Ru(MeCN)_6]^{2+}$ and stirred overnight. The solvent was removed *in vacuo* and the remaining solid was analyzed via ESI-MS. Mass spectrometry revealed no clusters possessing the isotopic envelope of the $[Ru(\textbf{Ni-1'})_3]^{2+}$ species; however, a trimetallic nickel species ($\{(\textbf{Ni-1'})_2Ni\}^{2+}$, *m/z* = 305) and an unidentifiable ruthenium species (*m/z* = 112) were consistently observed.

Crystallography

Crystallographic experimental data for all complexes is shown in Table VII-1. The $[(\textbf{Ni-1})Rh(CO)_2][PF_6]$ complex crystallizes in the orthorhombic space group $P2_12_12_1$. Selected metric data for this complex is listed in Table VII-2. This heterobimetallic, shown as a thermal ellipsoid plot in Figure VII-2, is comprised of a square planar NiN_2S_2 ligand that binds in a bidentate manner to a square planar Rh^I metal center via its thiolate sulfur donor atoms. The metalloligand, NiN_2S_2, displays a slight tetrahedral twist of 11.2˚ which is slightly smaller than the free ligand at 13˚.[11] The average deviation of N and S from the best least squares plane is 0.0188 Å. From this plane, the Ni^{II} deviates by 0.1443 Å and is displaced away from the Rh; the Rh-Ni distance is 2.871 Å. Of note is the hinge formed by the intersection of the NiN_2S_2 and

$S_2Rh(CO)_2$ planes. The dihedral angle of 106º is slightly larger than the analogous angle found in (**Ni-1**)Pd(Me)Cl, a heterobimetallic compound comprised of two square planes hinged by bridging thiolates.

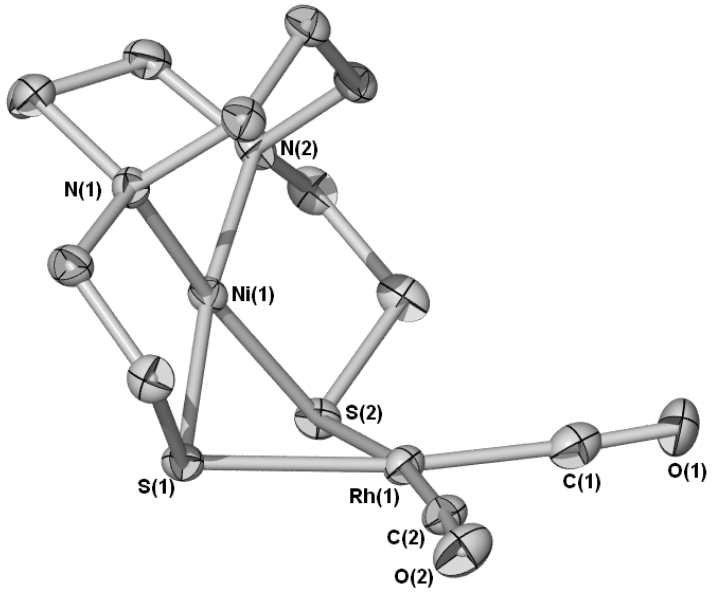

Figure VII-2. Thermal ellipsoid plot (50 % probability) of the $[(\textbf{Ni-1})Rh(CO)_2]^+$ cation with hydrogens omitted.

Table VII-1. Crystallographic experimental data for all complexes.

	[Rh(**Ni-1**)(CO)$_2$][PF$_6$]	[NEt$_4$]$_2${[(Ni(ema)Rh(CO)$_2$]}$_2$	[Rh(**Ni-1**)(CO)(PPh$_3$)][Cl]·H$_2$O	[Rh$_2$(**Ni-1'**)$_4$][O$_2$CCF$_3$]$_4$·3MeCN	[Rh(**Ni-1'**)$_3$][BF$_4$]$_3$
Formula	$C_{12}H_{20}F_6N_2NiRhS_2PO_2$	$C_{16}H_{28}N_3NiO_4RhS_2$	$C_{29}H_{39}ClN_2NiO_3PRhS_2$	$C_{52}H_{84}F_{12}N_{12}Ni_4O_8Rh_2S_8$	$C_{27}H_{54}B_3F_{12}N_6RhS_6$
Formula Weight	610.99	552.15	755.59	1930.46	1194.59
Temperature (K)	110(2)	110(2)	110(2)	110(2)	110(2)
Wavelength (Å)	0.71073	0.71073	0.71073	0.71073	1.54178
Z	4	32	2	2	3
Dcalcd (Mg/cm3)	2.037	1.692	1.67	1.795	1.884
m (mm^{-1})	2.206	1.849	15.32	1.807	8.169
Crystal System	orthorhombic	monoclinic	triclinic	triclinic	rhombohedral
Space Group	$P2_12_12_1$	*C2/c*	*P*-1	*P*-1	R3c
Unit Cell					
a(Å)	9.991(2)	27.950(5)	9.119(5)	12.611(3)	21.507(2)
b(Å)	11.550(3)	23.526(4)	11.111(5)	12.738(3)	21.507(2)
c(Å)	16.844(4)	28.457(5)	14.916(5)	13.248(3)	15.769(2)
α(°)	90	90		102.397(4)	90
β(°)	90	112.113(3)	79.333(5)	94.325(4)	90
γ(°)	90	90		118.550(4)	120
Volume (Å^3)	1943.7(8)	17336(5)	1467.5(12)	1786.0(8)	6316.6(12)
Goodness-of-fit	1.068	1.091	1.078	1.029	1.008
R_1[a], wR_2[b](%) [I>2s(I)]	0.0230, 0.0546	0.0551, 0.1273	0.0562, 0.1327	0.0433, 0.1149	0.0498, 0.0915
R_1[b], wR_2[b](%) all data	0.0233, 0.0548	0.0722, 0.1435	0.0715, 0.1429	0.0468, 0.1197	0.0707, 0.0972

[a] $R_1 = S||F_o|-|F_c||/SF_o$ [b] $wR_2 = [S[w(F_o^2-F_c^2)^2]/Sw(F_o^2)^2]^{1/2}$

Table VII-2. Selected metric data for [Rh(**Ni-1**)$(CO)_2$][PF_6].

Rh-Ni	2.871	C(1)-Rh(1)-C(2)	92.20(16)
Rh(1)-C(1)	1.872(4)	S(1)-Rh(1)-S(2)	76.53(3)
Rh(2)-C(2)	1.871(4)	S(1)-Ni(1)-S(2)	84.65(3)
Rh(1)-S(1)	2.365(1)	Rh(1)-C(1)-O(1)	176.5(3)
Rh(1)-S(2)	2.354(1)	Rh(1)-C(2)-O(2)	175.3(3)
Ni(1)-S(1)	2.176(9)		
Ni(1)-S(2)	2.166(1)	Dihedral angle	106
Ni(1)-N(1)	1.957(3)		
Ni(1)-N(2)	1.966(3)		

The square planar $S_2Rh(CO)_2$ moiety also has a slight tetrahedral twist of 11.6˚, and, consistent with the ν(CO) spectrum, the *cis* carbonyls are separated by an angle of 92.4˚. There are no intermolecular interactions within van der Waals distances. There are minor differences in the metric data between the free and bound NiN_2S_2 ligand. There is a slight elongation of the Ni-S distances as well as the concomitant decrease in Ni-N distances upon binding to a metal. The $\angle_{S\text{-}Ni\text{-}S}$ of 84.65(3)˚ is slightly smaller than that of the free ligand which is approximately 88˚. This feature, coupled with the decrease in angle of tetrahedral twist, suggest that the NiN_2S_2 ligand becomes more ordered and rigid when metallated. The **Ni-1*** analog, although not structurally characterized, would be expected to have a similar molecular structure to **Ni-1**. Based on findings from the $W(CO)_4$ series,[30,41] the major difference between the **Ni-1** and **Ni-1*** complexes with $Rh(CO)_2$ should be a larger hinge angle dictated by the steric bulk on the pendant thiolate arms of **Ni-1***.

The $[NEt_4]_2\{[Ni(ema)Rh(CO)_2]_2\}$ complex, prepared and analyzed in collaboration with Kayla Green, crystallizes in the monoclinic space group *C2/c*, with selected metric data listed in Table VII-3. Unlike the former compound, the molecular structure of this heterotetrametallic is that of two $S_2Rh(CO)_2$ planes, with *cis* carbonyl groups in each plane and two sulfurs each derived from separate NiN_2S_2 moieties. The

two square planar Rh units are bridged by two NiN_2S_2 moieties which point away from each other as shown in the thermal ellipsoid plot, Figure VII-3. A view of the molecule along the Rh···Rh vector shows the two two $S_2Rh(CO)_2$ moieties are roughly eclipsed with some staggering due to significant S-Rh-Rh-S torsion angles of 15.3 and 17.4º. The Rh···Rh distance of 3.217 Å is beyond bonding range yet close enough for van der Waals contact.[83] Each NiN_2S_2 metalloligand displays slight tetrahedral twists of 3.3 and 7.2º while each nickel atom deviates from the least squares N_2S_2 best planes of 0.0134 and 0.0293Å respectively.

Table VII-3. Selected metric data for $[NEt_4]_2\{[(Ni(ema))Rh(CO)_2]_2\}$.

Rh(1A)-C(1A)	1.872(6)	C(1A)-Rh(1A)-C(2A)	91.3(2)
Rh(1A)-C(2A)	1.873(6)	C(3A)-Rh(1A)-C(4A)	88.7(3)
Rh(2A)-C(3A)	1.876(6)	S(1A)-Rh(1A)-S(3A)	84.26(4)
Rh(2A)-C(4A)	1.888(7)	S(2A)-Rh(1A)-S(4A)	82.62(5)
Rh(1A)-S(1A)	2.406(1)		
Rh(1A)-S(3A)	2.378(1)	Rh(1A)-C(1A)-O(1A)	174.8(5)
Rh(2A)-S(2A)	2.349(1)	Rh(1A)-C(2A)-O(2A)	178.0(5)
Rh(2A)-S(4A)	2.427(1)	Rh(2A)-C(3A)-O(3A)	178.0(6)
R(1A)-Rh(2A)	3.217	Rh(2A)-C(4A)-O(4A)	172.0(5)
Ni(1A)-S(1A)	2.201(1)	S(1A)-Ni(1A)-S(2A)	98.82(5)
Ni(1A)-S(2A)	2.207(2)	S(3A)-Ni(2A)-S(4A)	98.36(5)
Ni(2A)-S(3A)	2.193(1)		
Ni(2A)-S(4A)	2.179(1)	Torsion angle	15.3
Ni(1A)-N(1A)	1.867(4)		17.4
Ni(1A)-N(2A)	1.865(4)		
Ni(1A)-N(3A)	1.846(4)		
Ni(2A)-N(4A)	1.861(4)		

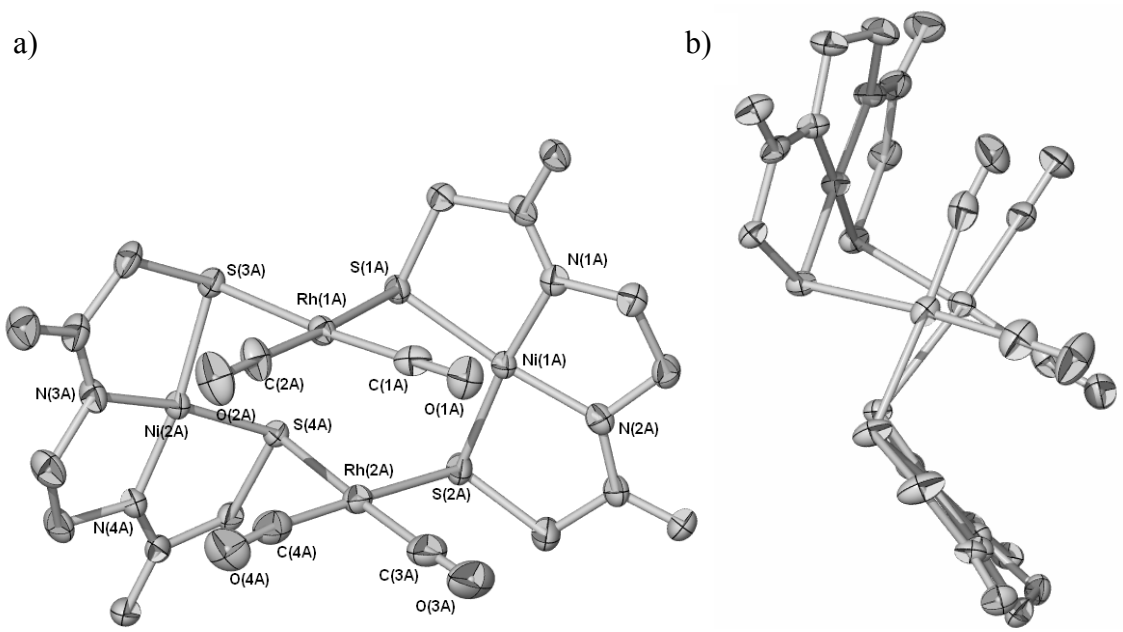

Figure VII-3. Thermal ellipsoid plot (50 % probability) with hydrogens omitted of the $[Ni(ema)Rh(CO)_2]_2^{2-}$ anion a) dicarbonyl planes pointed towards the viewer; b) viewed down Rh-Rh axis.

As described above, the rhodium atoms are enveloped in a square planar $SS'(CO)_2$ core, where the donor sulfur atoms come from each of the NiN_2S_2 ligands. The greater flexibility of this arrangement produces $SS'Rh(CO)_2$ moieties which are able to conform to a more regular square planar geometry with essentially neglible tetrahedral twists of 3.6 and 3.2º. The average least squares deviation from the best $SS'C_2$ is 0.0273 and 0.0161 Å respectively; the rhodium ions deviate from the $SS'C_2$ planes by Rh(1A) of 0.0369 and Rh(2A) of 0.0373 Å. An optimal square planar geometry consists of four 90º angles; this structure deviates slightly as evidenced by the S-Rh-S (84.26(4)º), S-Rh-C (~91.4(2)º, 93.0 (2) º), and C-Rh-C (91.3(2)º) angles of the donor atoms about the Rh center. The ability of the complex to adapt this preferred geometry about the Rh^I may be a key for explaining formation of the tetrametallic versus the $[(NiN_2S_2)Rh(CO)_2]^{2-}$ bimetallic structure.

There are minor differences in the metric data between the free and bound NiN_2S_2 ligand. There is a slight elongation of the Ni-S distances as well as the concomitant increase in Ni-N distances upon metalation. The tetrametallic cluster crystallizes with alternating channels of the counterion more than 3.3 Å away as seen in Figure VII-4.

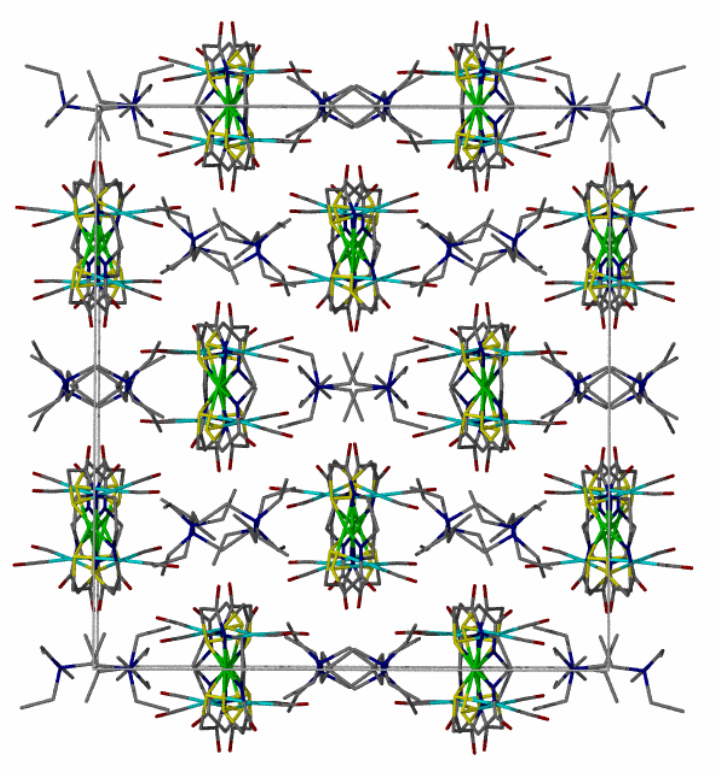

Figure VII-4. Packing diagram of $[Ni(ema)Rh(CO)_2]_2^{2-}$ with alternating channels of NEt_4 cations viewed down the c-axis.

The [(**Ni-1**)Rh(CO)(PPh_3)][Cl] complex crystallizes in the triclinic space group *P*-1, selected metric data is listed in Table VII-4. The molecular structure is that of a heteronuclear bimetallic shown in the thermal ellipsoid plot listed as Figure VII-5. The rigid square planar **Ni-1** unit coordinates to the Rh^I metal center in a bidentate mononucleating fashion. The Rh^I also adopts a square planar geometry with the CO and PPh_3 ligand completing the coordination sphere. A chloride ion a closest distance of

7.671 Å balances the charge on the Rh^{I} heterobimetallic; a H_2O water molecule is also located in the interstices of the unit cell. A decrease in the Ni-N and increase in Ni-S distances are also observed upon metallation. The S-Ni-S angle is pinched ca. 4° from the parent **Ni-1** complex as the thiolates form a μ-SR bridge to the Rh metal center, which opens up the N-Ni-N angle by 2°.

Table VII-4. Selected metric data for [Rh(**Ni-1**)(CO)(PPh_3)][Cl].

Rh-Ni	2.996	Rh(1)-C(11)-O(1)	175.8(4)
Rh(1)-S(1)	2.399(1)	S(1)-Rh(1)-S(2)	75.92(5)
Rh(1)-S(2)	2.372(1)	C(11)-Rh(1)-P(1)	91.7(2)
Rh(1)-P(1)	2.271(1)	S(1)-Ni(1)-S(2)	85.37(5)
Rh(1)-C(11)	1.843(5)		
		Dihedral angle	115
Ni(1)-S(1)	2.163(2)		
Ni(1)-S(2)	2.167(1)		
Ni(1)-N(1)	1.958(4)		
Ni(1)-N(2)	1.968(4)		

The μ-SR bridge formed between Rh^{I} and Ni^{II} metal centers produces a dihedral "hinge" angle, defined as the intersection of the NiN_2S_2 and RhS_2CP planes, of 115˚ and a Ni-Rh distance of 2.996 Å. The dihedral angle is ca. 14˚ larger than that observed for the Pd(**Ni-1**)(CH_3)(Cl) heterobimetallic, and 11˚ larger than that of [Rh(**Ni-1**)$(CO)_2$]$^{+}$. This is perhaps due to the bulky PPh_3 group that is positioned opposite to the NiN_2S_2 ligand. One of the aromatic rings on the PPh_3 group is above the RhS_2PC plane in front of the CH_2 groups of the diazacycle backbone, while the other two aromatic rings are below the plane. Most of the steric bulk of the ligands is above the RhS_2PC plane, which adds an attractive stereo-chemical feature similar to Pd(**Ni-1**)(CH_3)(Cl).

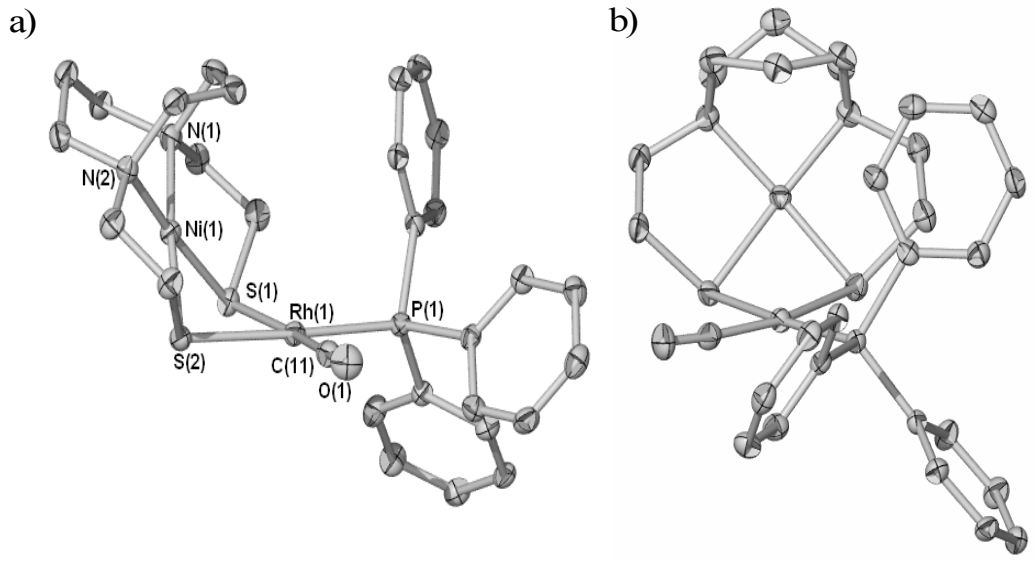

Figure VII-5. Thermal ellipsoid plot (50 % probability) with hydrogens omitted of the [Rh(**Ni-1**)(CO)(PPh_3)]$^+$ cation from the a) side b) front.

A topic of much discussion in this dissertation is the hinge formed by Ni(μ-SR)$_2$M' units. In Chapter III it was determined from molecular structure analysis of the (NiN_2S_2)$W(CO)_4$ series that the hinge angle directly increased with the steric bulk on the thiolate arms of the NiN_2S_2. In that series, the NiN_2S_2 unit is bound to a metal in octahedral coordination. The possible steric influence of the two axial carbonyls on the hinge angle groups was not addressed.

A comparison of the heterobimetallics in our collection which display a Ni(μ-SR)$_2$M' hinge in Figure VII-6 clearly shows that the complexes with edge-bridged square planar complexes have the smallest hinge angle. The Pd^{II} and the Rh^{I} with no steric encumbrance from the additional ligands on the d^8 metals have the smallest dihedral angle. In contrast, the [Rh(**Ni-1**)(CO)(PPh_3)]$^+$ complex shows an increase of 10˚ to reduce the interaction of the **Ni-1** diazacycle and a phenyl ring from the phosphine 3.4 - 4.0 Å away. A more dramatic effect is seen in the (**Ni-1**)$W(CO)_4$ complex where an

increase of the hinge angle reduces the interaction of the **Ni-1** diazacycle and a carbonyl group 3.7 - 3.8 Å away. For comparison, the computed H-S-H bond angle of H_2S is 92˚.[84] It would appear that the optimal hinge angle in absence of steric bulk is around 101˚.

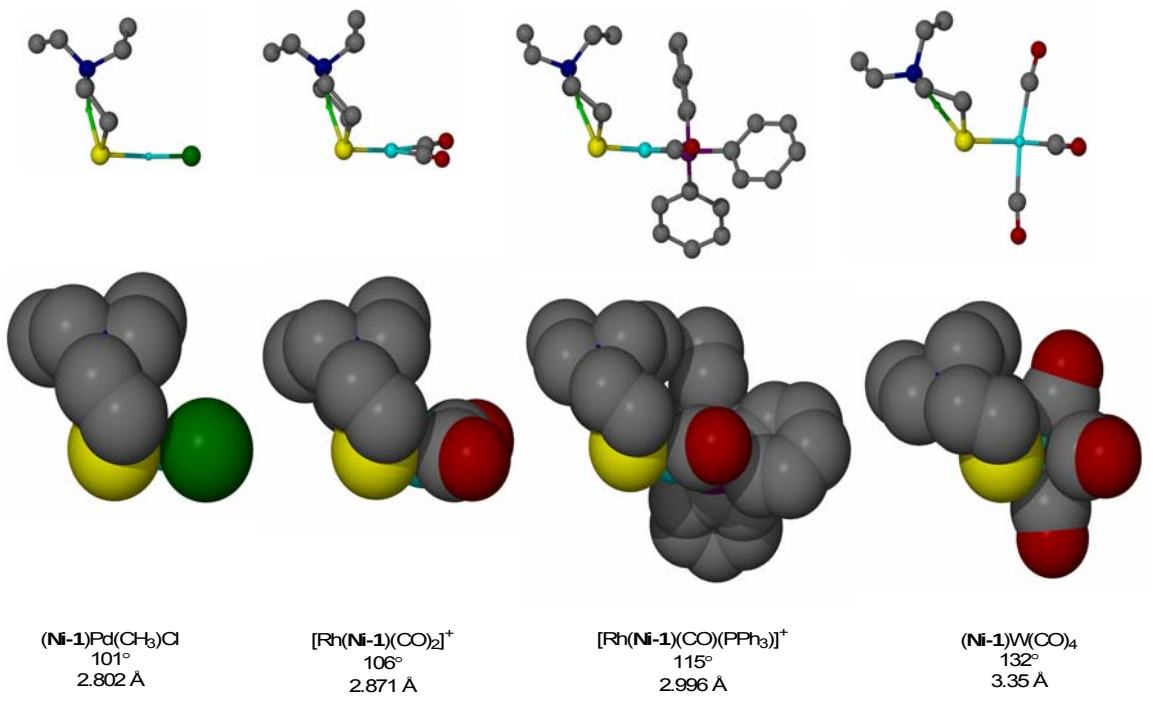

Figure VII-6. Profile view of heterobimetallic complexes which utilize **Ni-1** as a bidentate ligand shown as ball and stick and space filling models. Hinge angles and Ni-M' distances are listed below each structure.

The $[Rh_2(\mathbf{Ni\text{-}1}')_4][O_2CCF_3]_4$ complex crystallizes in the triclinic space group *P*-1 as a MeCN solvate; selected metric data is listed in Table VII-5. The two independent molecules in the unit cell show minor differences; therefore, only one will be discussed here. The molecular structure of the complex, shown in the thermal ellipsoid plot in Figure VII-7, is that of a C_4 paddlewheel. The tetracationic cluster crystallizes with two MeCN molecules bound axially to the dirhodium unit with a Rh-$N_{nitrile}$ distance of 2.183

Å. The cluster is of nearly perfect C_{4h} point group symmetry. There are four disordered trifluoroacetate anions within the lattice interstices with one MeCN molecule in the crystalline matrix. The crystal packing diagram in Figure VII-8 shows alternating channels of Rh_2Ni_4 clusters and trifluoroacetate ions more than 3.3 Å away.

Table VII-5. Selected metric data for $[Rh_2(\mathbf{Ni\text{-}1'})_4]^{4+}$.

Rh-Rh	2.893(8)	S(2)-Rh(1)-S(4)	90.59(3)	N(1)-Ni(1)-N(2)	82.77(17)
Rh-S(2)	2.361(1)	S(3A)-Rh(1)-S(2)	89.75(3)	N(4)-Ni(2)-N(3)	83.12(16)
Rh-S(4)	2.364(1)	S(3A)-Rh(1)-S(1A)	89.87(3)	S(1)-Ni(1)-S(2)	91.43(4)
Rh-N(5)	2.183(3)	S(1A)-Rh(1)-S(4)	89.56(4)	S(3)-Ni(2)-S(4)	91.69(4)
		S(1A)-Rh(1)-S(2)	176.31(3)		
Ni(1)-S(1)	2.122(1)	S(3A)-Rh(1)-S(4)	176.26(3)	Dihedral angle	132
Ni(1)-S(2)	2.130(1)	C(19)-N(5)-Rh(1)	176.7(3)		
Ni(1)-N(1)	1.910(3)	S(3A)-Rh(1)-Rh(1A)	91.86(3)		
Ni(1)-N(2)	1.920(4)	S(1A)-Rh(1)-Rh(1A)	91.74(3)		
		S(2)-Rh(1)-Rh(1A)	91.95(3)		
		S(4)-Rh(1)-Rh(1A)	91.85(3)		
		N(5)-Rh(1)-Rh(1A)	179.35(8)		

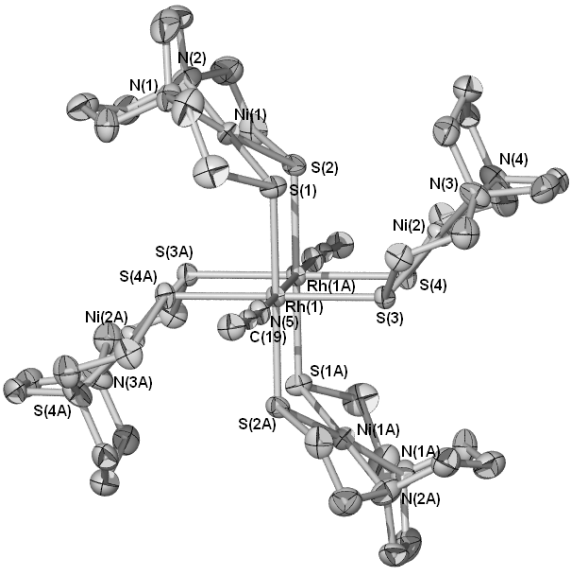

Figure VII-7. Thermal ellipsoid plot (50 % probability) of $[Rh_2(\mathbf{Ni\text{-}1'})_4]^{4+}$ with select atoms labeled and hydrogen atoms omitted.

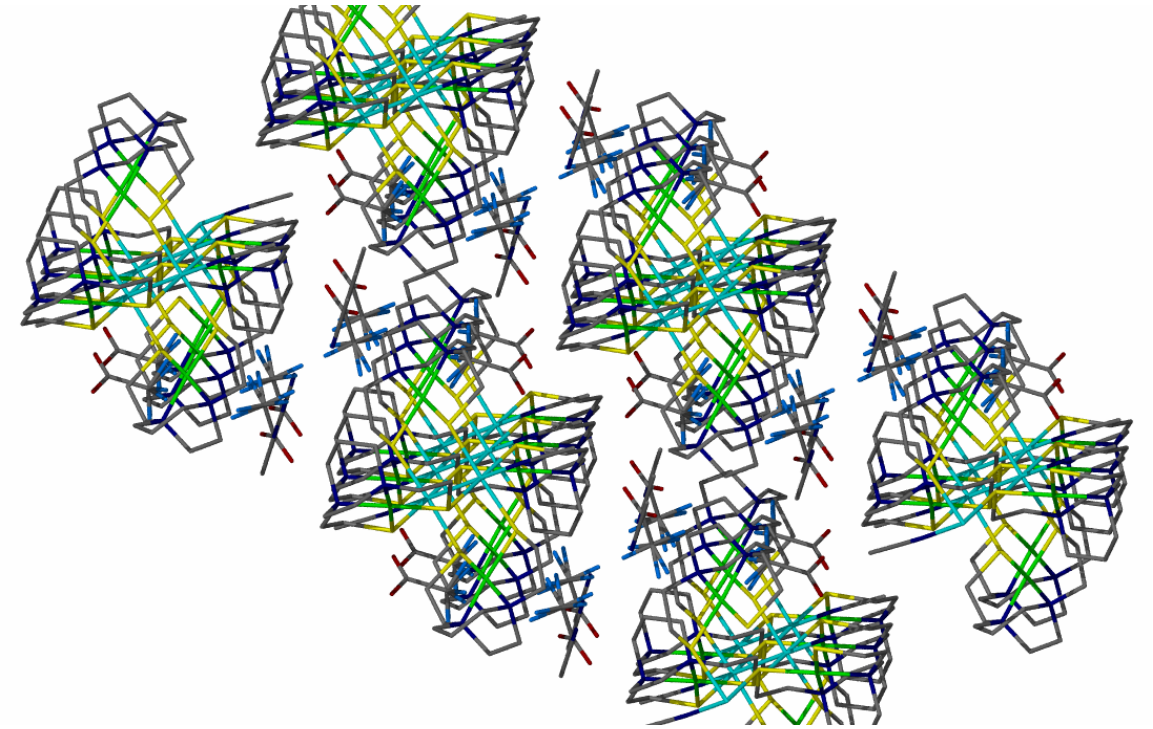

Figure VII-8. Packing diagram showing channels of Rh_2Ni_4 clusters and trifluoroacetate ions as viewed down the a-axis.

The Rh_2^{4+} coordination environment of the Rh_2Ni_4 clusters contains a Rh-Rh axis and eight sulfurs originating from the four NiN_2S_2 paddles. The Rh_2S_4 planes are mostly eclipsed displaying a S-Rh-Rh-S torsion angle of 0.3º notably smaller than the one found in the analogous Mo_2Ni_4 cluster at 1.5º.[54] The **Ni-1'** units display a very slight tetrahedral twist of no more than 4º and are in their common configurations. The **Ni-1'** units coordinate to the dirhodium unit via their donor sulfur atoms at an average Rh-S distance of 2.36 Å. These distances are comparable to the Pd_2Ni_4 analog reported in Chapter V. The complex with the longest metal-metal distance, Pd_2Ni_4, interestingly exhibits the smallest S-Ni-S bidentate bridging bite angle, 89.99(6)º. Like most dirhodium paddlewheel complexes, the dirhodium unit contains a single bond. In the case of $[Rh_2(\textbf{Ni-1'})_4]^{4+}$, the distance of 2.893 Å is on the long end of the range of metal-metal

distances for dirhodium complexes, which is 2.35 to 3.01 Å; examples are shown in Figure VII-9 as ball and stick representations.[14,85]

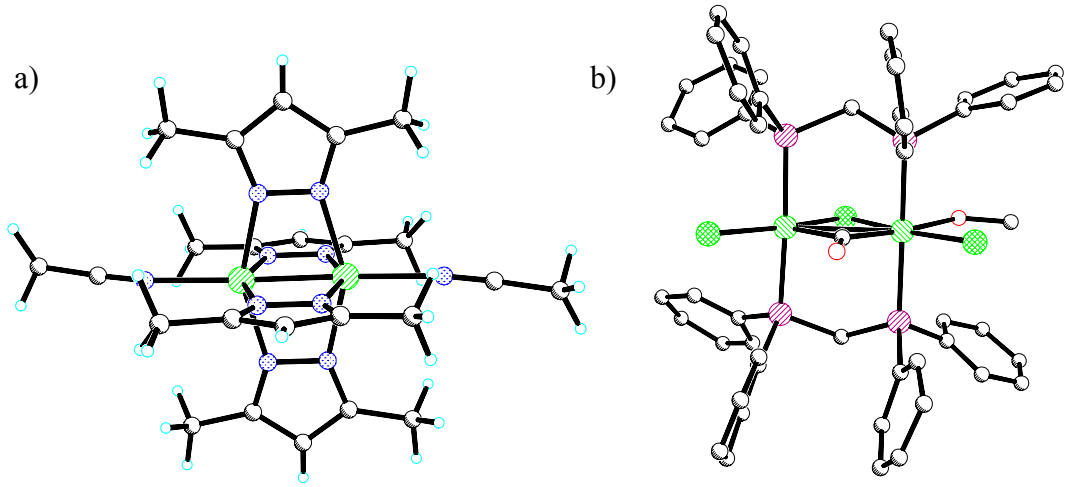

Figure VII-9. Molecular structures of dirhodium compounds with the longest and shortest Rh-Rh bonds respectively a) Rh_2(3,5-dimethylpyrazolato)$_4$·2MeCN, 2.353(3) Å b) Rh_2(CO)Cl(dppm)(MeOH)][PF_6]·2MeOH, 3.010(2) Å.

The [Rh(**Ni-1'**)$_3$][BF_4]$_3$ salt crystallizes as an enantiomerically pure sample in the rhombohedral space group *R*3c as its Δ optical isomer. Selected metric data is listed in Table VII-6. There are three independent molecules in the unit cell which show minor differences. The molecular structure of the $RhNi_3$ complex is that of a boat propeller in which three NiN_2S_2 ligands are bound in a chelating arrangement to a Rh^{III} ion thus saturating its coordination sphere and forming a pseudooctahedron. Neglecting the diazacycle framework, the molecular cation is of D_3 symmetry which is inherently chiral (see Figure VII-10). The unit cell contains a Rh(**Ni-1'**)BF_4 unit and this D_3 symmetry generates the entire molecule. The disordered BF_4^- ions are clustered around each of the tetranuclear cations and are more than 3.2 Å away as seen in Figure VII-11.

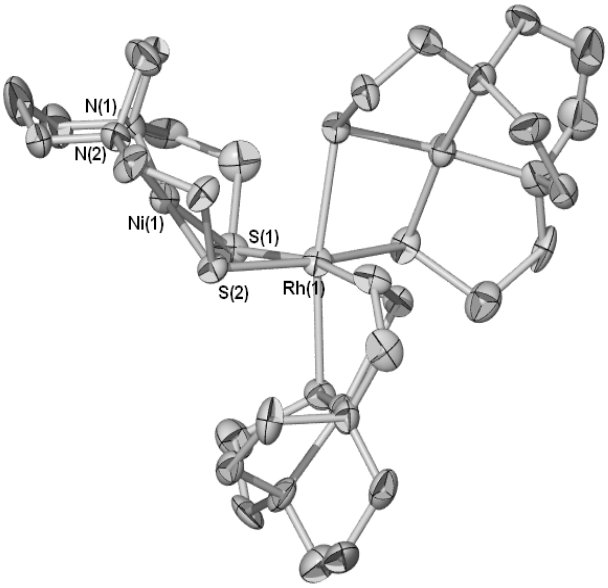

Figure VII-10. Thermal ellipsoid plot (50 % probability) of the $[Rh(\textbf{Ni-1}')_3]^{3+}$ cation with hydrogens omitted.

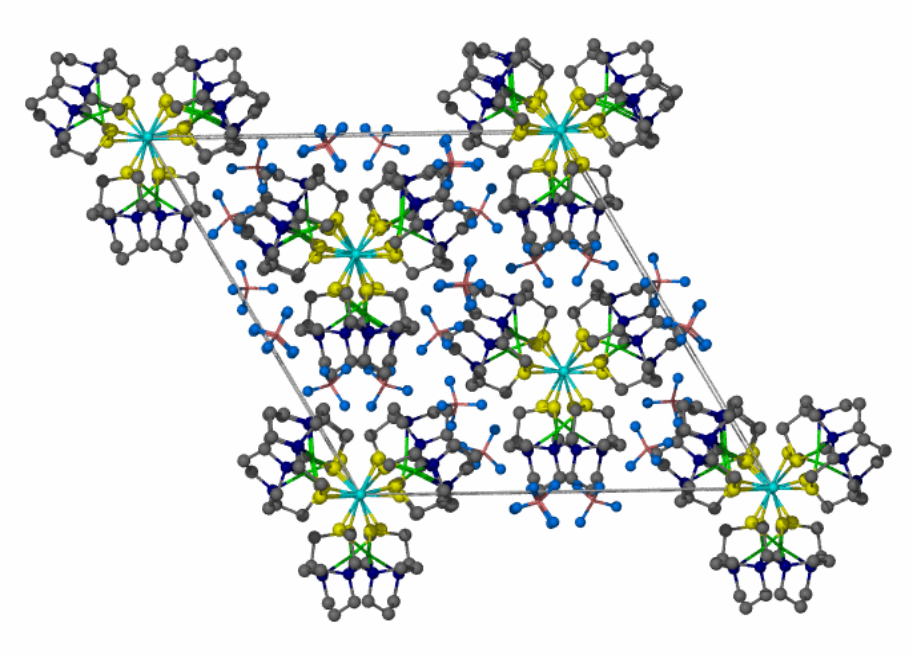

Figure VII-11. Packing diagram of the $[Rh(\textbf{Ni-1}')_3][BF_4]_3$ complex as viewed along the c-axis.

Table VII-6. Selected metric data for [Rh(**Ni-1'**)$_3$][BF$_4$]$_3$.

Rh-Ni	3.129	S(1)-Rh(1)-S(2)	79.30(9)
Rh(1)-S(1)	2.374(3)	S(1)-Ni(1)-S(2)	89.72(11)
Rh(1)-S(2)	2.383(3)	N(1)-Ni(1)-N(2)	83.5(4)
Ni(1)-S(1)	2.144(3)		
Ni(1)-S(2)	2.159(3)		
Ni(1)-N(1)	1.919(9)		
Ni(1)-N(2)	1.927(9)		

Electrochemistry

The compounds [Rh(**Ni-1'**)$_3$][I]$_3$ and [Rh$_2$(**Ni-1'**)$_4$][O$_2$CCF$_3$]$_4$ were analyzed in MeCN solution using the electrochemical methods of cyclic and square wave voltammetry. Analysis of the [Rh(**Ni-1'**)$_3$][I]$_3$ compound, shown in Figure VII-12, revealed two irreversible reductions in the cathodic region at E_{pc1} = -0.90 V and E_{pc2} = -1.64 V. A third reduction, at $E_{1/2}$ = -1.99 V, is reversible. These events are assigned to the $Ni^{2+/1+}$ reduction of the three NiN_2S_2 ligands. The reduction process occurring at -0.30 V has been not been assigned. Observation of this event is not consistently reproducible. This response is often very small, and we conclude it to be an impurity or decomposition product. The anodic region of the CV shows two irreversible oxidations at E_{pa1} = 0.48 V and E_{pa2} = 0.77 V. These oxidations are reasonably assigned to the oxidation of I^- to I_2.[86]

Analysis of [Rh$_2$(**Ni-1'**)$_4$][O$_2$CCF$_3$]$_4$ as shown in Figure VII-13, showed three irreversible reductions in the cathodic region at -0.47, -0.81, and -1.58 V assigned to reduction of the NiN_2S_2 ligands. Only three of the four nickel *cis*-thiolates exhibit redox activity within the MeCN solvent window. The anodic region showed an irreversible oxidation at 1.07 V. This oxidation is assigned to the $Rh_2^{4+/5+}$ oxidation. The recently reported *cis*-Rh$_2$(C$_6$H$_4$PPh$_2$)$_2$(MeCN)$_6$(BF$_4$)$_2$·0.5H$_2$O complex displayed a reversible $Rh_2^{4+/5+}$ oxidation at $E_{1/2}$ = 1.41 V.[87]

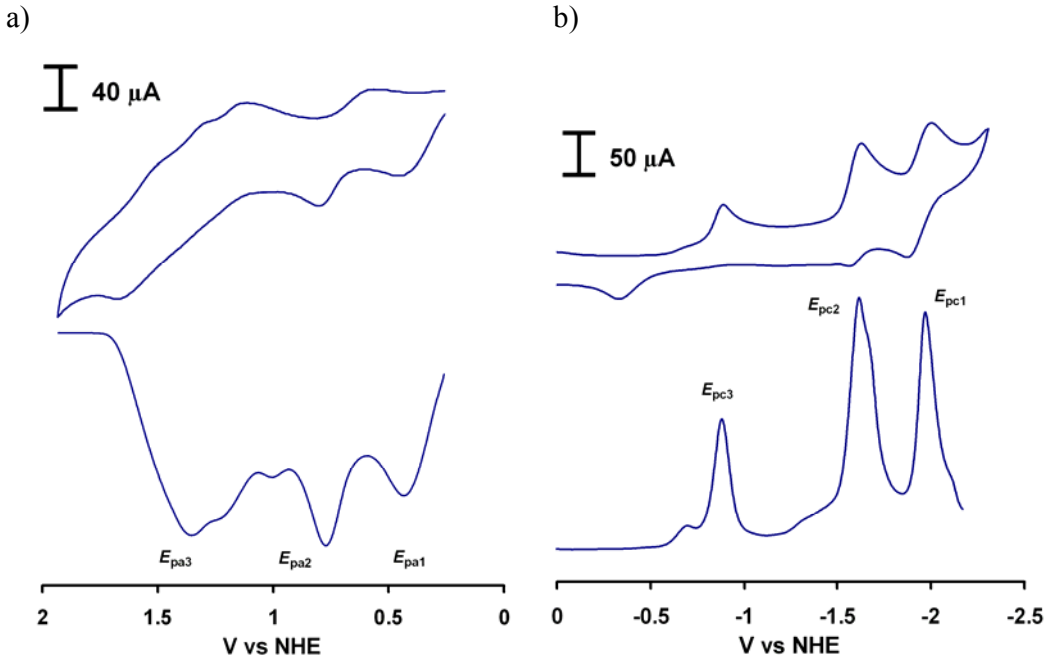

Figure VII-12. Cyclic and square wave voltammograms of the a) anodic and b) cathodic regions of a 1.0 mM solution of [Rh(**Ni-1'**)$_3$][I]$_3$ in 0.1 M *n*-Bu$_4$NBF$_4$ at a scan rate of 100 mV/ s.

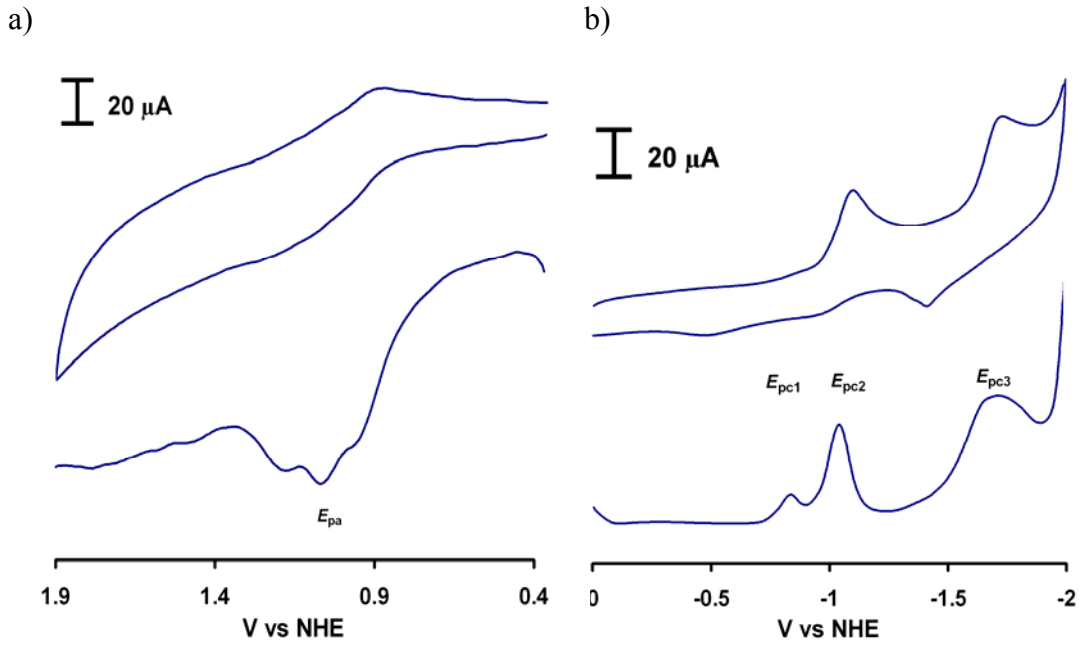

Figure VII-13. Cyclic and square wave voltammograms of the a) anodic and b) cathodic regions of a 0.1 mM solution of [Rh$_2$(**Ni-1'**)$_4$][O$_2$CCF$_3$]$_4$ in 0.1 M *n*-Bu$_4$NBF$_4$ at a scan rate of 100 mV/ s.

Rhodium reactivity

Studies were performed to investigate if the hexametallic $[Rh^{II}_2(\mathbf{Ni\text{-}1'})_4]^{4+}$ cluster can be synthesized from the $[Rh^{III}(\mathbf{Ni\text{-}1'})_3]^{3+}$ cluster in the presence of Rh^I. Thus, solutions of $[Rh(\mathbf{Ni\text{-}1'})_3][I]_3$ and $[Rh(cod)Cl]_2$ were reacted. To enforce a 1:2 rhodium to nickel stochiometry, **Ni-1'** was added as well. To drive the reaction to completion and to obtain a common counterion, chloride and iodide salts were precipitated with $TlPF_6$. The reagents were refluxed in 20 mL of MeCN overnight, the solvent removed *in vacuo*, and the remaining solid analyzed via ESI-MS. The isotopic envelope of greatest intensity was that of the $\{[Rh(\mathbf{Ni\text{-}1'})_3(MeCN)]^{3+}\}$ 325 (100%), followed by $\{[Rh(\mathbf{Ni\text{-}1'})_3{}^{3+}\}$ 311 (25.2%). It appears once the tetrametallic cluster is formed, the Rh-S bonds are stable; that is, chelate closing is highly favored and no open site is created for Rh^I to form a bond with Rh^{III}.

Scheme VII-5. Routes (successful and failed attempts) to the various polymetallic rhodium clusters.

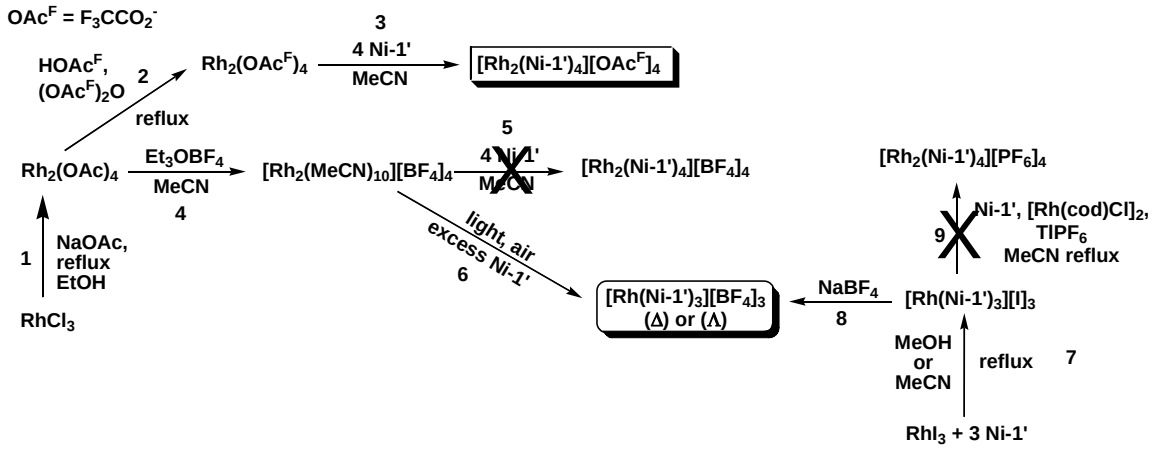

Reactivity of the RhNi complexes related to synthesis and interconversion of species is summarized in Scheme VII-5. Any product in this scheme can be synthesized

in a facile manner by starting from rhodium(III)halides. In reaction 1, $Rh_2(OAc)_4$is prepared from $RhCl_3$ and sodium acetate in refluxing ethanol. This can be converted to the trifluoroacetate via reaction 2 by refluxing in trifluoroacetic acid and trifluoroacetic anhydride. The hexametallic cluster, $[Rh_2(\mathbf{Ni\text{-}1'})_4]^{4+}$, can be formed upon mixing $Rh_2(OAc^F)_4$ with **Ni-1'** and MeCN (reaction 3). In reaction 4, $Rh_2(OAc)_4$ is converted to the decakis(acetonitrile) complex by refluxing with an excess of Et_3OBF_4 and MeCN for a period of seven days. In our hands, the **Ni-1'**/MeCN exchange to produce the BF_4^- salt of $[Rh_2(\mathbf{Ni\text{-}1'})_4]^{4+}$, reaction 5, was unsuccessful. Instead, reaction 6 occurred resulting in a tetrametallic species. This material can be synthesized directly through reactions 7 and 8, in which RhI_3 and three equivalents of **Ni-1'** were refluxed in MeCN, followed by anion exchange with $NaBF_4$. To investigate conversion of Rh^{III} and Rh^{I} source to yield Rh_2^{4+}, reaction 9 was performed. In this reaction, the product of reaction 8 was mixed with $TlPF_6$, **Ni-1'**, and $[Rh(cod)Cl]_2$. No products were obtained from this reaction.

CHAPTER VIII

SUMMARY AND CONCLUSIONS

The design of ligands which offer specific properties to transition metal complexes is a persistent endeavor in the fields of academic and industrial research. There has long been evidence in the literature noting the formation of heterometallic clusters in which two or more metals are bridged by thiolates. I have explored the extent to which such aggregates might be considered as normal coordination complexes wherein a NiN_2S_2 metallothiolate unit serves as an innocent ligand forming coordinate covalent bonds to a second metal. The long-term goal of my project was to explore the analogy between diphosphine and diimine ligands with *cis*-thiolato nickel compounds as metallodithiolate ligands and to advance them as an entirely new class of ligands.

To investigate the analogy of NiN_2S_2 to diphosphines as ligands, a series of $(NiN_2S_2)W(CO)_4$ complexes was synthesized; the complexes were structurally characterized, their infrared spectra obtained, and Cotton-Kraihanzel force constants calculated. Using CO ligands to report the electron density on the tungsten metal center, these complexes were ranked according to their donor abilities. The neutral complexes of this series are of essentially the same donor ability, whereas the dianion ($Ni(ema)^{2-}$), was the best donor as indicated by having the lowest ν(CO) stretching frequencies. In comparison to the more traditional ligands in the literature, i.e. those containing either N- or P-donor ligands, the NiN_2S_2 ligands have donor abilites much greater than

diphosphines. In fact, their donor abilities are much closer to diimine ligands like bipyridine.

X-ray structural analysis revealed two striking features in the series of $(NiN_2S_2)W(CO)_4$ complexes. The first feature is the hinge angle defined as the intersection of the NiN_2S_2 and S_2WC_2 planes. This hinge angle, ranging from 107 to 136˚, is directed by the steric bulk of the pendant thiolate arms on the NiN_2S_2 ligand and correlates with the Ni-W distances which range from 2.92 to 3.39 Å. The second feature is the bending of the CO ligands caused by intermolecular interactions of neighboring CO ligands on adjacent molecules.

Having established their donor abilities, ligand substitution studies were performed. Investigations with (**Ni-1'**)$W(CO)_4$ using the ν(CO) region of the infrared spectrum as a monitor showed substitution of the NiN_2S_2 ligand with excess monodentate phosphines is possible. This qualitative study proved unsuccessful for detailed kinetic information; however, it indicated similarity in affinity for the $W(CO)_4$ unit by phosphines and NiN_2S_2 metalloligands.

Kinetic studies performed on the (**Ni-1***)$W(CO)_4$ complex revealed a NiS_2 chelate ring opening mechanism proposed of the Acetyl CoA Synthase catalysis mechanism. A study by Don Darensbourg, Andrea Phelps, and co-workers showed that at high CO pressures and temperatures, the pentacarbonyl derivative is formed. In fact, crystallographic studies found the remaining chelate arm strengthens as evidenced by shorter W-S bond distances in the pentacarbonyl derivatives of both **Ni-1** and **Ni-1*** as

compared to the tetracarbonyls. There was no evidence suggesting the formation of $W(CO)_6$, indicating the remaining W-S bond is quite strong.

The aggregative ability of nickel *cis*-dithiolates may be controlled by the sulfur affinity of the exogenous metal or by modification of the NiN_2S_2 moiety itself. Thus the sulfinato species, Ni(mese-daco), was prepared. When reacted with $W(CO)_5$(THF) to probe the donor ability of the oxygenated species, the absence of CO bands in the IR spectrum suggested a labilizing effect by Ni(mese-daco) (or an oxidation of the CO ligands) similar to that observed for phosphine oxides. However, in the case of CuBr as electrophile a $CuNi_2$ trimetallic was isolated.

Metallodithiolates, aided by sulfur's affinity for aggregation, have served as the building block or subunit for myriad complexes found in the literature. The metallodithiolate ligands **Ni-1** and **Ni-1'** have been used in a number of metallations and bind to metals using one or both sulfur donor atoms to form coordinate-covalent bonds with an exogenous metal. When both S-donor atoms are used, the NiN_2S_2 unit can be either a bidentate ligand chelated to a single metal or a bidentate-bridging ligand binding two metals together. In this dissertation, these NiN_2S_2 units were reacted with various metals (W, Mo, Rh, Pd, Cu) resulting in bi- and trimetallics, C_4 paddlewheels, and propeller-shaped molecular constructions. The resultant polymetallic complexes were characterized via x-ray crystallography. In all cases, there were slight changes in the metric parameters of the metalloligand, indicated by an increase in the Ni-S distances with a concomitant decrease in the Ni-N distances. Additionally, the metallothiolate ligand becomes more ordered upon metallation.

The paddlewheel structures utilizing NiN_2S_2 units reported in the literature were formed serendipitously via the ability of the *cis*-dithiolate to scavenge metal ions from solution. The paddlewheel structures in this dissertation are the result of designed synthesis in which labile ligands are displaced from a preconstructed dimetal unit as a synthon. Each complex contains four NiN_2S_2 units which bind in a bidentate bridging fashion to a dimetal unit bound by its sulfur donor atoms. A series of hexametallic clusters was synthesized of the bond orders 4, 1, and 0. The clusters are formulated as $M_2Ni_4^{4+}$, where M = Mo, Rh, Pd. On stripping away the hydrocarbons of the metalloligand, the clusters are isostructural having an overall point group symmetry of C_{4h}. The Rh_2 complex crystallizes with two axial solvent molecules which is common for compounds of this family. These explorations have extended the range of metal-metal distances accommodated by metallothiolate ligands from 2.14 to 4.35 Å shown in Figure VIII-1.

Table VIII-1 compares the metric parameters for the C_4 and C_3 paddlewheel complexes from our library. The C_4 paddlewheel complexes, which vary in bond order, have similar S···S and Ni-S distances. All complexes are essentially of eclipsed conformations and have approximately the same dihedral angle. There is no difference to the S-Ni-S angle for the dipalladium compared to the free nickel *cis*-dithiolate. Like the C_4 paddlewheel complexes, the C_3 paddlewheels exhibit comparable S···S and Ni-S distances. The Zn_2 and Cu_2 structures have similar torsion and dihedral angles. The molecular structures of the two complexes are deformed, i.e., with a substantial stagger

tendency. The more ordered Ag_2 complex possesses a dihedral angle slightly greater than 90˚ and a torsion angle less than 5˚.

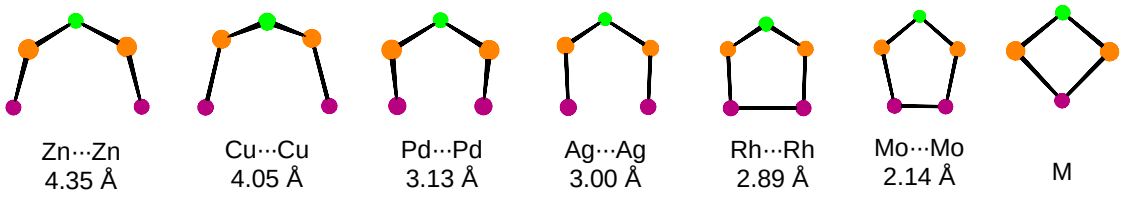

Figure VIII-1. Range of metal-metal distances accommodated by NiN_2S_2 units in our library of paddlewheel complexes.

Table VIII-1. Comparison of selected metric data for all paddlewheel complexes in our library which utilize **Ni-1'** as a bidentate, bridging ligand. Distances shown as averages.

	C_4 paddlewheels			C_3 paddlewheels		
	Mo_2	Rh_2	Pd_2	Ag_2	Cu_2	Zn_2
bond order	4	1	0	0	0	0
M---M	2.162(10)	2.893(8)	3.099(2)	3.00(1)	3.37(1)	4.28(1)
S---S	3.098	3.045	3.188	3.195	3.200	3.204
Ni-S	2.141(16)	2.124(11)	2.143(4)	2.170(2)	2.169(2)	2.168(2)
M-S	2.5179(14)	2.360(11)	2.332(4)	2.515(2)	2.355(2)	2.357(2)
S-Ni-S	92.62(6)	91.56(4)	95.49(15)	94.80(7)	95.0(1)	95.3(1)
Ni-S-M'	106.1(6)	114.71(4)	114.4(16)	91.52(6)	96.51(7)	107.95(6)
Dihedral angle[a]	128.7	129.8	131.6	97.1	102.5	107.6
Torsion angle[b]	0.9	0.3	0.8	4	22.9	26.3

[a] defined as the angle between the NiN_2S_2 and M_2S_2 planes
[b] defined as the S-M-M-S angle

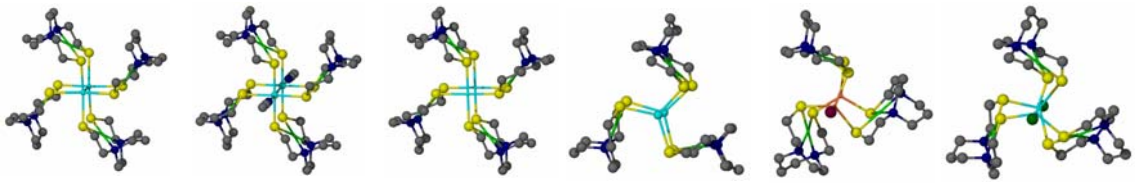

The complexes discussed in this dissertation are polymetallic clusters with high positive charges associated with them. For comparative purposes, all paddlewheel complexes from our library have been analyzed by electrochemistry. Electrochemical studies performed on these complexes revealed successive redox events. We conclude that the the redox chemistry of the NiN_2S_2 ligand can be deconvoluted from the redox active atoms which comprise the dimetal unit; nevertheless, the electrochemistry is complicated by dissociation of the NiN_2S_2 ligand. Sulfur metallation causes the reduction potential of the NiN_2S_2 ligand (~-2.0 V) to become more positive. With each subsequent reduction, the overall positive charge is lessened which consequently causes each successive reduction to be less accessible. Ligand exchange studies suggest NiN_2S_2 ligand dissociation in solution as evidenced by the formation of several mixed-ligand species identified via ESI-MS. The spiking of electrochemical solutions with free NiN_2S_2 found a slight enhancement of the most negative event; however, the effects of spiking were more prominent in the oxidative region as evidenced by the growth of a new peak corresponding to same potential as disulfide formation.

The cyclic voltammograms of the polymetallic clusters revealed multiple and overlapping redox events. Solvent dependent studies on a series of $Mo_2Ni_x(OAc)_{4-x}$ complexes, where x = 4, 3, 2, suggest partial NiN_2S_2 ligand dissociation evidenced by a mixture of strong and weakly defined peaks when the square wave voltammogram is recorded in coordinating solvents such as MeCN or DMF. However, when the square wave voltammogram is recorded in a poorly coordinating solvent such as THF, only four peaks of equal intensity are observed. This partial dissociation of NiN_2S_2 ligands was

observed in kinetic studies and stabilization studies performed on complexes in the $(NiN_2S_2)W(CO)_4$ series. This finding is supported by attempts to structurally characterize the Mo_2Ni_3 and Mo_2Ni_2 clusters resulting in the Mo_2Ni_4 cluster.

Electrochemical studies in DMF performed on the $Mo_2Ni_x(OAc)_{4-x}$ complexes in the series, x = 2 or 3, show noticeable similarities to MeCN in their cyclic and square wave voltammograms. Each complex shows a major redox event besieged by several lesser events which suggest either ligand dissociation or a significant structural rearrangement at this potential. These complexes proved unstable in any solvent used for electrochemical analysis.

Parenthetically, Bill Geiger and co-workers have performed work of a similar context, choosing to focus their efforts on how varying the supporting electrolyte effects the redox potentials on a series of polyferrocenyl complexes which themselves show, successive one-electron processes.[88] Increasing the size of the electrolyte anions from the smaller $[BF_4]^-$ or $[PF_6]^-$ ions to the significantly larger $[B(C_6F_5)_4]^-$ or $[BAr^F]^-$ ions showed a decrease in the conductivity of the solution and consequently more positive potentials by lessening ion paring.

Typically, nickel *cis*-dithiolates have been used to stabilize low or zero valent transition metals. My synthetic efforts have shown that NiN_2S_2 moieties are capable of stabilizing rhodium in multiple oxidation states. These works produced a heterobimetallic (Rh^I), another addition to our library of paddlewheel clusters (Rh^{II}), and a structural mimic to Rubpy complexes (Rh^{III}).

As a whole, NiN_2S_2 moieties are electron-rich ligands as determined by a fundamental organometallic study. The remarkable structural capability of these ligands in mono- and bidentate binding modes has been discussed herein. The hemi-labile property of NiN_2S_2 is consistent with that proposed for the mechanism of the ACS metalloenzyme and shows promise as a ligand in catalytic processes. However, it is up to the synthetic chemist to design ligands with the appropriate steric bulk to exploit this dissociative property to direct substrate to the metal center resulting in high yield and few side-products.

In the words of Sir Isaac Newton, "If I have seen further than others, it is by standing on the shoulders of giants." In the scientific community, our findings stand on the precedents set by giants who have come before us. Since the seminal discovery of nickel *cis*-dithiolates by Jicha and Busche and their use of NiN_2S_2 moieties as ligands to nickel and palladium documented over four decades ago, the field has progressed and the literature has chronicled numerous polymetallic complexes, sulfur alkylations and oxidations, the gauging of their donor abilities and electronic properties, its unearthing in a natural metalloenzyme, and will hopefully culminate with their use as ligands in industrial catalytic processes. The novelty of this work rests in that of a metal complex used as ligand which has its own intrinsic properties (hemi-lability, donor ability, steric bulk, etc.) being used to influence the reactivity of other metals. The evolution of the transition metal complexes has transcended traditional Werner chemistry, while at the same time remained true to classic chemical principles.

...when I started doing chemistry, I did it the way I fished – for the excitement, the discovery, the adventure, for going after the most elusive catch imaginable in uncharted seas. *K. Barry Sharpless*

REFERENCES

1. White, G. S.; Stephan, D. W. *Inorg. Chem.* **1985**, *24*, 1499.
2. Jicha, D. C.; Busch, D. H. *Inorg. Chem.* **1962**, *1*, 872.
3. Rao, P. V.; Bhaduri, S.; Jiang, J.; Holm, R. H. *Inorg. Chem.* **2004**, *43*, 5833.
4. Golden, M. L.; Jeffery, S. P.; Miller, M. L.; Reibenspies, J. H.; Darensbourg, M. Y. *Eur. J. Inorg. Chem.* **2004**, 231.
5. Rampersad, M. V.; Golden, M. L.; Miller, M. L.; Reibenspies, J. H.; Darensbourg, M. Y. *Manuscript in preparation.*
6. Miller, M. L.; Ibrahim, S. A.; Golden, M. L.; Darensbourg, M. Y. *Inorg. Chem.* **2003**, *42*, 2999.
7. Tuntulani, T.; Reibenspies, J. H.; Farmer, P. J.; Darensbourg, M. Y. *Inorg. Chem.* **1992**, *31*, 3497.
8. Jeffery, S. P.; Green, K. G.; Rampersad, M. V.; Reibenspies, J. H.; Darensbourg, M. Y. *Dalton Trans.* Submitted.
9. Golden, M. L.; Whaley, C. M.; Rampersad, M. V.; Reibenspies, J. H.; Hancock, R. D.; Darensbourg, M. Y. *Inorg. Chem.* **2005**, *44*, 875.
10. (a) Huang, W.; Jia, J.; Cummings, J.; Nelson, M.; Schneider, G.; Lindqvist, Y. *Structure* **1997**, *5*, 691. (b) Doukov, T. I.; Iverson, T. M.; Seravalli, J.; Ragsdale, S. W.; Drennan, C. L. *Science* **2002**, *298*, 567. (c) Darnault, C.; Volbeda, A.; Kim, E. J.; Legrand, P.; Vernède, X.; Lindahl, P. A.; Fontecilla-Camps, J. C. *Nat. Struct. Biol.* **2003**, *10*, 271. (d) Nagashima, S.; Nakasako, M.; Dohmae, N.; Tsujimura, M.;

Takio, K.; Odaka, M.; Yohda, M.; Kamiya, N.; Endo, I. *Nat. Struct. Biol.* **1998**, *5*, 347.

11. Mills, D. K.; Reibenspies, J. H.; Darensbourg, M. Y. *Inorg. Chem.* **1990**, *29*, 4364.
12. Smee, J. J.; Miller, M. L.; Grapperhaus, C. A.; Reibenspies, J. H.; Darensbourg, M. Y. *Inorg. Chem.* **2001**, *40*, 3601.
13. Li-Y.-Z.; Liu, J.-C.; Wang, Z.-P.; Li, Q.-X.; Sun, G.-C.; Wang, L. F.; Xia, C.-G. *Acta Cryst.* **2000**, *C56*, e286.
14. Farmer, P. J.; Solouki, T.; Mills, D. K.; Soma, T.; Russell, D. H.; Reibenspies, J. H.; Darensbourg, M. Y. *J. Am. Chem. Soc.* **1992**, *114*, 4601.
15. Cotton, F. A.; Walton, R. A.; Murillo, C. A. *Multiple Bonds Between Metal Atoms,* Spring Science and Business Media, Inc., New York, 3rd edn., 2005.
16. Stanley, G. G., Louisiana State University, http://chemistry.lsu.edu/stanley/webpub/4571-chap10-MM-bonding.pdf (accessed January 2006).
17. (a) Cen, W.; Lindenfield, P.; Fehlner, T. P. *J. Am. Chem. Soc.* **1992,** *114*, 5441**.** (b) Cotton, F. A.; Falvello, L. R.; Reid, Jr., A. H.; Tocher, J. H. *J. Organomet. Chem.* **1987**, *319*, 87. (c) Vega, A.; Calvo, V.; Manzur, J.; Spodine, E.; Saillard, J.-Y. *Inorg. Chem.* **2002**, 41, 5382. (d) Reddy, N. D.; Fanwick, P. E.; Walton, R. A. *Inorg. Chem.* **2001**, *40*, 1732. (e) Calvo-Pérez, V.; Fehlner, T. P.; Rheingold, A. L. *Inorg. Chem.* **1996**, *35*, 7289. (f) Fehlner, T. P.; Calvo-Pérez, V.; Cen. W. *J. Electr. Spectrosc. Related Phenom.* **1993**, *66*, 29. (g) Cooke, M. W.; Murphy, C. A.; Cameron, T. S.; Swarts, J. C.; Aquino, M. A. S. *Inorg. Chem. Commun.* **2000**, *3*, 721. (h) Cooke, M.

W.; Cameron, T. S.; Robertson, K. N.; Swarts, J. C.; Aquino, M. A. S. *Organometallics* **2002**, *21*, 5962. (i) Greaney, M. A.; Stiefel, E. I. *J. Chem. Soc., Chem. Commun.* **1992**, 1679.

18. (a) Lamotte, L.; Dideberg, O.; Dupont, L.; Durbut, P. *Cryst. Struct. Comm.* **1981**, *10*, 59. (b) Breakell, K. R.; Rettig, S. J.; Storr, A.; Trotter, J. *Can. J. Chem.* **1983**, *61*, 1659.

19. (a) Cotton, F. A.; Donahue, J. P.; Murillo, C. A. *Inorg. Chem.* **2001**, *40*, 2229. (b) Cotton, F. A.; Liu, C.-Y.; Murillo, C. A.; Wang, X. *Inorg. Chem.* **2003**, *42*, 4619. (c) Lu, J.; Harrison, W. T. A.; Jacobson, A. J. *Chem. Commun.* **1996**, 399. (d) Contakes, S. M.; Klausmeyer, K. K.; Rauchfuss, T. B. *Inorg. Chem.* **2000**, *39*, 2069. (e) Kim, Y.; Kim, S.-J.; Nam, W. *Acta Crystallogr.* **2000**, *C57*, 266. (f) Chapman, C. T.; Ciurtin, D. M.; Smith, M. D.; zur Loye, H.-C. *Solid State Sciences* **2002**, *4*, 1187. (g) Kuang, S.-M.; Fanwick, P. E.; Walton, R. A. *Inorg. Chem.* **2002**, *41*, 147. (h) Cotton, F. A.; Donahue, J. P.; Lin, C.; Murillo, C. A. *Inorg. Chem.* **2001**, *40*, 1234. (i) Cotton, F. A.; Daniels, L. M.; Lin, C.; Murillo, C. A. *J. Am. Chem. Soc.* **1999**, *121*, 4538. (j) Cotton, F. A.; Lin, C.; Murillo, C. A. *Inorg. Chem.* **2001**, *40*, 478. (k) Cotton, F. A.; Lin, C.; Murillo, C. A. *Acc. Chem. Res.* **2001**, *34*, 759.

20. (a) Cotton, F. A.; Dikarev, E. V.; Herrero, S. *Inorg. Chem.* **1998**, *37*, 490. (b) Abbott, E. H.; Bose, K. S.; Cotton, F. A.; Hall, W. T.; Sekutowski, J. C. *Inorg. Chem.* **1978**, *17*, 3240. (c) Campbell, F. L., III; Cotton, F. A.; Powell, G. L. *Inorg. Chem.* **1984**, *23*, 4222. (d) Cotton, F. A.; Dunbar, K. R.; Poli, R. *Inorg. Chem.* **1986**, *25*, 3700. (e) Fanwick, P. E.; Harwood, W. S.; Walton, R. A. *Inorg. Chim. Acta* **1986**, *122*, 7.

21. Gordon, A. J.; Ford, R. A. *The Chemist's Companion,* Wiley and Sons: New York, 1972; pp. 429-436.

22. Gagné, R. R.; Koval, C. A.; Lisensky, G. C. *Inorg. Chem.* **1980**, *19*, 2854.

23. SMART 1000 CCD, Bruker Analytical X-ray Systems: Madison, WI, 1999.

24. Sheldrick, G. 1990, SHELXTL-PLUS revison 4.11V, SHELXTL-PLUS users manual, Siemens Analytical X-ray Inst. Inc., Madison, WI, U.S.A.

25. Sheldrick, G. 1997, SHELXS-97 Program for Crystal Structure Solution, Institüt für Anorganische Chemie der Universität, Tammanstrasse 4, D-3400 Gottingen, Germany.

26. Sheldrick, G. 1997, SHELXL-97 Program for Crystal Structure Refinement, Institüt für Anorganische Chemie der Universität, Tammanstrasse 4, D-3400 Gottingen, Germany.

27. SAINT V6.63 "Program for Reduction of Area Detector Data" Bruker AXS Inc., Madison, WI, 53711-5373 U.S.A.

28. Barbour, L. J. *J. Supramol. Chem.* **2001***, 1,* 189.

29. Colpas, G. J.; Kumar, M.; Day, R. O.; Maroney, M. J. *Inorg. Chem.* **1990**, *29*, 4779.

30. Darensbourg, D. J.; Kump, R. L. *Inorg. Chem.* **1978**, *17*, 2680.

31. Rampersad, M. V.; Jeffery, S. P.; Golden, M. L.; Lee, J.; Reibenspies, J. H.; Ortiz, C. G.; Darensbourg, D. J.; Darensbourg, M. Y. *J. Am. Chem. Soc.* **2005**, *127*, 17323.

32. (a) Cotton, F. A.; Wiesinger, K. J. *Inorg. Chem.* **1991**, *30*, 871. (b) Shin, Y. K.; Nocera, D. G. *J. Am. Chem. Soc.* **1992**, *114*, 1264.

33. Cotton, F. A.; Reid Jr., A. H.; Schwotzer, W. *Inorg. Chem.* **1985**, *24*, 3965.

34. Cotton, F. A.; Liu, C.-Y.; Murillo, C. A. *Inorg. Chem.* **2004**, *43*, 2267.

35. Golden, M. L.; Rampersad, M. V.; Reibenspies, J. H.; Darensbourg, M. Y. *Chem. Commun.* **2003**, 1824.

36. Darensbourg, M. Y.; Font, I. Pala, M. Reibenspies, J. H. *J. Coord. Chem.* **1994**, *32*, 39.

37. Kruger, H. J.; Peng, G.; Holm, R. H. *Inorg. Chem.* **1991**, *30*, 734.

38. Slightly modified procedure of Rempel, G. A.; Legzdins, P.; Smith, H.; Wilkinson, G. *Inorg. Synth.* **1972**, *13*, 90.

39. Tolman, C. A. *Chem. Rev.* **1977**, *77*, 313.

40. Lai, C.-H.; Reibenspies, J. H.; Darensbourg, M. Y. *Angew. Chem. Int. Ed. Engl.* **1996**, *35*, 2390.

41. Rampersad, M. V.; Jeffery, S. P.; Reibenspies, J. H.; Ortiz, C. G.; Darensbourg, D. J.; Darensbourg, M. Y. *Angew. Chem. Int. Ed.* **2005**, *117*, 1243.

42. Grapperhaus, C. A.; Mullins, C. S.; Kozlowski, P. M.; Mashuta, M. S. *Inorg. Chem.* **2004**, *43*, 2859.

43. (a) Allen, F. H.; Kennard, O.; Taylor, R. *Acc. Chem. Res.* **1983**, *16*, 146. (b) Allen, F. H. A*cta Cryst.* **2002**, *B58*, 380.

44. (a) Huikan, W.; Lucas, C. R. *Inorg. Chem.* **1992**, *31*, 2354. (b) Cortes-Figueroa, J. E.; Zubkowski, J. D.; Valente, E. J. *J. Chem. Cryst.* **1998**, *28*, 217. (c) Reisner, G. M.; Bernal, I.; Dobson, G. R. *J. Organomet. Chem.* **1978**, *23*, 157.

45. (a) Saum, S. E.; Fronczek, F. R.; Laneman, S. A.; Stanley, G. G. *Inorg. Chem.* **1989**, *28*, 878. (b) Bienewald, F.; Ricard, L.; Mercier, F.; Mathey, F. *Tetrahedron Assym.*

1999, *10*, 4701. (c) Horng, D.-N.; Ueng, C.-H. *J. Organomet. Chem.* **1995**, *53*, 505. (d) Ye, Q.; Wu, Q.; Zhao, H.; Song, Y.-M.; Xue, X.; Xiong, R.-G.; Pang, S.-M.; Lee, G. H. *J. Organomet. Chem.* **2005**, *690*, 286. (e) Jinshun, H.; Qinrong, C.; Manfang, W.; Shimei, L. *Jiegou Huaxue* **1985**, *4*, 64. (f) Liu, F.; Chem, W.; You, X. *Anal. Sci.* **1985**, *4*, 64.

46. Cotton, F. A.; Kraihanzel, C. S. *J. Am. Chem. Soc.* **1962**, *84*, 4432.
47. Phelps, A. L.; Rampersad, M. V.; Fitch, S. B.; Darensbourg, M. Y.; Darensbourg, D. J. *Inorg. Chem.* **2006**, *45*, 119.
48. (a) Hirisivaara, L.; Haukka, M.; Pursiainen. *Eur. J. Inorg. Chem.* **2001**, 2255. (b) Sánchez-Peláez, A.-E.; Perpiñán, M.F. *J. Organomet. Chem.* **1991**, *405* 101. (c) Syzmańska-Buzar, T.; Glowiak, T.; Czeluśniak, I. *Polyhedron* **2002**, *21*, 1817.
49. (a) Benson, J. W.; Keiter, R. L.; Keiter, E. A.; Rheingold, A. L.; Yap., G. P. A.; Mainz, V. V. *Organometallics* **1998**, *17*, 4275. (b) Benson, J. W.; Keiter, R. L.; Keiter, E. A. *J. Organomet. Chem.* **1995**, *495*, 77. (c) Sellmann, D.; Weiß, R.; Knoch, F.; Moll, M. *J. Organomet. Chem.* **1990**, 3*91*, 327.
50. Golden, M. L.; Yarbrough, J. C.; Reibenspies, J. H.; Darensbourg, M. Y. *Inorg. Chem.* **2004**, *43*, 4207.
51. Kang, D.-X.; Poor, M.; Blinn, E. L.; Treichel, P. M. *Inorg. Chim. Acta* **1990**, *168*, 209.
52. (a) Lane, R. H.; Pantaleo, N. S.; Farr, J. K.; Coney, W. M.; Newton, M. G. *J. Am. Chem. Soc.* **1978**, *100*, 1610. (b) Henkel, G.; Betz, P.; Krebs, B. *Inorg. Chim. Acta* **1987**, *134*, 195.

53. Darensbourg, D. J.; Walker, N.; Darensbourg, M. Y. *J. Am. Chem. Soc.* **1980**, *102*, 1213.

54. Jeffery, S. P.; Lee, J.; Darensbourg, M. Y. *Chem. Commun*. **2005**, 1122.

55. Amoroso, A. J.; Chung, S. S. M.; Spencer, D. J. E.; Danks, J. P.; Glenny, M. W.; Blake, A. J.; Cooke, P. A.; Wilson, C.; Schröder, M. *Chem. Commun.* **2003**, 2020.

56. Burk, J. D.; Whitwell II, G. E.; Lemley, J. T.; Burlitch, J. M. *Inorg. Chem.* **1983**, *22*, 1306.

57. (a) Cotton, F. A.; Fanwick, P. E.; Niswander, R. H.; Sekutowski, J. C. *Acta Chem. Scand.* **1978**, *A32*, 663. (b) Ricard; L.; Karagiannidis, P.; Weiss, R. *Inorg. Chem.* **1973**, *9*, 2179.

58. Musie, G.; Farmer, P. J.; Tuntulani, T.; Reibenspies, J. H.; Darensbourg, M. Y. *Inorg. Chem.* **1996**, *35*, 2176.

59. Bleujerveld, R. H. T.; Vrieze, K. *Inorg. Chim. Acta* **1976**, *19*, 195.

60. Cotton, F. A.; Daniels, L. M.; Murillo, C. A.; Timmons, D. J.; Wilkinson, C. C. *J. Am. Chem. Soc.* **2002**, *124*, 9249.

61. Grapperhaus, C. A.; Darensbourg, M. Y. *Acc. Chem. Res.* **1998**, *31*, 451.

62. Jeffery, S. P. *Unpublished results*.

63. (a) Huang, Y.; Drake, R. L.; Stephan, D. W. *Inorg. Chem.* **1993**, *32*, 3022. (b) Konno, T.; Yonenobu, K.; Hidaka, J.; Okamoto, K. *Inorg. Chem.* **1994**, *33*, 861. (c) Gasanov, K. I.; Antsyshkina, A. S.; Sadikov, G. G.; Ivanova, N. A.; Mirzai, D. I.; Eimenko, I. A.; Sergienko, V. S. *Kristallografiya* **2002**, *47*, 668. (d) Gorbunova, Y.

E.; Mikhailov, Y. N.; Kurbakova, A. P.; Efimenko, I. A. *Koord. Khim.* **1993**, *19*, 322.

64. (a) Pauly, J. W.; Sander, J.; Kuppert, D.; Winter, M.; Reiss, G. J.; Zurcher, F.; Hoffmann, R.; Fassler, T. F.; Hegetschweiler, K. *Chem. Eur. J.* **2000**, *6*, 2830. (b) Zilbermann, I.; Maimon, E.; Cohen, H.; Meyerstein, D.; *Chem. Rev.* **2005**, *105*, 2609.
65. Golden, M. L. Ph.D. Dissertation, Texas A&M University, College Station, TX USA. 2004.
66. Santure, D. J.; Huffman, J. C.; Sattelberger, A. P. *Inorg. Chem.* **1985**, *24*, 371.
67. Jubran, N.; Meyerstein, D.; Koresh, J.; Cohen, H. J. *J. Chem. Soc., Dalton Trans.* **1986**, 2509.
68. (a) Tuntulani, T.; Musie, G.; Reibenspies, J. H.; Darensbourg, M. Y. *Inorg. Chem.* **1995**, *34*, 6279. (b) Farmer, P. J.; Reibenspies, J. H.; Lindahl, P. A.; Darensbourg, M. Y. *J. Am. Chem. Soc.* **1993**,*115,* 4665.
69. Hartman, J. R.; Cooper, S. R. *J. Am. Chem. Soc.* **1986**, *108*, 1202.
70. Karlin, K.; Zubieta, J., Eds. "Copper Coordination Chemistry: Biochemical and Inorganic Perspectives"; Adenine Press: Guilderland, NY, 1983.
71. Zhang, F.; Bau, S.; Yap, G. P. A.; Tarwade, V.; Fox, J. M. *J. Am. Chem. Soc.* **2005**, *127*, 10590.
72. Aguado, J. E.; Calhorda, M. J.; Costa, P. J.; Crespo, O. Félix, V.; Concepción Gimeno, M; Jones, P. G.; Laguna, A. *Eur. J. Inorg. Chem.* **2004**, 3038.

73. Tsuchiya, T.; Shimizu, T.; Hirabayashi, K.; Kamigata, N. *J. Org. Chem.* **2002**, *67*, 6632.

74. (a) Bryan, J. C.; Cotton, F. A.; Daniels, L. M.; Haefner, S. C.; Sattelberger, A. P. *Inorg. Chem.,* **1995**, *34*, 1875. (b) Prater, M. E.; Pence, L. E.; Clérac, R.; Finniss, G. M.; Campana, C.; Auban-Senzier, P.; Jerome, D.; Canadell, E.; Dunbar, K. R. *J. Am. Chem. Soc.,* **1999**, *121*, 8005.

75. Vella P.; Zubieta, J. *J. Inorg. Nucl. Chem.,* **1978**, *40*, 477.

76. (a) Della Guardia, R. A.; Thomas, J. K. *J. Phys. Chem.* **1983**, *87*, 990. (b) Schoonheydt, R. A.; De Pauw, P.; Vliers, D. De Schrijver, F. C. *J. Phys. Chem.* **1984**, *88*, 5113. (c) Ghosh, P. K.; Bard, A. J. *J. Phys. Chem.* **1984**, *88*, 5519.

77. De Armond, M. K.; Myrick, M. L. *Acc. Chem. Res.* **1989**, *22*, 364.

78. Dunbar, K. R. *J. Am. Chem. Soc.* **1988**, *110*, 8247.

79. James, C. A.; Morris, D. E.; Doorn, S. K.; Arrington, Jr., C. A.; Dunbar, K. R. *Inorg. Chim. Acta* **1996**, *242*, 91.

80. Green, K. G.; Jeffery, S. P.; Reibenspies, J. H. Darensbourg, M. Y. *J. Am. Chem. Soc.* Submitted.

81. Forster, D. *Adv. Organomet. Chem.* **1979**, *17*, 255.

82. Leigh, G. J.; Sanders, J. R.; Hitchcock, P. B.; Fernandes, J. S.; Togrou, M. *Inorg. Chimica Acta* **2002**, *330*, 197.

83. Bondi, A. *J. Phys. Chem*. **1964**, *68*, 441.

84. Hinchliffe, A.; Hughes, P. R. *J. Mol. Struct.* **1976**, *32*, 79.

85. (a) Barron, A. R.; Wilkinson, G.; Motevalli, M.; Hursthouse, M. B. *Polyhedron* **1985**, *4*, 1131. (b) Cotton, F. A.; Eagle, C. T.; Price, A. C. *Inorg. Chem.* **1988**, *27*, 4362.

86. Datta, J.; Bhattacharya, A.; Kundu, K. K. *Bull .Chem. Soc. Jpn.* **1988**, *61*, 1735.

87. Cotton, F. A.; Murillo, C. A.; Yu, R. *Inorg. Chem.* **2004**, *43*, 8394.

88. (a) LeSuer, R.; Geiger, W. E. *Angew. Chem. Int. Ed.* **2000**, *39*, 248. (b) Camire, N.; Mueller-Westerhoff, U. T.; Geiger, W. E. *J. Organomet. Chem.* **2001**, *637-639*, 823. (c) Barrière, F.; Camire, N.; Geiger, W. E.; Mueller-Westerhoff, U. T.; Sander, R. *J. Am. Chem. Soc.* **2002**, *124*, 7262. (d) LeSuer, R.; Buttolph, C.; Geiger, W. E. *Anal. Chem.* **2004**, *76*, 6395.

APPENDIX

TABLES OF STRUCTURAL DATA

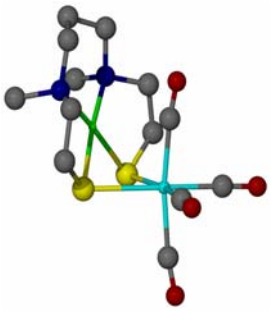

(Ni(bme-Me_2PDA)W$(CO)_4$

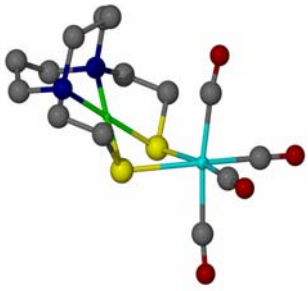

(**Ni-1**)W$(CO)_4$

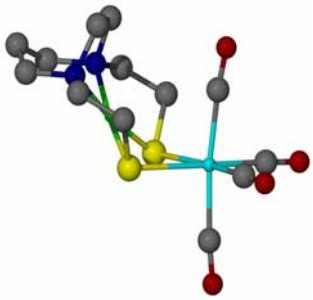

(**Ni-1'**)W$(CO)_4$

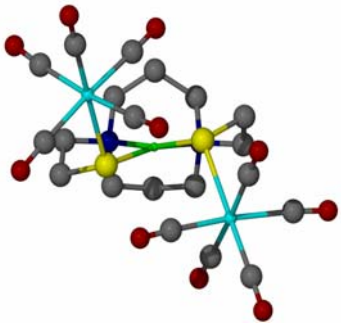

Ni-1$(W(CO)_5)_2$

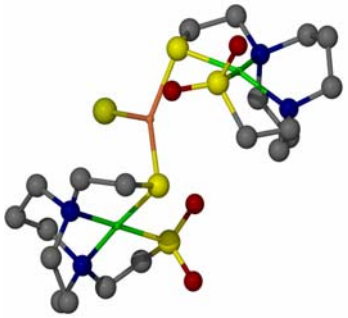

(Ni(mese-daco))$_2$CuBr

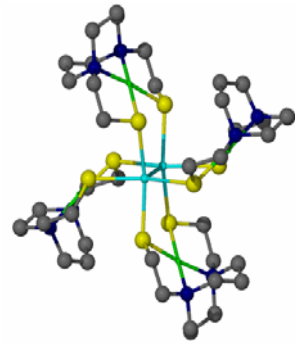

[Mo_2(**Ni-1**)$_4$][BF_4]$_4$

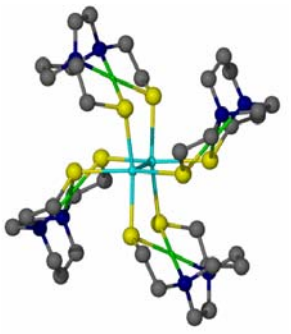

[Mo_2(**Ni-1'**)$_4$][BF_4]$_4$

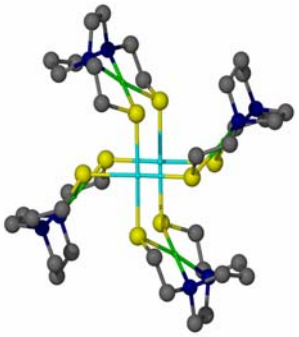

[Pd_2(**Ni-1'**)$_4$][Br]$_4$

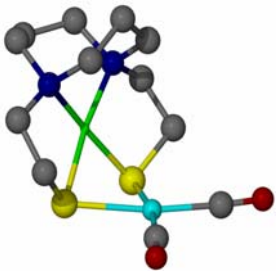

[Rh(**Ni-1**)$(CO)_2$][PF_6]

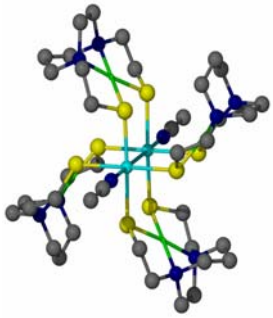

[Rh_2(**Ni-1'**)$_4$][O_2CCF_3]$_4$·2MeCN

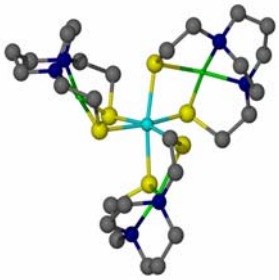

[Rh(**Ni-1'**)$_3$][BF_4]$_3$

Table A-1. Crystal data and structure refinement for $(Ni(bme\text{-}Me_2PDA))W(CO)_4$.

Empirical formula	C13 H20 N2 Ni O4 S2 W	
Formula weight	574.99	
Temperature	293(2) K	
Wavelength	0.71073 Å	
Crystal system	Orthorhombic	
Space group	Pnma	
Unit cell dimensions	a = 19.713(6) Å	α= 90°.
	b = 12.868(3) Å	β= 90°.
	c = 6.894(3) Å	γ = 90°.
Volume	1748.9(10) $Å^3$	
Z	4	
Density (calculated)	2.184 Mg/m^3	
Absorption coefficient	7.906 mm^{-1}	
F(000)	1112	
Crystal size	0.3 x 0.2 x 0.2 mm^3	
Theta range for data collection	2.07 to 23.28°.	
Index ranges	-14<=h<=21, -14<=k<=14, -7<=l<=7	
Reflections collected	7110	
Independent reflections	1326 [R(int) = 0.0313]	
Completeness to theta = 23.28°	100.0 %	
Absorption correction	None	
Refinement method	Full-matrix least-squares on F^2	
Data / restraints / parameters	1326 / 0 / 116	
Goodness-of-fit on F^2	1.296	
Final R indices [I>2sigma(I)]	R1 = 0.0389, wR2 = 0.1006	
R indices (all data)	R1 = 0.0434, wR2 = 0.1150	
Largest diff. peak and hole	4.942 and -1.528 $e.Å^{-3}$	

Table A-2. Bond lengths [Å] and angles [°] for (Ni(bme-Me_2PDA))$W(CO)_4$.

Ni(1)-N(1)	1.995(6)
Ni(1)-N(1)#1	1.995(6)
Ni(1)-S(1)#1	2.190(2)
Ni(1)-S(1)	2.190(2)
W(1)-C(3)	1.952(8)
W(1)-C(3)#1	1.952(8)
W(1)-C(1)	2.023(13)
W(1)-C(2)	2.057(12)
W(1)-S(1)#1	2.591(2)
W(1)-S(1)	2.591(2)
C(1)-O(1)	1.144(15)
C(2)-O(2)	1.136(13)
C(3)-O(3)	1.165(9)
C(4)-C(5)	1.520(10)
C(4)-S(1)	1.818(9)
C(5)-N(1)	1.491(9)
C(6)-N(1)	1.494(10)
C(7)-N(1)	1.486(10)
C(7)-C(8)	1.499(11)
C(8)-C(7)#1	1.499(10)
N(1)-Ni(1)-N(1)#1	98.3(4)
N(1)-Ni(1)-S(1)#1	172.71(19)
N(1)#1-Ni(1)-S(1)#1	88.92(18)
N(1)-Ni(1)-S(1)	88.92(18)
N(1)#1-Ni(1)-S(1)	172.71(19)
S(1)#1-Ni(1)-S(1)	83.83(11)
C(3)-W(1)-C(3)#1	89.9(4)
C(3)-W(1)-C(1)	87.4(3)
C(3)#1-W(1)-C(1)	87.4(3)
C(3)-W(1)-C(2)	85.5(3)
C(3)#1-W(1)-C(2)	85.5(3)

C(1)-W(1)-C(2)	170.0(4)
C(3)-W(1)-S(1)#1	169.3(2)
C(3)#1-W(1)-S(1)#1	100.6(2)
C(1)-W(1)-S(1)#1	95.0(2)
C(2)-W(1)-S(1)#1	93.3(2)
C(3)-W(1)-S(1)	100.6(2)
C(3)#1-W(1)-S(1)	169.3(2)
C(1)-W(1)-S(1)	95.0(2)
C(2)-W(1)-S(1)	93.3(2)
S(1)#1-W(1)-S(1)	68.75(9)
O(1)-C(1)-W(1)	172.9(9)
O(2)-C(2)-W(1)	170.8(8)
O(3)-C(3)-W(1)	178.4(6)
C(5)-C(4)-S(1)	110.3(6)
N(1)-C(5)-C(4)	111.8(6)
N(1)-C(7)-C(8)	113.0(7)
C(7)-C(8)-C(7)#1	113.5(10)
C(7)-N(1)-C(5)	105.9(5)
C(7)-N(1)-C(6)	108.8(6)
C(5)-N(1)-C(6)	109.2(6)
C(7)-N(1)-Ni(1)	118.2(4)
C(5)-N(1)-Ni(1)	107.4(4)
C(6)-N(1)-Ni(1)	107.2(5)
C(4)-S(1)-Ni(1)	99.4(3)
C(4)-S(1)-W(1)	113.8(2)
Ni(1)-S(1)-W(1)	78.25(7)

Symmetry transformations used to generate equivalent atoms:

#1 x,-y+1/2,z

Table A-3. Crystal data and structure refinement for (**Ni-1**)$W(CO)_4$.

Empirical formula	C14 H18 N2 Ni O4 S2 W	
Formula weight	584.98	
Temperature	293(2) K	
Wavelength	0.71073 Å	
Crystal system	Orthorhombic	
Space group	Pnma	
Unit cell dimensions	a = 13.397(4) Å	α= 90°.
	b = 12.386(4) Å	β= 90°.
	c = 11.005(3) Å	γ = 90°.
Volume	1826.2(10) $Å^3$	
Z	4	
Density (calculated)	2.128 Mg/m^3	
Absorption coefficient	7.573 mm^{-1}	
F(000)	1128	
Crystal size	0.3 x 0.2 x 0.2 mm^3	
Theta range for data collection	2.39 to 27.43°.	
Index ranges	-9<=h<=11, -16<=k<=8, -11<=l<=13	
Reflections collected	4764	
Independent reflections	1608 [R(int) = 0.1131]	
Completeness to theta = 27.43°	73.6 %	
Absorption correction	None	
Refinement method	Full-matrix least-squares on F^2	
Data / restraints / parameters	1608 / 0 / 121	
Goodness-of-fit on F^2	1.144	
Final R indices [I>2sigma(I)]	R1 = 0.0330, wR2 = 0.0886	
R indices (all data)	R1 = 0.0341, wR2 = 0.0895	
Largest diff. peak and hole	2.355 and -0.986 $e.Å^{-3}$	

Table A-4. Bond lengths [Å] and angles [°] for (**Ni-1**)$W(CO)_4$.

W(1)-C(2)	1.957(6)
W(1)-C(2)#1	1.957(6)
W(1)-C(1)	2.023(15)
W(1)-C(4)	2.047(11)
W(1)-S(5)#1	2.5792(14)
W(1)-S(5)	2.5792(14)
Ni(2)-N(2)#1	1.974(5)
Ni(2)-N(2)	1.974(5)
Ni(2)-S(5)#1	2.1893(15)
Ni(2)-S(5)	2.1893(15)
S(5)-C(12)	1.828(6)
C(7)-C(11)	1.510(7)
C(7)-N(2)	1.549(10)
O(2)-C(2)	1.173(7)
N(2)-C(6)	1.511(7)
N(2)-C(13)	1.512(7)
C(1)-O(1)	1.188(14)
C(6)-C(12)	1.524(7)
C(4)-O(4)	1.158(12)
C(10)-C(13)#1	1.526(7)
C(10)-C(13)	1.526(7)
C(11)-C(7)#1	1.510(7)
C(2)-W(1)-C(2)#1	90.7(3)
C(2)-W(1)-C(1)	86.6(3)
C(2)#1-W(1)-C(1)	86.6(3)
C(2)-W(1)-C(4)	88.0(3)
C(2)#1-W(1)-C(4)	88.0(3)
C(1)-W(1)-C(4)	172.4(3)
C(2)-W(1)-S(5)#1	170.1(2)
C(2)#1-W(1)-S(5)#1	98.53(18)
C(1)-W(1)-S(5)#1	97.57(19)

C(4)-W(1)-S(5)#1	88.57(19)
C(2)-W(1)-S(5)	98.53(18)
C(2)#1-W(1)-S(5)	170.1(2)
C(1)-W(1)-S(5)	97.57(19)
C(4)-W(1)-S(5)	88.57(19)
S(5)#1-W(1)-S(5)	72.08(6)
N(2)#1-Ni(2)-N(2)	91.5(3)
N(2)#1-Ni(2)-S(5)#1	90.34(14)
N(2)-Ni(2)-S(5)#1	177.54(15)
N(2)#1-Ni(2)-S(5)	177.54(15)
N(2)-Ni(2)-S(5)	90.34(14)
S(5)#1-Ni(2)-S(5)	87.76(8)
C(12)-S(5)-Ni(2)	93.9(2)
C(12)-S(5)-W(1)	116.4(2)
Ni(2)-S(5)-W(1)	88.88(5)
C(11)-C(7)-N(2)	112.2(6)
C(6)-N(2)-C(13)	107.0(5)
C(6)-N(2)-C(7)	108.1(5)
C(13)-N(2)-C(7)	110.7(4)
C(6)-N(2)-Ni(2)	111.7(3)
C(13)-N(2)-Ni(2)	108.5(4)
C(7)-N(2)-Ni(2)	110.8(3)
O(2)-C(2)-W(1)	177.1(6)
O(1)-C(1)-W(1)	171.7(7)
N(2)-C(6)-C(12)	109.1(5)
O(4)-C(4)-W(1)	175.5(8)
C(13)#1-C(10)-C(13)	115.0(6)
C(7)#1-C(11)-C(7)	118.9(8)
C(6)-C(12)-S(5)	105.0(4)
N(2)-C(13)-C(10)	113.6(6)

Symmetry transformations used to generate equivalent atoms:

#1 x,-y+1/2,z

Table A-5. Crystal data and structure refinement for (**Ni-1'**)$W(CO)_4$.

Empirical formula	C13 H18 N2 Ni O4 S2 W	
Formula weight	572.97	
Temperature	293(2) K	
Wavelength	0.71073 Å	
Crystal system	Orthorhombic	
Space group	Pnma	
Unit cell dimensions	a = 12.721(5) Å	α= 90°.
	b = 12.151(5) Å	β= 90°.
	c = 11(2) Å	γ = 90°.
Volume	1694(309) $Å^3$	
Z	4	
Density (calculated)	2.247 Mg/m^3	
Absorption coefficient	8.162 mm^{-1}	
F(000)	1104	
Crystal size	0.3 x 0.2 x 0.2 mm^3	
Theta range for data collection	2.45 to 23.46°.	
Index ranges	0<=h<=14, -13<=k<=13, -12<=l<=12	
Reflections collected	7249	
Independent reflections	7249 [R(int) = 0.0000]	
Completeness to theta = 23.46°	97.8 %	
Absorption correction	None	
Refinement method	Full-matrix least-squares on F^2	
Data / restraints / parameters	7249 / 0 / 116	
Goodness-of-fit on F^2	1.164	
Final R indices [I>2sigma(I)]	R1 = 0.0717, wR2 = 0.1761	
R indices (all data)	R1 = 0.0800, wR2 = 0.1815	
Largest diff. peak and hole	3.481 and -1.047 e.$Å^{-3}$	

Table A-6. Bond lengths [Å] and angles [°] for (**Ni-1'**)$W(CO)_4$.

W(1)-C(2)	1.96(15)
W(1)-C(2)#1	1.96(15)
W(1)-C(3)	2.03(8)
W(1)-C(1)	2.03(4)
W(1)-S(1)#1	2.6(2)
W(1)-S(1)	2.6(2)
Ni(1)-N(1)#1	1.93(14)
Ni(1)-N(1)	1.93(14)
Ni(1)-S(1)	2.17(16)
Ni(1)-S(1)#1	2.17(16)
S(1)-C(4)	1.84(3)
O(1)-C(1)	1.164(17)
O(2)-C(2)	1.17(9)
O(3)-C(3)	1.17(6)
N(1)-C(6)	1.501(8)
N(1)-C(7)	1.5(2)
N(1)-C(5)	1.50(3)
C(4)-C(5)	1.5(3)
C(6)-C(6)#1	1.564(14)
C(7)-C(8)	1.50(7)
C(8)-C(7)#1	1.50(7)
C(2)-W(1)-C(2)#1	91(9)
C(2)-W(1)-C(3)	88(6)
C(2)#1-W(1)-C(3)	88(6)
C(2)-W(1)-C(1)	87(5)
C(2)#1-W(1)-C(1)	87(5)
C(3)-W(1)-C(1)	172.6(10)
C(2)-W(1)-S(1)#1	171.8(3)
C(2)#1-W(1)-S(1)#1	97(8)
C(3)-W(1)-S(1)#1	91(7)
C(1)-W(1)-S(1)#1	95(6)

C(2)-W(1)-S(1)	97(8)
C(2)#1-W(1)-S(1)	171.8(3)
C(3)-W(1)-S(1)	91(7)
C(1)-W(1)-S(1)	95(6)
S(1)#1-W(1)-S(1)	75(8)
N(1)#1-Ni(1)-N(1)	83(7)
N(1)#1-Ni(1)-S(1)	171.1(7)
N(1)-Ni(1)-S(1)	92(8)
N(1)#1-Ni(1)-S(1)#1	92(8)
N(1)-Ni(1)-S(1)#1	171.1(7)
S(1)-Ni(1)-S(1)#1	92(9)
C(4)-S(1)-Ni(1)	93(4)
C(4)-S(1)-W(1)	111(3)
Ni(1)-S(1)-W(1)	86(10)
C(6)-N(1)-C(7)	110(4)
C(6)-N(1)-C(5)	111.2(5)
C(7)-N(1)-C(5)	108(4)
C(6)-N(1)-Ni(1)	101.3(4)
C(7)-N(1)-Ni(1)	113(8)
C(5)-N(1)-Ni(1)	113(7)
O(1)-C(1)-W(1)	174.7(11)
O(2)-C(2)-W(1)	178.6(6)
O(3)-C(3)-W(1)	174.9(10)
C(5)-C(4)-S(1)	107(3)
N(1)-C(5)-C(4)	111(3)
N(1)-C(6)-C(6)#1	109.6(3)
N(1)-C(7)-C(8)	114(6)
C(7)-C(8)-C(7)#1	115(9)

Symmetry transformations used to generate equivalent atoms:

#1 x,-y+1/2,z

Table A-7. Crystal data and structure refinement for **Ni-1**$(W(CO)_5)_2$.

Empirical formula	C40 H40 N4 Ni2 O20 S4 W4	
Formula weight	1877.82	
Temperature	110(2) K	
Wavelength	1.54178 Å	
Crystal system	Triclinic	
Space group	P-1	
Unit cell dimensions	a = 10.4829(7) Å	α= 106.304(5)°.
	b = 10.5887(7) Å	β= 96.606(4)°.
	c = 13.7992(8) Å	γ = 112.242(4)°.
Volume	1317.83(15) $Å^3$	
Z	1	
Density (calculated)	2.366 Mg/m^3	
Absorption coefficient	18.591 mm^{-1}	
F(000)	884	
Crystal size	0.24 x 0.24 x 0.01 mm^3	
Theta range for data collection	3.45 to 58.93°.	
Index ranges	-11<=h<=11, -11<=k<=11, -15<=l<=15	
Reflections collected	11485	
Independent reflections	3652 [R(int) = 0.0677]	
Completeness to theta = 58.93°	96.6 %	
Absorption correction	Semi-empirical from equivalents	
Max. and min. transmission	0.8359 and 0.0946	
Refinement method	Full-matrix least-squares on F^2	
Data / restraints / parameters	3652 / 60 / 335	
Goodness-of-fit on F^2	1.079	
Final R indices [I>2sigma(I)]	R1 = 0.0376, wR2 = 0.0849	
R indices (all data)	R1 = 0.0562, wR2 = 0.0942	
Extinction coefficient	0.00020(6)	
Largest diff. peak and hole	1.060 and -1.534 e.$Å^{-3}$	

Table A-8. Bond lengths [Å] and angles [°] for **Ni-1**$(W(CO)_5)_2$.

W(1A)-C(3A)	1.982(12)
W(1A)-C(1A)	2.010(11)
W(1A)-C(4A)	2.053(12)
W(1A)-C(5A)	2.071(11)
W(1A)-C(2A)	2.081(12)
W(1A)-S(1A)	2.572(3)
W(2A)-C(8A)	1.968(13)
W(2A)-C(7A)	2.035(13)
W(2A)-C(9A)	2.037(12)
W(2A)-C(6A)	2.038(12)
W(2A)-C(10A)	2.055(11)
W(2A)-S(2A)	2.571(2)
Ni(1A)-N(2A)	1.984(8)
Ni(1A)-N(1A)	1.984(7)
Ni(1A)-S(2A)	2.170(2)
Ni(1A)-S(1A)	2.186(3)
S(1A)-C(11A)	1.813(9)
S(2A)-C(20A)	1.831(9)
O(1A)-C(1A)	1.146(12)
O(2A)-C(2A)	1.120(13)
O(3A)-C(3A)	1.142(13)
O(4A)-C(4A)	1.138(13)
O(5A)-C(5A)	1.107(11)
O(6A)-C(6A)	1.147(13)
O(7A)-C(7A)	1.147(14)
O(8A)-C(8A)	1.168(14)
O(9A)-C(9A)	1.144(13)
O(10A)-C(10A)	1.130(12)
N(1A)-C(12A)	1.461(13)
N(1A)-C(16A)	1.497(13)
N(1A)-C(13A)	1.499(13)
N(2A)-C(18A)	1.497(13)

N(2A)-C(15A)	1.504(12)
N(2A)-C(19A)	1.505(12)
C(11A)-C(12A)	1.475(14)
C(13A)-C(14A)	1.503(15)
C(14A)-C(15A)	1.495(14)
C(16A)-C(17A)	1.516(14)
C(17A)-C(18A)	1.513(14)
C(19A)-C(20A)	1.494(14)

C(3A)-W(1A)-C(1A)	91.8(4)
C(3A)-W(1A)-C(4A)	92.1(4)
C(1A)-W(1A)-C(4A)	176.1(4)
C(3A)-W(1A)-C(5A)	86.9(4)
C(1A)-W(1A)-C(5A)	89.8(4)
C(4A)-W(1A)-C(5A)	90.0(4)
C(3A)-W(1A)-C(2A)	86.4(4)
C(1A)-W(1A)-C(2A)	92.8(4)
C(4A)-W(1A)-C(2A)	87.8(4)
C(5A)-W(1A)-C(2A)	172.9(4)
C(3A)-W(1A)-S(1A)	177.1(3)
C(1A)-W(1A)-S(1A)	90.9(3)
C(4A)-W(1A)-S(1A)	85.2(3)
C(5A)-W(1A)-S(1A)	92.1(3)
C(2A)-W(1A)-S(1A)	94.5(3)
C(8A)-W(2A)-C(7A)	93.4(4)
C(8A)-W(2A)-C(9A)	87.6(4)
C(7A)-W(2A)-C(9A)	91.1(4)
C(8A)-W(2A)-C(6A)	85.0(4)
C(7A)-W(2A)-C(6A)	90.4(4)
C(9A)-W(2A)-C(6A)	172.5(4)
C(8A)-W(2A)-C(10A)	92.1(4)
C(7A)-W(2A)-C(10A)	174.5(4)
C(9A)-W(2A)-C(10A)	89.0(4)
C(6A)-W(2A)-C(10A)	90.3(4)

C(8A)-W(2A)-S(2A)	174.5(3)
C(7A)-W(2A)-S(2A)	83.8(3)
C(9A)-W(2A)-S(2A)	97.2(3)
C(6A)-W(2A)-S(2A)	90.3(3)
C(10A)-W(2A)-S(2A)	90.7(3)
N(2A)-Ni(1A)-N(1A)	90.9(3)
N(2A)-Ni(1A)-S(2A)	90.8(2)
N(1A)-Ni(1A)-S(2A)	170.1(3)
N(2A)-Ni(1A)-S(1A)	170.4(3)
N(1A)-Ni(1A)-S(1A)	90.7(2)
S(2A)-Ni(1A)-S(1A)	89.25(9)
C(11A)-S(1A)-Ni(1A)	94.2(3)
C(11A)-S(1A)-W(1A)	109.4(4)
Ni(1A)-S(1A)-W(1A)	117.47(11)
C(20A)-S(2A)-Ni(1A)	97.8(3)
C(20A)-S(2A)-W(2A)	108.8(4)
Ni(1A)-S(2A)-W(2A)	113.39(10)
C(12A)-N(1A)-C(16A)	108.3(8)
C(12A)-N(1A)-C(13A)	109.1(7)
C(16A)-N(1A)-C(13A)	111.2(7)
C(12A)-N(1A)-Ni(1A)	110.8(5)
C(16A)-N(1A)-Ni(1A)	106.2(5)
C(13A)-N(1A)-Ni(1A)	111.2(6)
C(18A)-N(2A)-C(15A)	110.5(7)
C(18A)-N(2A)-C(19A)	108.0(7)
C(15A)-N(2A)-C(19A)	108.4(8)
C(18A)-N(2A)-Ni(1A)	106.2(6)
C(15A)-N(2A)-Ni(1A)	112.2(5)
C(19A)-N(2A)-Ni(1A)	111.4(5)
O(1A)-C(1A)-W(1A)	179.2(10)
O(2A)-C(2A)-W(1A)	173.8(10)
O(3A)-C(3A)-W(1A)	179.1(9)
O(4A)-C(4A)-W(1A)	178.4(9)
O(5A)-C(5A)-W(1A)	176.8(9)

O(6A)-C(6A)-W(2A)	174.8(9)
O(7A)-C(7A)-W(2A)	175.8(9)
O(8A)-C(8A)-W(2A)	177.2(10)
O(9A)-C(9A)-W(2A)	176.2(8)
O(10A)-C(10A)-W(2A)	177.2(8)
C(12A)-C(11A)-S(1A)	108.3(7)
N(1A)-C(12A)-C(11A)	111.0(8)
N(1A)-C(13A)-C(14A)	113.9(8)
C(15A)-C(14A)-C(13A)	115.3(9)
C(14A)-C(15A)-N(2A)	113.0(8)
N(1A)-C(16A)-C(17A)	116.0(9)
C(18A)-C(17A)-C(16A)	115.4(8)
N(2A)-C(18A)-C(17A)	114.1(8)
C(20A)-C(19A)-N(2A)	111.7(8)
C(19A)-C(20A)-S(2A)	108.5(6)

Symmetry transformations used to generate equivalent atoms:

Table A-9. Crystal data and structure refinement for $(Ni(mese\text{-}daco))_2CuBr$.

Empirical formula	C10 H20 Br0.50 Cu0.50 N2 Ni O2 S2	
Formula weight	394.84	
Temperature	110(2) K	
Wavelength	0.71073 Å	
Crystal system	Orthorhombic	
Space group	P2(1)2(1)2(1)	
Unit cell dimensions	a = 8.467(5) Å	α= 90°.
	b = 11.600(7) Å	β= 90°.
	c = 27.870(16) Å	γ = 90°.
Volume	2737(3) $Å^3$	
Z	8	
Density (calculated)	1.916 Mg/m^3	
Absorption coefficient	3.932 mm^{-1}	
F(000)	1616	
Crystal size	0.1 x 0.1 x 0.2 mm^3	
Theta range for data collection	2.28 to 25.00°.	
Index ranges	-5<=h<=9, -10<=k<=13, -33<=l<=32	
Reflections collected	5271	
Independent reflections	3685 [R(int) = 0.0809]	
Completeness to theta = 25.00°	88.7 %	
Absorption correction	None	
Refinement method	Full-matrix least-squares on F^2	
Data / restraints / parameters	3685 / 168 / 326	
Goodness-of-fit on F^2	1.019	
Final R indices [I>2sigma(I)]	R1 = 0.0770, wR2 = 0.1451	
R indices (all data)	R1 = 0.1353, wR2 = 0.1682	
Absolute structure parameter	0.0(3)	
Largest diff. peak and hole	0.858 and -0.824 e.$Å^{-3}$	

Table A-10. Bond lengths [Å] and angles [°] for $(Ni(mese\text{-}daco))_2CuBr$.

Ni(1)-N(2)	1.959(15)
Ni(1)-N(1)	1.967(15)
Ni(1)-S(1)	2.102(5)
Ni(1)-S(2)	2.159(6)
Ni(2)-N(4)	1.908(15)
Ni(2)-N(3)	1.994(12)
Ni(2)-S(3)	2.101(5)
Ni(2)-S(4)	2.152(4)
Cu(1)-S(2)	2.245(5)
Cu(1)-S(4)	2.248(5)
Cu(1)-Br(1)	2.421(3)
S(1)-O(1)	1.456(11)
S(1)-O(2)	1.465(14)
S(1)-C(1)	1.76(2)
S(2)-C(10)	1.80(2)
S(3)-O(3)	1.478(11)
S(3)-O(4)	1.493(13)
S(3)-C(11)	1.783(17)
S(4)-C(20)	1.811(18)
N(1)-C(2)	1.43(2)
N(1)-C(3)	1.536(19)
N(1)-C(6)	1.58(2)
N(2)-C(9)	1.47(2)
N(2)-C(8)	1.49(2)
N(2)-C(5)	1.54(2)
N(3)-C(12)	1.45(2)
N(3)-C(13)	1.51(2)
N(3)-C(16)	1.52(2)
N(4)-C(18)	1.45(2)
N(4)-C(19)	1.510(18)
N(4)-C(15)	1.59(2)
C(1)-C(2)	1.42(3)

C(3)-C(4)	1.50(2)
C(4)-C(5)	1.55(2)
C(6)-C(7)	1.51(3)
C(7)-C(8)	1.49(2)
C(9)-C(10)	1.46(2)
C(11)-C(12)	1.52(2)
C(13)-C(14)	1.52(2)
C(14)-C(15)	1.56(2)
C(16)-C(17)	1.57(2)
C(17)-C(18)	1.50(2)
C(19)-C(20)	1.50(2)

N(2)-Ni(1)-N(1)	91.9(6)
N(2)-Ni(1)-S(1)	177.6(5)
N(1)-Ni(1)-S(1)	89.4(5)
N(2)-Ni(1)-S(2)	89.9(5)
N(1)-Ni(1)-S(2)	178.1(5)
S(1)-Ni(1)-S(2)	88.9(2)
N(4)-Ni(2)-N(3)	91.6(6)
N(4)-Ni(2)-S(3)	175.1(5)
N(3)-Ni(2)-S(3)	88.0(4)
N(4)-Ni(2)-S(4)	91.0(4)
N(3)-Ni(2)-S(4)	163.7(5)
S(3)-Ni(2)-S(4)	90.75(18)
S(2)-Cu(1)-S(4)	130.80(19)
S(2)-Cu(1)-Br(1)	123.23(17)
S(4)-Cu(1)-Br(1)	105.97(14)
O(1)-S(1)-O(2)	113.7(7)
O(1)-S(1)-C(1)	101.0(10)
O(2)-S(1)-C(1)	108.1(11)
O(1)-S(1)-Ni(1)	115.0(6)
O(2)-S(1)-Ni(1)	117.5(6)
C(1)-S(1)-Ni(1)	98.6(7)
C(10)-S(2)-Ni(1)	97.0(7)

C(10)-S(2)-Cu(1)	107.6(7)
Ni(1)-S(2)-Cu(1)	95.65(19)
O(3)-S(3)-O(4)	114.5(7)
O(3)-S(3)-C(11)	106.7(8)
O(4)-S(3)-C(11)	105.7(8)
O(3)-S(3)-Ni(2)	121.1(5)
O(4)-S(3)-Ni(2)	106.9(5)
C(11)-S(3)-Ni(2)	100.1(6)
C(20)-S(4)-Ni(2)	98.4(5)
C(20)-S(4)-Cu(1)	103.1(7)
Ni(2)-S(4)-Cu(1)	97.32(17)
C(2)-N(1)-C(3)	113.0(16)
C(2)-N(1)-C(6)	104.5(14)
C(3)-N(1)-C(6)	108.7(13)
C(2)-N(1)-Ni(1)	113.6(12)
C(3)-N(1)-Ni(1)	107.3(11)
C(6)-N(1)-Ni(1)	109.6(12)
C(9)-N(2)-C(8)	112.1(16)
C(9)-N(2)-C(5)	103.7(13)
C(8)-N(2)-C(5)	110.0(14)
C(9)-N(2)-Ni(1)	111.8(12)
C(8)-N(2)-Ni(1)	110.1(11)
C(5)-N(2)-Ni(1)	108.9(12)
C(12)-N(3)-C(13)	106.0(12)
C(12)-N(3)-C(16)	107.6(14)
C(13)-N(3)-C(16)	113.8(14)
C(12)-N(3)-Ni(2)	113.8(10)
C(13)-N(3)-Ni(2)	115.9(11)
C(16)-N(3)-Ni(2)	99.7(9)
C(18)-N(4)-C(19)	111.5(14)
C(18)-N(4)-C(15)	109.2(14)
C(19)-N(4)-C(15)	102.9(13)
C(18)-N(4)-Ni(2)	106.7(11)
C(19)-N(4)-Ni(2)	111.1(11)

C(15)-N(4)-Ni(2)	115.6(11)
C(2)-C(1)-S(1)	112.3(17)
C(1)-C(2)-N(1)	114.1(18)
C(4)-C(3)-N(1)	114.0(16)
C(3)-C(4)-C(5)	110.3(15)
N(2)-C(5)-C(4)	114.0(15)
C(7)-C(6)-N(1)	113.8(16)
C(8)-C(7)-C(6)	115.3(16)
C(7)-C(8)-N(2)	116.4(16)
N(2)-C(9)-C(10)	113.1(16)
C(9)-C(10)-S(2)	107.0(15)
C(12)-C(11)-S(3)	105.1(12)
N(3)-C(12)-C(11)	113.0(12)
N(3)-C(13)-C(14)	111.4(13)
C(13)-C(14)-C(15)	113.1(16)
C(14)-C(15)-N(4)	110.2(15)
N(3)-C(16)-C(17)	112.7(15)
C(18)-C(17)-C(16)	114.4(15)
N(4)-C(18)-C(17)	114.3(15)
N(4)-C(19)-C(20)	109.0(14)
C(19)-C(20)-S(4)	110.4(12)

Symmetry transformations used to generate equivalent atoms:

Table A-11. Crystal data and structure refinement for $[Mo_2(\mathbf{Ni\text{-}1})_4][BF_4]_4$.

Empirical formula	C52 H98 B4 F16 Mo2 N14 Ni4 S8	
Formula weight	1949.88	
Temperature	110(2) K	
Wavelength	0.71073 Å	
Crystal system	Monoclinic	
Space group	P2(1)/n	
Unit cell dimensions	a = 11.319(5) Å	α= 90°.
	b = 23.770(10) Å	β= 96.057(8)°.
	c = 13.822(6) Å	γ = 90°.
Volume	3698(3) $Å^3$	
Z	2	
Density (calculated)	1.751 Mg/m^3	
Absorption coefficient	1.640 mm^{-1}	
F(000)	1992	
Crystal size	0.3 x 0.2 x 0.2 mm^3	
Theta range for data collection	2.49 to 23.39°.	
Index ranges	-12<=h<=12, -26<=k<=22, -13<=l<=15	
Reflections collected	15531	
Independent reflections	5274 [R(int) = 0.0960]	
Completeness to theta = 23.39°	97.5 %	
Absorption correction	None	
Refinement method	Full-matrix least-squares on F^2	
Data / restraints / parameters	5274 / 0 / 451	
Goodness-of-fit on F^2	1.048	
Final R indices [I>2sigma(I)]	R1 = 0.0769, wR2 = 0.1645	
R indices (all data)	R1 = 0.1183, wR2 = 0.1846	
Largest diff. peak and hole	2.161 and -0.963 $e.Å^{-3}$	

Table A-12. Bond lengths [Å] and angles [°] for $[Mo_2(\mathbf{Ni\text{-}1})_4][BF_4]_4$.

Mo(1)-Mo(1)#1	2.1425(18)
Mo(1)-S(4)	2.504(3)
Mo(1)-S(1)	2.518(2)
Mo(1)-S(2)	2.536(3)
Mo(1)-S(3)	2.544(3)
Ni(1)-N(2)	1.976(8)
Ni(1)-N(1)	1.984(8)
Ni(1)-S(3)#1	2.159(3)
Ni(1)-S(1)	2.171(3)
N(1)-C(2)	1.454(12)
N(1)-C(3)	1.502(12)
N(1)-C(6)	1.526(13)
S(1)-C(1)	1.807(10)
C(1)-C(2)	1.508(12)
Ni(2)-N(4)	1.972(7)
Ni(2)-N(3)	1.975(8)
Ni(2)-S(4)#1	2.154(3)
Ni(2)-S(2)	2.156(3)
N(2)-C(5)	1.491(12)
N(2)-C(8)	1.495(14)
N(2)-C(9)	1.523(13)
S(2)-C(10)	1.803(9)
N(3)-C(11)	1.483(12)
N(3)-C(15)	1.488(12)
N(3)-C(12)	1.529(12)
S(3)-C(19)	1.829(9)
S(3)-Ni(1)#1	2.159(3)
C(3)-C(4)	1.365(18)
N(4)-C(17)	1.482(11)
N(4)-C(14)	1.487(12)
N(4)-C(18)	1.498(13)
S(4)-C(20)	1.804(9)

S(4)-Ni(2)#1	2.154(3)
C(4)-C(5)	1.439(18)
C(6)-C(7)	1.429(16)
C(7)-C(8)	1.506(19)
C(9)-C(19)#1	1.505(13)
C(10)-C(11)	1.523(13)
C(12)-C(13)	1.472(13)
C(13)-C(14)	1.521(14)
C(15)-C(16)	1.522(14)
C(16)-C(17)	1.493(15)
C(18)-C(20)#1	1.512(13)
C(19)-C(9)#1	1.505(13)
C(20)-C(18)#1	1.512(13)
N(5)-C(21)	1.108(15)
C(21)-C(22)	1.48(2)
N(6)-C(23)	1.146(13)
C(23)-C(24)	1.434(16)
N(7)-C(25)	1.141(16)
C(25)-C(26)	1.485(18)
B(1)-F(1)	1.357(16)
B(1)-F(3)	1.388(14)
B(1)-F(2)	1.396(14)
B(1)-F(4)	1.408(14)
B(2)-F(5)	1.356(18)
B(2)-F(8)	1.368(17)
B(2)-F(6)	1.38(2)
B(2)-F(7)	1.389(17)

Mo(1)#1-Mo(1)-S(4)	97.95(8)
Mo(1)#1-Mo(1)-S(1)	97.57(8)
S(4)-Mo(1)-S(1)	90.22(8)
Mo(1)#1-Mo(1)-S(2)	101.32(8)
S(4)-Mo(1)-S(2)	160.68(9)
S(1)-Mo(1)-S(2)	88.59(8)

Mo(1)#1-Mo(1)-S(3)	102.13(8)
S(4)-Mo(1)-S(3)	86.40(8)
S(1)-Mo(1)-S(3)	160.29(9)
S(2)-Mo(1)-S(3)	88.25(9)
N(2)-Ni(1)-N(1)	90.6(3)
N(2)-Ni(1)-S(3)#1	90.8(3)
N(1)-Ni(1)-S(3)#1	177.6(3)
N(2)-Ni(1)-S(1)	175.9(2)
N(1)-Ni(1)-S(1)	90.4(2)
S(3)#1-Ni(1)-S(1)	88.05(10)
C(2)-N(1)-C(3)	107.0(8)
C(2)-N(1)-C(6)	111.0(8)
C(3)-N(1)-C(6)	110.9(8)
C(2)-N(1)-Ni(1)	110.3(6)
C(3)-N(1)-Ni(1)	112.9(7)
C(6)-N(1)-Ni(1)	104.8(6)
C(1)-S(1)-Ni(1)	96.9(3)
C(1)-S(1)-Mo(1)	108.4(3)
Ni(1)-S(1)-Mo(1)	114.24(10)
C(2)-C(1)-S(1)	106.1(7)
N(4)-Ni(2)-N(3)	91.1(3)
N(4)-Ni(2)-S(4)#1	90.6(2)
N(3)-Ni(2)-S(4)#1	174.8(2)
N(4)-Ni(2)-S(2)	177.0(2)
N(3)-Ni(2)-S(2)	90.3(2)
S(4)#1-Ni(2)-S(2)	87.77(10)
C(5)-N(2)-C(8)	108.9(8)
C(5)-N(2)-C(9)	106.3(8)
C(8)-N(2)-C(9)	110.1(8)
C(5)-N(2)-Ni(1)	115.4(6)
C(8)-N(2)-Ni(1)	104.5(6)
C(9)-N(2)-Ni(1)	111.5(6)
C(10)-S(2)-Ni(2)	99.0(3)
C(10)-S(2)-Mo(1)	109.6(3)

Ni(2)-S(2)-Mo(1)	112.71(11)
N(1)-C(2)-C(1)	112.1(8)
C(11)-N(3)-C(15)	109.9(7)
C(11)-N(3)-C(12)	106.9(7)
C(15)-N(3)-C(12)	111.5(7)
C(11)-N(3)-Ni(2)	111.8(6)
C(15)-N(3)-Ni(2)	100.8(6)
C(12)-N(3)-Ni(2)	115.8(6)
C(19)-S(3)-Ni(1)#1	98.4(3)
C(19)-S(3)-Mo(1)	108.8(3)
Ni(1)#1-S(3)-Mo(1)	111.21(12)
C(4)-C(3)-N(1)	117.2(10)
C(17)-N(4)-C(14)	111.9(7)
C(17)-N(4)-C(18)	109.9(7)
C(14)-N(4)-C(18)	106.6(8)
C(17)-N(4)-Ni(2)	102.4(5)
C(14)-N(4)-Ni(2)	115.7(6)
C(18)-N(4)-Ni(2)	110.5(5)
C(20)-S(4)-Ni(2)#1	98.5(3)
C(20)-S(4)-Mo(1)	108.1(3)
Ni(2)#1-S(4)-Mo(1)	115.31(11)
C(3)-C(4)-C(5)	125.7(14)
C(4)-C(5)-N(2)	115.9(10)
C(7)-C(6)-N(1)	116.3(10)
C(6)-C(7)-C(8)	125.4(12)
N(2)-C(8)-C(7)	116.8(9)
C(19)#1-C(9)-N(2)	111.8(8)
C(11)-C(10)-S(2)	106.7(6)
N(3)-C(11)-C(10)	112.4(8)
C(13)-C(12)-N(3)	111.4(8)
C(12)-C(13)-C(14)	116.7(9)
N(4)-C(14)-C(13)	112.4(8)
N(3)-C(15)-C(16)	113.6(8)
C(17)-C(16)-C(15)	116.3(8)

N(4)-C(17)-C(16)	114.9(8)
N(4)-C(18)-C(20)#1	111.8(7)
C(9)#1-C(19)-S(3)	106.9(7)
C(18)#1-C(20)-S(4)	105.9(7)
N(5)-C(21)-C(22)	179.5(16)
N(6)-C(23)-C(24)	178.6(11)
N(7)-C(25)-C(26)	175.5(18)
F(1)-B(1)-F(3)	110.0(10)
F(1)-B(1)-F(2)	110.3(10)
F(3)-B(1)-F(2)	109.9(10)
F(1)-B(1)-F(4)	109.6(10)
F(3)-B(1)-F(4)	109.2(10)
F(2)-B(1)-F(4)	107.8(10)
F(5)-B(2)-F(8)	112.9(15)
F(5)-B(2)-F(6)	110.9(13)
F(8)-B(2)-F(6)	106.6(12)
F(5)-B(2)-F(7)	109.9(12)
F(8)-B(2)-F(7)	106.5(12)
F(6)-B(2)-F(7)	109.8(15)

Symmetry transformations used to generate equivalent atoms:

#1 -x+1,-y+2,-z+2

Table A-13. Crystal data and structure refinement for $[Mo_2(\mathbf{Ni\text{-}1}')_4][BF_4]_4$.

Empirical formula	C44 H84 B4 F16 Mo2 N12 Ni4 S8	
Formula weight	1811.67	
Temperature	110(2) K	
Wavelength	0.71073 Å	
Crystal system	Monoclinic	
Space group	P2(1)/n	
Unit cell dimensions	a = 12.693(4) Å	α= 90°.
	b = 20.039(5) Å	β= 109.659(4)°.
	c = 14.166(4) Å	γ = 90°.
Volume	3393.3(16) $Å^3$	
Z	2	
Density (calculated)	1.773 Mg/m^3	
Absorption coefficient	1.779 mm^{-1}	
F(000)	1840	
Crystal size	0.3 x 0.2 x 0.2 mm^3	
Theta range for data collection	2.65 to 23.28°.	
Index ranges	-14<=h<=14, -22<=k<=19, -15<=l<=11	
Reflections collected	14270	
Independent reflections	4870 [R(int) = 0.0201]	
Completeness to theta = 23.28°	99.6 %	
Absorption correction	None	
Refinement method	Full-matrix least-squares on F^2	
Data / restraints / parameters	4870 / 10 / 406	
Goodness-of-fit on F^2	1.055	
Final R indices [I>2sigma(I)]	R1 = 0.0584, wR2 = 0.1515	
R indices (all data)	R1 = 0.0618, wR2 = 0.1559	
Largest diff. peak and hole	3.107 and -0.692 $e.Å^{-3}$	

Table A-14. Bond lengths [Å] and angles [°] for $[Mo_2(\mathbf{Ni\text{-}1}')_4][BF_4]_4$.

Mo(1)-Mo(1)#1	2.1625(10)
Mo(1)-S(2)	2.5073(14)
Mo(1)-S(1)	2.5132(14)
Mo(1)-S(4)	2.5148(14)
Mo(1)-S(3)	2.5326(14)
S(1)-C(1)	1.843(5)
S(1)-Ni(1)	2.1493(15)
Ni(1)-N(1)	1.920(4)
Ni(1)-N(2)	1.926(4)
Ni(1)-S(3)#1	2.1456(15)
N(1)-C(5)	1.490(7)
N(1)-C(3)	1.495(7)
N(1)-C(2)	1.504(7)
C(1)-C(2)	1.507(8)
Ni(2)-N(4)	1.917(5)
Ni(2)-N(3)	1.923(5)
Ni(2)-S(2)	2.1330(16)
Ni(2)-S(4)#1	2.1401(16)
S(2)-C(9)	1.850(7)
N(2)-C(4)	1.489(7)
N(2)-C(7)	1.491(7)
N(2)-C(8)	1.501(7)
S(3)-C(17)	1.842(5)
S(3)-Ni(1)#1	2.1456(15)
N(3)-C(11)	1.475(8)
N(3)-C(10)	1.498(9)
N(3)-C(14)	1.538(11)
C(3)-C(4)	1.533(8)
N(4)-C(13)	1.394(10)
N(4)-C(15)	1.487(10)
N(4)-C(16)	1.553(9)
S(4)-C(18)	1.855(6)

S(4)-Ni(2)#1	2.1401(16)
N(5)-C(19)	1.147(9)
C(5)-C(6)	1.504(8)
C(6)-C(7)	1.521(8)
N(6)-C(21)	1.138(9)
C(8)-C(17)#1	1.504(7)
C(9)-C(10)	1.467(10)
C(11)-C(12)	1.476(10)
C(12)-C(13)	1.430(12)
C(14)-C(15)	1.598(12)
C(16)-C(18)#1	1.471(10)
C(17)-C(8)#1	1.504(7)
C(18)-C(16)#1	1.471(10)
C(19)-C(20)	1.452(10)
C(21)-C(22)	1.460(11)
B(1)-F(3)	1.380(7)
B(1)-F(1)	1.392(7)
B(1)-F(4)	1.394(7)
B(1)-F(2)	1.401(7)
B(2A)-F(5A)	1.367(16)
B(2A)-F(8A)	1.371(18)
B(2A)-F(7A)	1.411(17)
B(2A)-F(6A)	1.413(18)
B(2B)-F(8B)	1.367(14)
B(2B)-F(5B)	1.369(13)
B(2B)-F(6B)	1.388(14)
B(2B)-F(7B)	1.421(14)

Mo(1)#1-Mo(1)-S(2)	99.81(4)
Mo(1)#1-Mo(1)-S(1)	100.22(4)
S(2)-Mo(1)-S(1)	87.82(5)
Mo(1)#1-Mo(1)-S(4)	101.47(4)
S(2)-Mo(1)-S(4)	158.70(5)
S(1)-Mo(1)-S(4)	87.43(5)

Mo(1)#1-Mo(1)-S(3)	101.29(4)
S(2)-Mo(1)-S(3)	89.45(5)
S(1)-Mo(1)-S(3)	158.47(5)
S(4)-Mo(1)-S(3)	87.40(5)
C(1)-S(1)-Ni(1)	97.04(18)
C(1)-S(1)-Mo(1)	112.21(18)
Ni(1)-S(1)-Mo(1)	106.99(6)
N(1)-Ni(1)-N(2)	82.98(18)
N(1)-Ni(1)-S(3)#1	175.41(14)
N(2)-Ni(1)-S(3)#1	92.61(13)
N(1)-Ni(1)-S(1)	91.84(14)
N(2)-Ni(1)-S(1)	174.82(13)
S(3)#1-Ni(1)-S(1)	92.58(6)
C(5)-N(1)-C(3)	110.9(4)
C(5)-N(1)-C(2)	111.2(4)
C(3)-N(1)-C(2)	110.9(4)
C(5)-N(1)-Ni(1)	106.6(3)
C(3)-N(1)-Ni(1)	106.0(3)
C(2)-N(1)-Ni(1)	111.0(3)
C(2)-C(1)-S(1)	105.8(4)
N(4)-Ni(2)-N(3)	83.7(2)
N(4)-Ni(2)-S(2)	174.92(17)
N(3)-Ni(2)-S(2)	92.05(15)
N(4)-Ni(2)-S(4)#1	91.58(16)
N(3)-Ni(2)-S(4)#1	174.95(16)
S(2)-Ni(2)-S(4)#1	92.63(6)
C(9)-S(2)-Ni(2)	96.0(2)
C(9)-S(2)-Mo(1)	111.9(3)
Ni(2)-S(2)-Mo(1)	106.03(6)
C(4)-N(2)-C(7)	110.9(4)
C(4)-N(2)-C(8)	110.9(4)
C(7)-N(2)-C(8)	111.1(4)
C(4)-N(2)-Ni(1)	105.9(3)
C(7)-N(2)-Ni(1)	107.1(3)

C(8)-N(2)-Ni(1)	110.7(3)
N(1)-C(2)-C(1)	110.0(4)
C(17)-S(3)-Ni(1)#1	96.18(18)
C(17)-S(3)-Mo(1)	112.47(18)
Ni(1)#1-S(3)-Mo(1)	106.22(6)
C(11)-N(3)-C(10)	116.4(5)
C(11)-N(3)-C(14)	108.0(5)
C(10)-N(3)-C(14)	108.6(6)
C(11)-N(3)-Ni(2)	107.6(4)
C(10)-N(3)-Ni(2)	111.5(4)
C(14)-N(3)-Ni(2)	104.0(4)
N(1)-C(3)-C(4)	109.7(4)
C(13)-N(4)-C(15)	112.4(5)
C(13)-N(4)-C(16)	113.2(6)
C(15)-N(4)-C(16)	106.0(6)
C(13)-N(4)-Ni(2)	108.1(5)
C(15)-N(4)-Ni(2)	106.4(4)
C(16)-N(4)-Ni(2)	110.5(4)
C(18)-S(4)-Ni(2)#1	96.78(19)
C(18)-S(4)-Mo(1)	113.06(19)
Ni(2)#1-S(4)-Mo(1)	105.16(6)
N(2)-C(4)-C(3)	110.1(4)
N(1)-C(5)-C(6)	112.5(4)
C(5)-C(6)-C(7)	115.7(5)
N(2)-C(7)-C(6)	111.6(4)
N(2)-C(8)-C(17)#1	110.1(4)
C(10)-C(9)-S(2)	107.8(5)
C(9)-C(10)-N(3)	109.7(6)
N(3)-C(11)-C(12)	114.3(5)
C(13)-C(12)-C(11)	117.5(6)
N(4)-C(13)-C(12)	114.5(6)
N(3)-C(14)-C(15)	109.4(5)
N(4)-C(15)-C(14)	107.7(5)
C(18)#1-C(16)-N(4)	108.0(5)

C(8)#1-C(17)-S(3)	106.9(4)
C(16)#1-C(18)-S(4)	105.5(4)
N(5)-C(19)-C(20)	178.1(8)
N(6)-C(21)-C(22)	178.8(8)
F(3)-B(1)-F(1)	108.7(5)
F(3)-B(1)-F(4)	108.8(5)
F(1)-B(1)-F(4)	109.7(5)
F(3)-B(1)-F(2)	110.2(5)
F(1)-B(1)-F(2)	109.7(5)
F(4)-B(1)-F(2)	109.6(5)
F(5A)-B(2A)-F(8A)	110.0(19)
F(5A)-B(2A)-F(7A)	111.4(19)
F(8A)-B(2A)-F(7A)	110.1(15)
F(5A)-B(2A)-F(6A)	112(2)
F(8A)-B(2A)-F(6A)	107.5(15)
F(7A)-B(2A)-F(6A)	105.9(14)
F(8B)-B(2B)-F(5B)	110.3(14)
F(8B)-B(2B)-F(6B)	109.0(11)
F(5B)-B(2B)-F(6B)	110.4(13)
F(8B)-B(2B)-F(7B)	110.7(11)
F(5B)-B(2B)-F(7B)	107.4(13)
F(6B)-B(2B)-F(7B)	109.0(11)

Symmetry transformations used to generate equivalent atoms:

#1 -x+1,-y+2,-z+1

Table A-15. Crystal data and structure refinement for $[Pd_2(\mathbf{Ni\text{-}1}')_4][Br]_4$

Empirical formula	C42 H93 Br4 N8 Ni4 O6 Pd2 S8	
Formula weight	1830.00	
Temperature	110(2) K	
Wavelength	0.71069 Å	
Crystal system	Triclinic	
Space group	P-1	
Unit cell dimensions	a = 11.116(5) Å	α= 92.754(5)°.
	b = 13.000(5) Å	β= 92.599(5)°.
	c = 23.214(5) Å	γ = 105.543(5)°.
Volume	3222(2) $Å^3$	
Z	2	
Density (calculated)	1.886 Mg/m^3	
Absorption coefficient	4.478 mm^{-1}	
F(000)	1842	
Crystal size	0.3 x 0.2 x 0.2 mm^3	
Theta range for data collection	0.88 to 23.32°.	
Index ranges	-9<=h<=12, -14<=k<=12, -25<=l<=25	
Reflections collected	14322	
Independent reflections	9163 [R(int) = 0.0557]	
Completeness to theta = 23.32°	98.0 %	
Absorption correction	None	
Refinement method	Full-matrix least-squares on F^2	
Data / restraints / parameters	9163 / 0 / 643	
Goodness-of-fit on F^2	1.084	
Final R indices [I>2sigma(I)]	R1 = 0.0915, wR2 = 0.2158	
R indices (all data)	R1 = 0.1379, wR2 = 0.2559	
Largest diff. peak and hole	3.872 and -2.022 $e.Å^{-3}$	

Table A-16. Bond lengths [Å] and angles [°] for $[Pd_2(\mathbf{Ni\text{-}1}')_4][Br]_4$.

Pd(1)-S(6)	2.319(4)
Pd(1)-S(7)#1	2.329(4)
Pd(1)-S(5)#1	2.334(4)
Pd(1)-S(8)	2.345(4)
Pd(1)-Pd(1)#1	3.099(2)
Pd(2)-S(3)#2	2.332(4)
Pd(2)-S(4)	2.332(4)
Pd(2)-S(1)#2	2.333(4)
Pd(2)-S(2)	2.336(4)
Pd(2)-Pd(2)#2	3.104(2)
Ni(1)-N(1)	1.916(12)
Ni(1)-N(2)	1.948(14)
Ni(1)-S(1)	2.160(4)
Ni(1)-S(2)	2.167(4)
Ni(2)-N(4)	1.921(12)
Ni(2)-N(3)	1.930(12)
Ni(2)-S(3)	2.141(4)
Ni(2)-S(4)	2.144(4)
Ni(3)-N(5)	1.918(12)
Ni(3)-N(6)	1.948(13)
Ni(3)-S(6)	2.141(4)
Ni(3)-S(5)	2.162(4)
Ni(4)-N(7)	1.925(13)
Ni(4)-N(8)	1.929(12)
Ni(4)-S(7)	2.156(4)
Ni(4)-S(8)	2.162(4)
S(1)-C(1)	1.827(13)
S(1)-Pd(2)#2	2.333(4)
S(2)-C(9)	1.848(15)
S(3)-C(10)	1.846(13)
S(3)-Pd(2)#2	2.332(4)
S(4)-C(18)	1.824(13)

S(5)-C(19)	1.850(17)
S(5)-Pd(1)#1	2.334(4)
S(6)-C(27)	1.855(17)
S(7)-C(28)	1.850(16)
S(7)-Pd(1)#1	2.329(4)
S(8)-C(36)	1.858(15)
N(1)-C(3)	1.466(18)
N(1)-C(5)	1.502(19)
N(1)-C(2)	1.52(2)
N(2)-C(8)	1.447(19)
N(2)-C(4)	1.516(19)
N(2)-C(7)	1.514(19)
N(3)-C(14)	1.48(2)
N(3)-C(11)	1.49(2)
N(3)-C(12)	1.50(2)
N(4)-C(16)	1.45(2)
N(4)-C(13)	1.50(2)
N(4)-C(17)	1.53(2)
N(5)-C(23)	1.47(2)
N(5)-C(20)	1.52(2)
N(5)-C(21)	1.54(2)
N(6)-C(25)	1.43(2)
N(6)-C(22)	1.46(2)
N(6)-C(26)	1.56(2)
N(7)-C(29)	1.47(2)
N(7)-C(32)	1.49(2)
N(7)-C(30)	1.50(2)
N(8)-C(34)	1.43(2)
N(8)-C(31)	1.45(2)
N(8)-C(35)	1.54(2)
C(1)-C(2)	1.45(2)
C(3)-C(4)	1.52(2)
C(5)-C(6)	1.50(2)
C(6)-C(7)	1.49(2)

C(8)-C(9)	1.55(2)
C(10)-C(11)	1.49(2)
C(12)-C(13)	1.55(2)
C(14)-C(15)	1.43(2)
C(15)-C(16)	1.38(2)
C(17)-C(18)	1.47(2)
C(19)-C(20)	1.45(2)
C(21)-C(22)	1.61(3)
C(23)-C(24)	1.53(2)
C(24)-C(25)	1.46(3)
C(26)-C(27)	1.42(2)
C(28)-C(29)	1.50(2)
C(30)-C(31)	1.53(2)
C(32)-C(33)	1.48(2)
C(33)-C(34)	1.46(3)
C(35)-C(36)	1.45(2)
O(1ME)-C(1ME)	1.44(3)
O(2ME)-C(2ME)	1.37(2)
O(3ME)-C(3ME)	1.37(3)
O(4ME)-C(4ME)	1.41(3)
O(5ME)-C(5ME)	1.38(2)
O(6ME)-C(6ME)	1.47(3)

S(6)-Pd(1)-S(7)#1	88.79(14)
S(6)-Pd(1)-S(5)#1	178.00(15)
S(7)#1-Pd(1)-S(5)#1	90.82(14)
S(6)-Pd(1)-S(8)	89.74(15)
S(7)#1-Pd(1)-S(8)	177.23(15)
S(5)#1-Pd(1)-S(8)	90.57(15)
S(6)-Pd(1)-Pd(1)#1	91.08(11)
S(7)#1-Pd(1)-Pd(1)#1	95.65(11)
S(5)#1-Pd(1)-Pd(1)#1	90.90(11)
S(8)-Pd(1)-Pd(1)#1	86.72(11)
S(3)#2-Pd(2)-S(4)	178.33(13)

S(3)#2-Pd(2)-S(1)#2	89.21(13)
S(4)-Pd(2)-S(1)#2	90.30(13)
S(3)#2-Pd(2)-S(2)	90.23(13)
S(4)-Pd(2)-S(2)	90.19(13)
S(1)#2-Pd(2)-S(2)	177.45(13)
S(3)#2-Pd(2)-Pd(2)#2	90.51(10)
S(4)-Pd(2)-Pd(2)#2	91.10(10)
S(1)#2-Pd(2)-Pd(2)#2	92.39(10)
S(2)-Pd(2)-Pd(2)#2	90.11(10)
N(1)-Ni(1)-N(2)	81.7(5)
N(1)-Ni(1)-S(1)	91.0(4)
N(2)-Ni(1)-S(1)	171.9(4)
N(1)-Ni(1)-S(2)	173.0(4)
N(2)-Ni(1)-S(2)	91.6(4)
S(1)-Ni(1)-S(2)	95.60(15)
N(4)-Ni(2)-N(3)	82.3(5)
N(4)-Ni(2)-S(3)	172.7(4)
N(3)-Ni(2)-S(3)	91.1(4)
N(4)-Ni(2)-S(4)	91.0(4)
N(3)-Ni(2)-S(4)	171.9(4)
S(3)-Ni(2)-S(4)	95.37(15)
N(5)-Ni(3)-N(6)	83.2(6)
N(5)-Ni(3)-S(6)	172.8(4)
N(6)-Ni(3)-S(6)	90.1(4)
N(5)-Ni(3)-S(5)	91.2(4)
N(6)-Ni(3)-S(5)	173.7(4)
S(6)-Ni(3)-S(5)	95.31(17)
N(7)-Ni(4)-N(8)	81.1(5)
N(7)-Ni(4)-S(7)	91.9(4)
N(8)-Ni(4)-S(7)	171.5(4)
N(7)-Ni(4)-S(8)	172.3(4)
N(8)-Ni(4)-S(8)	91.4(4)
S(7)-Ni(4)-S(8)	95.43(17)
C(1)-S(1)-Ni(1)	97.2(5)

C(1)-S(1)-Pd(2)#2	109.1(5)
Ni(1)-S(1)-Pd(2)#2	113.40(16)
C(9)-S(2)-Ni(1)	96.5(5)
C(9)-S(2)-Pd(2)	108.1(5)
Ni(1)-S(2)-Pd(2)	114.75(16)
C(10)-S(3)-Ni(2)	99.1(4)
C(10)-S(3)-Pd(2)#2	108.3(5)
Ni(2)-S(3)-Pd(2)#2	114.86(16)
C(18)-S(4)-Ni(2)	97.1(5)
C(18)-S(4)-Pd(2)	109.0(5)
Ni(2)-S(4)-Pd(2)	114.59(17)
C(19)-S(5)-Ni(3)	96.1(6)
C(19)-S(5)-Pd(1)#1	109.7(6)
Ni(3)-S(5)-Pd(1)#1	114.21(18)
C(27)-S(6)-Ni(3)	97.8(6)
C(27)-S(6)-Pd(1)	108.0(6)
Ni(3)-S(6)-Pd(1)	114.68(19)
C(28)-S(7)-Ni(4)	96.2(5)
C(28)-S(7)-Pd(1)#1	109.1(6)
Ni(4)-S(7)-Pd(1)#1	111.31(17)
C(36)-S(8)-Ni(4)	96.3(5)
C(36)-S(8)-Pd(1)	107.6(6)
Ni(4)-S(8)-Pd(1)	117.05(17)
C(3)-N(1)-C(5)	112.4(12)
C(3)-N(1)-C(2)	108.8(12)
C(5)-N(1)-C(2)	109.0(12)
C(3)-N(1)-Ni(1)	108.1(9)
C(5)-N(1)-Ni(1)	105.7(9)
C(2)-N(1)-Ni(1)	113.0(9)
C(8)-N(2)-C(4)	110.2(13)
C(8)-N(2)-C(7)	113.0(12)
C(4)-N(2)-C(7)	108.9(11)
C(8)-N(2)-Ni(1)	111.5(10)
C(4)-N(2)-Ni(1)	107.0(9)

C(7)-N(2)-Ni(1)	106.0(10)
C(14)-N(3)-C(11)	115.6(14)
C(14)-N(3)-C(12)	108.4(12)
C(11)-N(3)-C(12)	109.8(13)
C(14)-N(3)-Ni(2)	105.5(10)
C(11)-N(3)-Ni(2)	110.3(9)
C(12)-N(3)-Ni(2)	106.6(9)
C(16)-N(4)-C(13)	108.6(12)
C(16)-N(4)-C(17)	115.9(14)
C(13)-N(4)-C(17)	106.1(13)
C(16)-N(4)-Ni(2)	107.2(11)
C(13)-N(4)-Ni(2)	107.3(9)
C(17)-N(4)-Ni(2)	111.3(9)
C(23)-N(5)-C(20)	113.4(14)
C(23)-N(5)-C(21)	110.7(12)
C(20)-N(5)-C(21)	108.8(13)
C(23)-N(5)-Ni(3)	106.2(9)
C(20)-N(5)-Ni(3)	112.2(10)
C(21)-N(5)-Ni(3)	105.1(9)
C(25)-N(6)-C(22)	114.5(14)
C(25)-N(6)-C(26)	110.1(16)
C(22)-N(6)-C(26)	106.4(15)
C(25)-N(6)-Ni(3)	105.9(11)
C(22)-N(6)-Ni(3)	108.7(11)
C(26)-N(6)-Ni(3)	111.3(10)
C(29)-N(7)-C(32)	112.4(14)
C(29)-N(7)-C(30)	110.7(13)
C(32)-N(7)-C(30)	108.1(13)
C(29)-N(7)-Ni(4)	112.3(10)
C(32)-N(7)-Ni(4)	105.9(10)
C(30)-N(7)-Ni(4)	107.2(10)
C(34)-N(8)-C(31)	114.0(14)
C(34)-N(8)-C(35)	111.3(15)
C(31)-N(8)-C(35)	107.4(14)

C(34)-N(8)-Ni(4)	106.5(10)
C(31)-N(8)-Ni(4)	107.2(10)
C(35)-N(8)-Ni(4)	110.4(10)
C(2)-C(1)-S(1)	109.2(10)
C(1)-C(2)-N(1)	110.8(12)
N(1)-C(3)-C(4)	110.2(11)
N(2)-C(4)-C(3)	109.1(12)
C(6)-C(5)-N(1)	111.7(13)
C(7)-C(6)-C(5)	116.4(14)
C(6)-C(7)-N(2)	112.3(12)
N(2)-C(8)-C(9)	110.6(13)
C(8)-C(9)-S(2)	105.7(10)
C(11)-C(10)-S(3)	103.8(10)
C(10)-C(11)-N(3)	114.2(13)
N(3)-C(12)-C(13)	109.6(12)
N(4)-C(13)-C(12)	108.6(12)
C(15)-C(14)-N(3)	113.4(14)
C(16)-C(15)-C(14)	118.6(15)
C(15)-C(16)-N(4)	114.2(15)
C(18)-C(17)-N(4)	108.3(13)
C(17)-C(18)-S(4)	107.2(10)
C(20)-C(19)-S(5)	108.4(13)
C(19)-C(20)-N(5)	109.6(14)
N(5)-C(21)-C(22)	109.1(12)
N(6)-C(22)-C(21)	107.9(13)
N(5)-C(23)-C(24)	111.4(14)
C(25)-C(24)-C(23)	120.0(16)
N(6)-C(25)-C(24)	109.7(16)
C(27)-C(26)-N(6)	108.5(15)
C(26)-C(27)-S(6)	107.4(14)
C(29)-C(28)-S(7)	106.5(12)
N(7)-C(29)-C(28)	111.9(13)
N(7)-C(30)-C(31)	108.5(13)
N(8)-C(31)-C(30)	110.1(14)

C(33)-C(32)-N(7)	113.7(16)
C(34)-C(33)-C(32)	114.9(17)
N(8)-C(34)-C(33)	111.8(18)
C(36)-C(35)-N(8)	109.0(15)
C(35)-C(36)-S(8)	106.9(12)

Symmetry transformations used to generate equivalent atoms:

#1 -x+1,-y+2,-z+1 #2 -x,-y+1,-z

Table A-17. Crystal data and structure refinement for [Rh(**Ni-1**)$(CO)_2$][PF_6].

Empirical formula	C12 H20 F6 N2 Ni O2 Rh S3	
Formula weight	596.10	
Temperature	110(2) K	
Wavelength	0.71073 Å	
Crystal system	Orthorhombic	
Space group	P2(1)2(1)2(1)	
Unit cell dimensions	a = 9.991(2) Å	α= 90°.
	b = 11.550(3) Å	β= 90°.
	c = 16.844(4) Å	γ = 90°.
Volume	1943.7(8) $Å^3$	
Z	4	
Density (calculated)	2.037 Mg/m^3	
Absorption coefficient	2.206 mm^{-1}	
F(000)	1188	
Crystal size	0.30 x 0.10 x 0.10 mm^3	
Theta range for data collection	2.14 to 24.99°.	
Index ranges	-11<=h<=11, -13<=k<=8, -19<=l<=20	
Reflections collected	9616	
Independent reflections	3316 [R(int) = 0.0239]	
Completeness to theta = 24.99°	98.2 %	
Absorption correction	Semi-empirical from equivalents	
Max. and min. transmission	0.8095 and 0.5574	
Refinement method	Full-matrix least-squares on F^2	
Data / restraints / parameters	3316 / 0 / 244	
Goodness-of-fit on F^2	1.068	
Final R indices [I>2sigma(I)]	R1 = 0.0230, wR2 = 0.0546	
R indices (all data)	R1 = 0.0233, wR2 = 0.0548	
Absolute structure parameter	-0.012(15)	
Largest diff. peak and hole	0.734 and -0.460 e.$Å^{-3}$	

Table A-18. Bond lengths [Å] and angles [°] for [Rh(**Ni-1**)$(CO)_2$][PF_6].

Rh(1)-C(2)	1.871(4)
Rh(1)-C(1)	1.872(4)
Rh(1)-S(2)	2.3540(10)
Rh(1)-S(1)	2.3648(10)
Rh(1)-Ni(1)	2.8708(6)
Ni(1)-N(1)	1.957(3)
Ni(1)-N(2)	1.966(3)
Ni(1)-S(2)	2.1644(10)
Ni(1)-S(1)	2.1756(9)
S(1)-C(3)	1.835(3)
S(2)-C(12)	1.830(3)
S(3)-F(3)	1.600(2)
S(3)-F(4)	1.602(2)
S(3)-F(5)	1.602(2)
S(3)-F(6)	1.603(2)
S(3)-F(1)	1.607(2)
S(3)-F(2)	1.611(2)
O(1)-C(1)	1.139(5)
O(2)-C(2)	1.136(4)
N(1)-C(4)	1.503(4)
N(1)-C(5)	1.505(4)
N(1)-C(8)	1.516(4)
N(2)-C(10)	1.500(4)
N(2)-C(11)	1.511(4)
N(2)-C(7)	1.513(5)
C(3)-C(4)	1.506(5)
C(5)-C(6)	1.529(5)
C(6)-C(7)	1.513(5)
C(8)-C(9)	1.532(5)
C(9)-C(10)	1.521(5)
C(11)-C(12)	1.502(5)

C(2)-Rh(1)-C(1)	92.20(16)
C(2)-Rh(1)-S(2)	169.84(11)
C(1)-Rh(1)-S(2)	97.50(12)
C(2)-Rh(1)-S(1)	94.13(11)
C(1)-Rh(1)-S(1)	171.59(11)
S(2)-Rh(1)-S(1)	76.53(3)
C(2)-Rh(1)-Ni(1)	127.85(10)
C(1)-Rh(1)-Ni(1)	123.68(11)
S(2)-Rh(1)-Ni(1)	47.69(2)
S(1)-Rh(1)-Ni(1)	47.91(2)
N(1)-Ni(1)-N(2)	92.09(11)
N(1)-Ni(1)-S(2)	170.17(9)
N(2)-Ni(1)-S(2)	91.04(8)
N(1)-Ni(1)-S(1)	91.12(8)
N(2)-Ni(1)-S(1)	172.06(9)
S(2)-Ni(1)-S(1)	84.65(3)
N(1)-Ni(1)-Rh(1)	117.00(8)
N(2)-Ni(1)-Rh(1)	118.39(8)
S(2)-Ni(1)-Rh(1)	53.54(3)
S(1)-Ni(1)-Rh(1)	53.77(3)
C(3)-S(1)-Ni(1)	97.04(12)
C(3)-S(1)-Rh(1)	109.25(12)
Ni(1)-S(1)-Rh(1)	78.31(3)
C(12)-S(2)-Ni(1)	98.16(12)
C(12)-S(2)-Rh(1)	114.65(12)
Ni(1)-S(2)-Rh(1)	78.77(3)
F(3)-S(3)-F(4)	90.30(13)
F(3)-S(3)-F(5)	89.84(12)
F(4)-S(3)-F(5)	90.24(12)
F(3)-S(3)-F(6)	179.55(14)
F(4)-S(3)-F(6)	90.11(12)
F(5)-S(3)-F(6)	90.34(12)
F(3)-S(3)-F(1)	89.67(14)
F(4)-S(3)-F(1)	179.95(17)

F(5)-S(3)-F(1)	89.79(12)
F(6)-S(3)-F(1)	89.93(14)
F(3)-S(3)-F(2)	90.43(13)
F(4)-S(3)-F(2)	90.27(12)
F(5)-S(3)-F(2)	179.43(13)
F(6)-S(3)-F(2)	89.39(12)
F(1)-S(3)-F(2)	89.71(12)
C(4)-N(1)-C(5)	108.7(3)
C(4)-N(1)-C(8)	107.5(3)
C(5)-N(1)-C(8)	111.1(3)
C(4)-N(1)-Ni(1)	111.4(2)
C(5)-N(1)-Ni(1)	114.6(2)
C(8)-N(1)-Ni(1)	103.29(19)
C(10)-N(2)-C(11)	108.9(3)
C(10)-N(2)-C(7)	110.7(3)
C(11)-N(2)-C(7)	108.3(3)
C(10)-N(2)-Ni(1)	104.4(2)
C(11)-N(2)-Ni(1)	110.3(2)
C(7)-N(2)-Ni(1)	114.1(2)
O(1)-C(1)-Rh(1)	176.5(3)
O(2)-C(2)-Rh(1)	175.5(3)
C(4)-C(3)-S(1)	106.4(2)
N(1)-C(4)-C(3)	111.8(3)
N(1)-C(5)-C(6)	112.0(3)
C(7)-C(6)-C(5)	115.5(3)
N(2)-C(7)-C(6)	112.4(3)
N(1)-C(8)-C(9)	113.8(3)
C(10)-C(9)-C(8)	115.5(3)
N(2)-C(10)-C(9)	114.0(3)
C(12)-C(11)-N(2)	111.7(3)
C(11)-C(12)-S(2)	106.3(2)

Symmetry transformations used to generate equivalent atoms:

Table A-19. Crystal data and structure refinement for $[Rh_2(\mathbf{Ni\text{-}1'})_4][O_2CCF_3]_4$.

Empirical formula	C26 H42 F6 N6 Ni2 O4 Rh S4	
Formula weight	965.23	
Temperature	110(2) K	
Wavelength	0.71073 Å	
Crystal system	Triclinic	
Space group	P-1	
Unit cell dimensions	a = 12.611(3) Å	α= 102.397(4)°.
	b = 12.738(3) Å	β= 94.325(4)°.
	c = 13.248(3) Å	γ = 118.550(4)°.
Volume	1786.0(8) $Å^3$	
Z	2	
Density (calculated)	1.795 Mg/m^3	
Absorption coefficient	1.807 mm^{-1}	
F(000)	982	
Crystal size	0.30 x 0.20 x 0.20 mm^3	
Theta range for data collection	1.88 to 25.00°.	
Index ranges	-9<=h<=14, -15<=k<=12, -15<=l<=15	
Reflections collected	9336	
Independent reflections	6143 [R(int) = 0.0131]	
Completeness to theta = 25.00°	97.9 %	
Absorption correction	None	
Max. and min. transmission	0.7138 and 0.6131	
Refinement method	Full-matrix least-squares on F^2	
Data / restraints / parameters	6143 / 12 / 498	
Goodness-of-fit on F^2	1.029	
Final R indices [I>2sigma(I)]	R1 = 0.0433, wR2 = 0.1149	
R indices (all data)	R1 = 0.0468, wR2 = 0.1197	
Largest diff. peak and hole	2.051 and -0.712 e.$Å^{-3}$	

Table A-20. Bond lengths [Å] and angles [°] for $[Rh_2(\mathbf{Ni\text{-}1'})_4][O_2CCF_4]_4$.

Rh(1)-N(5)	2.183(3)
Rh(1)-S(3)#1	2.3540(11)
Rh(1)-S(1)#1	2.3600(11)
Rh(1)-S(2)	2.3606(11)
Rh(1)-S(4)	2.3635(11)
Rh(1)-Rh(1)#1	2.8925(8)
Ni(1)-N(1)	1.910(3)
Ni(1)-N(2)	1.920(4)
Ni(1)-S(1)	2.1224(11)
Ni(1)-S(2)	2.1302(11)
Ni(2)-N(4)	1.912(4)
Ni(2)-N(3)	1.913(4)
Ni(2)-S(4)	2.1211(12)
Ni(2)-S(3)	2.1234(11)
S(1)-C(1)	1.868(5)
S(1)-Rh(1)#1	2.3599(11)
S(2)-C(9)	1.851(4)
S(3)-C(10)	1.849(4)
S(3)-Rh(1)#1	2.3540(11)
S(4)-C(18)	1.848(4)
N(1)-C(2)	1.473(6)
N(1)-C(3)	1.488(6)
N(1)-C(6)	1.545(7)
N(2)-C(5)	1.458(6)
N(2)-C(7)	1.480(6)
N(2)-C(8)	1.527(6)
N(3)-C(12)	1.481(6)
N(3)-C(11)	1.502(6)
N(3)-C(15)	1.506(6)
N(4)-C(14)	1.481(6)
N(4)-C(17)	1.500(6)
N(4)-C(16)	1.509(6)

N(5)-C(19)	1.111(5)
C(1)-C(2)	1.457(8)
C(3)-C(4)	1.496(7)
C(4)-C(5)	1.474(7)
C(6)-C(7)	1.571(8)
C(8)-C(9)	1.434(7)
C(10)-C(11)	1.483(6)
C(12)-C(13)	1.487(7)
C(13)-C(14)	1.490(7)
C(15)-C(16)	1.558(7)
C(17)-C(18)	1.485(6)
C(19)-C(20)	1.482(6)
C(21)-O(2)	1.237(6)
C(21)-O(1)	1.232(6)
C(21)-C(22A)	1.540(7)
C(22A)-F(1A)	1.321(11)
C(22A)-F(3A)	1.339(12)
C(22A)-F(2A)	1.349(11)
C(23)-O(4)	1.226(5)
C(23)-O(3)	1.240(5)
C(23)-C(24A)	1.530(7)
C(24A)-F(6A)	1.325(12)
C(24A)-F(4A)	1.345(12)
C(24A)-F(5A)	1.357(13)
N(6)-C(25)	1.147(8)
C(25)-C(26)	1.434(8)

N(5)-Rh(1)-S(3)#1	88.79(9)
N(5)-Rh(1)-S(1)#1	88.31(9)
S(3)#1-Rh(1)-S(1)#1	89.87(3)
N(5)-Rh(1)-S(2)	88.01(9)
S(3)#1-Rh(1)-S(2)	89.75(3)
S(1)#1-Rh(1)-S(2)	176.31(3)
N(5)-Rh(1)-S(4)	87.50(9)

S(3)#1-Rh(1)-S(4)	176.26(3)
S(1)#1-Rh(1)-S(4)	89.56(4)
S(2)-Rh(1)-S(4)	90.59(3)
N(5)-Rh(1)-Rh(1)#1	179.35(8)
S(3)#1-Rh(1)-Rh(1)#1	91.86(3)
S(1)#1-Rh(1)-Rh(1)#1	91.74(3)
S(2)-Rh(1)-Rh(1)#1	91.95(3)
S(4)-Rh(1)-Rh(1)#1	91.85(3)
N(1)-Ni(1)-N(2)	82.77(17)
N(1)-Ni(1)-S(1)	93.24(12)
N(2)-Ni(1)-S(1)	175.52(12)
N(1)-Ni(1)-S(2)	174.49(12)
N(2)-Ni(1)-S(2)	92.46(12)
S(1)-Ni(1)-S(2)	91.43(4)
N(4)-Ni(2)-N(3)	83.12(16)
N(4)-Ni(2)-S(4)	92.65(12)
N(3)-Ni(2)-S(4)	175.38(12)
N(4)-Ni(2)-S(3)	174.42(12)
N(3)-Ni(2)-S(3)	92.42(11)
S(4)-Ni(2)-S(3)	91.69(4)
C(1)-S(1)-Ni(1)	94.65(17)
C(1)-S(1)-Rh(1)#1	108.12(17)
Ni(1)-S(1)-Rh(1)#1	114.14(5)
C(9)-S(2)-Ni(1)	95.61(15)
C(9)-S(2)-Rh(1)	108.65(16)
Ni(1)-S(2)-Rh(1)	114.00(4)
C(10)-S(3)-Ni(2)	96.16(14)
C(10)-S(3)-Rh(1)#1	108.69(14)
Ni(2)-S(3)-Rh(1)#1	115.58(4)
C(18)-S(4)-Ni(2)	95.99(14)
C(18)-S(4)-Rh(1)	110.13(14)
Ni(2)-S(4)-Rh(1)	115.07(4)
C(2)-N(1)-C(3)	113.1(4)
C(2)-N(1)-C(6)	111.1(4)

C(3)-N(1)-C(6)	107.5(4)
C(2)-N(1)-Ni(1)	111.3(3)
C(3)-N(1)-Ni(1)	106.8(3)
C(6)-N(1)-Ni(1)	106.7(3)
C(5)-N(2)-C(7)	112.7(4)
C(5)-N(2)-C(8)	111.3(4)
C(7)-N(2)-C(8)	106.4(4)
C(5)-N(2)-Ni(1)	108.0(3)
C(7)-N(2)-Ni(1)	108.1(3)
C(8)-N(2)-Ni(1)	110.4(3)
C(12)-N(3)-C(11)	113.0(4)
C(12)-N(3)-C(15)	109.3(3)
C(11)-N(3)-C(15)	108.4(4)
C(12)-N(3)-Ni(2)	106.0(3)
C(11)-N(3)-Ni(2)	112.1(3)
C(15)-N(3)-Ni(2)	107.8(3)
C(14)-N(4)-C(17)	112.5(4)
C(14)-N(4)-C(16)	110.5(3)
C(17)-N(4)-C(16)	108.6(4)
C(14)-N(4)-Ni(2)	107.0(3)
C(17)-N(4)-Ni(2)	111.2(3)
C(16)-N(4)-Ni(2)	106.9(3)
C(19)-N(5)-Rh(1)	176.7(3)
C(2)-C(1)-S(1)	108.2(4)
C(1)-C(2)-N(1)	110.6(4)
N(1)-C(3)-C(4)	113.5(4)
C(5)-C(4)-C(3)	118.1(4)
N(2)-C(5)-C(4)	110.5(4)
N(1)-C(6)-C(7)	108.6(4)
N(2)-C(7)-C(6)	108.3(4)
C(9)-C(8)-N(2)	109.3(4)
C(8)-C(9)-S(2)	108.7(3)
C(11)-C(10)-S(3)	108.2(3)
C(10)-C(11)-N(3)	108.9(3)

N(3)-C(12)-C(13)	112.9(4)
C(12)-C(13)-C(14)	117.1(4)
N(4)-C(14)-C(13)	112.4(4)
N(3)-C(15)-C(16)	109.0(3)
N(4)-C(16)-C(15)	108.9(3)
C(18)-C(17)-N(4)	108.9(4)
C(17)-C(18)-S(4)	107.5(3)
N(5)-C(19)-C(20)	178.0(4)
O(2)-C(21)-O(1)	129.0(5)
O(2)-C(21)-C(22A)	113.8(4)
O(1)-C(21)-C(22A)	117.1(5)
F(1A)-C(22A)-F(3A)	103.6(13)
F(1A)-C(22A)-F(2A)	107.9(12)
F(3A)-C(22A)-F(2A)	104.5(13)
F(1A)-C(22A)-C(21)	111.1(7)
F(3A)-C(22A)-C(21)	118.2(17)
F(2A)-C(22A)-C(21)	110.9(12)
O(4)-C(23)-O(3)	130.6(4)
O(4)-C(23)-C(24A)	113.8(4)
O(3)-C(23)-C(24A)	115.4(4)
F(6A)-C(24A)-F(4A)	107.9(13)
F(6A)-C(24A)-F(5A)	99.0(13)
F(4A)-C(24A)-F(5A)	103.0(12)
F(6A)-C(24A)-C(23)	112.2(10)
F(4A)-C(24A)-C(23)	114.2(10)
F(5A)-C(24A)-C(23)	118.9(11)
N(6)-C(25)-C(26)	179.5(7)

Symmetry transformations used to generate equivalent atoms:

#1 -x,-y+1,-z

Table A-21. Crystal data and structure refinement for $[Rh(\mathbf{Ni\text{-}1}')_3][BF_4]_3$.

Empirical formula	C54 H108 B6 F24 N12 Ni6 Rh2 S12	
Formula weight	2389.18	
Temperature	110(2) K	
Wavelength	1.54178 Å	
Crystal system	Rhombohedral	
Space group	R3c	
Unit cell dimensions	a = 21.507(2) Å	α= 90°.
	b = 21.507(2) Å	β= 90°.
	c = 15.769(2) Å	γ = 120°.
Volume	6316.6(12) $Å^3$	
Z	3	
Density (calculated)	1.884 Mg/m^3	
Absorption coefficient	8.169 mm^{-1}	
F(000)	3636	
Crystal size	0.10 x 0.01 x 0.01 mm^3	
Theta range for data collection	4.11 to 58.74°.	
Index ranges	-22<=h<=23, -23<=k<=20, -17<=l<=17	
Reflections collected	7075	
Independent reflections	1893 [R(int) = 0.1284]	
Completeness to theta = 58.74°	99.4 %	
Absorption correction	None	
Max. and min. transmission	0.9228 and 0.4955	
Refinement method	Full-matrix least-squares on F^2	
Data / restraints / parameters	1893 / 11 / 173	
Goodness-of-fit on F^2	1.008	
Final R indices [I>2sigma(I)]	R1 = 0.0498, wR2 = 0.0915	
R indices (all data)	R1 = 0.0707, wR2 = 0.0972	
Absolute structure parameter	0.01(2)	
Largest diff. peak and hole	0.667 and -0.512 $e.Å^{-3}$	

Table A-22. Bond lengths [Å] and angles [°] for [Rh(**Ni-1'**)$_3$][BF$_4$]$_3$.

Rh(1)-S(1)#1	2.374(3)
Rh(1)-S(1)#2	2.374(3)
Rh(1)-S(1)	2.374(3)
Rh(1)-S(2)#2	2.383(3)
Rh(1)-S(2)#1	2.383(3)
Rh(1)-S(2)	2.383(3)
Ni(1)-N(1)	1.919(9)
Ni(1)-N(2)	1.927(9)
Ni(1)-S(1)	2.144(3)
Ni(1)-S(2)	2.159(3)
S(1)-C(1)	1.826(12)
S(2)-C(9)	1.842(9)
N(1)-C(3)	1.466(14)
N(1)-C(6)	1.502(12)
N(1)-C(2)	1.502(13)
N(2)-C(5)	1.495(13)
N(2)-C(8)	1.502(13)
N(2)-C(7)	1.515(13)
C(1)-C(2)	1.511(16)
C(3)-C(4)	1.48(2)
C(4)-C(5)	1.469(17)
C(6)-C(7)	1.588(15)
C(8)-C(9)	1.487(13)
B(1A)-F(3A)	1.33(2)
B(1A)-F(1A)	1.35(2)
B(1A)-F(4A)	1.38(3)
B(1A)-F(2A)	1.46(3)
B(1B)-F(3B)	1.33(2)
B(1B)-F(1B)	1.35(2)
B(1B)-F(4B)	1.38(3)
B(1B)-F(2B)	1.44(3)

S(1)#1-Rh(1)-S(1)#2	89.14(10)
S(1)#1-Rh(1)-S(1)	89.14(10)
S(1)#2-Rh(1)-S(1)	89.14(10)
S(1)#1-Rh(1)-S(2)#2	168.07(9)
S(1)#2-Rh(1)-S(2)#2	79.30(9)
S(1)-Rh(1)-S(2)#2	93.57(9)
S(1)#1-Rh(1)-S(2)#1	79.30(9)
S(1)#2-Rh(1)-S(2)#1	93.57(9)
S(1)-Rh(1)-S(2)#1	168.07(9)
S(2)#2-Rh(1)-S(2)#1	98.35(8)
S(1)#1-Rh(1)-S(2)	93.57(9)
S(1)#2-Rh(1)-S(2)	168.07(9)
S(1)-Rh(1)-S(2)	79.30(9)
S(2)#2-Rh(1)-S(2)	98.35(8)
S(2)#1-Rh(1)-S(2)	98.35(8)
N(1)-Ni(1)-N(2)	83.5(4)
N(1)-Ni(1)-S(1)	92.0(3)
N(2)-Ni(1)-S(1)	169.5(3)
N(1)-Ni(1)-S(2)	170.1(3)
N(2)-Ni(1)-S(2)	93.1(3)
S(1)-Ni(1)-S(2)	89.72(11)
C(1)-S(1)-Ni(1)	93.4(4)
C(1)-S(1)-Rh(1)	113.0(4)
Ni(1)-S(1)-Rh(1)	87.47(9)
C(9)-S(2)-Ni(1)	92.7(3)
C(9)-S(2)-Rh(1)	115.3(4)
Ni(1)-S(2)-Rh(1)	86.90(10)
C(3)-N(1)-C(6)	111.5(9)
C(3)-N(1)-C(2)	107.8(9)
C(6)-N(1)-C(2)	112.1(8)
C(3)-N(1)-Ni(1)	112.2(8)
C(6)-N(1)-Ni(1)	102.0(6)
C(2)-N(1)-Ni(1)	111.3(7)
C(5)-N(2)-C(8)	109.6(8)

C(5)-N(2)-C(7)	110.6(9)
C(8)-N(2)-C(7)	113.8(8)
C(5)-N(2)-Ni(1)	109.6(7)
C(8)-N(2)-Ni(1)	110.6(6)
C(7)-N(2)-Ni(1)	102.4(6)
C(2)-C(1)-S(1)	104.6(8)
N(1)-C(2)-C(1)	110.0(8)
N(1)-C(3)-C(4)	111.7(11)
C(5)-C(4)-C(3)	115.1(13)
C(4)-C(5)-N(2)	112.5(10)
N(1)-C(6)-C(7)	109.3(8)
N(2)-C(7)-C(6)	108.3(8)
C(9)-C(8)-N(2)	111.5(8)
C(8)-C(9)-S(2)	106.7(7)
F(3A)-B(1A)-F(1A)	110.3(18)
F(3A)-B(1A)-F(4A)	112(2)
F(1A)-B(1A)-F(4A)	116.6(19)
F(3A)-B(1A)-F(2A)	103.9(18)
F(1A)-B(1A)-F(2A)	107(2)
F(4A)-B(1A)-F(2A)	105.9(16)
F(3B)-B(1B)-F(1B)	110(2)
F(3B)-B(1B)-F(4B)	107(2)
F(1B)-B(1B)-F(4B)	108(2)
F(3B)-B(1B)-F(2B)	109(2)
F(1B)-B(1B)-F(2B)	112(2)
F(4B)-B(1B)-F(2B)	110(2)

Symmetry transformations used to generate equivalent atoms:

#1 -x+y,-x,z #2 -y,x-y,z

VITA

Stephen Paul Jeffery was born on April 22, 1978 in Houston, TX. After attending many schools in the continental United States and Canada due to his parents' itinerant lifestyle in construction, he began his college career at Texas A&M University and completed his Bachelor of Science degree from Texas A&M University in December of 2000. He continued his graduate education at Texas A&M and earned his doctorate under Dr. Marcetta Y. Darensbourg. He can be contacted through his parents, Curtis and Leona Jeffery, at 2426 Donovan View, Dickinson, TX 77539, (281) 337-4576.